

METAL/POLYMER INTERACTIONS

by

Gregory Mills Porta

Dissertation submitted to the faculty of the  
Virginia Polytechnic Institute and State University  
in partial fulfillment of the requirements for the degree of

DOCTOR OF PHILOSOPHY

in

Chemistry

APPROVED:

---

Dr. L. T. Taylor, Chairman

---

Dr. B. E. Hanson

---

Dr. J. G. Dillard

---

Dr. J. E. McGrath

---

Dr. L. C. Burton

September, 1989  
Blacksburg, Virginia

# METAL/POLYMER INTERACTIONS

by

Gregory M. Porta

Committee Chairman: Larry T. Taylor  
Chemistry

(ABSTRACT)

Polyimides by nature are highly resistive materials which exhibit exceptional thermal and chemical stabilities. Yet, there are a number of instances in which a polymeric material displaying low resistance and featuring similar physical, chemical, and thermal characteristics as polyimide would be desirable. Toward this goal, multilayered polyimide composite films have been produced through the homogeneous incorporation of copper salts and complexes into poly(amide acid) followed by thermal processing. In this way, highly anisotropic copper containing composite films have been obtained which feature a surface or near-surface layer of copper metal or copper oxide as the conductive medium.

The surface resistivity of the composites is lowered up to ten orders of magnitude relative to unmodified polyimide films. However, in many cases, the discontinuity of the copper containing layer limits the attainment of near-theoretical resistivity. Hence, evaluation of the composites by a variety of analytical techniques has been used to develop structure-process-property relationships in order to optimize the electrical properties of these materials.

The surface treatment of polymeric materials by glow discharge is known to improve their adhesive strength when in contact with a large number of other substances, be they polymeric, metallic, or ceramic in nature. Many efforts have been made to characterize this phenomenon, however in most instances, details

concerning the interfacial structure and adhesion mechanism are not fully understood.

The second part of this Dissertation describes the structure and chemistry occurring in the interfacial region between sputter-coated titanium metal, and both plasma pretreated and nonpretreated polyethylene terephthalate (PET) film. The effect of plasma pretreatment on nonmetallized PET is discussed as well. Upon application of a gaseous plasma, titanium/polyester adhesion increases dramatically following metallization compared to the nonpretreated analog. In order to relate this phenomenon to a physical and/or chemical change X-ray photoelectron spectroscopy, Auger electron spectroscopy, transmission electron microscopy, as well as, surface Fourier transform infrared spectrometry have been used to characterize both the surface and interfacial regions of these films.

## ACKNOWLEDGEMENTS

Over the years there have been a number of people who have been instrumental in shaping my academic career. It is with great pleasure that I acknowledge their influence in my life:

I sincerely thank Dr. Timothy J. McNeese, who guided my undergraduate research project at the Loyola College of Maryland, for kindling my interest in inorganic chemistry. He strongly encouraged me to pursue graduate study in this field.

I would like to thank Dr. Larry T. Taylor for directing my research during my doctoral program. His unrestrained approach to research provided me with an opportunity to explore many avenues in the field of my research, to which I am very grateful. Also, I thank the other members of my research committee: Dr. John G. Dillard, Dr. James E. McGrath, Dr. Brian E. Hanson, and Dr. Larry C. Burton who during various aspects of this work provided helpful hints and discussions.

I sincerely appreciate Dr. James D. Rancourt for collaborating in both of my research projects. This association has been very fruitful and it has been a pleasure working with him. Furthermore, I wish to acknowledge the guidance provided by \_\_\_\_\_ in obtaining surface analyses and the assistance provided by my wife \_\_\_\_\_ for the electron microscopy. I would also like to thank \_\_\_\_\_, for without whose collaboration, the metallized polyester project would not have been possible.

I wish to thank my parents \_\_\_\_\_ for all their support, encouragement, and cooperation during my academic career.

Finally, with sincere gratitude, I acknowledge the National Aeronautics and Space Administration Langley Research Center, and the Virginia Center for Innovative Technology for their generous financial support of this research.

## **DEDICATION**

**This Dissertation is dedicated**

**to my wife,**

**without whose support and love this degree would not  
have been possible.**

## TABLE OF CONTENTS

COVER PAGE .....	i
ABSTRACT .....	ii
ACKNOWLEDGEMENTS .....	iv
DEDICATION .....	vi
TABLE OF CONTENTS .....	vii
LIST OF FIGURES .....	xi
LIST OF SCHEMES .....	xvii
LIST OF TABLES .....	xviii
I. INTRODUCTION .....	1
PART 1.	
II. HISTORICAL .....	5
III. EXPERIMENTAL .....	11
A. Copper Doped Film Preparation .....	11
1. Monomers .....	11
2. Dopants .....	11
3. Solvent .....	14
4. Polymers .....	14
B. Polymer Film Characterization .....	16
1. Elemental Analysis .....	16
2. Differential Scanning Calorimetry .....	16
3. Thermogravimetric Analysis .....	19
4. Auger Electron Spectroscopy .....	19
5. X-ray Photoelectron Spectroscopy .....	19
6. Scanning and Transmission Electron Microscopy .....	20
7. Energy-dispersive X-ray Analysis .....	20
8. Room Temperature Electrical Resistivity Measurements ..	20
9. Variable Temperature Electrical Resistivity Measurements .....	20

## RESULTS AND DISCUSSION

IV.	THE STRUCTURE OF COPPER/POLYIMIDE MULTI-LAYERED COMPOSITES .....	22
	A. Preliminary .....	22
	B. General Characteristics .....	22
	C. Copper Modified (1X) BTDA-ODA Polyimide Films .....	23
	D. Copper Modified (2X) BTDA-ODA and (1X, 2X) BTDA-APB Polyimide Films .....	33
	E. Copper Modified (1X, 2X) BDSDA-ODA Polyimide Films .....	46
	F. Copper/Polyimide Composite Formation .....	56
	G. A Comparison: Copper-Doped Soluble Polyimide and Condensation Polyimide Films .....	64
V.	ELECTRICAL AND THERMAL CHARACTERISTICS OF COPPER CONTAINING POLYIMIDE FILMS .....	70
	A. Preliminary .....	70
	B. Thermal Properties .....	70
	C. Electrical Properties .....	74
VI.	THE DEVELOPMENT OF PROCESS-PROPERTY RELATIONSHIPS FOR COPPER-DOPED BTDA-APB POLYIMIDE FILMS .....	87
	A. Preliminary .....	87
	B. The Statistical Experimental Design .....	87
	C. Process-Property Relationships .....	90
	D. High Temperature Processing of Copper-Doped BTDA-APB Polyimide Films .....	106
	E. High Temperature Processing of Copper-Doped BTDA-ODA Polyimide Films .....	117
VII.	CONCLUSIONS AND FUTURE WORK .....	130
PART 2.		
VIII.	HISTORICAL .....	134
	A. Polyester Film .....	134
	B. Sputtering .....	136
	C. Surface Treatments .....	137

IX. EXPERIMENTAL .....	142
A. Plasma Pretreatment and Metallization of Poly(ethylene terephthalate) Film .....	142
1. Polyester Film .....	142
2. Plasma Pretreatment Gases .....	142
3. Plasma Processing .....	142
4. Film Metallization .....	142
B. Film Characterization .....	144
1. X-ray Photoelectron Spectroscopy .....	144
2. Auger Electron Spectroscopy .....	144
3. Transmission Electron Microscopy .....	144
4. Fourier Transform Electron Spectrometry .....	144
5. Contact Angle Analysis .....	144
6. Residual Gas Spectrometric Analysis .....	144
7. Mechanical Analysis .....	145
 RESULTS AND DISCUSSION	
X. THE EFFECT OF PLASMA TREATMENT ON THE SURFACE PROPERTIES OF POLY(ETHYLENE TEREPHTHALATE) FILM .....	146
A. Preliminary .....	146
B. X-ray Photoelectron Analysis of ICI-442 Polyester Film .....	146
C. Surface Characterization of Plasma Treated ICI-442 Polyester Film by X-ray Photoelectron Spectroscopy .....	152
D. Attenuated Total Reflectance Fourier Transform Infrared Spectrometric (ATR-FT-IR) Study of Plasma Pretreated ICI-442 Polyester Film .....	164
E. Residual Gas Analysis of the Treatment Gas Mixture Before and After Plasma Initiation .....	173
F. Static Contact Angle Analysis of Nontreated and Plasma Treated ICI-442 Polyester Film .....	180
XI. THE INTERFACIAL CHEMISTRY OF TITANIUM COATED POLYESTER FILMS .....	182
A. Preliminary .....	182
B. Auger Electron Depth Profiling and X-ray Photoelectron Spectroscopy .....	182
C. Transmission Electron Microscopic Analysis. ....	197
XII. THE APPLICATION OF STATISTICAL EXPERIMENTAL DESIGNS TO DETERMINE PROCESS-PROPERTY RELATIONSHIPS OF TITANIUM COATED POLYESTER FILMS .....	201
A. Preliminary .....	201
B. Factorial I. ....	201
C. Factorial II .....	208
D. Factorial III .....	213

XIII. CONCLUSIONS AND FUTURE WORK .....	219
XIV. APPENDIX .....	224
REFERENCES .....	225
VITA .....	234

## LIST OF FIGURES

### Part I

Figure 1.	Schematic drawing of the polymer reactor vessel. ....	15
Figure 2.	Schematic drawing of the wet breathing air apparatus. ....	17
Figure 3.	The XPS Cu(2p) spectrum of Cu(TFA) <sub>2</sub> . ....	25
Figure 4.	The XPS Cu(2p) spectrum of the wet-air-cured 1X-doped BTDA-ODA film. ....	26
Figure 5.	The XPS O(1s) spectrum of the wet-air-cured 1X-doped BTDA-ODA film. ....	28
Figure 6.	The XPS survey spectrum of the wet-air-cured 1X-doped BTDA-ODA film before and after argon ion etching. ....	29
Figure 7.	Auger electron spectroscopic depth profile of the wet-air-cured 1X-doped BTDA-ODA film. ....	30
Figure 8.	Transmission electron cross section of the surface region of the wet-air-cured 1X-doped BTDA-ODA film. ....	32
Figure 9.	Transmission electron cross section of particulate matter within a dry-air-cured 1X-doped BTDA-ODA film. ....	35
Figure 10.	Energy dispersive X-ray analysis of the particulate matter within a dry-air-cured 1X-doped BTDA-ODA film. ....	36
Figure 11.	The XPS Cu(2p) spectrum of the wet-air-cured 2X-doped BTDA-ODA film. ....	37
Figure 12.	The XPS O(1s) spectrum of the wet-air-cured 2X-doped BTDA-ODA film. ....	38
Figure 13.	Auger electron spectroscopic depth profile of the nitrogen-cured 2X-doped BTDA-ODA film. ....	40
Figure 14.	Auger electron spectroscopic depth profile of the dry-air-cured 2X-doped BTDA-APB film. ....	41
Figure 15.	Scanning electron micrograph of the wet-air-cured 2X-doped BTDA-ODA film. ....	42
Figure 16.	Scanning electron micrograph of the wet-air-cured 2X-doped BTDA-ODA film after treatment with forming gas (5% H <sub>2</sub> /95% N <sub>2</sub> ). ....	44

Figure 17.	Transmission electron cross section of the surface region of the wet-air-cured 2X-doped BTDA-ODA film. ....	45
Figure 18.	The XPS Cu(2p) spectrum of the wet-air-cured 2X-doped BDSDA-ODA film after argon ion etching. ....	48
Figure 19.	The XPS S(2p) spectrum of the wet-air cured 2X-doped BDSDA-ODA film (A) before and (B) after argon ion etching. ....	49
Figure 20.	Auger electron spectroscopic depth profile of the wet-air-cured 1X-doped BDSDA-ODA film. ....	51
Figure 21.	Auger electron spectroscopic depth profile of the wet-air-cured 2X-doped BDSDA-ODA film. ....	52
Figure 22.	Transmission electron cross section of a dry-air-cured 1X-doped BDSDA-ODA film. ....	53
Figure 23.	Transmission electron cross-section of the surface region of the wet-air-cured 1X-doped BDSDA-ODA film. ....	54
Figure 24.	Transmission electron cross-section of the surface region of the wet-air-cured 2X-doped BDSDA-ODA film. ....	55
Figure 25.	Schematic drawing of the temperature and imidization gradients resulting from the solvent and water flux within a curing film. ....	60
Figure 26.	Chemical structure of Polyimide XU-218. ....	65
Figure 27.	The XPS Cu(2p) spectrum of Cu(TFA) <sub>2</sub> modified BTDA-DAPI and Cu(TFA) <sub>2</sub> modified XU-218 films. ....	66
Figure 28.	Scanning transmission electron cross sections of (A) Cu(TFA) <sub>2</sub> modified BTDA-DAPI and (B) Cu(TFA) <sub>2</sub> modified XU-218. ....	68
Figure 29.	The thermogravimetric profile of nondoped and Cu(TFA) <sub>2</sub> doped BTDA-ODA films. ....	73
Figure 30.	Electron path through a tri-layered composite film. ....	79
Figure 31.	Two probe electrode resistivity measurement of a tri-layered film following argon ion etching. ....	81
Figure 32.	"Air-Side" electrical resistivity as a function of temperature for the 1X-doped and 2X-doped wet-air-cured BTDA-ODA films. ....	84
Figure 33.	"Air-Side" electrical resistivity as a function of temperature for the Cu(TFA) <sub>2</sub> -doped BTDA-APB films. ....	85

Figure 34.	"Air-Side" electrical resistivity as a function of temperature for the wet-air-cured and dry-air-cured 1X-doped BTDA-ODA films. ....	86
Figure 35.	The XPS F(1s) spectrum of a sample which contains both inorganic and organic fluorine components. ....	96
Figure 36.	Optical micrograph of factorial sample #3. ....	98
Figure 37.	Auger electron spectroscopic line scan of the "air-side" surface of factorial sample #3. ....	99
Figure 38.	Guarded electrode geometry for surface resistivity measurements. ....	101
Figure 39.	Resistivity versus temperature for $\text{Cu}(\text{TFA})_2$ modified BTDA-APB films cured to $200^\circ\text{C}$ and $300^\circ\text{C}$ . ....	104
Figure 40.	The thermogravimetric profile of $\text{Cu}(\text{TFA})_2$ modified BTDA-APB films cured to $200^\circ\text{C}$ and $300^\circ\text{C}$ . ....	105
Figure 41.	Differential scanning calorimetric analysis of a $\text{Cu}(\text{TFA})_2$ modified BTDA-APB film cured to $200^\circ\text{C}$ . ....	107
Figure 42.	Differential scanning calorimetric analysis of a $\text{Cu}(\text{TFA})_2$ modified BTDA-APB film cured to $300^\circ\text{C}$ . ....	108
Figure 43.	Scanning electron micrographs of a 2X-doped wet-air-cured BTDA-APB film (A) before and (B) after post-processing. ....	110
Figure 44.	Transmission electron cross section of the surface region of a 2X-doped wet-air-cured BTDA-APB film (A) before and (B) after post-processing. ....	111
Figure 45.	The thermogravimetric profile of $\text{Cu}(\text{TFA})_2$ -doped and nondoped BTDA-APB films cured to $300^\circ\text{C}$ . ....	114
Figure 46.	The XPS Cu(2p) spectrum of a 2X-doped dry-air-cured BTDA-APB film post-processed in nitrogen. ....	116
Figure 47.	Transmission electron cross section of the surface region of a 20% solids 1X-doped wet-air-cured BTDA-ODA film. ....	119
Figure 48.	Transmission electron cross section of the surface region of a 23% solids 1X-doped wet-air-cured BTDA-ODA film. ....	120
Figure 49.	Transmission electron cross section of the surface region of a 25% solids 1X-doped wet-air-cured BTDA-ODA film. ....	121

Figure 50.	Auger electron spectroscopic depth profile of a 1X-doped BTDA-ODA film post-processed in dry air at 350°C for 1 hr.	126
Figure 51.	Auger electron spectroscopic depth profile of a 1X-doped BTDA-ODA film post-processed in nitrogen at 350°C for 1 hr. ....	127

## Part II

Figure 52.	Schematic drawing of a glow discharge sputtering device of the planar diode type. ....	138
Figure 53.	Schematic drawing of a planar magnetron sputtering system. ....	143
Figure 54.	The XPS C(1s) spectrum of raw ICI-442 polyester film. ....	148
Figure 55.	The XPS O(1s) spectrum of raw ICI-442 polyester film. ....	150
Figure 56.	Plot of the change in elemental composition versus plasma exposure for ICI-442 polyester film at a 15° take-off angle. ...	153
Figure 57.	Plot of the change in elemental composition versus plasma exposure for ICI-442 polyester film at a 90° take-off angle. ...	154
Figure 58.	The XPS O(1s) spectrum of both plasma pretreated and nontreated ICI-442 polyester film. ....	157
Figure 59.	The curve resolved XPS O(1s) spectrum of plasma pretreated ICI-442 polyester film. ....	158
Figure 60.	The XPS C(1s) spectrum of both plasma pretreated and nontreated ICI-442 polyester film. ....	160
Figure 61.	Plot of the change in concentration of oxygen species versus plasma exposure for ICI-442 polyester film at a 15° take-off angle. ....	161
Figure 62.	The ATR-IR spectrum of nontreated ICI-442 polyester film. ...	165
Figure 63.	The carbonyl region of both plasma pretreated and nontreated ICI-442 polyester film obtained by ATR-IR. ....	166
Figure 64.	The effect of plasma exposure on the carbonyl region of ICI-442 polyester film obtained by ATR-IR. The difference spectra are shown (plasma treated spectrum - nontreated spectrum). ....	168

Figure 65.	The effect of plasma exposure on the -OH stretching region of ICI-442 polyester film obtained by ATR-IR. The difference spectra are shown (plasma treated spectrum - nontreated spectrum). .....	169
Figure 66.	The C-O region of both plasma pretreated and nontreated ICI-442 polyester film obtained by ATR-IR. ....	171
Figure 67.	The effect of plasma exposure on the C-O region of ICI-442 polyester film obtained by ATR-IR. The difference spectra are shown (plasma treated spectrum - nontreated spectrum). ....	172
Figure 68.	The thermogravimetric profile of nontreated and plasma pretreated ICI-442 polyester film. ....	176
Figure 69.	The behavior of titanium/polyester adhesion versus plasma exposure. ....	179
Figure 70.	The AES depth profile of a typical titanium coated ICI-442 polyester film. ....	184
Figure 71.	The XPS Ti(2p) spectrum of both plasma pretreated and nontreated titanium coated ICI-442 polyester film following argon ion etching. ....	186
Figure 72.	The XPS O(1s) spectrum of both plasma pretreated and nontreated titanium coated ICI-442 polyester film following argon ion etching. ....	189
Figure 73.	The XPS C(1s) spectrum of both plasma pretreated and nontreated titanium coated ICI-442 polyester film following argon ion etching. ....	190
Figure 74.	The XPS O(1s) spectrum of the metal containing fracture surface of a nontreated titanium coated ICI-442 polyester film. ....	193
Figure 75.	The XPS O(1s) spectrum of both plasma pretreated and nontreated ICI-442 polyester film coated with a thin layer of titanium. ....	195
Figure 76.	The XPS C(1s) spectrum of both plasma pretreated and nontreated ICI-442 polyester film coated with a thin layer of titanium. ....	196
Figure 77.	Transmission electron micrograph of the metallized surface of a typical titanium coated ICI-442 polyester film. ....	198

Figure 78.	Schematic drawing of both normal and biased electrode configurations. ....	211
Figure 79.	Schematic drawing of the electrode configuration with the drum cylinder as the anode. ....	223

## LIST OF SCHEMES

### Part I

Scheme 1.	Synthesis and cure of a doped polyimide film. ....	18
Scheme 2.	Probable $\text{Cu}(\text{TFA})_2$ reaction routes leading to the formation of $\text{CuO}$ . ....	57
Scheme 3.	Alternative reactive pathway leading to the formation of $\text{CuO}$ from $\text{Cu}(\text{TFA})_2$ . ....	59

### Part II

Scheme 4.	Initial synthesis of poly(ethylene terephthalate). ....	135
Scheme 5.	Commonly reported thermal and photolytic decomposition mechanisms of poly(ethylene terephthalate). ....	163
Scheme 6.	Poly(ethylene terephthalate) decomposition routes leading to the formation of $\text{CO}$ and $\text{CO}_2$ . ....	178
Scheme 7.	Possible polyester oxygen-titanium metal interactions and products. ....	188

## LIST OF TABLES

### Part I

Table I.	Structures and Data Pertaining to Monomers Used in This Study. ....	12
Table II.	Data Pertaining to the Dopants Used in This Study. ....	13
Table III.	General Properties of Cu(TFA) <sub>2</sub> -Doped and Nondoped Polyimide Films. ....	24
Table IV.	Morphological Features of Cu(TFA) <sub>2</sub> -Doped Polyimide Films as Deduced from TEM Data. ....	34
Table V.	Additive Conversion and Volume Fraction of Copper Species. ....	62
Table VI.	Thermal Properties of Cu(TFA) <sub>2</sub> -Doped and Nondoped Polyimide Films. ....	71
Table VII.	DC Electrical Resistivity of Cu(TFA) <sub>2</sub> -Doped Polyimide Films. ....	75
Table VIII.	Calculated Vs. Experimental Surface Resistivity. ....	77
Table IX.	Processing Variables Used in the Experimental Strategy. ....	89
Table X.	The Statistical Experimental Design. ....	91
Table XI.	Surface Electrical Resistivities of Copper-Doped BTDA-APB Polyimide Films. ....	93
Table XII.	Film Properties and the Influence of Processing Variables. ...	94
Table XIII.	D.C. Electrical Properties of Cu(TFA) <sub>2</sub> modified BTDA-APB Polyimide Films. ....	102
Table XIV.	General Characteristics of Post-Processed BTDA-APB Polyimide Films. ....	112
Table XV.	Morphological Features of Post-Processed BTDA-APB Polyimide Films as Deduced From TEM Data. ....	115
Table XVI.	Surface Electrical Resistivities of Cu(TFA) <sub>2</sub> -Doped BTDA-APB Polyimide Films. ....	118
Table XVII.	Effect of Percent Solids On the Surface Electrical Resistivity of Cu(TFA) <sub>2</sub> -Doped BTDA-ODA Polyimide Films. ....	123

Table XVIII.	Morphological Features of Post-Processed Cu(TFA) <sub>2</sub> -Doped BTDA-ODA Polyimide Films as Deduced From TEM Data. ....	128
Table XIX.	Surface Electrical Resistivities of Post-Processed Cu(TFA) <sub>2</sub> -Doped BTDA-ODA Polyimide Films. ....	129

**Part II**

Table XX.	Binding Energy Assignments for Nontreated ICI-442 Polyester Film. ....	149
Table XXI.	Surface Elemental Composition of Nontreated ICI-442 Polyester Film. ....	151
Table XXII.	RGA Mass Spectral Data of the Glow Discharge. ....	174
Table XXIII.	Deposition Characteristics of Titanium Coated Polyester Film. ....	199
Table XXIV.	Experimental Design of Factorial I. ....	203
Table XXV.	Statistical Results of Factorial I. ....	204
Table XXVI.	UV Spectral Characteristics of Gaseous Plasmas. ....	207
Table XXVII.	Experimental Design of Factorial II. ....	209
Table XXVIII.	Statistical Results of Factorial II. ....	212
Table XXIX.	Experimental Design of Factorial III. ....	215
Table XXX.	Statistical Results of Factorial III. ....	216
Table XXXI.	Statistical Significance of All Process Variables Studied. ....	218

## I. INTRODUCTION

It is becoming increasingly important to understand the nature of polymer and metal interactions. Both have properties so unique unto themselves that it is sometimes difficult to perceive such an unlikely combination. But, it is these properties once combined that produce materials that again have many useful benefits. In everyday life, we are surrounded by reminders of this special relationship. To list a few; polymeric adhesives are used to bind metals in household goods, automobiles, and even "high tech" planes and spacecraft; polymers are applied to metals as protective coatings and insulating layers; thin layers of metals are used to coat polymeric substrates for decorative, conductive, and optical uses; and polymer/metal composites are used in electrical and structural applications. However, as more and more elaborate and unique materials are used and produced, it becomes imperative that their interaction be studied.

Polymers by nature are generally highly resistive materials which exhibit a variety of mechanical, thermal, and chemical properties. These features make them a boon to the electronics industry where they find a multitude of uses as insulators in a number of applications.[1] A few, such as, polyethylene, polypropylene, polyester, and polyimide account for most of the polymers used commercially in this area. The choice of a particular material naturally depends upon being able to reach a compromise among a whole range of considerations, including availability, ease of fabrication and cost.

However, there are a number of instances in which a polymeric material displaying low resistivity would be desirable. A lightweight, moldable, highly conductive material has long been recognised as a worthwhile goal to strive for,

and considerable scientific effort has been devoted to this.[2] Apart from the obvious market for a conductive material, substances with intermediate electrical properties would also be useful (e.g. for static charge dispersal)[3], resistive heaters[4], and graded insulation[1], among others). In the past, this problem has been attempted to be solved through the production of new conductive polymeric materials or the modification of existing materials. Although new conductive polymers have been produced which are relatively stable, a number of other problems have kept them from anything but the experimental stage.[5]

Of far more current importance is the external modification of plastics. Metal plating processes, such as, electroless deposition, vacuum evaporation deposition, and vacuum sputter deposition are the most commonly used.[6] In electroless deposition, metals are deposited upon the substrate by action of a metal salt (usually nickel or gold) with a reducing agent (e.g. sodium borohydride, sodium hypophosphite) in the presence of a catalyst.[7] In contrast to other electrochemical techniques, no electrodes or power supply is needed. Electroless plating is used in the production of circuit boards and chip packaging.

Vacuum evaporation is a process whereby a metal or inorganic compound is heated to the point that it will vaporize under vacuum conditions.[8] The substrate must be cool enough so that the metal vapors, once they contact the surface, will condense. Because the process is directional, fixturing must be provided to insure that all surfaces to be coated are in a line of sight from the vaporizing source to the surface to be metallized. Evaporated metal coatings have many uses; cadmium is used primarily for corrosion resistance on high tensile steel parts, gold and silver are used for decorative purposes, and copper

is used primarily in electronic circuits. The inorganic coatings are mainly employed to protect the substrate from scratches.

In vacuum sputter deposition, energetic particles generated in a plasma bombard the material to be deposited dislodging atoms which travel through the chamber and impact on the substrate to form the coating.[9] Vacuum sputtering is a particularly effective method because of its applicability to virtually any coating material. In contrast to vacuum evaporation, alloys such as stainless steel and compounds such as  $\text{Al}_2\text{O}_3$  can be effectively deposited in stoichiometric form. Again, vacuum sputtering is a line of sight process which restricts complicated substrates to fixturing. The high rate that materials are sputtered makes it an ideal technique for metallizing films where high processing speeds are achieved.

While all of the external plating processes discussed above may be viable routes to more "surface" conductive materials (not forgetting the multitude of other uses), poor adhesion of metal-to-polymer plagues many systems. This is one aspect of metal/polymer interaction that needs further study. Many efforts have been made to characterize this phenomenon; however, details concerning the interfacial structure and adhesion mechanism are not fully understood in most instances.

In the second half of this dissertation, one metal/polymer system in particular was explored. The purpose of this research was to determine the effect of plasma treatment, a technique used to promote metal/polymer adhesion, on a poly(ethylene terephthalate) substrate and to ascertain the physical and/or chemical effects of this process which allow improved adhesion to vacuum sputtered titanium metal. The determination of process-property relationships

was also undertaken to provide a means to improve existing levels of titanium/polyester adhesion.

The third most commonly used method for producing conductive plastics is internal modification. Internal modification has traditionally relied upon the heterogeneous incorporation of graphite, metal or conducting compound in some form (e.g. spheroids, fibers, etc.) within the polymer matrix.[10] Some uses of metal-filled polymers include; resistors, thermistors, electrodes, heating elements, EMI/RFI shielding, and switching power supplies. However, this method also required the use of relatively large mass loadings in order to approach the percolation threshold and achieve significant conductivity. The bulk material properties in these systems also began to deviate due to the large amount of conductor introduced.

An alternative approach to those mentioned has been followed in hopes of avoiding the aforementioned shortcomings. The purpose of this research was to create surface and volume conductive polymeric films stable at high temperatures for aerospace and electronic applications. Highly anisotropic metal containing polyimide films have been produced through the homogeneous incorporation of inorganic salts and complexes within the polyimide precursor, poly(amide acid), followed by thermal imidization (cyclodehydration). Surface conductive materials were produced in essentially one processing step by an internal process that requires low mass loading (< 5.0%) and provides exceptional conductor/polymer adherence. The first half of this dissertation provides the results of this endeavor.

## II. HISTORICAL

Linear polyimides are used extensively as structural materials in the aerospace and electronics industries because of their toughness, flexibility, high thermooxidative stability, solvent resistance, and low dielectric constant.[11] However, the processing of these materials is often tedious compared to other plastics. The soluble poly(amide acid) precursor must first be dissolved in a high boiling solvent, and later reacted to the polyimide by heating to an extremely high temperature. During the high temperature cure, significant amounts of solvent and water are also evolved making the preparation of large scale parts extremely difficult.

Despite the difficulty in processing these materials, polyimides are often produced as thin films and coatings, which are used as laminate materials, passivation layers, wire coatings, and adhesives.[12] The high surface area/volume ratio in these applications precludes a number of problems. However, as possible uses for these materials increase, polyimide processability becomes more and more of a potential burden.

A number of modifications have been developed to overcome this problem. Some of the first attempts to improve polyimide processability involved the use of meta-substituted aromatic diamines.[13] Additional advances in this area have included the incorporation of diamines and/or dianhydrides containing flexible bridging units such as ether, carbonyl, sulfur, fluoroalkyl, and sulfone, which impart mobility to the otherwise rigid polyimide chain. For example, St. Clair prepared a novel polyimide by reaction of 3,3',4,4'-benzophenonetetracarboxylic acid dianhydride and 3,3'-diaminophenylsulfone.[14] Although this material was

not soluble in its unend-capped form, it did possess thermoplastic tendencies and could be processed in the 260°C to 325°C temperature range.

A thermally stable polyimide that possesses reasonable solubility and processability characteristics is available from Ciba-Geigy (Polyimide XU-218).[15] The highly unsymmetrical nature of the aliphatic diamine that is employed to produce this material provides many of its unique properties. Successful attempts to improve the processability of polyimides has also centered around the use of aromatic monomers containing bulky side groups to disrupt chain packing.[16]

One method of modifying polyimides to improve their processability that has received a significant research effort is the formation of copolymers. Poly(amide imides)[17], poly(ester imides)[18] and poly(siloxane imides)[19,20] have been produced by a number of researchers. Although each is processable and possess a reasonable balance of mechanical and electrical properties, the materials exhibit substantially poorer thermal stability than the comparable aromatic polyimides.

As of late, considerable research efforts have taken place to modify the electrical properties of polyimides. Being insulators, a number of modifications have been introduced to increase their conductivity. There are generally two approaches to obtaining conductive or semi-conductive polyimides. As mentioned in the Introduction, the first approach involves the heterogeneous doping of polyimides with conductive particles, fibers, or flakes. Carbon black-filled polyimides have been shown to reduce the inherent resistance significantly; however, the materials are quite brittle and must be reinforced with glass fibers.[21]

Metal-filled polymers offer another means of heterogeneously modifying polyimides to improve conductivity. Several factors influence the use of metals in plastics. Some metals, including copper, tend to catalyze the degradation of some plastics.[22] In addition, some metals easily oxidize at the particle's surface, effectively rendering the composite material nonconductive. Sheer and Turner have reported that the oxidation of aluminum particles will effectively insulate the metal core, making modified plastics nonconductive up to very high filler concentrations.[23] Gold which does not oxidize and silver which is the most conductive metal are in general too expensive to use because of the high mass loadings involved. Because of the high density of metal compared to polymers and the lack of reinforcement exhibited by metal particles and fibers, it is desirable to minimize the concentration of metal used to form an electrically conducting polymer composite.

A second approach, homogeneous modification, has also been used to enhance the electrical characteristics of polyimides with relative success. Homogeneous incorporation requires a metallic additive, generally a metal salt or complex, which is soluble in the poly(amide acid) matrix. In this way, it was hoped that molecular composites would be formed that would induce conductivity and require low mass loading. Angelo first described the doping of polyimide precursors with metal ions in this fashion. Composite films were described consisting of a homogeneous mixture of (4,4'-diaminodiphenyl)methane, pyromellitic dianhydride, and bis(acetylacetonato)copper(II).[24] The volume resistivity of these films was reduced six orders of magnitude as compared to the non-doped controls.

The work of Angelo was later extended by Ezzell et al., who studied films resulting from the addition of various Cu(I) and Cu(II) compounds to various

polyimide precursors.[25] High-quality doped films were produced that exhibited lower thermal stabilities, higher softening temperatures, and lower electrical resistivities than the polymer alone. Surface segregation and chemical conversion of the dopant occurred during the curing process.

A number of researchers have employed palladium salts and complexes to lower the electrical resistivity of polyimides. Korshak et al. describe experiments wherein palladium(II) hydroxide was incorporated into polyimides to obtain a palladium metal surface layer.[26] In another set of studies, the addition of lithium tetrachloropalladate and bis(dimethylsulfide)dichloropalladium resulted in modified polyimides containing palladium in the metallic state.[27,28] The volume resistivity of these films was reported to have been reduced by more than ten orders of magnitude.

The electrical resistivity of polyimides has also been lowered by incorporation of silver salts and complexes. Auerbach described the use of silver nitrate as an additive.[29] Silver mirrors and/ or thin film silver conductors were produced by dissolving silver nitrate into commercial poly(amide acids) followed by thermal curing under a carbon blanket at 360°C in an oxygen containing atmosphere. Surface conductivities as low as 1 ohm were reported, comparable to vapor deposited silver films. In a later study, Boggess and Taylor described the surface enrichment of fully-cured polyimides with silver, following the addition of AgNO<sub>3</sub> and a number of silver inorganic complexes into poly(amide acid).[30]

Polyimides have also been modified with cobalt chloride.[31,32] A reduced surface resistivity was realized and was attributed to a surface cobalt oxide layer. No reduction in volume resistivity was observed for these films. A similar study was performed to determine if an interaction exists between cobalt and the

potential donor atoms of either poly(amide acid) in solution or the polyimide.[33] Results from UV-visible spectra indicated little or no interaction.

Although thermal curing has been most frequently used to enhance the electrical properties of homogeneously modified polyimides, several authors have reported alternative techniques. Auerbach has described the use of lasers to reduce metal salts within a polyimide matrix.[34,35] Krishnaswamy et al. have reported the patterning of gold mercaptide and silver nitrate doped poly(amide acid) films with an electron beam.[36,37] The cross-linking of the metal doped poly(amide acid) resulted in reduced solubility of the exposed regions which led to successful patterning. After E-beam processing, thermal curing brought the metal to the surface leading to continuous conductive silver lines, or gold agglomerations approximately 20-30 um in diameter.

Haushalter and Krause reported that free-standing films of pyromellitic dianhydride and 4,4'-oxydianiline could accept electrons from a solution of specific inorganic reducing agents, forming stable anion radicals and dianions on the imide functionality.[38] These latter species could then be used to reduce metal ions from solution to deposit metal particles or films on the surface of the polyimide.

Recently, Mazur and Reich reported a similar method wherein metal interlayers were electrochemically grown within a polyimide film.[39] In this study, films of polyimide coated on the surface of an electrode accepted electrons, via redox reactions, while cations from solution permeate from the opposite surface. When the electrolyte solution contains salts of metals whose reduction potentials are more positive than that for the polymer, zerovalent metals (gold, copper, and silver) may be deposited as thin electrical conductors embedded within the polymer.

As exhibited above, a number of ways in which the electrical characteristics of polyimides can be modified have been reported. The complexity of the modification varies from an elementary thermal processing cycle to the application of a variety of processing reagents and conditions. The technique of Taylor et al. [27,30,31] is especially attractive for its simplicity wherein the homogeneous dispersal of an inorganic additive into poly(amide acid) followed by thermal curing results in surface conductive films. It is this approach which was used to modify the polyimide films discussed in Part I of this Dissertation.

### III. EXPERIMENTAL

#### A. Copper Doped Film Preparation

##### 1. Monomers

The monomers selected for this research are shown in Table I while additional information is provided below.

BTDA: 3,3',4,4'-benzophenonetetracarboxylic dianhydride was obtained from either Gulf Chemical Co., The Kriskev Co., or Allco Chemical Corp. In all cases, BTDA was vacuum dried at 100°C before use.

BDSDA: 4,4'-Bis(3,4-dicarboxyphenoxy)diphenyl sulfide dianhydride was obtained from NASA, Langley Research Center (Hampton, Virginia) or M&T Chemical Co. and vacuum dried at 100°C prior to use.

ODA: 4,4'-oxydianiline, also named 4,4'-bis(aminophenyl)ether was received from Aldrich Chemical Co. in two purities. Standard grade ODA was purified by sublimation at 180°C and 1 torr before use. Zone-refined ODA was used as acquired.

APB: 1,3'-diaminodiphenyl ether was obtained from National Starch And Chemical Corp. APB was purified by recrystallization from xylenes (85°C) and vacuum dried at 100°C before use.

DAPI: 5,6-amino-1-(4'-aminophenyl)-1,3,3'-trimethylindane was received from Ciba-Geigy Corp. and vacuum dried at 100°C before use.

##### 2. Dopants

The dopants used in this research are shown Table II.

CuCl<sub>2</sub>: Copper(II) chloride was obtained from Aldrich Chemical Co. and used as received.

Table I  
Structures and Data Pertaining to Monomers Used in This Study

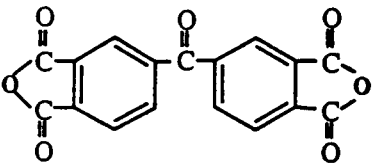
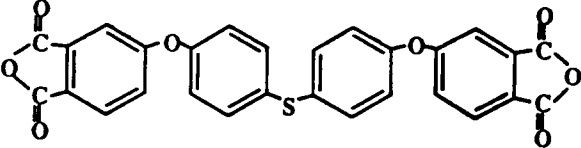
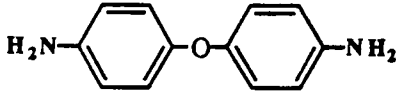
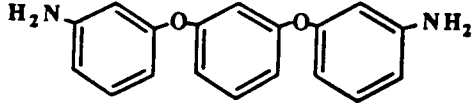
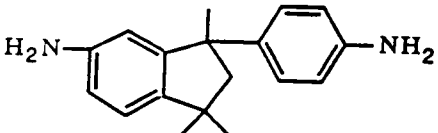
Abbreviations and Structure	CAS #	FW	m.p. (°C)
<p style="text-align: center;"><b>BTDA</b></p> 	[2421-28-5]	322.23	215-217
<p style="text-align: center;"><b>BDSDA</b></p> 	[52256-85-6]	510.48	---
<p style="text-align: center;"><b>ODA</b></p> 	[101-80-4]	200.24 (dec.)	188-190
<p style="text-align: center;"><b>APB</b></p> 	[5735-36-6]	292.13	
<p style="text-align: center;"><b>DAPI</b></p> 	[36468-18-2]	266.40	---

Table II  
Data Pertaining to the Dopants Used in This Study

Formula	CAS#	FW
$\text{CuCl}_2$	[7447-39-4]	134.44
$\text{Cu}(\text{AcAc})_2$	[13395-16-9]	263.56
$\text{Cu}(\text{TFA})_2$	[7440-50-8]	371.50

$\text{Cu}(\text{AcAc})_2$ : Bis(acetylacetonato)copper(II), also known as Cu(II) 2,4-Pentanedionate, was obtained from Alfa Chemical Co. and used as received.

$\text{Cu}(\text{TFA})_2$ : Bis(trifluoroacetylacetonato)copper(II) was synthesized as per literature reference [25] and purified through sublimation at  $105^\circ\text{C}$  and 1 torr prior to use.

### 3. Solvent

DMAC: Reagent grade N,N-dimethylacetamide purchased from Aldrich Chemical Co. was used to dissolve all monomers prior to addition of dopant. Before use, DMAC was distilled in glass, stored over molecular sieves under a nitrogen atmosphere and sparged with dry nitrogen.

### 4. Polymers

The precursor poly(amide acid) was formed by the reaction of the appropriate dianhydride and diamine in DMAC. The percent solids of these solutions was varied between 18% and 25%. A nitrogen-purged glass septum bottle (Figure 1.) was charged with the diamine (4.00 mmol) followed by the addition of the respective quantity of DMAC. After complete dissolution, the dianhydride (4.00 mmol) was added, and the consequent pale yellow solution was mechanically stirred for 1 h. Following thorough mixing, the copper dopant (0.50, 1.00, or 2.00 mmol) was added to the resultant poly(amide acid), and the solution stirred for an additional 2 h. Films employing 0.50, 1.00, and 2.00 mmol of additive will be known as 0.5X-, 1.0X-, and 2.0X-doped films, respectively.

Thin films were produced by casting the "copper-poly(amide acid)" solution via a doctor blade (18-mil or 36-mil gap) onto a dust-free soda lime glass plate following the solution's centrifugation for 5 min at ca. 1500 rpm. Unless stated otherwise, the films were pre-cured at  $80^\circ\text{C}$  for 20 min and subsequently

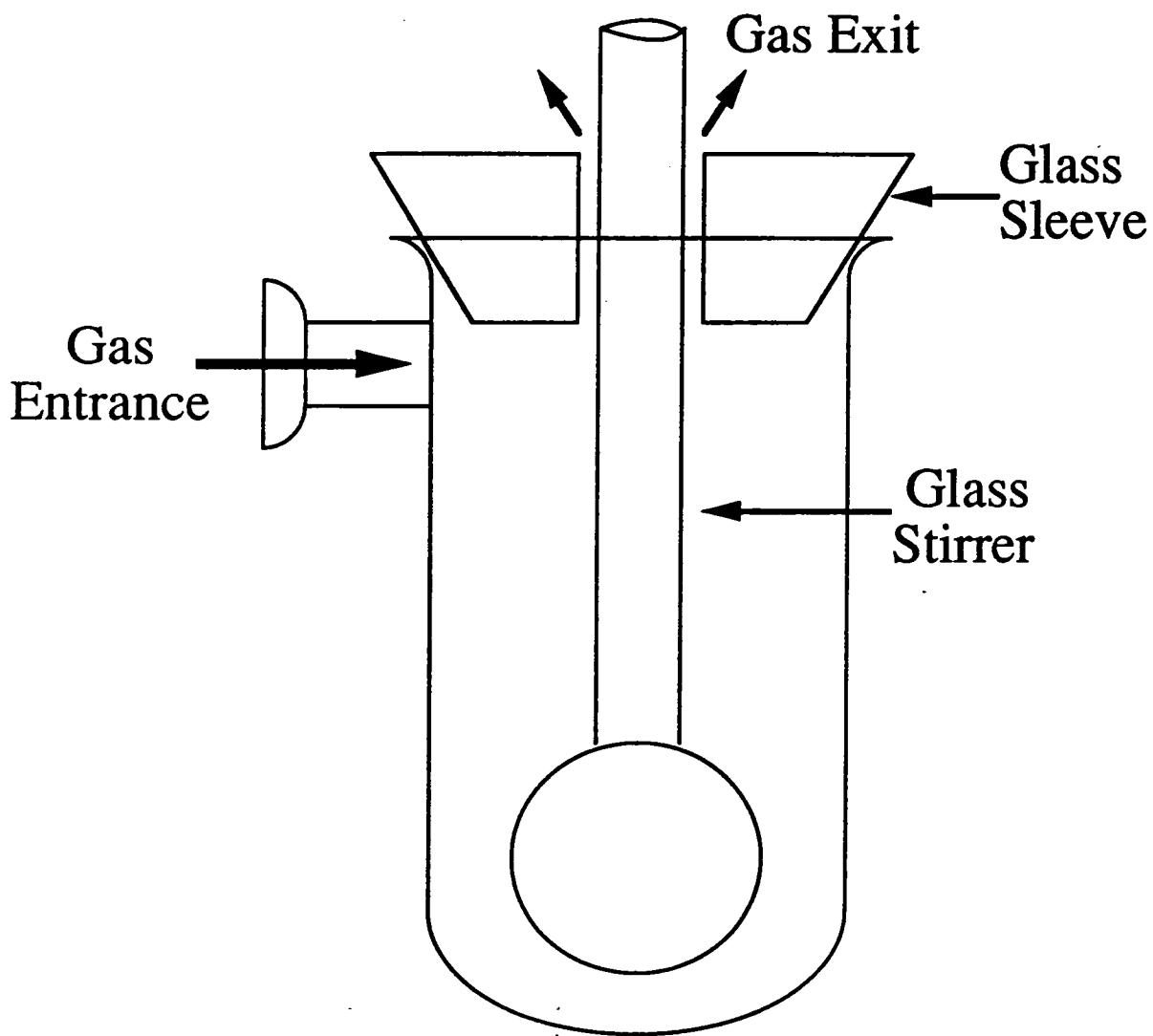


Figure 1. Schematic drawing of the polymer reactor vessel.

thermally imidized under controlled atmosphere at 100, 200, and 300°C each for 1 h, respectively. Samples were either cured in dry breathing air, wet breathing air (100% R.H.), or dry nitrogen. The wet breathing air curing atmosphere was produced by bubbling the bottled air through water at 25°C, as shown in Figure 2. After cooling to room temperature, the films were removed from the glass plate by peeling with a razor blade. A schematic representation of the doped film preparation is given in Scheme 1.

Fully imidized soluble Polyimide XU-218 dissolved in DMAC was also doped with  $\text{Cu}(\text{TFA})_2$  at 1X and 2X levels. The casting procedure and curing cycle were the same as that discussed above for the condensation polyimides. Films were cured in dry and wet breathing air only. XU-218 was received from Ciba-Geigy Corp. and vacuum dried at 100°C before use.

## B. Polymer Film Characterization

### 1. Elemental Analysis

Elemental analyses were obtained from Galbraith Analytical Laboratories, Knoxville, TN.

### 2. Differential Scanning Calorimetry

Differential scanning calorimetric analysis was performed using a Perkin-Elmer Model DSC-4 Differential Scanning Calorimeter at 20.0°C/min heating rate with a dynamic nitrogen purge. Two 0.25" diameter disks of each sample were encapsulated in aluminum sample pans prior to analysis. An empty aluminum sample pan was used as the reference for all analyses.

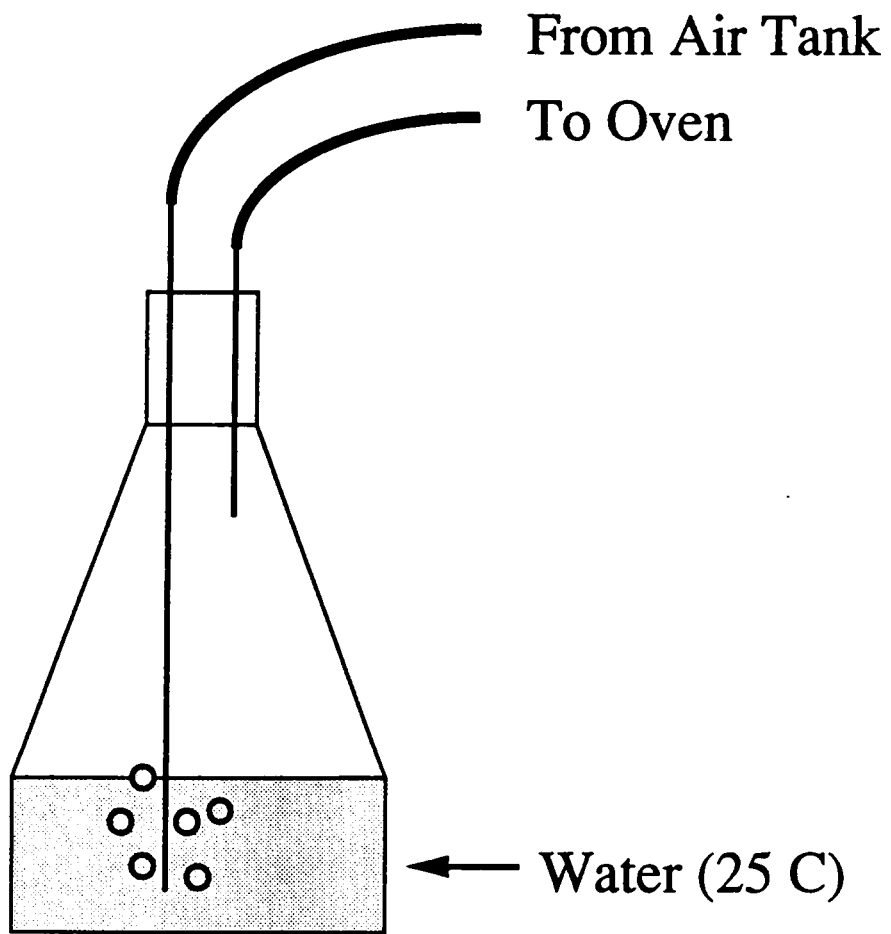
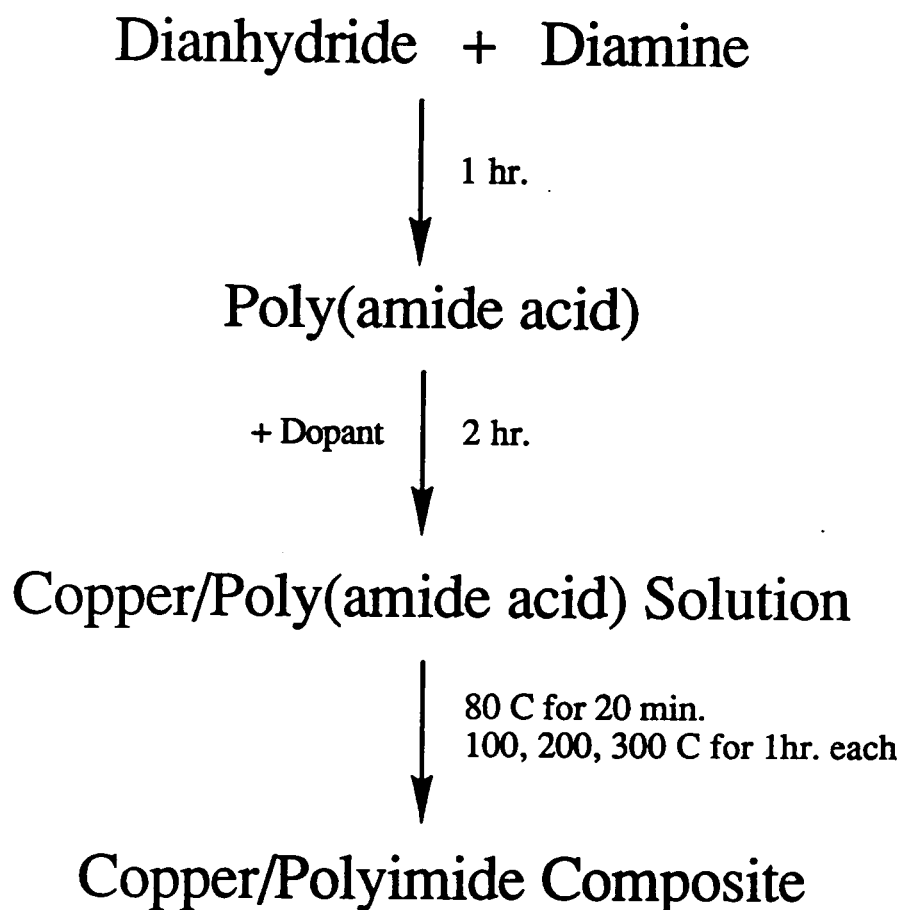


Figure 2. Schematic drawing of the wet breathing air apparatus.



Scheme 1. Synthesis and cure of a doped polyimide film.

### 3. Thermogravimetric Analysis

Thermogravimetric analysis was performed with a Perkin-Elmer Model TGS-2 Thermogravimetric system at 10.0°C heating rate with a dynamic air or nitrogen purge (50 mL/min) to determine the thermooxidative and thermal stability, respectively. Samples (0.25" diameter) were prepared with a hole punch to achieve consistent surface area. Two samples were analysed together typically weighing 5.0 ± 0.5 mg.

### 4. Auger Electron Spectroscopy

Auger electron spectra and depth profiles (approximately 30 Å/min via argon ion etching) were recorded with a Perkin-Elmer Phi Model 610 Scanning Auger Microprobe system. Typical electron beam voltage was 1.5 kV with a beam current of 30 μA. The ion beam used for concurrent Ar sputter etching was operated with an accelerating voltage of 4kV and an ion current of 5 μA/cm<sup>2</sup>. The ion gun was rastered within a 2 X 2 mm square for most analyses. Tantalum oxide was used as a standard to determine the rate of sputtering or sputter depth with time (30 Å/min). Following placement of the samples onto aluminum mounts with double sided tape, the edges of each sample were coated with a colloidal graphite solution enabling optimum electrical contact with the mount to avoid charge buildup.

### 5. X-ray Photoelectron Spectroscopy

X-ray photoelectron spectra were obtained with a Perkin-Elmer Phi Model 5300 ESCA system using a magnesium anode ( $K\alpha = 1253.6$  eV) at 250 W (14 keV, 18 mA). Normal XPS analysis uses an exit angle of 90°. However, a grazing exit angle of 15° was often used to intensify the signal from the outer surface composition. Operating pressures were in the range of  $5 \times 10^{-8}$  torr. Samples were attached onto aluminum mounts with doubled-sided transparent

tape. The binding energies were referenced to the aromatic C(1s) photopeak at 284.6 eV.[40] The atomic concentrations were evaluated from the photopeak areas using standard sensitivity factors located in the software available with the PHI 5300 system.

#### 6. Scanning and Transmission Electron Microscopy

Scanning and transmission micrographs (SEM and TEM) were taken with either a Philips Model 420 Scanning Transmission Microscope (STEM) or a Jeol 100 CX-II Transmission Electron Microscope. Samples prepared for TEM analysis were embedded in Polyscience ultralow viscosity resin and cured for 8 h at 70°C. Samples were then sectioned to between 500 and 800 Å with a Reichert-Jung ultramicrotome using a Microstar diamond knife. The thin sections were then placed on 200-mesh copper or nylon grids prior to analysis.

#### 7. Energy-Dispersive X-ray Analysis

Energy-dispersive x-ray spectra were obtained from the Philips STEM by using a Tracor-Northern 5500 EDAX attachment.

#### 8. Room Temperature Electrical Resistivity Measurements

Room temperature surface and volume direct current electrical resistivities of 85 mm diameter polymer films were determined with a Keithley high-voltage source (Model 240A), a Keithley electrometer (Model 610C), and a Keithley three-probe electrode assembly (Model 6105 resistivity adapter). In all cases, a +100 VDC potential was applied to the sample during analysis.

#### 9. Variable Temperature Electrical Resistivity Measurements

Variable temperature electrical resistivity determinations (VTERM) were obtained with a computer-controlled instrument developed in our laboratory.[41] The system controls sample temperature, atmosphere, electrification time, and surface or volume measurement mode. The electrode geometry for the variable

temperature test cell is the same as the Keithley resistivity adapter. During analysis, the samples were poled with +100 VDC in vacuum.

## IV. THE STRUCTURE OF COPPER/POLYIMIDE MULTILAYERED COMPOSITES

### A. Preliminary

Incorporation of bis(trifluoroacetylacetonato)copper (II) into poly(amide acid) solutions produces multi-layered composite films upon curing. Internal and near-surface structure is strongly dependent on the dopant concentration and specific polyimide precursor monomers. Three polyimide systems were used to determine the effect of monomer molecular structure and polymer glass transition temperature on the microcomposite surface structure. In general, this process has yielded uniform Cu and CuO dispersions of very small particle size developing from phase separation of the additive. However, in some instances, a highly diffuse copper phase is produced resulting from a polymer/dopant chemical interaction which increases the solubility of the dopant in the matrix. It is the object of this chapter to describe the structural characteristics of copper-modified polyimide films resulting from the in situ thermal decomposition of  $\text{Cu}(\text{TFA})_2$ . A structural comparison between copper-doped condensation and soluble polyimides is also undertaken.

### B. General Characteristics

Fully imidized nondoped BTDA-ODA, BDSDA-ODA, and BTDA-APB each produced high-quality transparent yellow free-standing films that are very flexible and thermooxidatively stable ( $>550^\circ\text{C}$ ). BTDA-ODA provides a high- $T_g$  polyimide ( $285^\circ\text{C}$ ) while BTDA-APB and BDSDA-ODA have a  $T_g$  of approximately  $210$  and  $215^\circ\text{C}$ , respectively. The addition of  $\text{Cu}(\text{TFA})_2$  to each of

the pre-polyimides yielded reproducible and in most cases, flexible films (Table III). Due to the casting conditions there were two distinct surfaces on each film. The surface of BTDA-ODA and BTDA-APB films that was in direct contact with the curing atmosphere (atmosphere side) appeared brown or gray with distinct metallic character, while that of BDSDA-ODA seemed shiny yet nonmetallic. The surface of each film in contact with the glass substrate (glass side) was dull brown and in all cases not metallic.

### C. Copper Modified (1X) BTDA-ODA Polyimide Films

The surface and near-surface composition of the copper modified polyimide films was ascertained in part through the use of X-ray photoelectron spectroscopy.[42,43] In general, Cu(2p) photopeaks are well-defined with large separation.[44] In Cu(TFA)<sub>2</sub>, copper is in the +2 oxidation state, thereby exhibiting satellite photopeaks appearing on the higher binding energy side of the 2p<sub>1/2</sub> and 2p<sub>3/2</sub> main photopeaks (Figure 3). The absence of satellite structure would indicate a Cu(I) or Cu(0) species.

XPS of the atmosphere side of 1X-doped BTDA-ODA films cured in dry air or nitrogen obtained with a take-off angle of 90° for maximum sampling depth shows insubstantial copper in any form at or near the surface. Alternatively, the wet-air-cured film reveals the existence of Cu(2p) photopeaks, albeit of low intensity (1.1 at. %), which are devoid of satellite structure suggesting reduction of Cu(TFA)<sub>2</sub> to a Cu(I) or Cu(0) species (Figure 4). The absence of a F(1s) signal provides further evidence that the copper species present is not Cu(TFA)<sub>2</sub>. Reduction of Cu(TFA)<sub>2</sub> to Cu<sub>2</sub>O would be easily observable through the presence of an oxide oxygen photopeak (<530 eV). Yet, only one oxygen

Table III  
General Properties of Cu(TFA)<sub>2</sub>-Doped and Nondoped Polyimide Films

<u>Polyimide</u>	<u>Curing Atmosphere</u>	<u>Additive<sup>a</sup> Level</u>	<u>Color</u>	<u>Flexibility</u>
BTDA-ODA	Dry Air	1.00X	Brown	Brittle
	Wet Air	1.00X	Brown	Flexible
	Nitrogen	1.00X	Brown	Flexible
	Dry Air	2.00X	Gray	Flexible
	Wet Air	2.00X	Gray	Flexible
	Nitrogen	2.00X	Gray	Flexible
BTDA-APB	Dry Air	1.00X	Gray	Flexible
	Wet Air	1.00X	Gray	Flexible
	Dry Air	2.00X	Gray	Flexible
	Wet Air	2.00X	Gray	Flexible
BDSDA-ODA	Dry Air	1.00X	Brown	Brittle
	Wet Air	1.00X	Brown	Brittle
	Dry Air	2.00X	Brown	Brittle
	Wet Air	2.00X	Brown	Brittle

<sup>a</sup>Nondoped films are flexible and yellow.

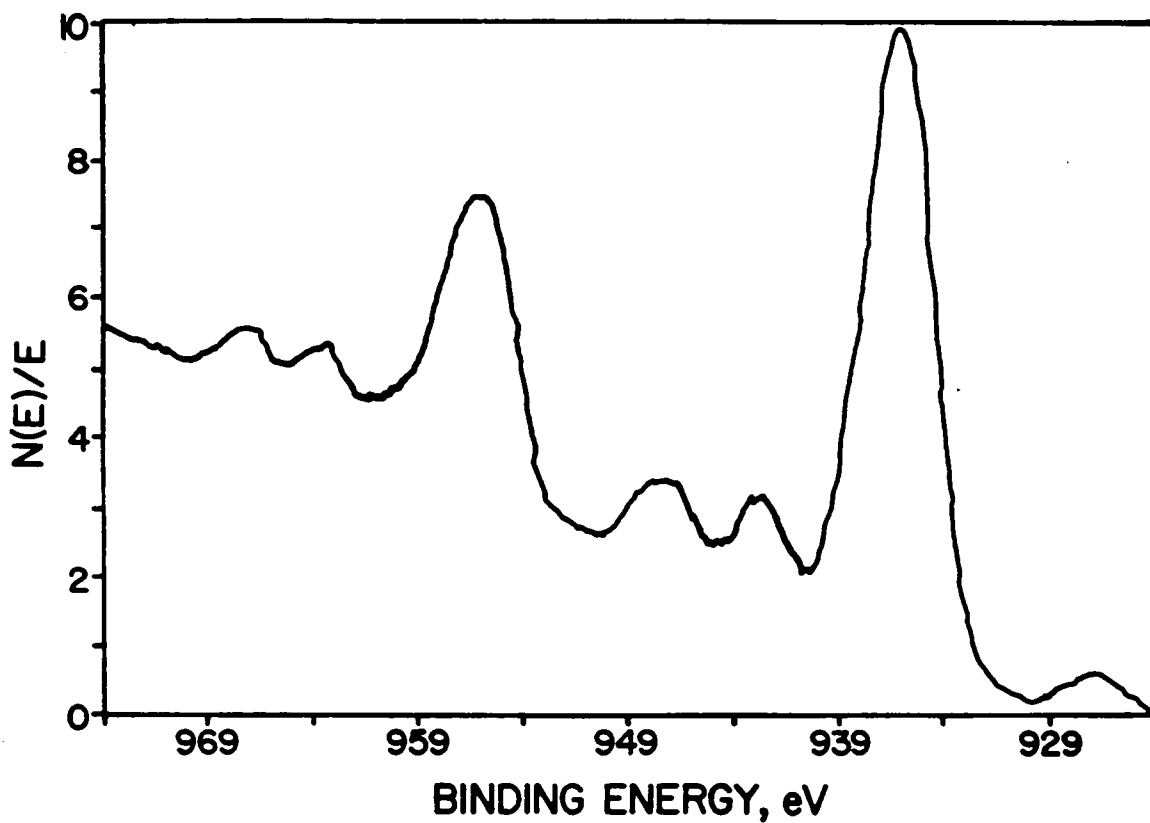


Figure 3. The XPS Cu(2p) spectrum of Cu(TFA)<sub>2</sub>.

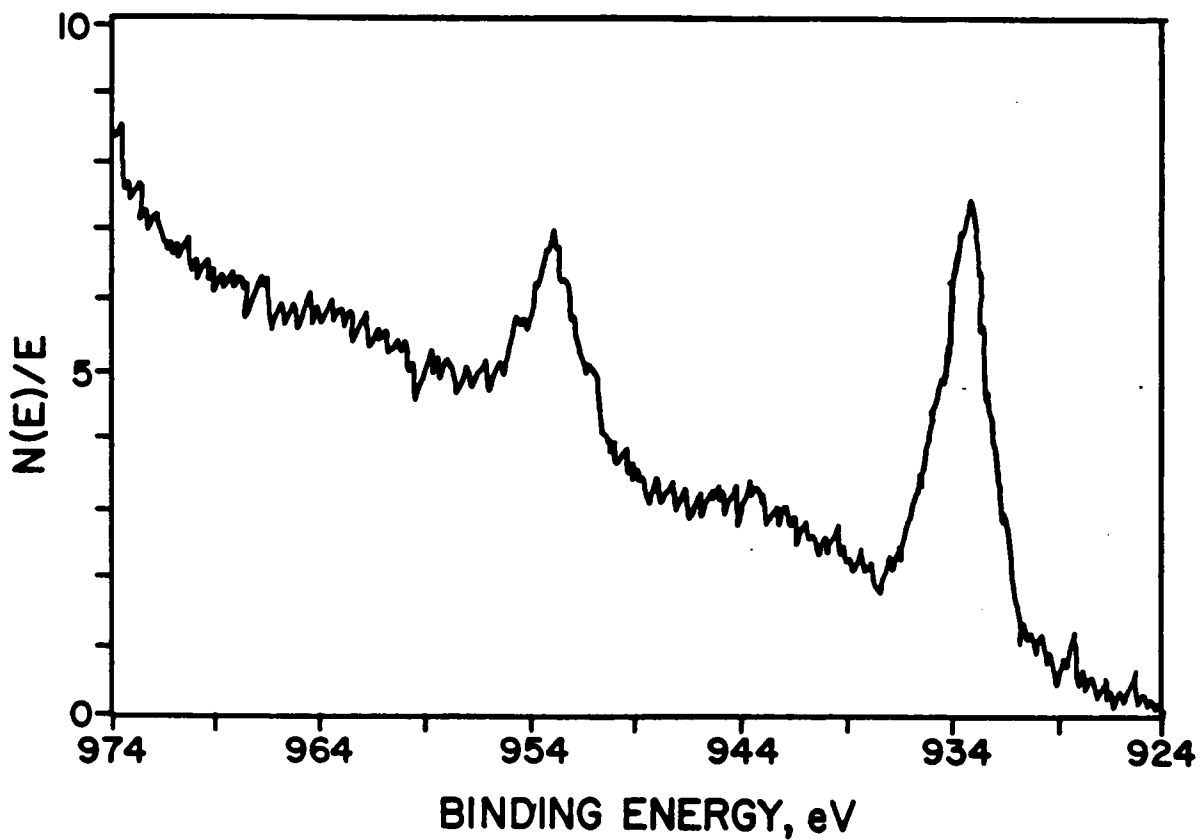


Figure 4. The XPS Cu(2p) spectrum of the wet-air-cured 1X-doped BTDA-ODA film.

photopeak is observed ( $\sim 532$  eV) in the XPS O(1s) spectrum characteristic of both carbonyl and ether oxygen in the polymer backbone as shown in Figure 5. The lack of an oxide oxygen or appreciable fluorine suggests that the copper species is, in fact, metallic copper. Application of ( $15^\circ$  take-off angle) grazing angle XPS to the film cured in moist air finds negligible copper at the surface. Taking into account the decrease in the observation depth of grazing angle XPS, the presence of a thin organic overlayer residing above the copper deposit is implied. Similar overlayers have been observed for cobalt- [45] and gold- [46] containing polyimide films.

To directly observe the underlying copper deposit by XPS, argon ion etching was employed on the wet-air-cured film in situ prior to the analysis. Following a 10-min etch at approximately  $5 \text{ \AA}/\text{min}$ , the Cu(2p) photopeaks became very intense (Figure 6), indicative of a much higher copper concentration ( $\sim 44$  at. %). As in the unetched film, the absence of satellite structure, fluorine, and oxide oxygen provided evidence that  $\text{Cu}(\text{TFA})_2$  is reduced to Cu(0). The organic overlayer may be judged to be at least  $30\text{-}50 \text{ \AA}$  thick as evidenced by the sputter rate and sputter time. Despite the fact that the copper concentration is relatively high in the sub-surface, significant amounts of carbon, nitrogen, and oxygen are still observed, which suggests that the copper present in this portion of the film is intermixed with the polyimide matrix.

Depth profiles via Auger electron spectroscopy (AES) in conjunction with argon ion etching of the films cured in dry air or nitrogen do not present any indication of significant copper accumulation within the first  $400 \text{ \AA}$  of the surface. On the other hand, the Auger depth profile of the film cured in wet air displays the onset of a significant copper deposit beginning approximately 5 min into the profile (Figure 7). A three-layered structure is therefore suggested which has a

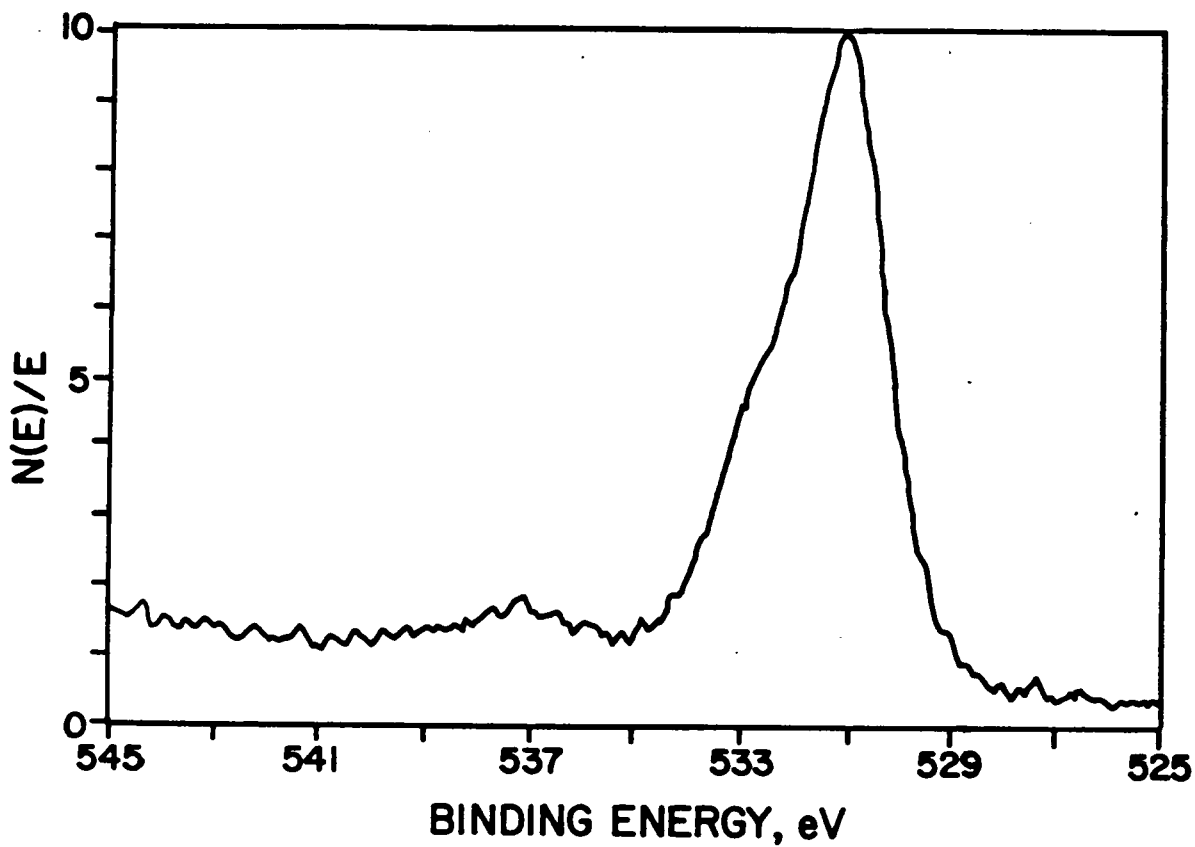


Figure 5. The XPS O(1s) spectrum of the wet-air-cured 1X-doped BTDA-ODA film.

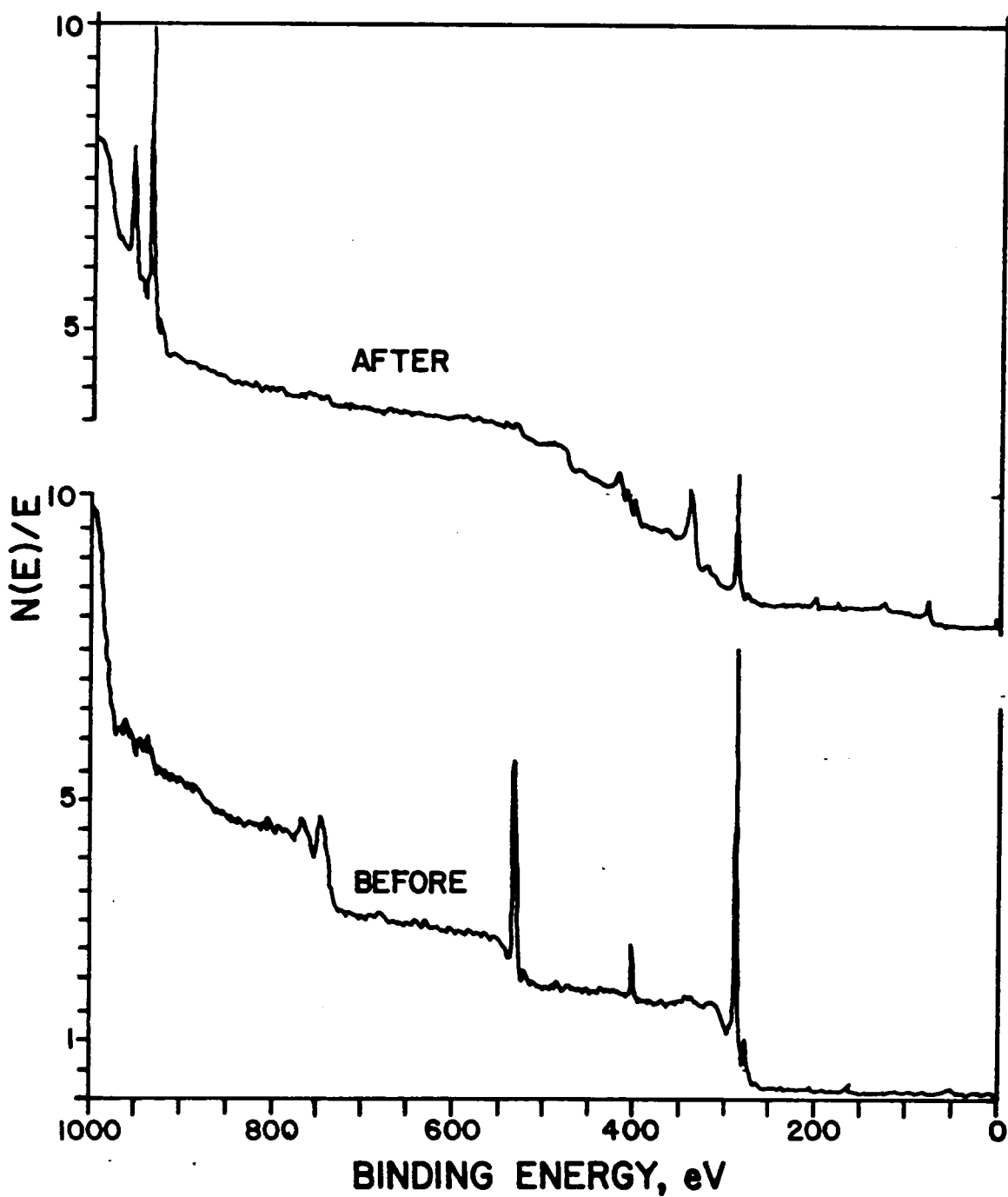


Figure 6. The XPS survey spectrum of the wet-air-cured 1X-doped BTDA-ODA film before and after argon ion etching.

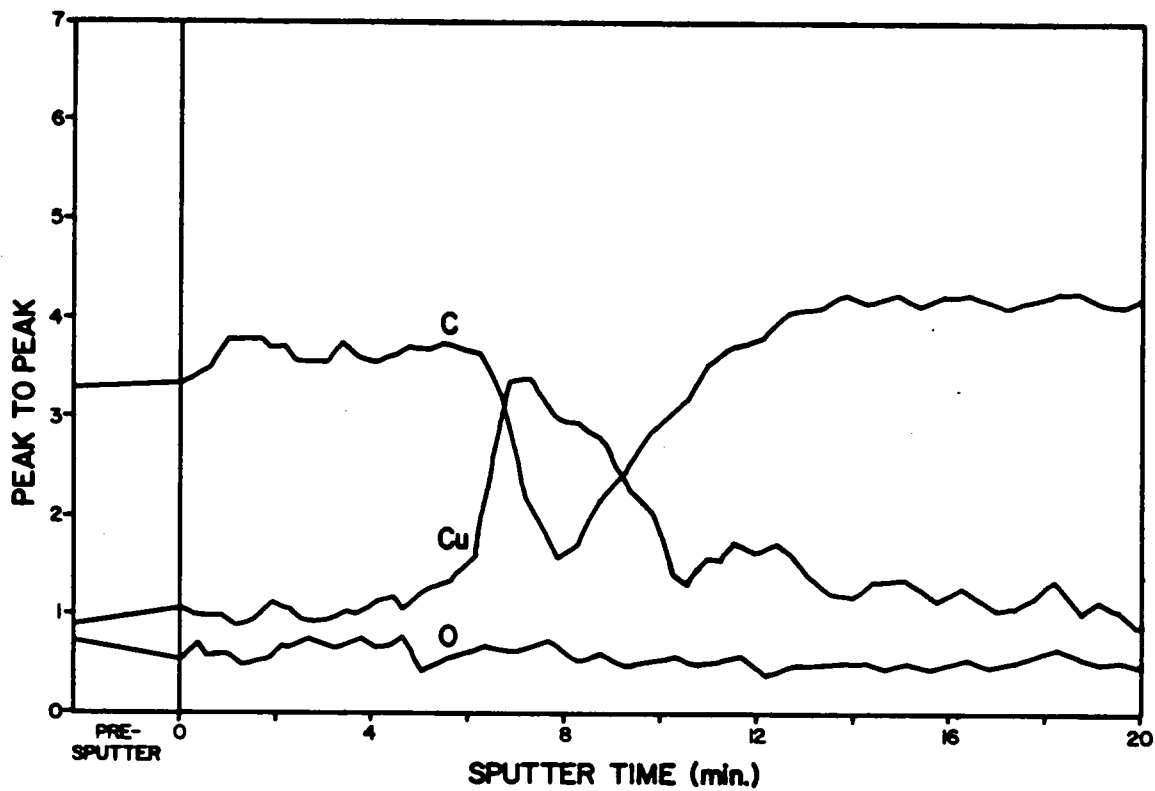


Figure 7. Auger electron spectroscopic depth profile of the wet-air-cured 1X-doped BTDA-ODA film.

copper layer positioned between a thin polymeric overlayer and the bulk polyimide. It is known, however, that ion bombardment may cause reduction of metal compounds, including copper in some instances.[47] Therefore, an Auger depth profile was taken of a CuO film that had been vacuum deposited onto a polyimide substrate. The profile of this sample exhibited copper and oxygen patterns characteristic of copper oxide (1:1 at. %), thus furnishing evidence that sputtering and electron- and/or ion-induced copper reduction is slow or negligible at the low sputtering rates used and that the elemental copper detected within the film is not an artifact of the etching process. In many instances, ion sputtering has been shown to change or "damage" polymeric surfaces.[48,49] In our studies the carbon signal is used as an elemental tag for the organic component in the Auger depth profile. Profile data should be considered only in a qualitative sense, irrespective of the chemical state of the carbon species and whether damage has or has not occurred.

To obtain a total view of the internal structure, ultramicrotomed cross sections of the films were examined by transmission electron microscopy (TEM). Visual proof of a three layered structure is observed for the 1X-doped BTDA-ODA film cured in wet air (Figure 8). Surprisingly, similar near-surface structure is found in the dry-air-cured and nitrogen-cured BTDA-ODA films. The depth at which metallic enrichment occurs for these samples is, however, below that attempted by AES with concurrent ion milling and achievable by XPS. Thicknesses of the polymer overlayer and the metallic layer are approximately 60 and  $50 \text{ \AA} \pm 10 \text{ \AA}$ , respectively, for the wet-air-cured film. The samples cured in dry air exhibited respective layer thicknesses of 400 and  $45 \text{ \AA}$ , while those cured in dry nitrogen had thicknesses of approximately 350 and  $60 \text{ \AA}$ .

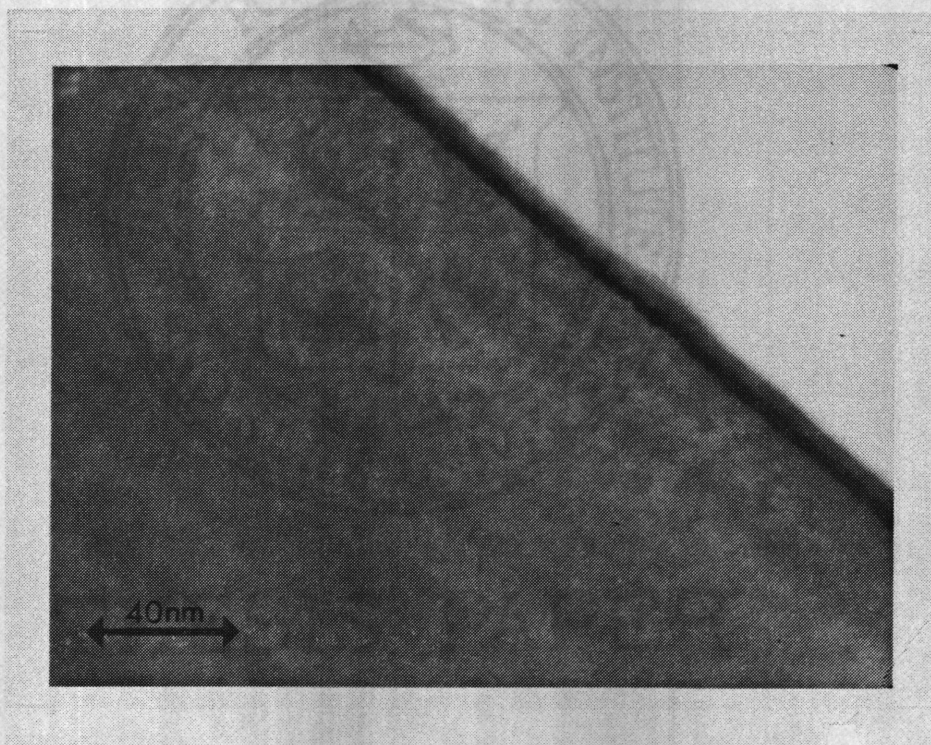


Figure 8. Transmission electron cross section of the surface region of the wet-air-cured 1X-doped BTDA-ODA film.

The bulk polymer is, regardless of curing atmosphere, devoid of any other particulate matter, other than the near-surface layer, to a depth of at least 50,000 Å from the atmosphere side of the films. We term this region the "depletion zone" (Table IV). Below this area spherical agglomerations roughly 3000-5000 Å in diameter are present, as shown in Figure 9. Energy-dispersive X-ray analysis of the particles reveals that they are copper in nature (Figure 10). Whether they consist of elemental copper or  $\text{Cu}(\text{TFA})_2$  is unknown since EDAX could detect only elements with atomic number 11 or greater. Similar agglomerates have been observed in  $\text{CoCl}_2$  doped polyimides wherein EDAX identified the material as containing Co and Cl.[50] No copper material in any form has been detected by TEM on the glass side of the 1X BTDA-ODA films or the films yet to be discussed.

#### D. Copper Modified (2X) BTDA-ODA and (1X, 2X) BTDA-APB

##### Polyimide Films.

XPS applied to the "air-side" of 2X-doped BTDA-ODA films and all  $\text{Cu}(\text{TFA})_2$ -doped BTDA-APB films reveals strong Cu(2p) photopeaks with satellite structure (Figure 11). The presence of a Cu(II) species is apparent; yet, the lack of a F(1s) photopeak suggests that the copper does not exist as  $\text{Cu}(\text{TFA})_2$ . Significant amounts of copper ranging between 15 and 40 at. % are observed on each film surface, although substantial amounts of polyimide carbon and oxygen are still present, which again supports metal-polymer intermixing. An additional O(1s) photopeak is detected (~529 eV) that is not present in the nondoped polyimide spectrum. The higher binding energy peak can be confidently assigned to the polymer oxygens (carbonyl, ether) [51], while the lower energy photopeak is due to the presence of oxide oxygen as shown in Figure 12. The +2 oxidation state

Table IV

Morphological Features of Cu(TFA)<sub>2</sub>-Doped Films As Deduced from TEM Data

<u>Polyimide</u>	<u>Curing Atmosphere</u>	<u>Additive Level</u>	<u>Overlayer</u>	<u>Cu Layer Thickness, Å</u>	<u>Depletion Zone Thickness, μm</u>
BTDA-ODA	Dry Air	1.00X	Yes (60Å)	45	5.4
	Wet Air	1.00X	Yes (400Å)	50	7.1
	Nitrogen	1.00X	Yes (350Å)	60	5.1
	Dry Air	2.00X	No	350	2.2
	Wet Air	2.00X	No	400	2.4
	Nitrogen	2.00X	No	420	2.4
BTDA-APB	Dry Air	1.00X	No	620	15.1
	Wet Air	1.00X	No	530	14.5
	Dry Air	2.00X	No	700	10.7
	Wet Air	2.00X	No	820	12.1
BDSDA-ODA	Dry Air	1.00X	No	---	18.7
	Wet Air	1.00X	No	200	17.6
	Dry Air	2.00X	No	---	17.6
	Wet Air	2.00X	No	300	12.3

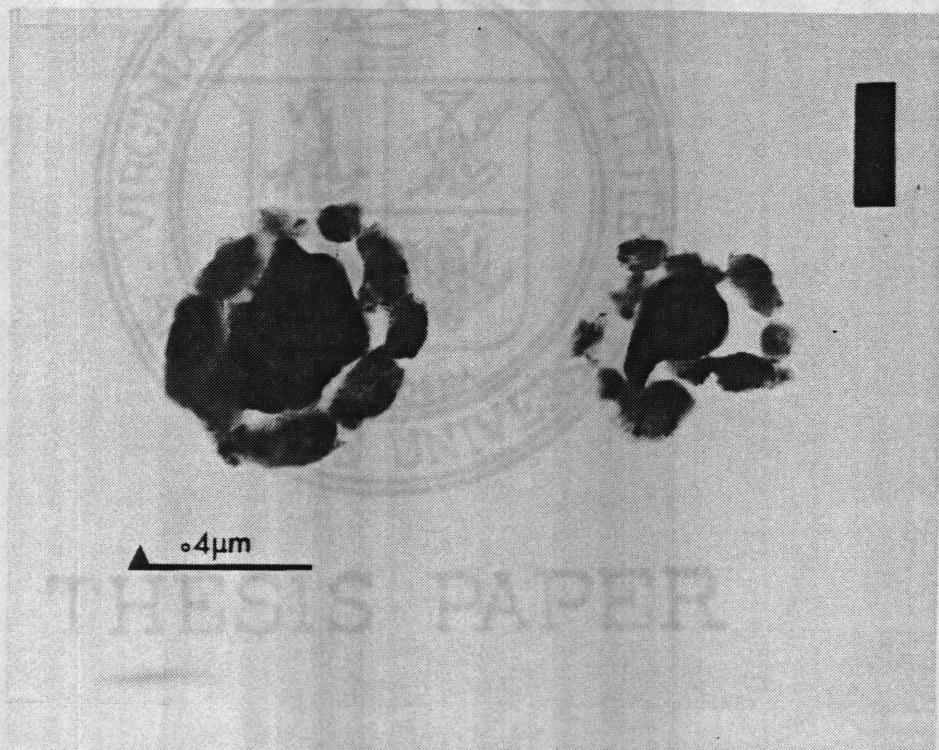


Figure 9. Transmission electron cross section of particulate matter within a dry-air-cured 1X-doped BTDA-ODA film.

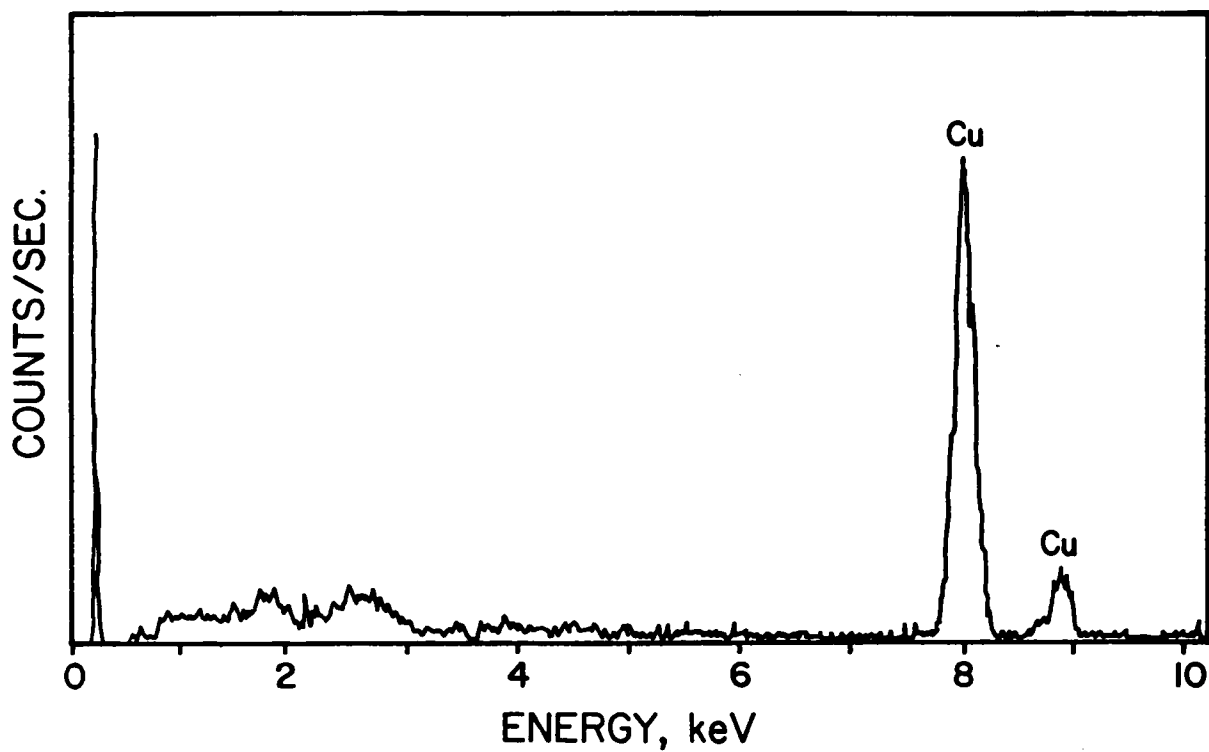


Figure 10. Energy dispersive X-ray analysis of the particulate matter within a dry-air-cured 1X-doped BTDA-ODA film.

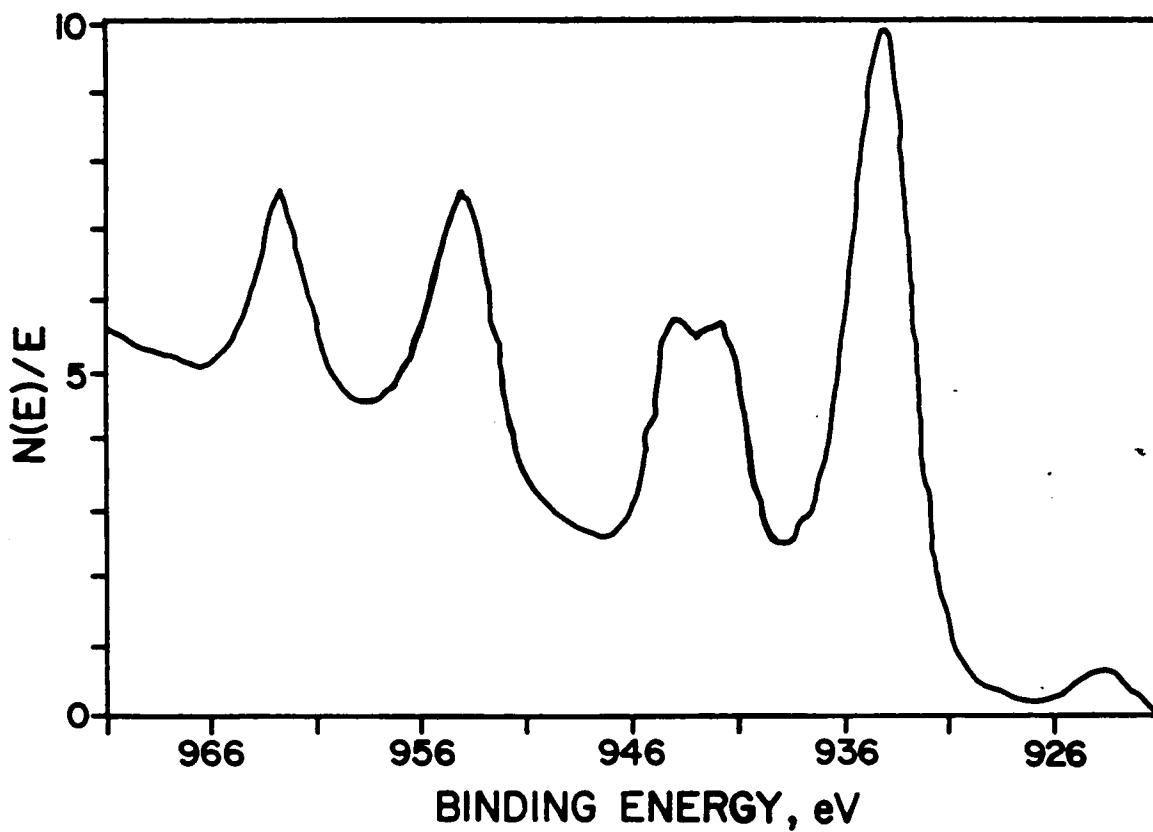


Figure 11. The XPS Cu(2p) spectrum of the wet-air-cured 2X-doped BTDA-ODA film.

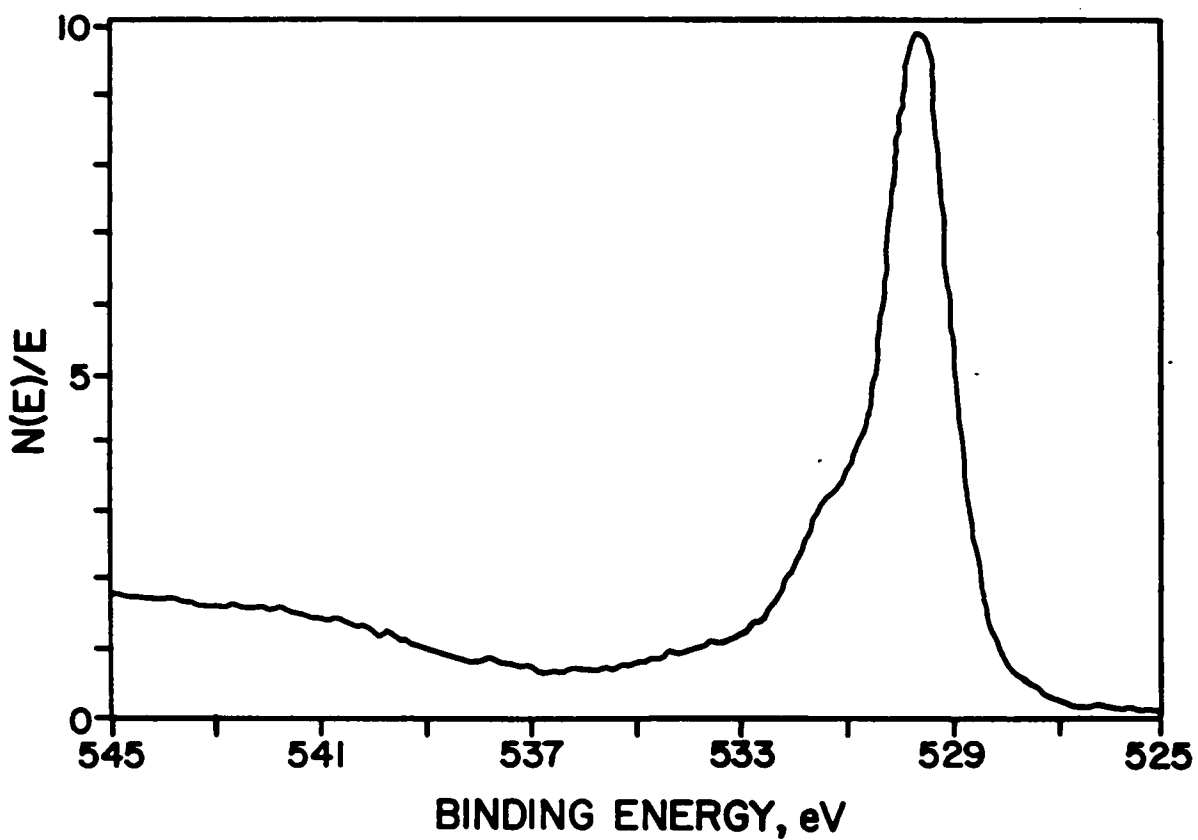


Figure 12. The XPS O(1s) spectrum of the wet-air-cured 2X-doped BTDA-ODA film.

of the copper species along with the 1:1 ratio of the surface copper and oxide oxygen concentrations indicates the presence of CuO on these films. Grazing angle XPS shows no change in the relative atomic concentrations of each element within the analysis depth.

Depth profiling with Auger electron spectroscopy assisted by an argon ion etch provided further evidence of a bilayered structure for the 2X-doped BTDA-ODA dry air and nitrogen cured films along with the 1X-doped BTDA-APB wet-air-cured film (Figure 13). On the other hand, the 2X-doped BTDA-ODA wet-air-cured film and all of the 2X-doped BTDA-APB films did not show this behavior because the copper containing deposit could not be penetrated during the 20-min etching period (Figure 14). In each profile, the oxygen signal intensity steadily followed that of copper throughout the spectrum, indicating that copper is present only as CuO. Significant amounts of fluorine were absent from all profiles.

Scanning secondary electron micrographs of the 2X-doped BTDA-ODA films exhibit rough, granular surfaces of uniform particle size ( $\sim 400 \text{ \AA}$ ) shown in Figure 15. This morphological character indicates that copper is present as the unconventional brown oxide and may provide superior adhesive properties.[52] Micrographs of the 1X- and 2X-doped BTDA-APB films displayed comparable morphology with a small variation in particle size. Surface structure is unaffected by choice of curing atmosphere. The CuO layer of these films, however, may be partially reduced to elemental copper by reheating the films to  $300^{\circ}\text{C}$  in a forming gas (5%  $\text{H}_2$ /95%  $\text{N}_2$ ) atmosphere. An approximate 75% conversion to metal can be realized according to XPS through reduction of the oxide oxygen component from 25 to 7 at. %. Surface chemical reduction results in a change in

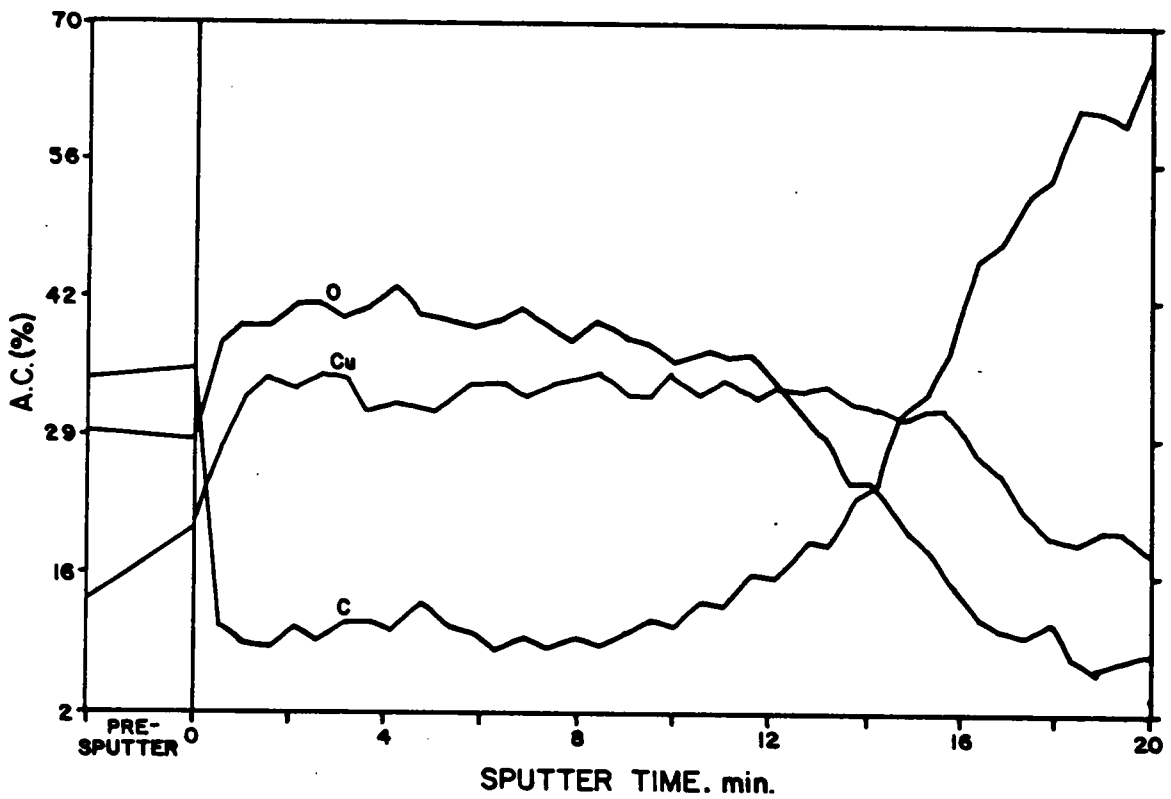


Figure 13. Auger electron spectroscopic depth profile of the nitrogen-cured 2X-doped BTDA-ODA film.

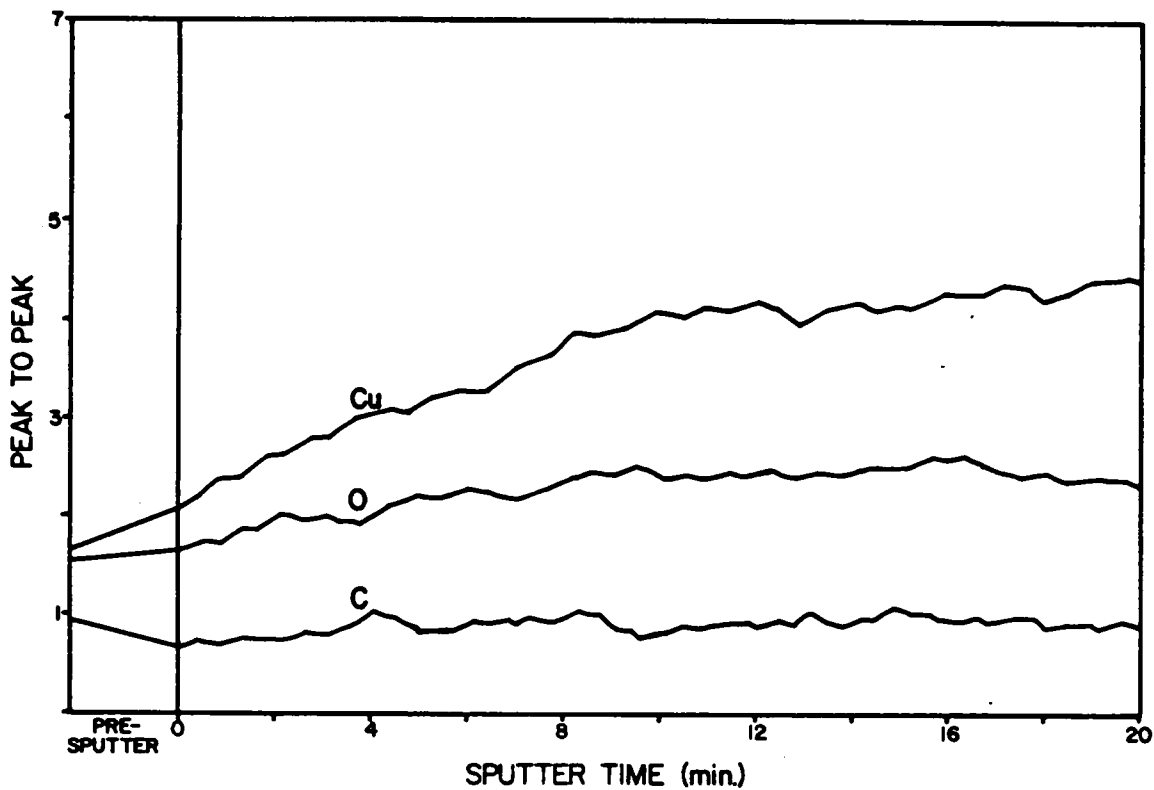


Figure 14. Auger electron spectroscopic depth profile of the dry-air-cured 2X-doped BTDA-APB film.

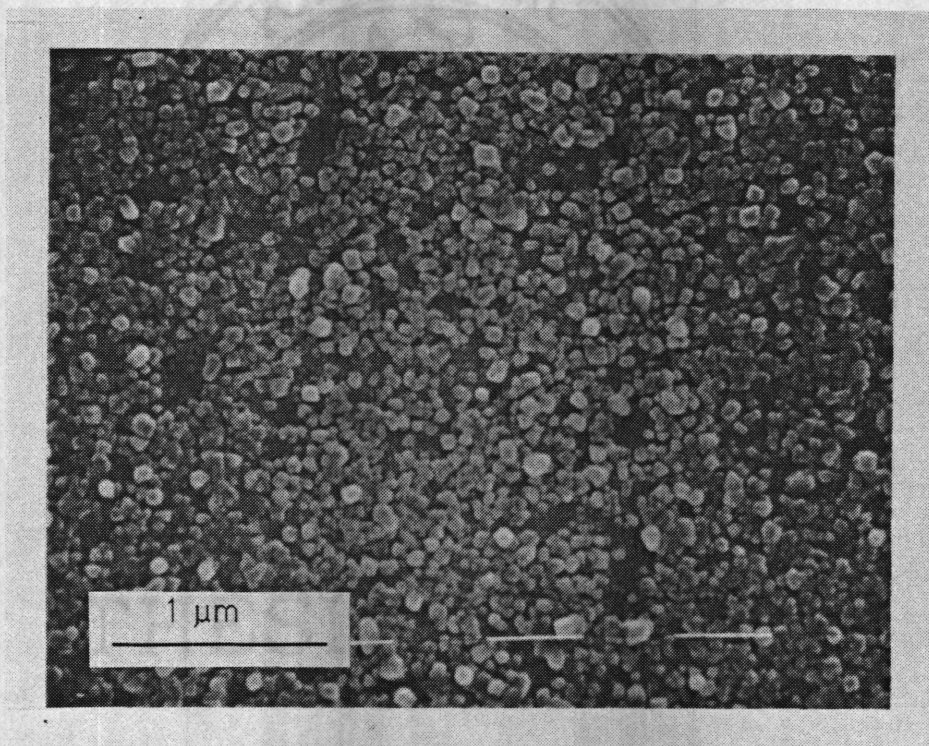


Figure 15. Scanning electron micrograph of the wet-air-cured 2X-doped BTDA-ODA film.

morphology as observed by SEM (Figure 16; i.e., upon reduction, the granular particles agglomerate and the surface becomes smoother).

Transmission electron microscopic analysis of ultramicrotomed cross sections visually portrays the bilayered structure of these films (Figure 17). Thicknesses of the CuO layer for the 2X-doped BTDA-ODA films range between 350 and 420 Å. The thickest CuO layers were observed in doped BTDA-APB films (Table IV). Several trends in these data were noted: (1) within a particular polyimide matrix, the thickness of the copper-containing surface deposit increases with additional concentration of dopant, (2) the increase in copper thickness is accompanied by an increase in the breadth of the depletion zone, and (3) for equivalent dopant concentrations and curing conditions, BTDA-APB films always contain larger copper deposits and depletion zones than BTDA-ODA films.

Within an identical volume, doubling the dopant concentration effectively doubles the potential reservoir of dopant available for the formation of a layer or deposit. The flux of the dopant through a given volume at a constant rate would control the effective size of a zone depleted of the additive. The 2X-doped films would necessarily take longer to exhaust the sub-surface region of additive over an equivalent curing period than a 1X-doped film as long as the total amount removed per unit time is significantly less than the overall local dopant concentration. This being valid, the depletion zone of a 1X-doped film should therefore be larger than that of a 2X-doped film. The flux of dopant should also be influenced by the glass transition temperature of the polyimide, especially if the additive is dispersed on a molecular scale wherein higher mobility would be expected. This fine dispersal of additive is verified by transmission electron microscopy, where TEMs of partially cured films (to 200°C) did not exhibit additive aggregation in any form. BTDA-APB has a  $T_g$  75°C below that of BTDA-

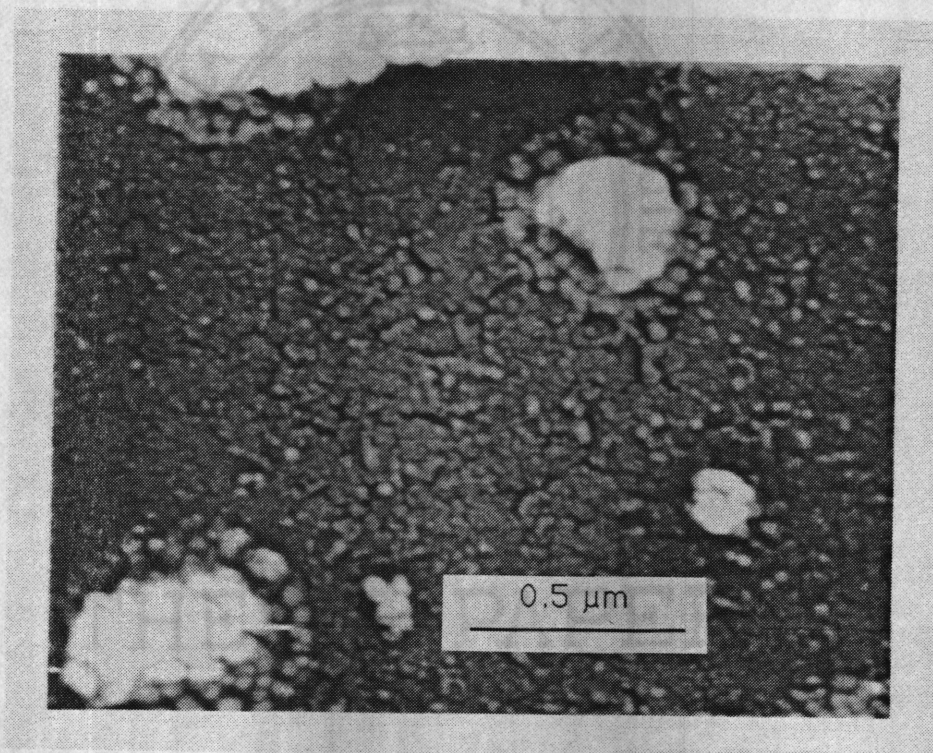


Figure 16. Scanning electron micrograph of the wet-air-cured 2X-doped BTDA-ODA film after treatment with forming gas (5% H<sub>2</sub>/95% N<sub>2</sub>).

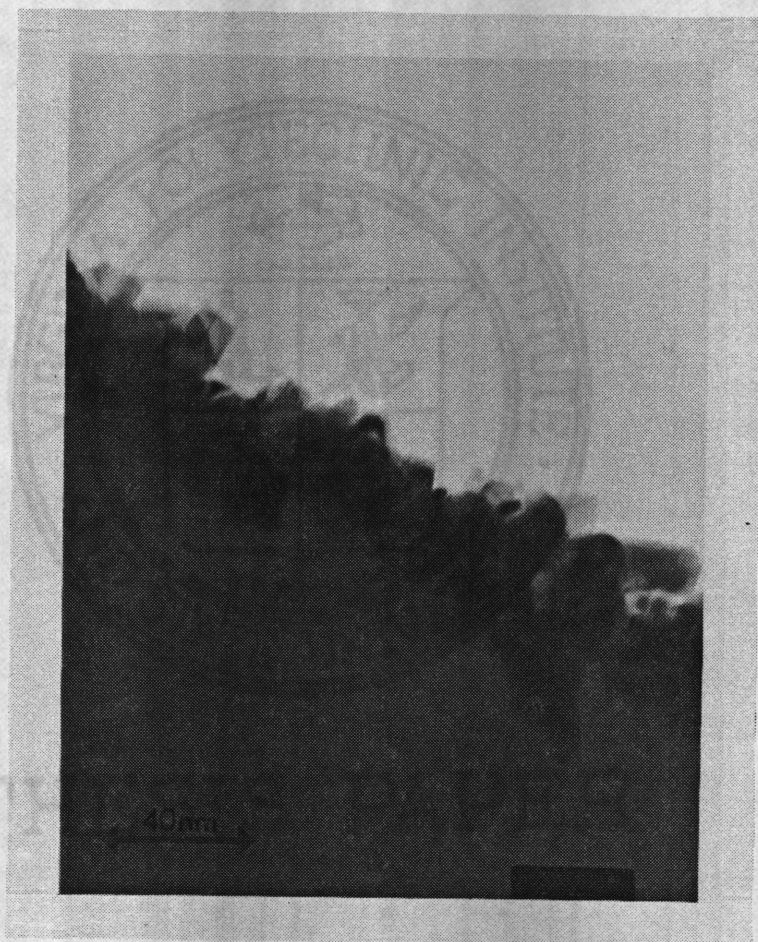


Figure 17. Transmission electron cross section of the surface region of the wet-air-cured 2X-doped BTDA-ODA film.

ODA. Since the  $T_g$  is attained earlier for BTDA-APB and a temperature 85°C higher than the  $T_g$  is ultimately reached during cure of BTDA-APB as compared to 15°C higher for BTDA-ODA, more material would be expected to become available over the curing period to enrich the surface layer in the BTDA-APB matrix. Consequently, this should enlarge the width of the depletion zone.

#### E. Copper Modified BDSDA-ODA Polyimide Films

Analysis of the surface and near-surface "air-side" regions of 1X-doped BDSDA-ODA films by X-ray photoelectron spectroscopy revealed weak Cu(2p) photopeak structure (i.e., 1.0 at. % and 2.3 at. % copper for the dry-air- and wet-air-cured films, respectively). If the dopant were homogeneously dispersed, a theoretical volume fraction of 0.3 at. % copper would be expected. In contrast, the 2X dry-air-cured BDSDA-ODA film exhibits negligible surface copper enrichment, while the wet-air-cured analog contains 6 at. % copper. For the 2X wet-air-cured film (1) Cu(2p) satellite structure is evident, (2) fluorine is undetected, and (3) an oxide oxygen signal is observed. These observations are not apparent for both 1X-doped BDSDA-ODA films. Otherwise, each film displays carbon, oxygen, nitrogen, and sulfur photopeaks characteristic of BDSDA-ODA.

A 15-min argon ion etch ( $\sim 5 \text{ \AA}/\text{min}$ ) followed by XPS analysis was used to probe the sub-surface region of the doped BDSDA-ODA films. The dry-air-cured 1X- and 2X-doped films showed no change in atomic concentration relative to the pre-sputtered films discussed above, signifying the presence of a homogeneous near-surface region sparsely populated by copper. The 1X- and 2X-doped wet-air-cured films, on the other hand, exhibited a distinct change in chemical composition following etching. Loss of satellite structure was observed for both

samples (Figure 18). The amount of copper present also increased after sputtering to approximately 8 and 21 at. % for the 1X- and 2X-doped wet-air-cured films, respectively. Fluorine concentration was negligible (<0.3 at. %), as was oxide oxygen. However a new sulfur(2p) photopeak (~163.4 eV) arose at lower energy from the polyimide S(2p) photopeak (168.6 eV, Figure 19). Approximately 1.5 at. % sulfur is present on the etched surface of these films. Several inorganic copper compounds have S(2p) binding energies similar to the new sulfur photopeak, CuS at 161.2 eV and Cu<sub>2</sub>S at 162.4 eV, [53] which suggests an inorganic in nature. It appears that some form of dopant/ matrix interaction is present when BDSDA-ODA is used since sulfur may be obtained only from the polymer backbone. The higher binding energy of the new sulfur species compared to the copper sulfides cited indicates that the copper is likely chelated to the polyimide sulfur instead of the sulfur being abstracted from the polymer backbone to form some distinct molecular compound. Ohki et al. [54] have shown strong interactions between thioethers and a number of metals including copper resulting in metal chelate complexes. This is in apparent contrast to the copper-doped BTDA-ODA and BTDA-APB films where dopant/matrix chemical interaction is negligible. The presence of a new sulfur species as well as the loss of Cu(2p) satellite structure suggests that the near-surface region of both films is composed of a mixture of elemental copper and a copper/sulfur component since the limited amount of sulfur (~1.5 at. %) cannot bind the large quantity of copper that exists in this region alone.

AES with ion milling provides a similar view of the surface and near-surface regions to that obtained by XPS. Twenty-minute profiles of the dry-air-cured films display essentially copper-free regions comprised totally of polyimide. Alternatively, the 1X-doped wet-air-cured film exhibits a moderate copper

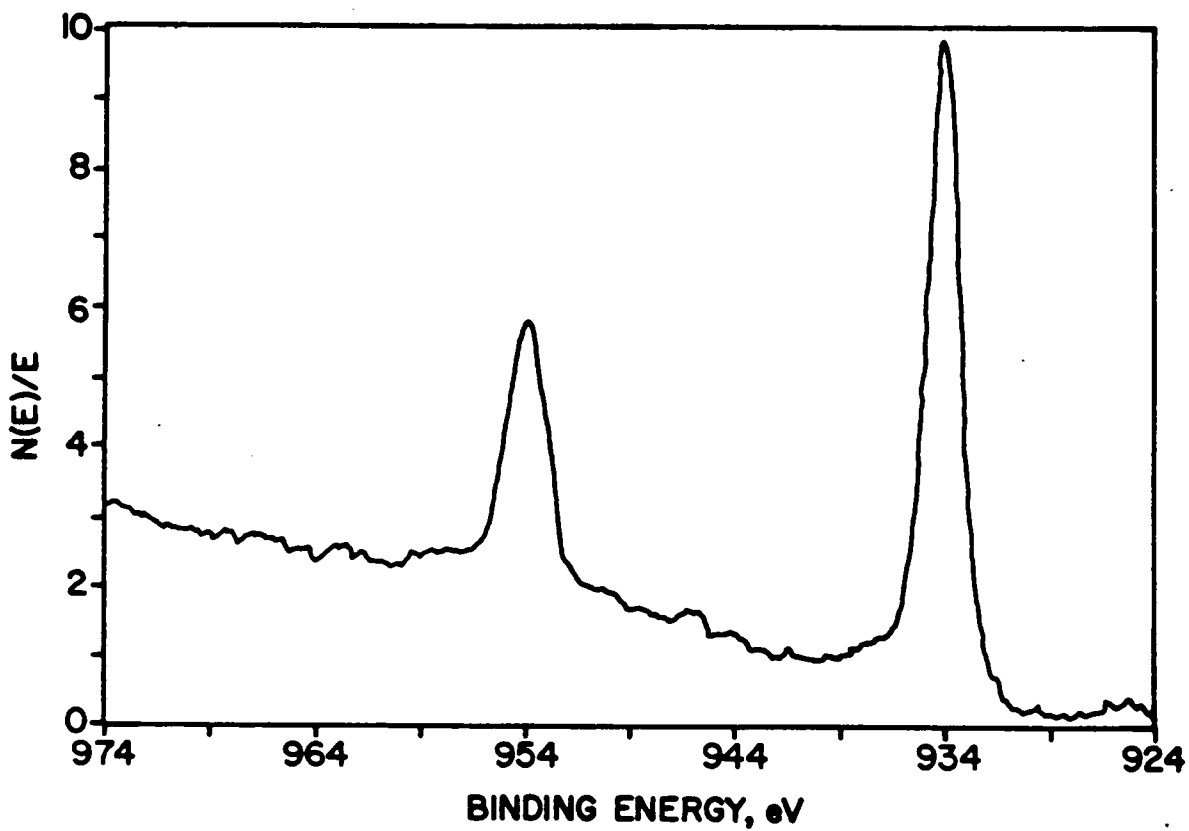


Figure 18. The XPS Cu(2p) spectrum of the wet-air-cured 2X-doped BDSDA-ODA film after argon ion etching.

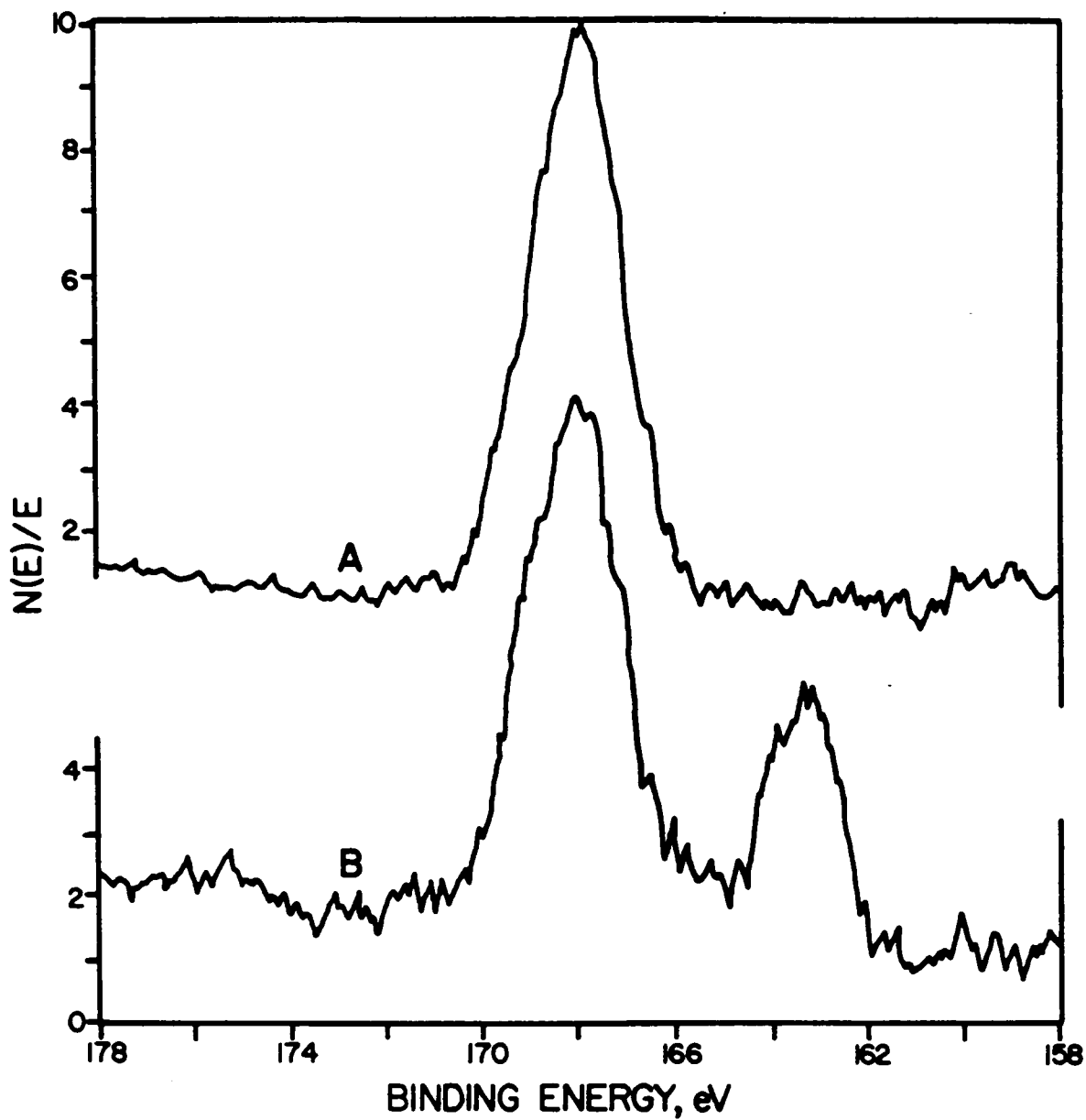


Figure 19. The XPS S(2p) spectrum of the wet-air-cured 2X-doped BDSDA-ODA film (A) before and (B) after argon ion etching.

concentration with irregular dispersions of sulfur throughout the profile (Figure 20). Similarly, the depth profile of the 2X-doped wet-air-cured film is comprised of a copper oxide layer followed by a region composed predominantly of copper and sulfur (Figure 21).

Transmission electron micrographs of the 1X and 2X dry-air cured ultramicrotomed films are characterized by large depletion zones (where no dopant aggregation occurs) which span 70-85% of the total film thickness from the atmosphere side of the film. These zones reside above regions of polyimide that contain dispersed copper-containing aggregates (Figure 22). A discontinuous surface composed of discrete copper-containing particles approximately 200 Å in diameter is observed on the atmosphere surface of the 1X wet-air-cured ultramicrotomed film (Figure 23). The 2X wet-air-cured film, on the other hand, displays a rather thick (~300 Å) continuous surface layer (Figure 24). Below the surface layer of each wet-air-cured film, a large depletion zone is again followed by a region that consists of widely dispersed copper-containing particles suspended in the polyimide matrix. The aggregates found in this region are on the order of 800 Å for all BDSDA-ODA films, significantly smaller than those found in the bulk of doped BTDA-ODA and BTDA-APB films. Energy-dispersive X-ray analysis detected both sulfur and copper in the aggregates. Whether the sulfur/copper species coat the particles or form an integral part of the aggregate is unknown.

The large depletion zones observed in all of the doped BDSDA-ODA films are most likely due to the copper/sulfur interaction. This interaction would lead to a large amount of copper, in some form, dispersed on a molecular scale, thereby accounting for smaller particles and larger depletion zones in comparison to the other polyimide systems under study. The large number of thioether groups

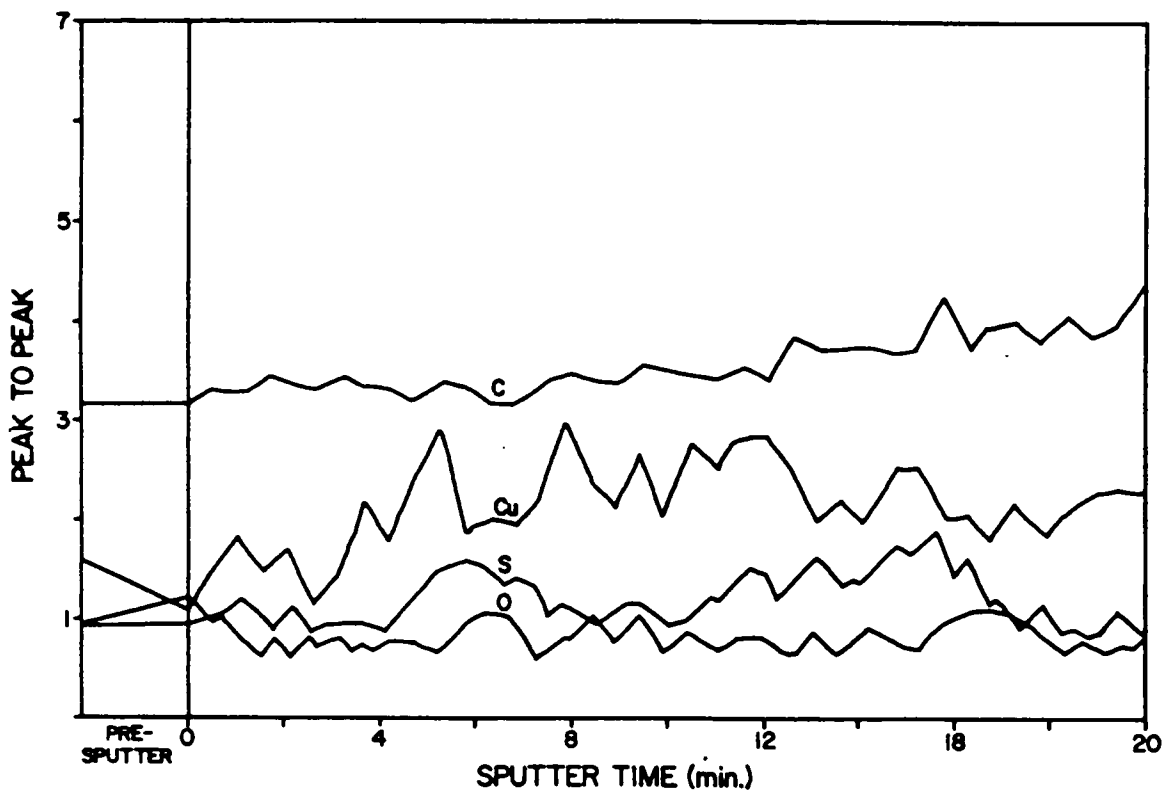


Figure 20. Auger electron spectroscopic depth profile of the wet-air-cured 1X-doped BDSDA-ODA film.

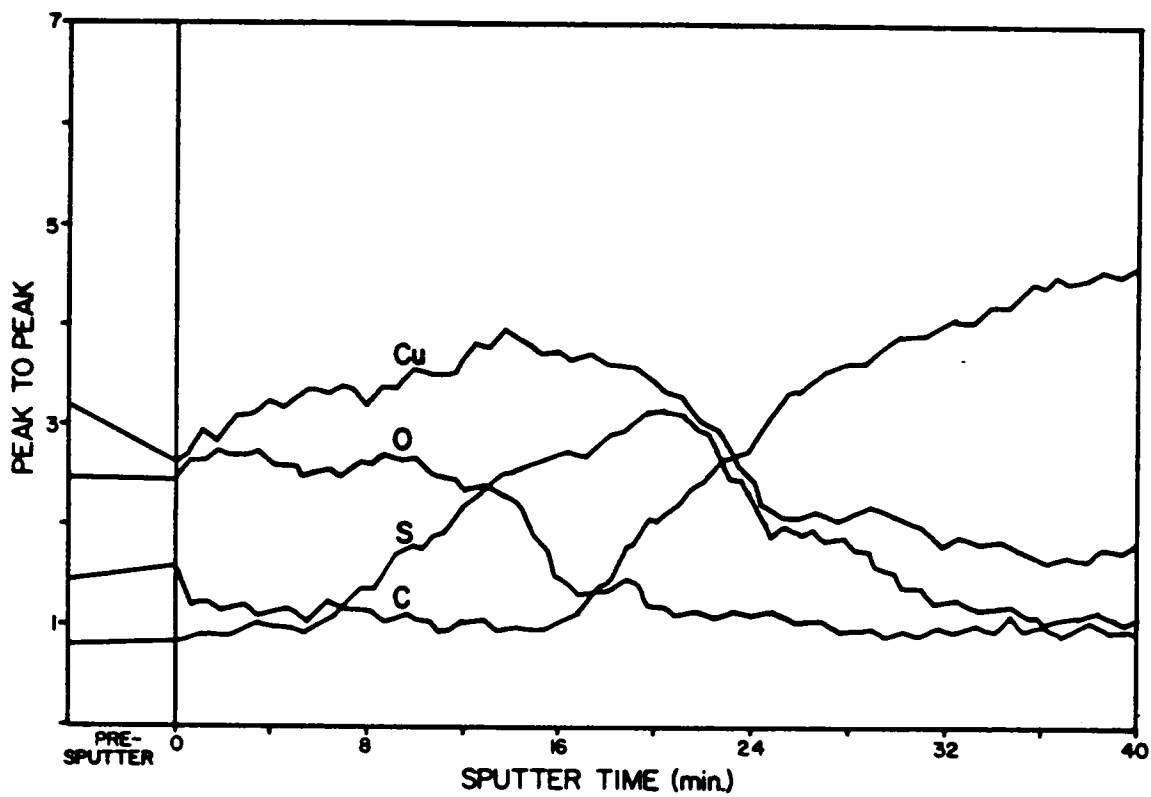


Figure 21. Auger electron spectroscopic depth profile of the wet-air-cured 2X-doped BDSDA-ODA film.

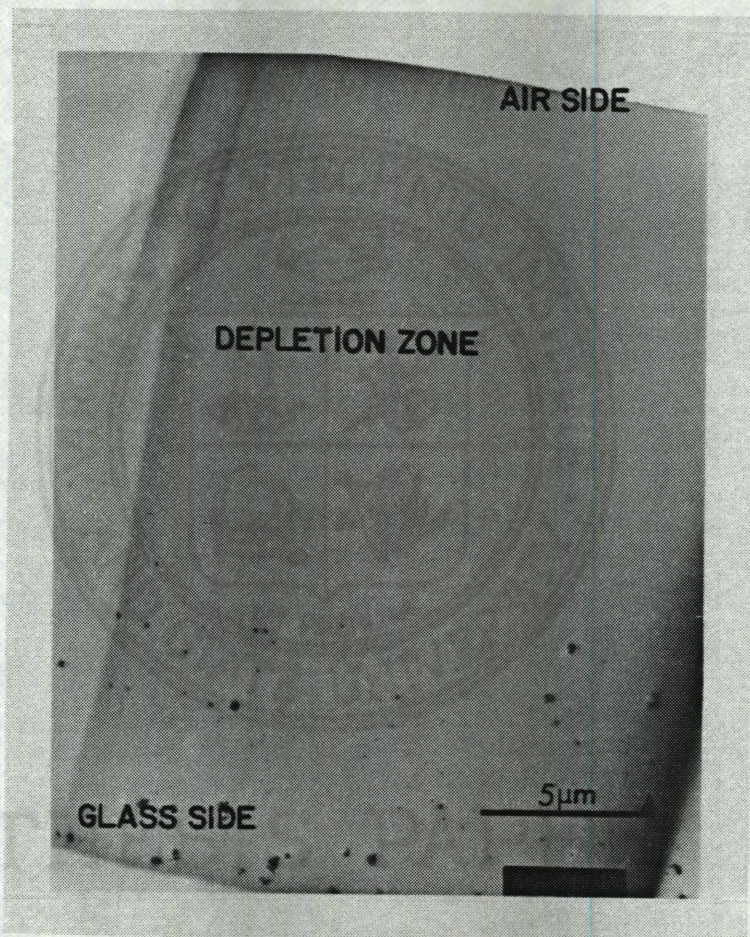


Figure 22. Transmission electron cross section of a dry-air-cured 1X-doped BDSDA-ODA film.

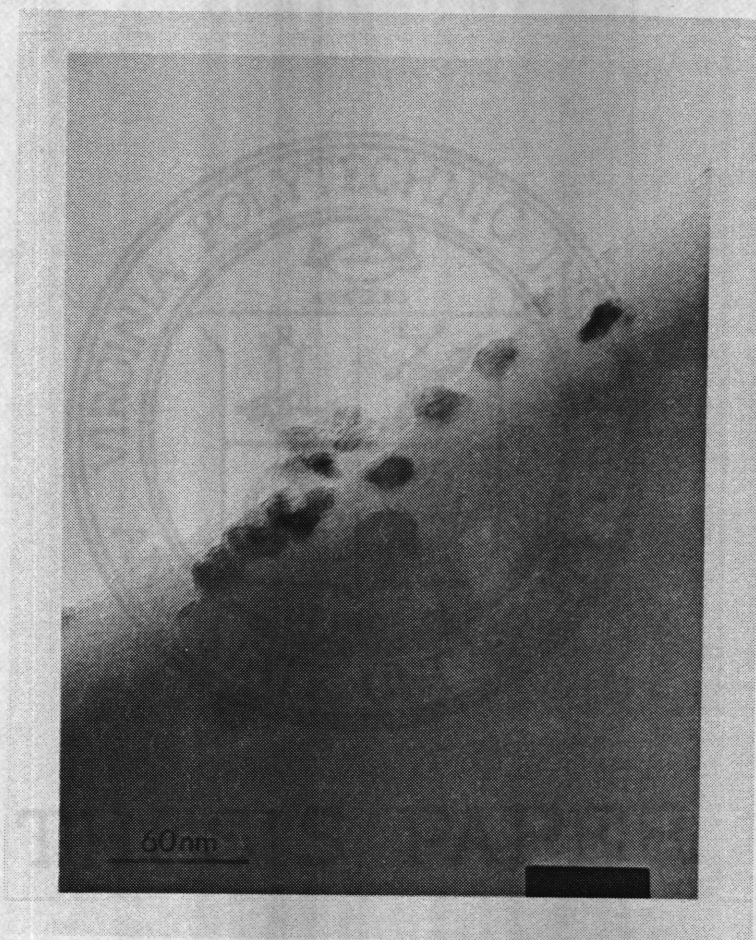


Figure 23. Transmission electron cross section of the surface region of the wet-air-cured 1X-doped BDSDA-ODA film.

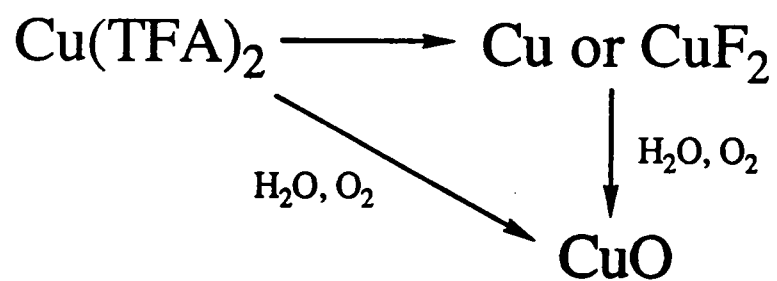


Figure 24. Transmission electron cross section of the surface region of the wet-air-cured 2X-doped BDSDA-ODA film.

theoretically available to react with a copper atom, which is 4 times the amount of initial additive molecules, could bind to and restrict additive mobility even at the higher curing temperatures. This immobilization could result in the small amount of internal agglomeration that is observed experimentally. The flexibility of the doped BDSDA-ODA films is poor. This in all likelihood, is due to the interaction between the thioether group and the copper dopant because nondoped films are extremely flexible and the doping of BTDA-ODA and BTDA-APB does not result in embrittlement.

#### F. Copper/Polyimide Composite Formation

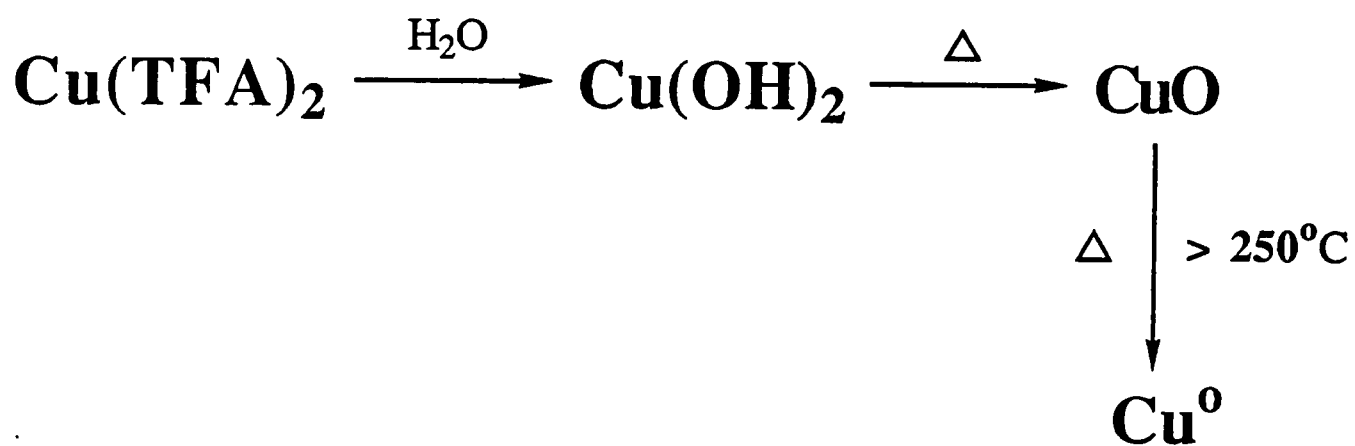
It is highly useful to consider in a qualitative sense how these varied, highly anisotropic metal-containing films are formed, given the fact that the dopant and cure temperature schedule is fixed. A working hypothesis is considered that takes into account the variable polymer matrix and cure atmosphere. It is based upon the concept that the solubility of the dopant is reduced during the thermal conversion of poly(amide acid) to polyimide, thereby promoting phase separation of a large portion of the additive.  $\text{Cu}(\text{TFA})_2$ , now a partially soluble second component, migrates to or near the atmosphere surface from the bulk during imidization.  $\text{Cu}(\text{TFA})_2$  may either thermally decompose to copper metal, whereby it is oxidized by reaction with atmospheric oxygen, atmospheric water, or the water of imidization, or  $\text{Cu}(\text{TFA})_2$  may interact with the same components to produce  $\text{CuO}$  directly (Scheme 2). It has been shown previously that metal beta-diketonates thermally decompose to the metallic state at temperatures as low as  $250^\circ\text{C}$ . [55,56] Water of imidization is apparently the reactant leading to formation of the  $\text{CuO}$  observed in the 2X-cured BTDA-ODA films. If the migrating dopant approaches the surface but does not come in contact with the curing



Scheme 2. Probable  $\text{Cu}(\text{TFA})_2$  reaction routes leading to the formation of  $\text{CuO}$ .

atmosphere two routes to the production of copper metal are feasible. First, it is possible that the dopant may thermally decompose to Cu(0), as described in Scheme 2, without subsequent oxidation (BTDA-ODA) which may also create a more active site for polymer/dopant interactions to take place (BDSDA-ODA). Second, it is also possible that a Cu(OH)<sub>2</sub>-CuO-Cu(0) reactive pathway (Scheme 3) is likely. Cu(OH)<sub>2</sub> may be an intermediate in the formation of CuO from Cu(TFA)<sub>2</sub> produced by reaction of the dopant with the water of imidization. CuO at higher temperatures (>250°C) can then thermally reduce in the polymer matrix to Cu(0). The reduction of CuO to Cu(0) has a positive heat of formation above 250°C.[57] Once formed, copper metal may (BDSDA-ODA) or may not (BTDA-ODA) react with the polymer matrix.

Phase separated material unable to migrate upward aggregates to form particles analogous to spherulites in a microphase separated copolymer, near the glass side of the film. This may be understood as follows. The portion of the film in contact with the glass substrate is the hottest region, while the surface in contact with the atmosphere is the coolest. This is due to the continual solvent loss (DMAC and the water of imidization) occurring at the atmosphere side of the film (Figure 25). The resulting temperature gradient would cause the percent imidization which is temperature dependent, to be greater at the glass side of the film during cure, thereby leading to a solubility gradient throughout the bulk of the film. In other words, material would begin to phase separate sooner at the glass side. Surface segregation could occur by having a certain portion of the dopant not yet immobilized by local polymerization seek the more soluble region above it. This would cause a front of the additive to eventually reach the air side of the film, where it may react further to form copper and copper oxide.



Scheme 3. Alternative reactive pathway leading to the formation of CuO from Cu(TFA)<sub>2</sub>.

# Additive Migration

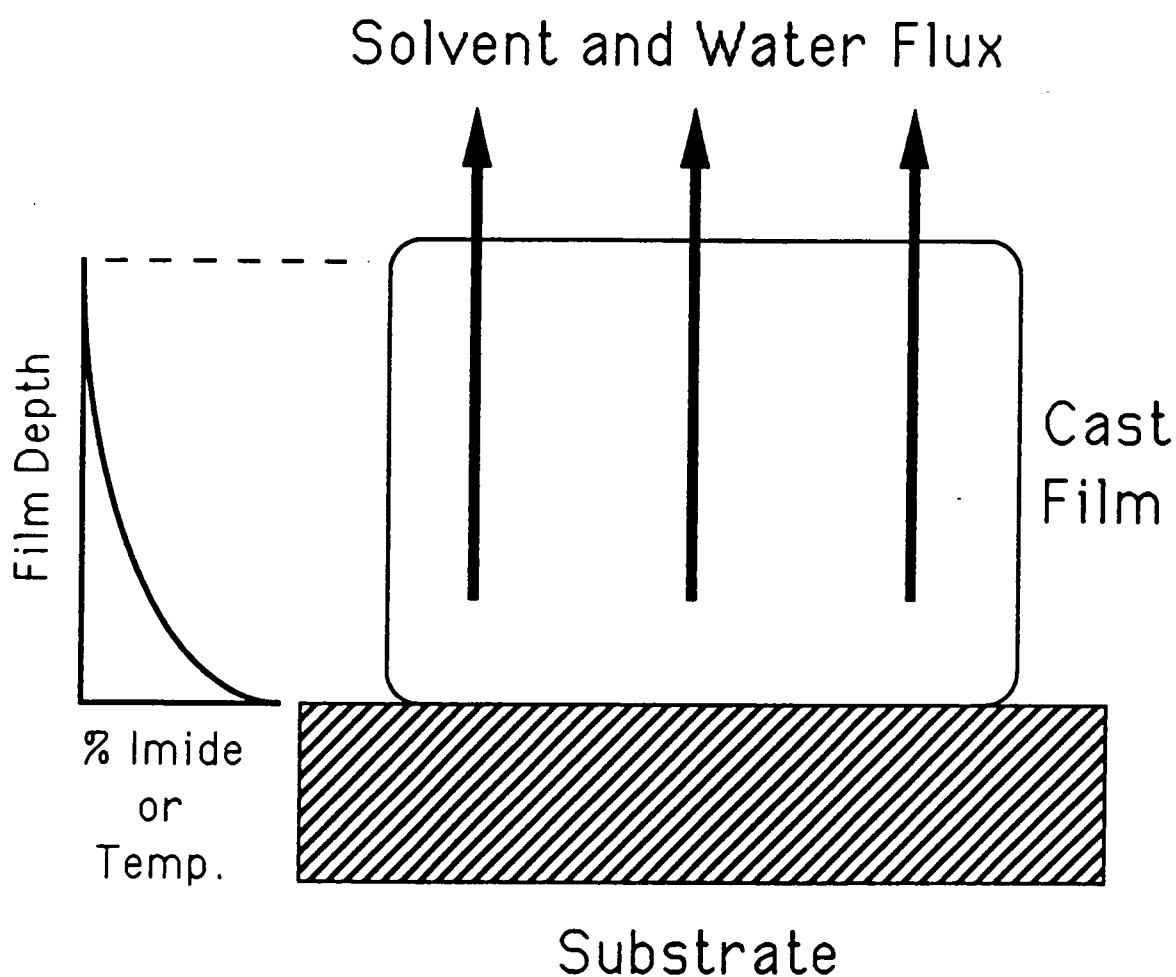


Figure 25. Schematic drawing of the temperature and imidization gradients resulting from solvent and water flux within a curing film.

For any doped film, no more than 5% of the copper initially mixed with the poly(amide acid) is lost throughout the curing process as determined by elemental analysis. This is somewhat surprising since  $\text{Cu}(\text{TFA})_2$  sublimates readily at approximately  $150^\circ\text{C}$  at atmospheric pressure; however, in the polymer matrix sublimation apparently does not occur. Since the presence of fluorine in the film is expected, it can be used as a tag for unreacted  $\text{Cu}(\text{TFA})_2$ . An estimate of the conversion of the additive to some other form within the film can be made by using the results of the fluorine elemental analysis. Theoretically, if one measures the volume of aggregated material at and below the surface of a portion of the film on a TEM micrograph, assuming all particles and layers were homogeneous, and if one specified the chemical nature of the aggregates ( $\text{Cu}(\text{TFA})_2$ ,  $\text{CuO}$ ,  $\text{Cu}$ ), a comparison could be made with the volume of material expected (if evenly dispersed through the film) using the percent additive conversion, the doping level, and the density of the components (see Appendix).

Table V provides the results of these estimates. As shown, the volume of particulate matter observed by TEM could not wholly account for the copper present in the film. Thus, even in the so-called "depletion zone" there exists a significant amount of finely dispersed copper either soluble in molecular form or too small for TEM to detect. Table V also provides information concerning the relative solubility of  $\text{Cu}(\text{TFA})_2$  in each polyimide matrix used. The large difference between the theoretical and experimental volume fractions for the doped BDSDA-ODA films as compared to the other doped matrices supports a higher level of solubility in BDSDA-ODA. A reduced solubility for BTDA-APB as compared to BTDA-ODA is also suggested. The wet-air-cured films display surface deposits denoting some additional effect as exemplified by the doped BDSDA-ODA films. It is possible that the increase in surface moisture from the

Table V

Additive Conversion and Volume Fraction of Copper Species

<u>Polyimide</u>	<u>Curing Atmosphere</u>	<u>Additive Level</u>	<u>Exptl</u>		<u>% Conversion<sup>c</sup></u>	<u>Theoret<sup>b</sup></u>	<u>V<sub>f</sub> Exptl<sup>a</sup></u>
			<u>%Cu</u>	<u>%F</u>			
BTDA-ODA	Wet Air	1.00X	2.4	1.7	62	0.062	0.042
	Wet Air	2.00X	4.8	2.4	72	0.084	0.056
BTDA-APB	Dry Air	1.00X	2.2	1.6	58	0.047	0.041
BDSDA-ODA	Dry Air	1.00X	2.0	1.2	66	0.040	0.005
	Wet Air	2.00X	4.3	2.4	68	0.069	0.014

<sup>a</sup>Volume fraction of particulate matter obtained from TEM. <sup>b</sup>Theoretical volume fraction of particulate matter taking into account additive conversion. <sup>c</sup>Percentage of initial amount of Cu(TFA)<sub>2</sub> reacted during cure, obtained from elemental analysis:

$$\frac{V(\text{spheres}) + V(\text{layer})}{V(\text{total})} = V(\text{f}) \text{ of particulate matter within the doped film.}$$

$$\% \text{ Conversion} = \frac{(\text{Cu/F})_{\text{reacted}}}{(\text{Cu/F})_{\text{initial}}} \times 100$$

moist-air purge may decrease the solubility of the additive in the surface region, thereby inducing phase separation at lower temperatures. It has been reported that atmospheric moisture increases the tensile modulus of fully cured polyimides above room temperature [58], which may modify the solubility characteristics of the doped polyimide films. Otherwise, the effect of curing atmosphere on the ultimate surface structure obtained is minor. It is more likely that the curing atmosphere has a pronounced effect on dopant reactivity. The use of wet air should increase the rate of CuO formation from  $\text{Cu}(\text{TFA})_2$  relative to dry air and nitrogen curing atmospheres due to surface moisture enrichment. Likewise, curing in dry air should increase the rate of CuO formation as compared to a nitrogen atmosphere.

There exists the likelihood that phase separation may begin at a certain temperature resulting from continual solvent loss (DMAC) in the film rather than the imidization process. Partially cured  $\text{Cu}(\text{TFA})_2$ -doped films do not display aggregation below approximately  $225^\circ\text{C}$ . The solubility of  $\text{Cu}(\text{TFA})_2$  in DMAC is considerable ( $>0.2$  mol/L), allowing for the possibility of total dissolution even at the higher curing temperatures present in the film during cure. Several films were doped with bis(acetylacetonato)copper(II),  $\text{Cu}(\text{AcAc})_2$ , which has a solubility in DMAC of  $\sim 0.01$  mol/L. By doping just under the solubility threshold, one would expect that a small loss of DMAC would cause the  $\text{Cu}(\text{AcAc})_2$  to phase separate if dopant solubility did not depend on the nature of the polymer matrix. Partial curing of these films to  $200^\circ\text{C}$  still produces films devoid of any internal aggregation, while fully cured films exhibit internal spherical particles of small size ( $\sim 100$  Å). The amount of DMAC within the film at  $200^\circ\text{C}$  cannot be sufficient to fully solubilize the additive. It is therefore concluded that the matrix itself acts to hold the dopant in solution at least up to a certain percent imidization.

## G. A Comparison: Copper-Doped Soluble Polyimide And Condensation Polyimide

A logical extension of these studies was to prepare and characterize copper-modified polyimide films wherein formation of a poly(amide acid) is eliminated. The use of Polyimide XU-218 (Figure 26), having high thermal stability, high glass transition temperature, and good solubility in many common solvents, affords such an opportunity. Poly(amide acid) solutions of BTDA and DAPI provided the condensation polyimide analogue of XU-218. Curing of the  $\text{Cu}(\text{TFA})_2$ -doped poly(amide acid) film (unlike its doped soluble polyimide counterpart) releases water and results in formation of the polyimide. If the phase separation is characteristic of the imidization process as suggested in the previous section, the pre-imidized XU-218 matrix should result in differing structural features.

In the case of  $\text{Cu}(\text{TFA})_2$  doping (dry air), the poly(amide acid) yields a highly anisotropic structure containing a surface layer of  $\text{CuO}$  as evidenced by X-ray photoelectron spectroscopy. In contrast,  $\text{Cu}(\text{TFA})_2$ -modified XU-218 soluble polyimide appears to have no copper on the air-side surface for comparable scan times (i.e. XPS spectra were typical of the nondoped XU-218 films). This is dramatically illustrated in Figure 27 where doped XU-218 exhibited no copper photopeaks on the air-side, whereas modified BTDA-DAPI showed strong  $\text{Cu}$  ( $2p_{1/2,3/2}$ ) signals, which reflect both  $\text{Cu}(\text{II})$  and  $\text{Cu}(0)$  near the air-side surface. Furthermore doubling the amount of  $\text{Cu}(\text{TFA})_2$  doping (2X) in XU-218 did not result in a detectable copper photopeak. On the other hand, an oxide oxygen photopeak and a weak signal due to fluorine was found in the modified BTDA-DAPI films. The chemical nature of the copper surface deposit on the BTDA-DAPI films appears to be a mixture of species, e.g.,  $\text{Cu}(\text{TFA})_2$ ,  $\text{CuO}$ , and  $\text{Cu}$  metal.

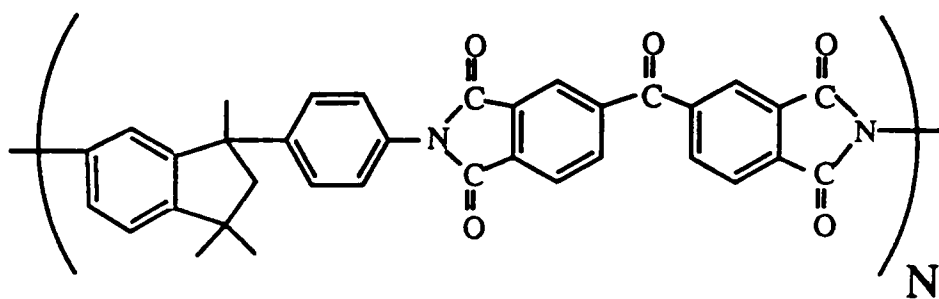


Figure 26. Chemical structure of Polyimide XU-218.

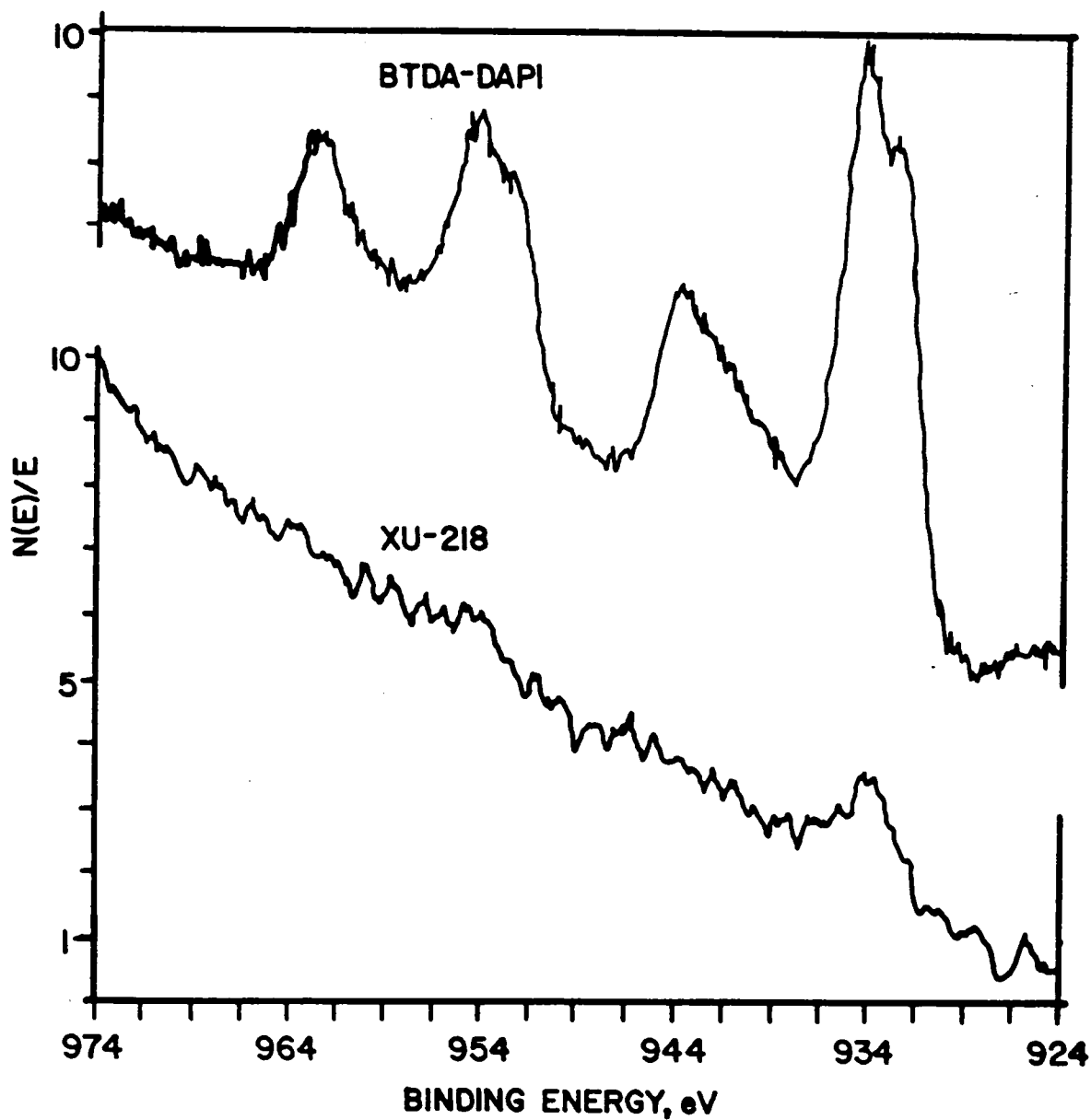


Figure 27. The XPS Cu(2p) spectrum of  $\text{Cu}(\text{TFA})_2$  modified BTDA-DAPI and  $\text{Cu}(\text{TFA})_2$  modified XU-218 films.

Argon ion milling experiments have been performed with Auger electron spectroscopic monitoring on both copper modified XU-218 and BTDA-DAPI. Surprisingly, no increased concentration of copper was noted near the surface of either film. In fact both depth profiles were identical despite the XPS observation that BTDA-DAPI contained appreciable surface Cu while XU-218 did not. Ultramicrotomed cross-sections of both films have been examined by scanning transmission electron microscopy (Figure 28). For the doped XU-218 material no metal deposits were noted on either surface as expected, although the bulk of the film demonstrated the deposition of relatively large amounts of additive. In contrast, the modified BTDA-DAPI films showed discrete metal-containing domains of approximately  $0.1\ \mu\text{m}$  in diameter on the air-side surface. In the bulk, considerable metal had precipitated. The distance between the surface copper domains was measured to be approximately  $0.5\ \mu\text{m}$  on average. Since the Auger electron beam is  $1\ \mu\text{m}$  in diameter and the copper domains are highly segregated, the Cu Auger signal will be rather small in comparison to the polyimide response rendering it undetectable. For both copper-doped BTDA-DAPI and XU-218, the glass side of the film was devoid of all copper-containing material.

The presence of copper oxide on the surface of doped BTDA-DAPI films and the absence of the same on doped XU-218 films provide further support for the film formation hypothesis denoted in Section F. of this Chapter. As exhibited by subsequent  $\text{Cu}(\text{TFA})_2$ -doped condensation polyimides, a possible solubility gradient within the film forces a portion of the dopant to the atmosphere side of the film where it reacts, and in the case of BTDA-DAPI forms  $\text{CuO}$ . This gradient being due to temperature variations resulting in progressive concentrations of

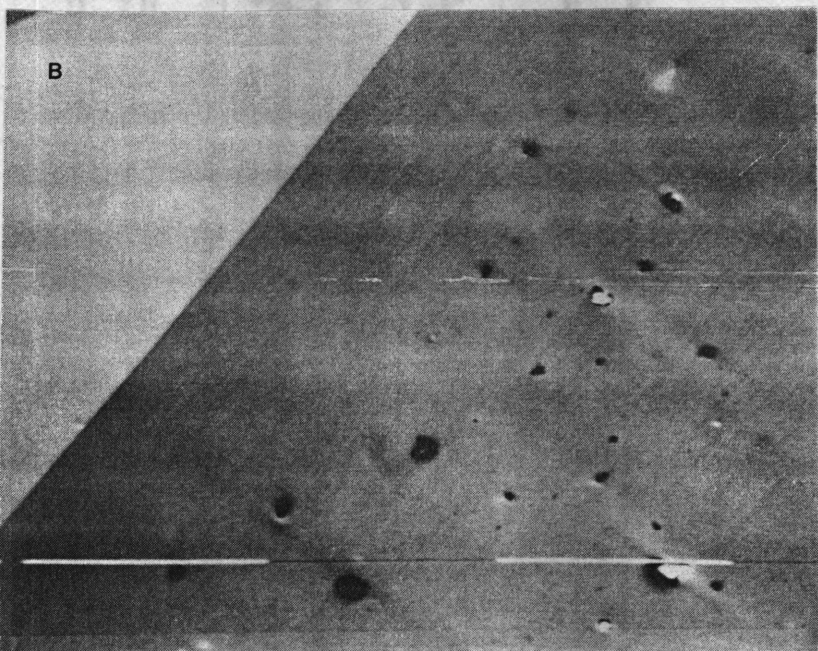
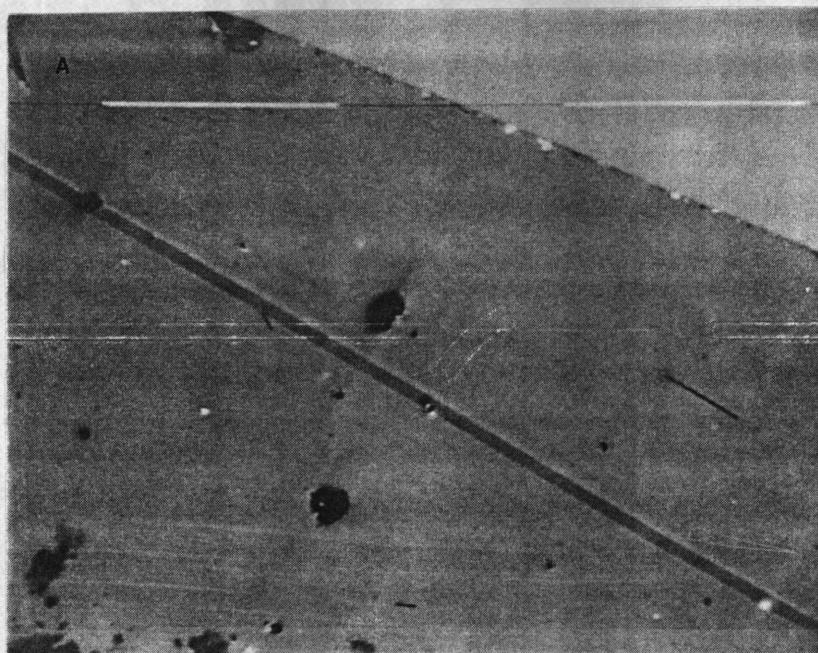


Figure 28. Scanning transmission electron cross sections of (A)  $\text{Cu}(\text{TFA})_2$  modified BTDA-DAPI and (B)  $\text{Cu}(\text{TFA})_2$  modified XU-218 films.

polyimide and poly(amide acid) in the film. On the other hand, use of a soluble polyimide would preclude the formation of a solubility gradient since the matrix is fully imidized prior to thermal processing. No solubility gradient would be expected, hence the dopant would phase separate after loss of a certain portion of DMAC at higher temperatures (the existence of DMAC now being the only reason for the dopant to remain soluble in the matrix). However, once phase separation has occurred, only localized aggregation would be expected; there would not be a driving force for additive surface segregation. In this way, doping of XU-218 resulted only in internal precipitation of additive, no surface enrichment was found.

## V. ELECTRICAL AND THERMAL CHARACTERISTICS OF COPPER CONTAINING POLYIMIDE FILMS

### A. Preliminary

The doping of poly(amide acid) solutions with  $\text{Cu}(\text{TFA})_2$  followed by thermal curing produces a variety of films with differing structural and chemical characteristics. It is these characteristics though that ultimately control the electrical and thermal properties of the modified films. Surface or near-surface copper enrichment creates conductive pathways across the film. The presence of dopant/polymer interactions also determines the point at which thermal transitions occur. It is the object of this Chapter to discuss in detail how the structural and chemical nature of the doped films affects properties such as these, as well as providing support for the observations and hypotheses presented in the previous Chapter.

### B. Thermal Properties

Each of the polyimide samples was evaluated by differential scanning calorimetry to determine the glass transition temperature (Table VI). The general observation is that the glass transition temperature of BTDA-ODA > BDSDA-ODA > BTDA-APB, respectively whether or not the films have been doped with  $\text{Cu}(\text{TFA})_2$ . However, differences in the effect of doping a particular polyimide matrix relative to the nondoped matrix have been noted. The glass transition temperature of copper-doped BTDA-ODA and BTDA-APB films is substantially lower than those obtained from the nondoped films. This is in apparent contrast

Table VI

Thermal Properties of Cu(TFA)<sub>2</sub>-Doped and Nondoped Polyimide Films

<u>Polyimide</u>	<u>Curing Atmosphere</u>	<u>Additive Level</u>	<u>PDT(°C)<sup>a</sup></u>	<u>AGT(°C)<sup>b</sup></u>
BTDA-ODA	Dry Air	1.00X	428(498,N <sub>2</sub> )	271
	Wet Air	1.00X	432	274
	Nitrogen	1.00X	438	271
	Dry Air	2.00X	415	277
	Wet Air	2.00X	444	276
	Nitrogen	2.00X	420	274
BTDA-APB	Dry Air	1.00X	465	201
	Wet Air	1.00X	475(533,N <sub>2</sub> )	202
	Dry Air	2.00X	494	205
	Wet Air	2.00X	499	201
BDSDA-ODA	Dry Air	1.00X	442	221
	Wet Air	1.00X	467	221
	Dry Air	2.00X	452(552,N <sub>2</sub> )	220
	Wet Air	2.00X	447	225

<sup>a</sup>PDT: BTDA-ODA = 553; BTDA-APB = 607 (601,N<sub>2</sub>); BDSDA-ODA = 580°C.

<sup>b</sup>AGT: BTDA-ODA = 285; BTDA-ODA = 211; BDSDA-ODA = 216°C.

to polyimide films doped with silver [60], cobalt [31,45], and tin [32] compounds wherein the glass transition temperatures of all films, irrespective of the diamine/dianhydride combination, were reported to be higher than their nondoped counterparts. The doped poly(amide acid) precursors may be considered "homogeneous" mixtures. With this in mind, the additive in the matrix may be considered a plasticizer at this stage since in general plasticizers are considered to form true, homogeneous solutions with polymers. This is the opposite of the action of fillers which produce heterogeneous mixtures that increase the glass transition temperature.

Alternatively, doping BDSDA-ODA polyimide films increases the glass transition relative to nondoped BDSDA-ODA films (Table VI). One of the general functional requirements of a plasticizer is that it must not interact chemically with the polymer matrix. It has been shown that  $\text{Cu}(\text{TFA})_2$  does not seem to interact chemically with either BTDA-ODA or BTDA-APB. However, a polymer/dopant interaction is present in  $\text{Cu}(\text{TFA})_2$ -doped BDSDA-ODA arising from the reactivity of the thioether backbone linkage. The additive then may restrict the mobility of the polymer backbone increasing the apparent glass transition temperature. The cure atmosphere or doping level does not appear to affect the  $T_g$  of any copper-doped polyimide appreciably.

Doping polyimide films with  $\text{Cu}(\text{TFA})_2$  has a pronounced effect on the thermal and thermooxidative stability of each film (Table VI). The stabilities are referenced to  $T_{10}$ ; a single parameter corresponding to the temperature at which 10% weight loss occurs.[61,62] Thermooxidative stabilities are reduced by at least  $100^\circ\text{C}$  as compared to the nondoped analogue (Figure 29). Thermal stability in an inert atmosphere is reduced less ( $\sim 70^\circ\text{C}$ ). The large difference between the polymer decomposition temperature (PDT) or  $T_{\text{max}}$  (temperature

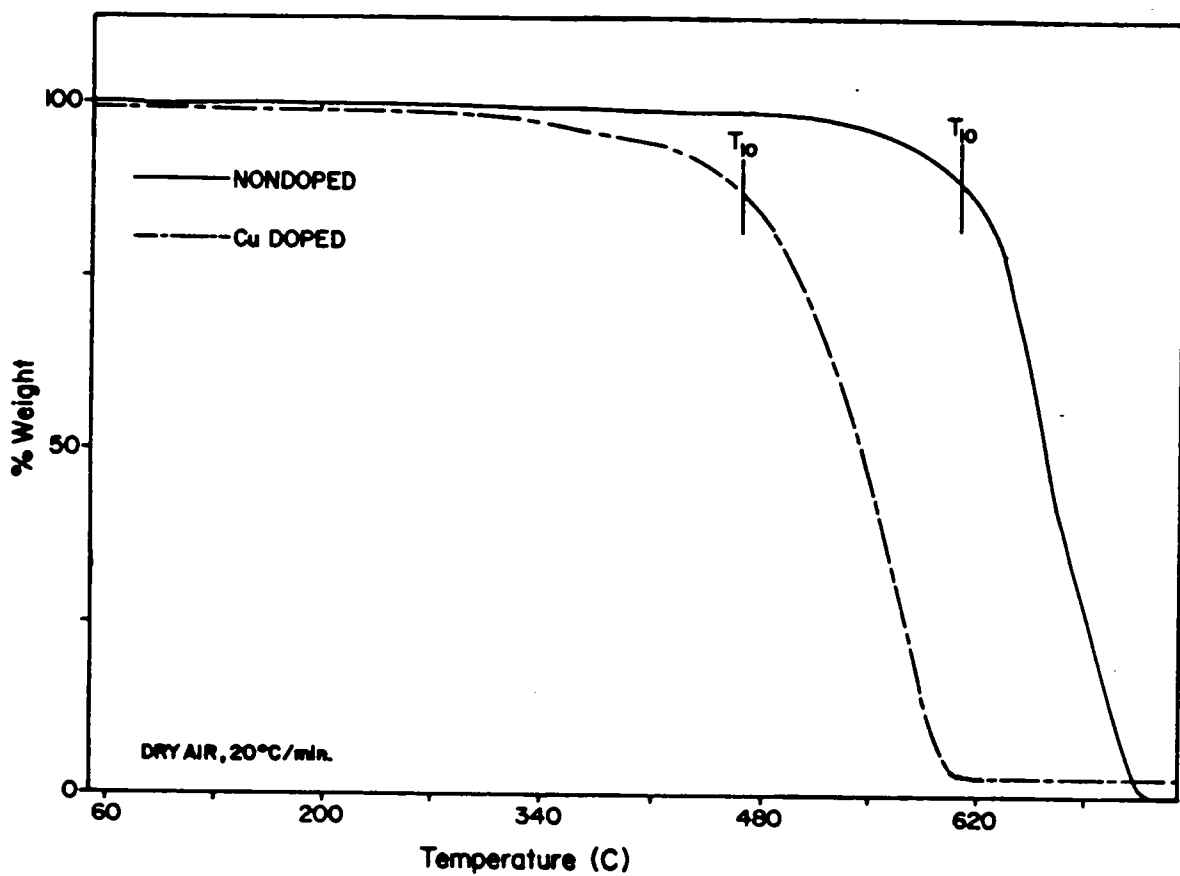


Figure 29. The thermogravimetric profile of nondoped and  $\text{Cu}(\text{TFA})_2$ -doped BTDA-ODA films.

where the decomposition rate is maximum) for the doped films versus the PDT for nondoped polyimides suggests the presence of a dopant-catalyzed decomposition mechanism. Since the presence of oxygen lowers the PDT drastically, an oxidative decomposition pathway, wherein the metal component activates the oxidizing agent, is most likely responsible for reduced stability.

### C. Electrical Properties

Surface resistivities of  $\text{Cu}(\text{TFA})_2$ -doped polyimide films measured in vacuum at  $25^\circ\text{C}$  are substantially lower, in most cases, than non-doped films, while volume resistivities are not appreciably affected (Table VII). The lowered surface resistivities (atmosphere surface) can be accounted for by the surface or near-surface enrichment in the form of elemental copper or copper oxide that occurs in many of the samples studied. Since the copper containing layers are very thin relative to the overall film thickness (25-50  $\mu\text{m}$ ) and the unreacted additive is nonionic, predictably the volume resistivity is unaffected in the doped films.

Variation of the polyimide matrix controls the magnitude of improvement in surface resistivity. For instance, the absence of at least a semi-continuous conductive pathway in the BDSDA-ODA doped films has resulted in little gain in surface conductivity relative to the nondoped film. Only one BDSDA-ODA doped film (2X, wet-air-cured) appears to contain a relatively uninterrupted surface layer composed of a mixture of  $\text{CuO}$  and a copper/sulfur compound. Yet even this film is highly resistive. This suggests a preponderance of the polyimide matrix that would destroy conductive paths. The large amount of polyimide carbon and oxygen detected by XPS supports this notion. Owing to the dominant chemical interaction between the polymer and additive in these films, other processing

Table VII  
DC Electrical Resistivity<sup>a</sup> of Cu(TFA)<sub>2</sub>-Doped Polyimide Films

<u>Polyimide</u> <sup>b</sup>	<u>Curing Atmosphere</u>	<u>Additive Level</u>	<u>Log Volume Resistivity</u>	<u>Log Surface Resistivity</u> <sup>c</sup>
BTDA-ODA	Dry Air	1.00X	16.2	17.2
	Wet Air	1.00X	16.8	11.4
	Nitrogen	1.00X	~17.0	16.8
	Dry Air	2.00X	~17.0	14.1
	Wet Air	2.00X	~17.0	13.6
	Nitrogen	2.00X	~17.0	14.3
BTDA-APB	Dry Air	1.00X	~17.0	16.0
	Wet Air	1.00X	~17.0	15.7
	Dry Air	2.00X	~17.0	15.5
	Wet Air	2.00X	~17.0	14.8
BDSDA-ODA	Dry Air	1.00X	~17.0	~17.0
	Wet Air	1.00X	~17.0	~17.0
	Dry Air	2.00X	~17.0	16.7
	Wet Air	2.00X	~17.0	16.9

<sup>a</sup>Temperature = 25°C.

<sup>b</sup>Nondoped polymers: log P(v) = 10<sup>18</sup> ohm-cm; log P(s) = 10<sup>17</sup> ohm.

<sup>c</sup>Curing atmosphere side.

variables such as dopant level and curing atmosphere are overshadowed such that they do not appear to affect film electrical properties.

Unlike BDSDA-ODA films, those composed of BTDA-ODA or BTDA-APB produce films with significant reduction in surface resistivity. The Cu(0) or CuO surface enrichment no doubt enhances the electrical properties since both have lower surface resistivity than the polyimide matrix. The wet-air-cured 1X-doped BTDA-ODA films in particular have produced the lowest measured resistivity. As noted previously, the dopant level has a pronounced effect on the surface or near-surface structure of the Cu(TFA)<sub>2</sub>-doped BTDA-ODA films. The thickness of the overlayer as well as the continuity of the elemental copper layer below it readily affect measured surface resistivity of the 1X-doped films. Table VIII provides data comparing calculated surface resistivities with experimentally obtained values for a number of doped films.

Surface mode electrical resistivity was calculated according to the following equation:

$$P(s) = 53.4 \frac{PL}{20} + \frac{P'}{53.46L'} + \frac{PL}{22.9} \quad (1)$$

where: 53.4, 20.0 and 22.9 = surface mode cell constants

P = polymer overlayer surface  
resistivity

L = overlayer thickness  
(if present)

P' = metallic layer surface  
resistivity

Table VIII  
Calculated Vs. Experimental Surface Resistivity<sup>a</sup>

<u>Polyimide</u>	<u>Curing Atmosphere</u>	<u>Additive Level</u>	<u>Calculated Surface Resistivity<sup>b</sup> (ohms)</u>	<u>Experimental Surface Resistivity (ohms)</u>
BTDA-ODA	Dry Air	1.00X	2.0X10 <sup>13</sup> (4.6X10 <sup>-1</sup> )	1.5X10 <sup>17</sup>
	Wet Air	1.00X	3.0X10 <sup>12</sup> (2.3X10 <sup>-1</sup> )	2.3X10 <sup>11</sup>
	Nitrogen	1.00X	1.8X10 <sup>13</sup> (5.2X10 <sup>-1</sup> )	8.2X10 <sup>16</sup>
	Dry Air	2.00X	1.2X10 <sup>9</sup>	1.1X10 <sup>14</sup>
	Wet Air	2.00X	1.0X10 <sup>9</sup>	1.1X10 <sup>14</sup>
	Nitrogen	2.00X	2.4X10 <sup>9</sup>	2.7X10 <sup>14</sup>
BTDA-APB	Dry Air	1.00X	1.6X10 <sup>9</sup>	1.0X10 <sup>16</sup>
	Wet Air	1.00X	1.9X10 <sup>9</sup>	7.0X10 <sup>15</sup>
	Dry Air	2.00X	1.3X10 <sup>9</sup>	5.2X10 <sup>15</sup>
	Wet Air	2.00X	1.2X10 <sup>9</sup>	7.7X10 <sup>14</sup>

<sup>a</sup>Temperature = 25°C.

<sup>b</sup>Resistivity value in parenthesis exhibits the effect of negating the overlayer contribution.

$L'$  = metallic layer thickness

Resistivity values used for the polymer overlayer, elemental copper layer, and CuO layer were  $1 \times 10^{18}$  ohms-cm,  $1 \times 10^{-5}$  ohms-cm, and  $1 \times 10^4$  ohms-cm, respectively. In nearly every case, the calculated resistivity is lower than the resistivity measured experimentally. It is assumed in the calculation that the copper or copper oxide layer is completely homogeneous which is refuted by previous structural analysis. These calculations are, therefore, biased and do not consider the innate discontinuity of the layers which is surely present.

The overlayer that exists on the atmosphere surface of 1X-doped BTDA-ODA films has a significant effect on the electrical properties. Any current passed along the surface of these films must successfully pass through a highly resistive overlayer varying in thickness, travel along the copper strata, then pass again through the overlayer upon exit (Figure 30). Between the films of this particular group, the polymer overlayer thickness attenuates the calculated resistivity by an order of magnitude. The larger difference realized experimentally is attributed to the seemingly higher continuity of the elemental copper layer in the wet-air-cured film with respect to the dry air and nitrogen cured films. TEM analysis displays less coherent copper enrichment for both of the latter films. The overlayer itself nonetheless profoundly curtails the potential reduction in surface resistivity. If the overlayer's effect was negated, as shown in the third column of Table VIII, expected resistivity would be much lower. The theoretical effect of the polymer overlayer then would be to increase the surface resistivity by 10 or 11 orders of magnitude.

In order to verify the actual effect the overlayer has on the measured electrical properties, argon ion etching was used to remove the overlayer thereby exposing the copper layer to direct electrical measurement. Etching was

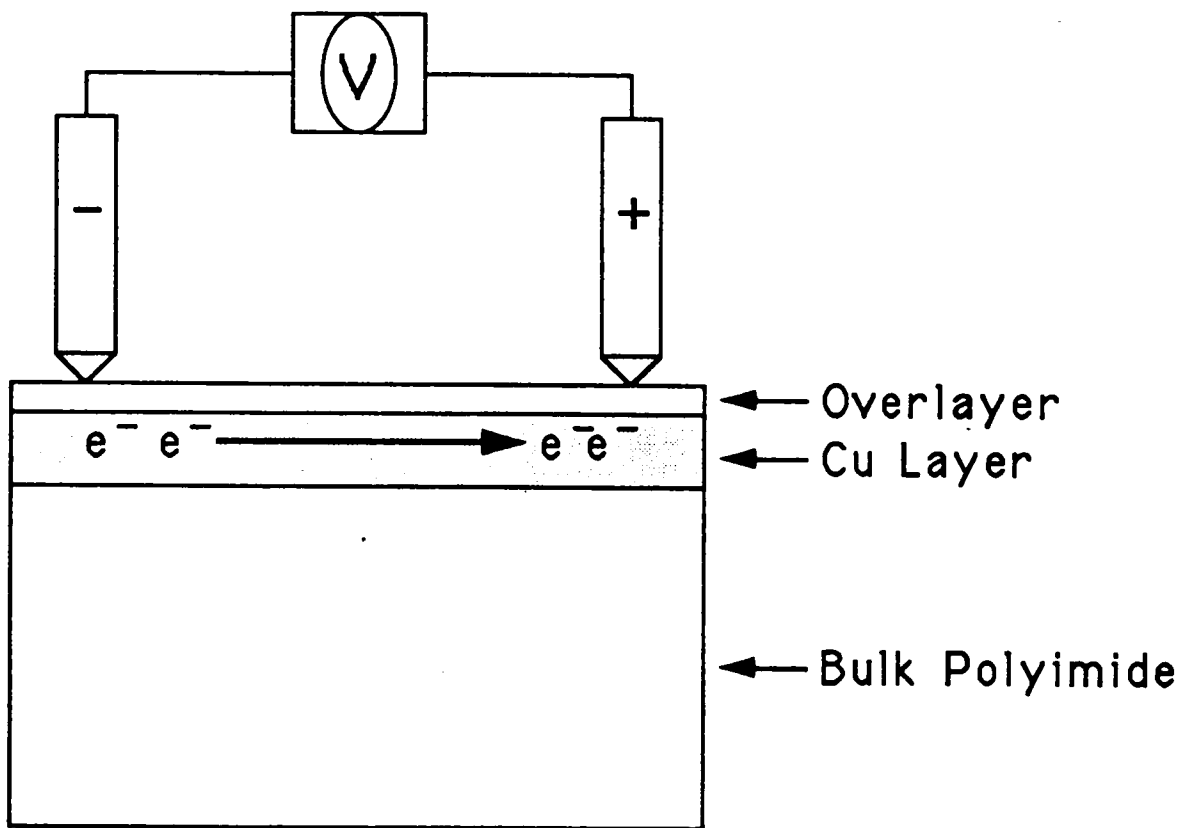


Figure 30. Electron path through a tri-layered composite film.

monitored by XPS and ceased when intense Cu(2p) photopeaks were observed. Following etching, the sample was removed from the vacuum chamber and its surface resistivity immediately measured by the two probe technique (Figure 31). Resistance values less than  $10^6$  ohms were measured; yet, the resistivities were significantly greater than the calculated values with the overlayer removed. The effect of the overlayer then, while great, does not completely account for the high resistivities observed for the 1X-doped films. Metal domain discontinuity must therefore play a major role in adversely affecting electrical properties.

The 2X-doped BTDA-ODA films and the doped BTDA-APB films provide materials with moderate reductions in surface resistivity. This being in part due to both the simple structure (two layers), as compared with the films previously discussed, and the chemical nature of the copper containing surface layer. First, the absence of an overlayer results in a less complicated conductive pathway devoid of the attenuated properties that would result. And second, the higher intrinsic volume resistivity of CuO ( $1 \times 10^4$  ohm-cm) relative to copper metal precludes the formation of a truly conductive surface. Measured surface resistivities for both 2X-doped BTDA-ODA and all BTDA-APB films were substantially higher than the calculated values (Table VIII). Again, this most likely arises from the discontinuity in the CuO surface layer where the polyimide component acts as a barrier to conduction. As considered previously, curing atmosphere and dopant level have minor effects on the structure of BTDA-APB films, therefore, they do not alter the outcome of surface electrical properties. Measured resistivities less than two orders of magnitude in difference up to  $250^\circ\text{C}$  are observed for films produced with the various combinations of curing atmosphere and dopant level. For 2X-doped BTDA-ODA films, curing

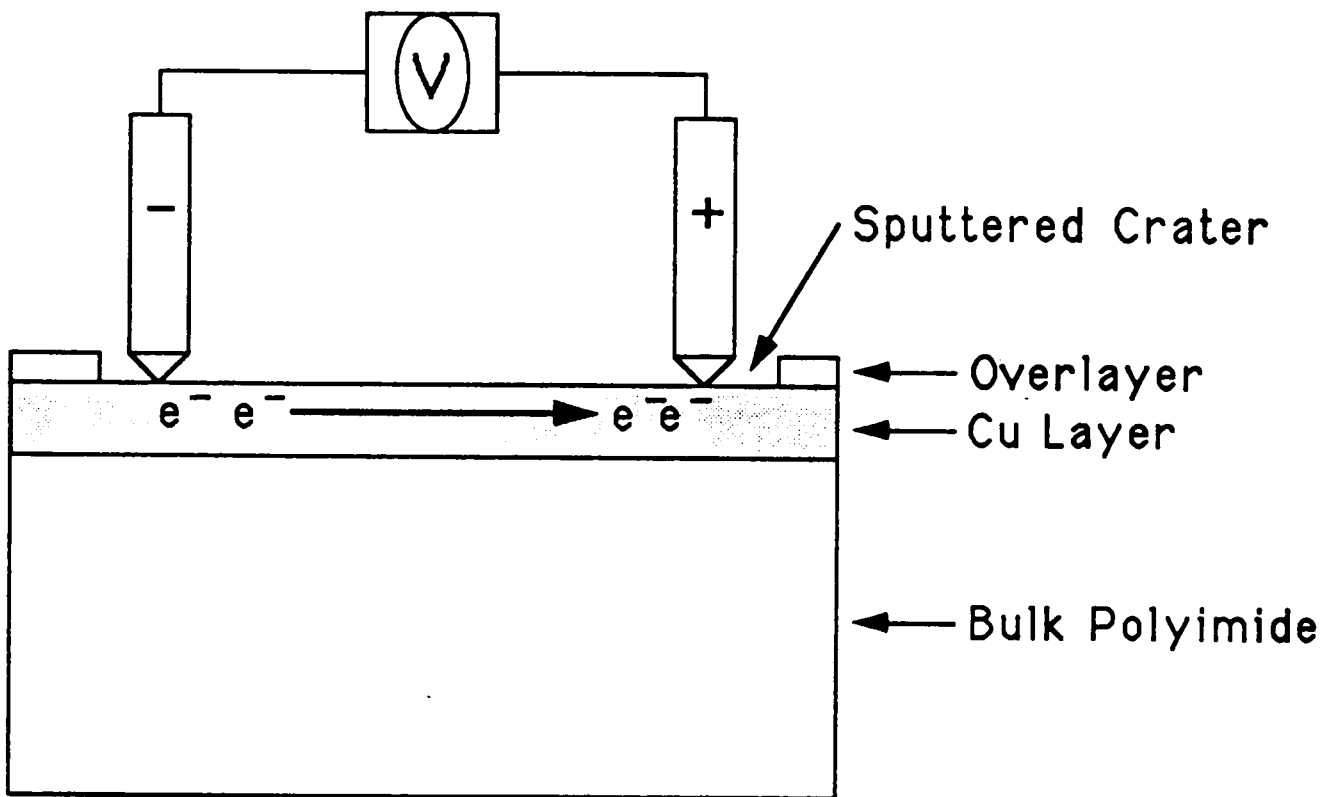


Figure 31. Two probe electrode resistivity measurement of a tri-layered film following argon ion etching.

atmosphere does not seriously affect the measured values; yet, the doping level does alter film structure producing a bi-layered material versus the tri-layered films established with the 1X-doped films. Resistivity differences between wet air, dry air, and nitrogen cured 2X BTDA-ODA films are less than one order of magnitude for temperatures between 30°C and 250°C.

Besides the inherent discontinuity present within the CuO layer, it has been noticed that when a film is removed from the glass plate "curling" sometimes occurs which could cause the CuO domains to rupture, thereby further eliminating conductive pathways. Recently, several tin doped polyimide films produced in our laboratory displayed resistivity increases of 3 or more orders of magnitude upon removal from the glass plate supporting this hypothesis. This phenomenon indicates that significant stresses may be generated within the film during cure. Once the film is physically detached from the glass plate, "curling" occurs to relieve these internal stresses. Hofer [63] has found that stresses build-up in fully cured polyimide films during cooling. If so, these stresses most likely do not affect the structure of the films, since quench-cooling of doped films cured to 300°C results in films with fully formed surface layers.

Surface electrical resistivity decreases with increasing temperature regardless of the polyimide formulation and curing parameters. This behavior is characteristic of insulators and semiconductors and is expected of the doped polyimide films considering their structure and chemical characteristics. CuO, a known semiconductor, is apparent on the surface of most copper doped films which exhibit the trend in electrical response with temperature noted above. It is also shown that the overlayer residing over an elemental copper layer, which should display an increase in resistivity with increasing temperature, alters the surface electrical properties enormously. The resistive nature of the overlayer

then should attenuate the higher temperature electrical response to a significant degree. However, the elemental copper layer being an electrical conductor should exhibit an increase in resistivity with increasing temperature. The opposing trends in resistivity with temperature may result in a net slope that is less than what would be expected.

The 1X-doped BTDA-ODA films which display overlayers show an approximately two order of magnitude decrease in surface resistivity with a temperature rise of 155°C (Figure 32). The 2X-doped BTDA-ODA films, however, exhibit approximately a four order of magnitude decrease in surface resistivity over the same temperature span. This is most probably the result of the conflicting nature of the overlayer and the copper layer beneath it in the 1X-doped films. Surface resistivity behavior within a particular polyimide series that have the same structural characteristics is constant from 25°C up to 250°C in most cases. For the doped BTDA-APB films measured resistivities varying less than two orders of magnitude to 250°C are observed (Figure 33). Resistivity differences between the 2X-doped BTDA-ODA films are less than one order of magnitude for temperatures between 30°C and 250°C. Similar behavior is observed for the doped BDSDA-ODA films. Only the 1X-doped BTDA-ODA films show large differences in electrical resistivities throughout the temperature range (Figure 34). The differences in the overlayer thickness and the continuity of the elemental copper layer provide this behavior.

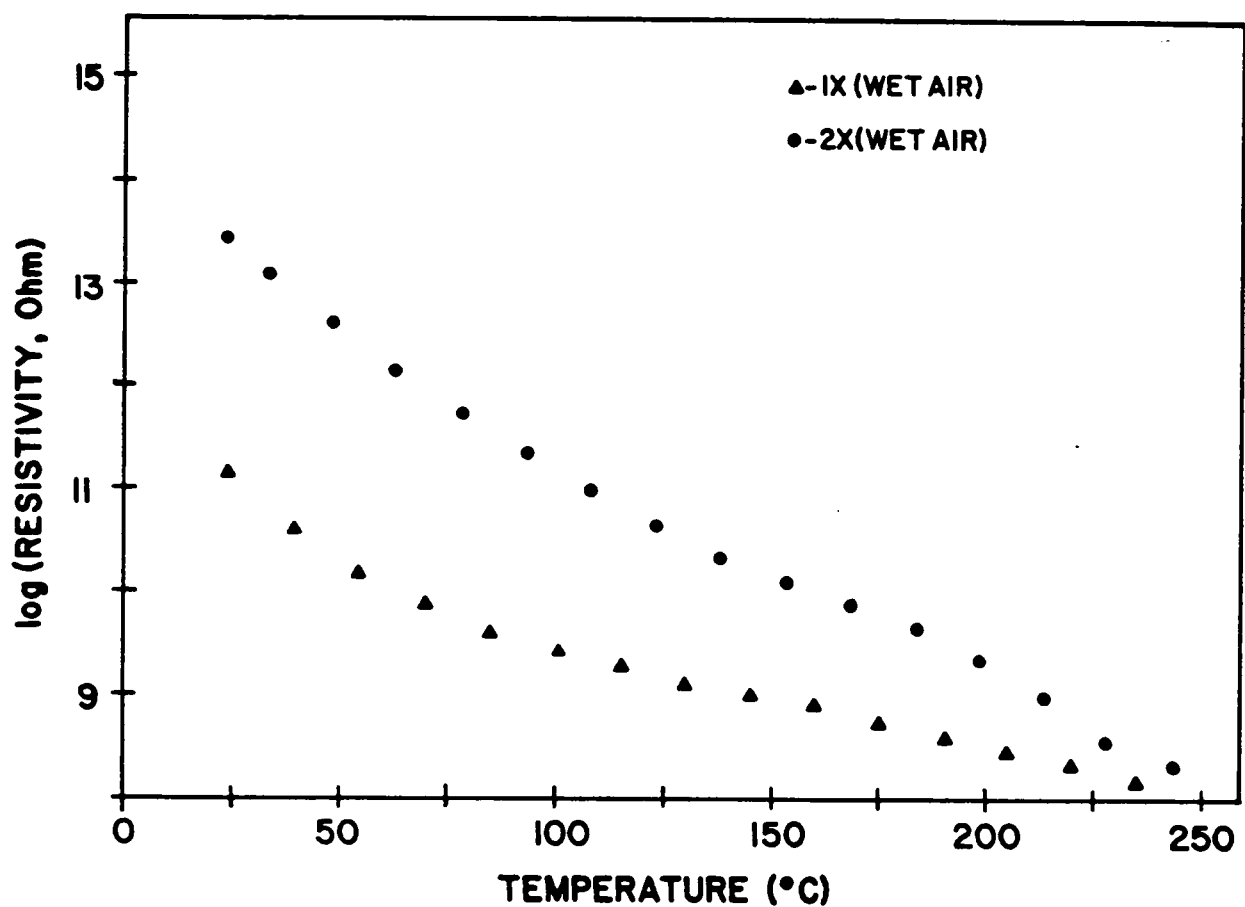


Figure 32. "Air-side" electrical resistivity as a function of temperature for the 1X-doped and 2X-doped wet-air-cured BTDA-ODA films.

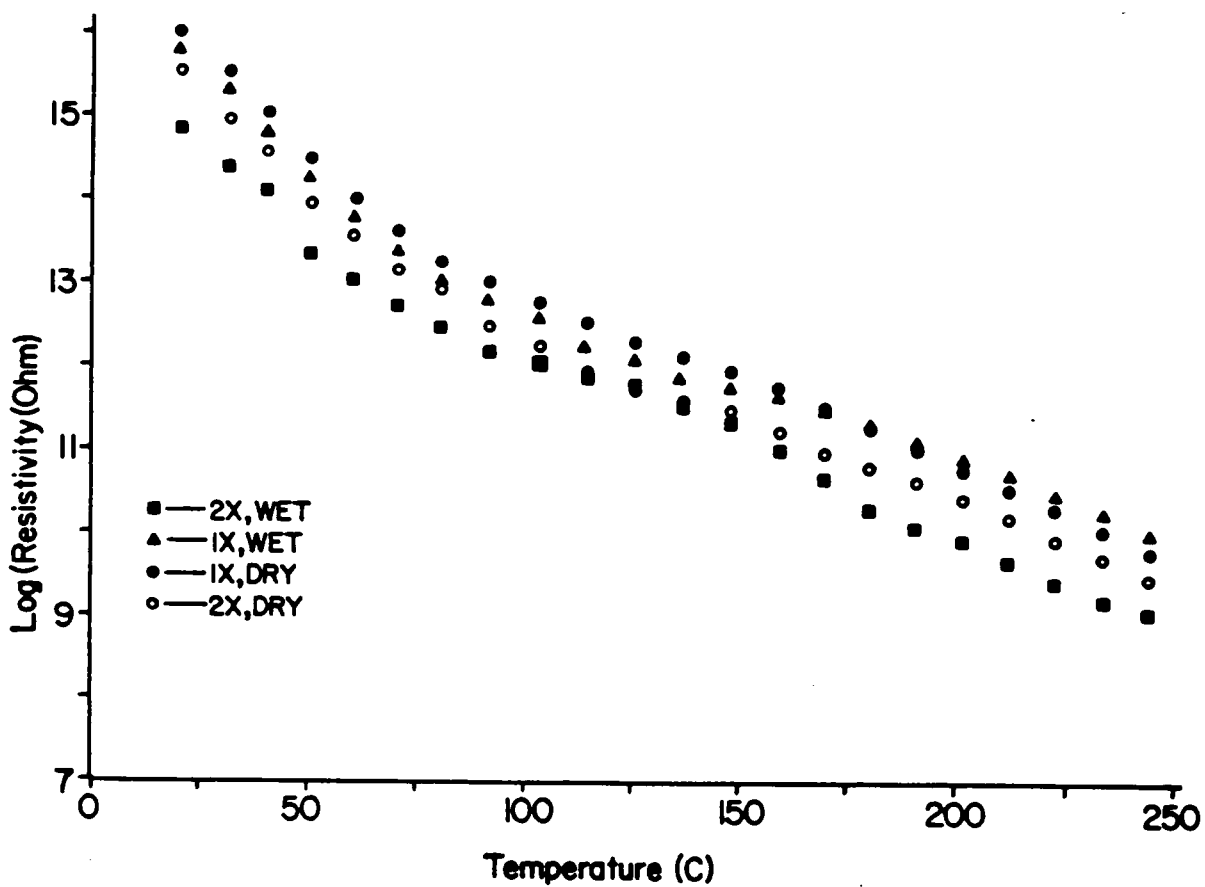


Figure 33. "Air-Side" electrical resistivity as a function of temperature for the  $\text{Cu}(\text{TFA})_2$ -doped BTDA-APB films.

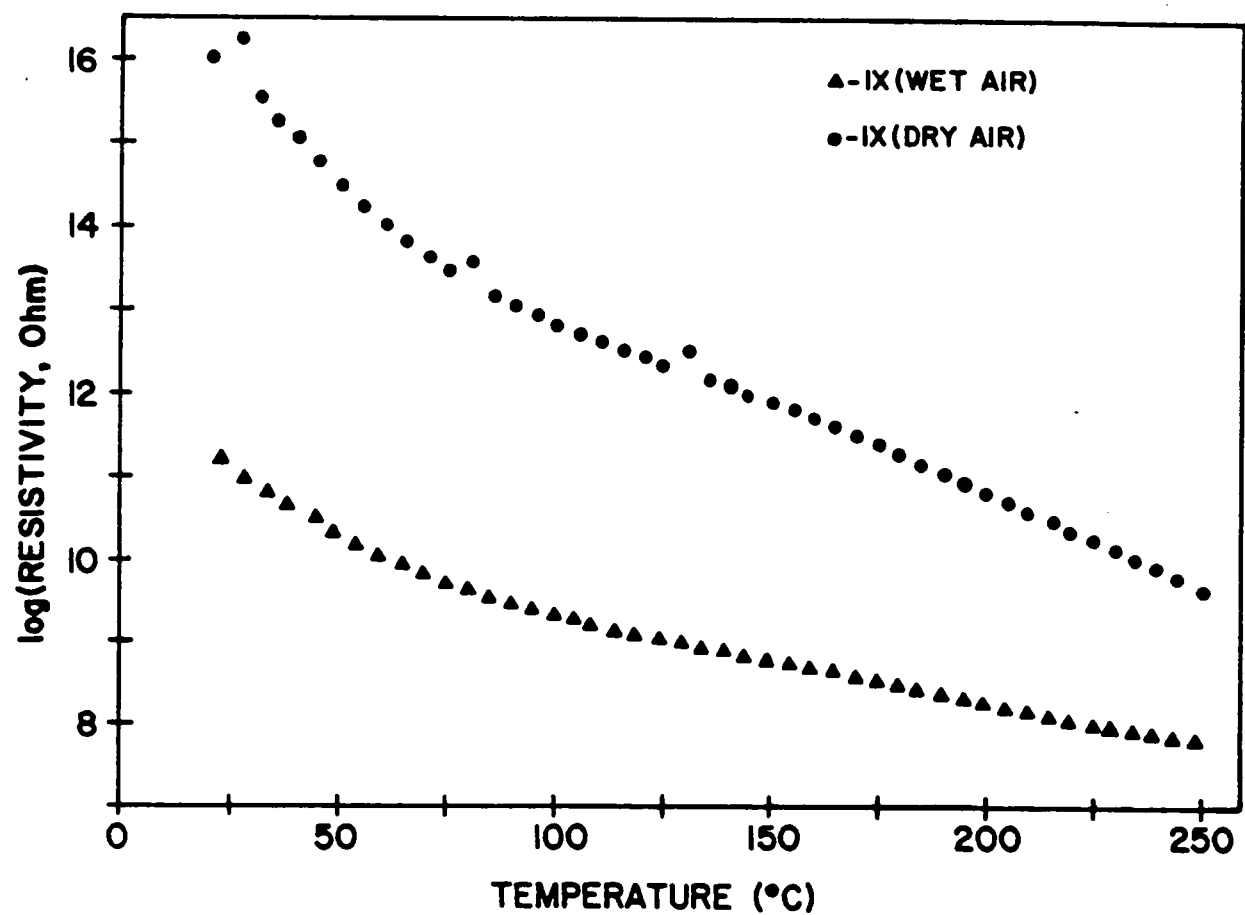


Figure 34. "Air-Side" electrical resistivity as a function of temperature for the wet-air-cured and dry-air-cured 1X-doped BTDA-ODA films.

## **VI. THE DEVELOPMENT OF PROCESS-PROPERTY RELATIONSHIPS FOR COPPER-DOPED BTDA-APB POLYIMIDE FILMS**

### **A. Preliminary**

It was shown in the previous chapters that surface or near-surface copper containing layers may be produced in polyimide films through the homogeneous incorporation of organo-copper complexes into the poly(amide acid) precursor prior to cure. The room temperature surface resistivities of these films exhibit up to a seven order of magnitude decrease relative to nondoped polyimide films. While this procedure yielded a significant increase in conductivity, the measured resistivities fall far short of those theoretically expected for the copper metal and copper oxide domains found. This is believed to be due to the poor inherent continuity that evolves during the production of these multi-layered systems. In order to improve our understanding of the process-property relationships encountered in the production of copper-doped polyimide films such that continuity of metal containing layers or deposits may be improved, surface migration maximized and near-theoretical resistivities attained, a method of statistically designed experimentation was implemented. A fractional factorial screening analysis of Plackett-Burman design was undertaken to provide such information. The majority of this Chapter has been allotted to the evaluation and discussion of this experimental technique.

### **B. The Statistical Experimental Design**

Factorial and fractional factorial design methodology have been used by a number of authors [64,65] to develop process-property relationships for numerous situations ranging from product yield or efficiency maximization to the

attainment of superior mechanical or chemical properties through processing. Potential advantages include (1) higher efficiency than one-factor-at-a-time experimentation. This increase in efficiency is manifested by larger gains in information per experiment (i.e. a smaller number of experiments are needed to produce equivalent amounts of information). (2) The minimization of error through hidden replication and randomization inherent in these designs. By randomizing experimental trials, bias error, whose numerical value tends to remain constant or follows a consistent pattern over time, is reduced to low levels. Also random error, whose numerical value changes from one moment to the next, is minimized by the moderate amount of replication that is introduced in the design. And (3) the ability to determine process variable interactions if present. In many situations, one-factor-at-a-time experimentation may give misleading conclusions in problems that have variable interactions.

The classical strategy is innately inadequate to handle these conditions. Yet, problems such as these are easily handled by factorial designs. The screening analysis used in this research provides the benefits of the former two, but has the disadvantage of assuming that interactions between processing variables are negligible. In this way, this approach affords considerable information with the minimum number of experiments. Screening designs are also useful in situations, such as this one, where the number of important processing variables is unknown. In the screening stage, one determines which variables are important and should be carried into future stages of more indepth study, while the remaining variables are discarded. "Discarded" means that the variable will be held constant at a convenient level or a level that is economically favorable.

It is important when defining a factorial experiment that one choose the most important processing variables. Table IX displays the process variables chosen

**Table IX**  
**Processing Variables Used in the Experimental Strategy**

<u>Processing Variable</u>	<u>Variable Range</u>	
	<u>Minima<sup>a</sup></u>	<u>Maxima<sup>b</sup></u>
Dopant Level	0.5X	2.0X
Cure Atmosphere	Moist Air	Dry Air
Casting Substrate	Glass	Polyimide
B-Stage Time	20 min.	120 min.
Conversion Temp.	200°C	300°C
Conversion Time	30 min.	120 min.

<sup>a</sup>Designated (-).  
<sup>b</sup>Designated (+).

for this design that have been shown to (or are thought to) influence the final structure and chemical composition of copper doped BTDA-APB films. The doped BTDA-APB matrix was chosen for this study because it is the simplest in terms of overall film structure and the chemistry which occurs in the formation of the conductive layer. For each processing variable, a suitable range (high and low) must be determined. In a screening analysis, a suitable choice of the range is critical due to the lack of midpoint correlation. In more elaborate designs (higher number of experiments), midpoint correlation provides information on any curvature of the response variable that may exist in the experimental region. The second column of Table IX exhibits the range chosen for each process variable under study.

A screening analysis of Plackett-Burman design was next implemented. A 12 X 12 design matrix was used which is known to be the most effective for less than seven processing variables.[66] Table X displays a portion of the design matrix (6 X 12) relative to the variables under study. Note the second column which exhibits experiment randomization and the hidden replication within the matrix (i.e. both high and low values are split equally (six) within each column). The six columns not shown in Table X are used to determine the mean and standard deviation of each dependent or "response" variable. Once each film has been characterized with respect to some property (dependent variable), the data are processed through relatively simple calculations which will not be discussed here but can be found elsewhere.[67]

### C. Process-Property Relationships

It will be useful to review the results of the previous Chapter in a limited way to emphasize the information provided by the experimental design. Several

Table X  
The Statistical Experimental Design

<u>Expt. Number</u>	<u>Expt. Sequence</u>	<u>Processing Variable<sup>a</sup></u>					
		1	2	3	4	5	6
1	3	-	-	+	-	-	-
2	5	-	+	-	-	-	-
3	10	+	-	-	-	+	+
4	1	-	-	-	+	+	+
5	8	-	-	+	+	+	-
6	9	-	+	+	+	-	+
7	11	+	+	+	-	+	-
8	12	+	+	-	+	-	-
9	6	+	-	+	-	-	+
10	7	-	+	-	-	+	-
11	4	+	-	-	+	-	-
12	2	+	+	+	+	+	+

<sup>a</sup> 1 = Dopant Level, 2 = Cure Atmosphere, 3 = Casting Substrate, 4 = B-stage Time, 5 = Conversion Temp., 6 = Conversion Time.

Cu(TFA)<sub>2</sub>-doped BTDA-APB films were produced prior to this study. Each film was comprised of a CuO deposit residing on the surface of the polyimide film. Table XI compares the experimental and calculated surface resistivities for a group of these copper-doped polyimide films. Surface resistivities up to four orders of magnitude less than the non-doped analogues are produced through this process. But compared to the calculated values a large discrepancy in the observed values is noted for the bilayered films. The discrepancy is due to poor continuity within the metal containing layer.

Table XII describes six properties which were used in characterizing certain aspects of the cured film's surface metal containing deposit. The processing variables that proved relevant in controlling the magnitude of the property (relative to a 90% confidence interval) are given in decreasing order of significance. The right-hand column displays the average values of each property for both processing extremes. From the information given in Table XII, the processing variables may be split into two groups that are defined by certain behavior. Group I, which consists of conversion temperature and dopant level, are processing variables that affect dopant migration/phase separation and are responsible for the amount of additive that reaches the surface of the film. For example at 200°C, the amount of solvent in the film along with the presence of a large amount of unreacted poly(amide acid) keeps the dopant solubilized in the polymer matrix. At this point migration is minimal and surface enrichment does not occur. But, at 300°C, the rate of imidization increases significantly depleting the bulk of poly(amide acid) functionality along with the loss of almost all solvent. When this occurs, a large portion of the additive becomes insoluble and phase separates within the matrix allowing the dopant that does not become trapped locally to migrate to the surface. Dopant level also affects surface enrichment by

Table XI

Surface Electrical Resistivities of Copper-Doped BTDA-APB Polyimide Films<sup>a</sup>

<u>Sample</u>	<u>Experimental (ohm)</u>	<u>Calculated (ohm)</u>
Prior Doped Films	1.1 X 10 <sup>14</sup> 5.2 X 10 <sup>15</sup>	1.0 X 10 <sup>9</sup> 1.3 X 10 <sup>9</sup>
Factorial Film #3	5.3 X 10 <sup>9</sup>	3.2 X 10 <sup>8</sup>
Post-Processed Film <sup>b</sup>	9.5 X 10 <sup>9</sup>	5.6 X 10 <sup>8</sup>

<sup>a</sup>T = 25°C, Applied Voltage = 100 VDC.

<sup>b</sup>T<sub>max</sub> = 350°C, Wet Air Cured, t<sub>max</sub> = 1 hr.

**Table XII**  
**Film Properties and the Influence of Processing Variables**

<u>Property Monitored</u> <sup>a</sup>	<u>Average Property Critical Variable</u>	<u>Extremes (Minima vs. Maxima)</u>
A. Surface Copper Concentration	1. Conversion Temp. 2. Dopant Level	[1.6 vs. 23.3 atom%] [10.8 vs. 15.9 atom%]
B. Surface Deposit Thickness	1. Conversion Temp.	[0 vs. 2540 Å]
C. Surface Electrical Resistivity	1. Conversion Temp. 2. Conversion Time	[10 <sup>13</sup> vs. 10 <sup>11</sup> ohm] [10 <sup>12</sup> vs. 10 <sup>11</sup> ohm]
D. Surface Fluorine Concentration	1. Dopant Level 2. Conversion Time 3. Cure Atmosphere	[1.4 vs. 11.1 atom%] [9.4 vs. 3.1 atom%] [8.3 vs. 4.1 atom%]
E. Types of Surface Fluorine <sup>b</sup>	1. Cure Atmosphere 2. Conversion Time 3. Conversion Temp.	2 vs. 1 1 vs. 0 1 vs. 2
F. Surface CuO	1. Conversion Temp. 2. Cure Atmosphere	[40 vs. 99 % CuO] [30 vs. 95 % CuO]

<sup>a</sup>Cured Film.

<sup>b</sup>Inorganic or Organic fluorine.

increasing the localized additive concentration at any point within the film. The results listed in Table XII support this notion in that greater conversion temperature increases the amount of copper present, the amount of fluorine present and the thickness of the surface copper deposit. Higher dopant level is also shown to increase the amount of copper and fluorine present. Conversion temperature would therefore be expected and is observed to indirectly influence the measured surface electrical resistivity.

A second group of variables may also be defined that affect the chemical state of the copper enriched surface. Scheme 2 of Chapter IV exhibited a proposed reaction pathway for the decomposition of  $\text{Cu(TFA)}_2$ . In the presence of high temperature and atmospheric  $\text{O}_2$  and/or  $\text{H}_2\text{O}$ ,  $\text{Cu(TFA)}_2$  may undergo decomposition directly to  $\text{CuO}$ . Alternatively, high temperature may first induce the decomposition of  $\text{Cu(TFA)}_2$  to  $\text{CuF}_2$  which may then undergo hydrolysis/dehydration to  $\text{CuO}$ . Inorganic fluorine has been detected on the surface of a number of films, albeit in small amounts, and only in the presence of significant quantities of organic fluorine which serves as an elemental tag for the unreacted dopant. Figure 35 displays the XPS F(1s) spectrum of a film that contains both surface organic (688.1 eV) and inorganic fluorine. The inorganic fluorine photopeak appears at approximately 684.0 eV very close to the reported value of 684.1 eV for  $\text{CuF}_2$ . [68] Accordingly, a small  $\text{Cu}(2p_{3/2})$  photopeak appeared at approximately 936.8 eV. [68] Curing atmosphere and conversion time both may affect this reaction scheme. The use of moist air should propel the reaction toward higher  $\text{CuO}$  formation independent of which reaction route is followed. Whereas, the use of dry air may considerably slow both reactions.

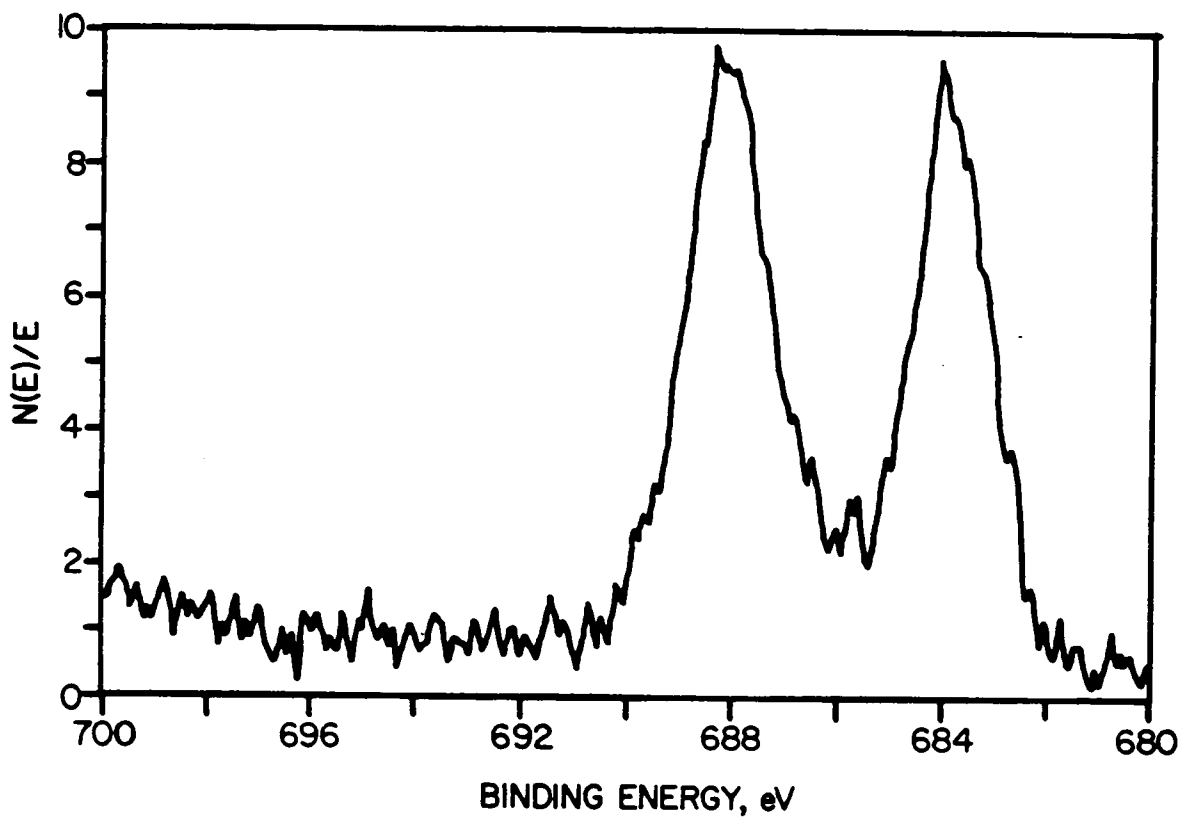


Figure 35. The XPS F(1s) spectrum of a sample which contains both inorganic and organic fluorine components.

Conversion time is considered to be a kinetic effect, whereby subjecting the sample to the curing atmosphere for extended periods of time results in near-complete formation of CuO from Cu(TFA)<sub>2</sub>.

Of the six process variables initially studied, four either affect the continuity or the chemical state of the surface copper-containing layer. The length of the B-stage and the type of casting substrate have a negligible effect on these properties. Sample #3 of the factorial design exemplifies the optimal conditions suggested to produce the most continuous and conductive film. Processing conditions were 2X doping level, moist-air-curing atmosphere, 300°C conversion temperature, and 2 hr conversion time. The measured surface resistivity has been reduced greatly (Table XI) compared to the films produced prior to the application of the statistical design. The amount of surface copper (~30 at. %) and the thickness of the CuO layer (~3100 Å) relative to those previously produced (~25 at. %) and (~500 Å) partly account for the observed decrease. The theoretical resistivity is nearly attained by sample #3. Unlike those films produced earlier, the continuity of the CuO layer is greatly enhanced allowing for a more efficient conductive pathway through the surface of the film.

Although surface resistivity is reduced, sample #3 had relatively poor mechanical properties. The film was brittle and exhibited extreme surface phase separation. Figure 36 show the lamellar type surface phase separation as observed by optical microscopy. Alternating domains of surface CuO and polyimide are present on a large scale. Auger lines scans (Figure 37) of the surface reveal that the pitted regions consist of CuO while the smooth regions are polyimide. This behavior is only observed for this particular film and is not present in the others produced in the factorial design. In all other cases where a

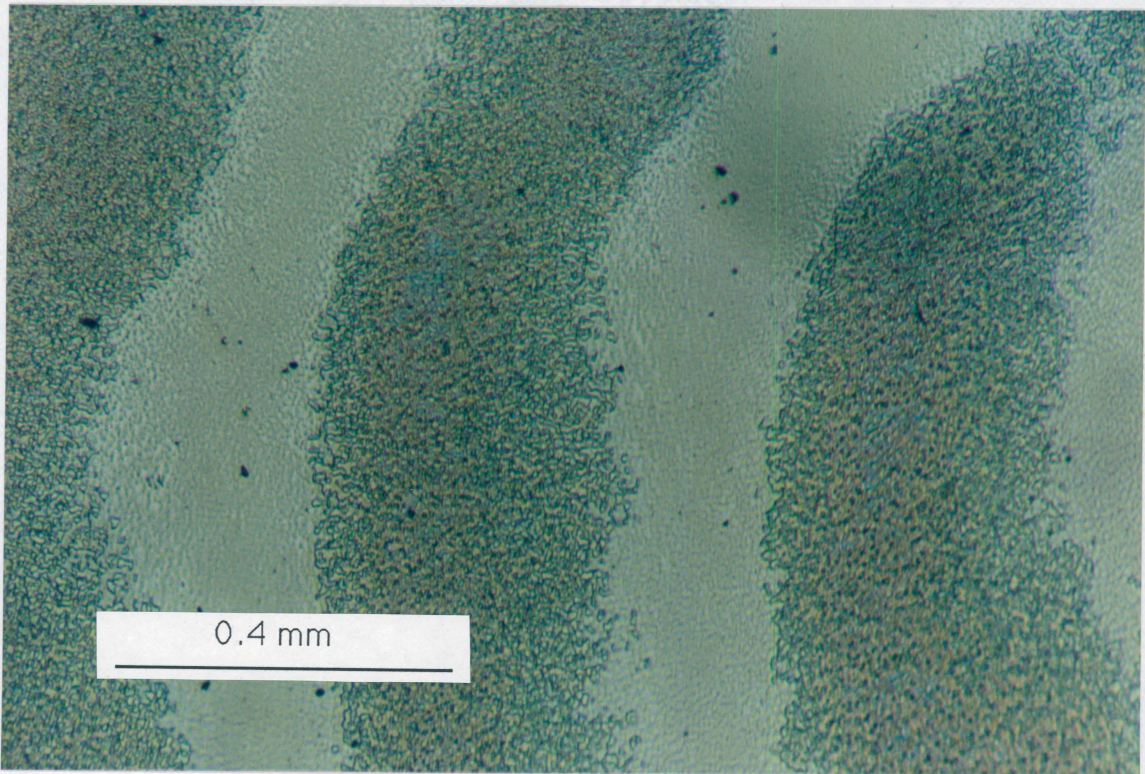


Figure 36. Optical micrograph of factorial sample #3.

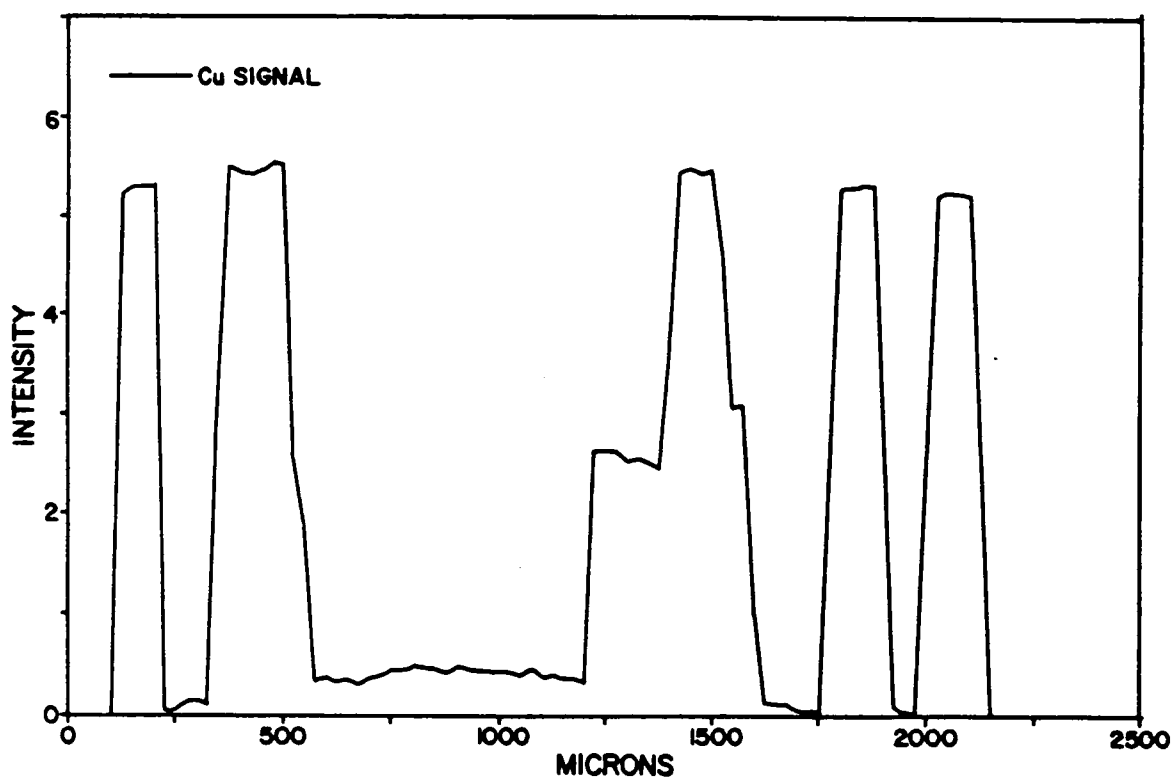


Figure 37. Auger electron spectroscopic line scan of the "air-side" surface of factorial sample #3.

significant surface copper concentration is present, copper oxide and/or  $\text{Cu}(\text{TFA})_2/\text{CuF}_2$  is homogeneously dispersed on the polyimide surface. No lateral surface phase separation is observed. Previously, it has been reported that the presence of moisture increases the modulus of fully cured non-doped polyimides.[58] This phenomenon may occur in the doped films thereby causing an increase in the internal stresses that might result in irregular phase separation. This would be most likely for sample #3 where the extent of imidization would be at its highest (300°C for 2 hours) in the presence of moist air. Several portions of sample #3 also exhibited internal cohesive failure supporting the notion of high stress build-up (i.e. circular portions of the film were peeled away from an intact layer in contact with the glass plate).

In addition to the room temperature electrical properties, each of the films produced in the factorial design was studied at elevated temperatures. Surface resistivity of the atmosphere-side of each film was determined in vacuum as a function of temperature using a guarded electrode system (Figure 38). The resistivity data from the first heating and cooling cycles are summarized in Table XIII. Because sample #3 was extremely brittle it could not be reliably evaluated by this electrical method. Thus, the formal statistics could not be applied to these samples but the effect of each level (high or low) of a particular processing variable could still be assessed. For example, averaging the air-side resistivity data determined during the first cooling cycle for each of the conversion temperatures reveals that films cured to 300°C have a much lower surface resistivity than those cured only to 200°C ( $6.6 \times 10^{10}$  versus  $2.8 \times 10^{14}$  ohm). No other variable investigated has an affect on the atmosphere-side resistivity that is this large.

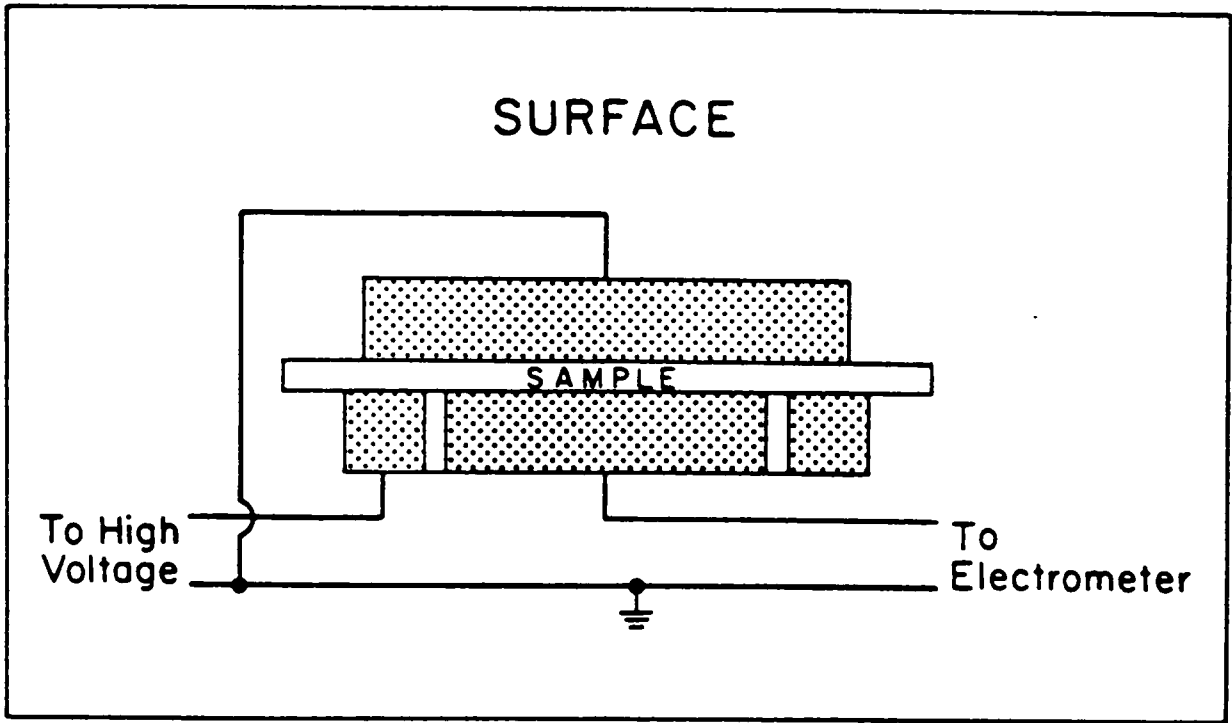


Figure 38. Guarded electrode geometry for surface resistivity measurements.

Table XIII

D.C. Electrical Properties of Cu(TFA)<sub>2</sub>-Modified BTDA-APB Polyimide Films

<u>Trial</u>	<u>Log<sub>10</sub></u> <u>[Surface Resistivity (ohm) at 175°C]</u>		<u>Hysteresis</u>	<u>Conversion</u>
	<u>First Heat.</u>	<u>First Cool.</u>		<u>Temperature(°C)</u>
1	13.8	14.9	-	200
2	14.5	15.4	-	200
3				300
4	12.3	11.2	+	300
5	11.5	10.3	+	300
6	14.4	15.4	-	200
7	14.2	12.3	+	300
8	12.0	14.4	-	200
9	15.1	15.0	-	200
10	11.2	9.5	+	300
11	11.7	11.6	+	200
12	12.6	10.8	+	300

It has already been shown that conversion temperature is responsible for the phase separation of the dopant in the polyimide matrix thereby influencing the size and continuity of the surface CuO layer. In contrast to the resistivity determined during the first cooling cycle, the resistivity determined during the first heating cycle was not dependent upon any of the variables investigated. The reason for this behavior is that the first cooling cycle and subsequent heating/cooling cycles result in similar surface resistivities but each is markedly different from that obtained during the first heating cycle creating a hysteresis loop (Figure 39). To assess this electrical hysteresis, the ratio of the resistivity determined at 175°C during the first heating cycle ( $P_H$ ) to that determined at 175°C during the first cooling cycle ( $P_C$ ) was evaluated and for simplicity was called either "+" ( $P_H > P_C$ ) or "-" ( $P_H < P_C$ ). All samples cured to 300°C have positive hysteresis while those cured only to 200°C, in general, had negative hysteresis (Figure 39).

The explanation for the greater resistivity observed during the first cooling cycle compared to the first heating cycle was thought to be due to factors such as residual solvent, residual water of imidization and possibly a lower glass transition temperature in the partially cured (200°C) films. Thermogravimetric analysis revealed that the films cured to 200°C had a greater mass loss upon heating to 250°C compared to those previously cured to 300°C (Figure 40). This mass loss can be due to both residual solvent (DMAC) and residual water of imidization. Direct identification of either cannot be obtained from the thermogravimetric experiment. In fact, some mass loss may be due to sublimation of  $\text{Cu}(\text{TFA})_2$ ; but previous evidence (Chapter IV) has shown this, if a reality, to be very small. However, differential scanning calorimetry verifies that the polymer films cured to 200°C are only partially imidized because the polymer

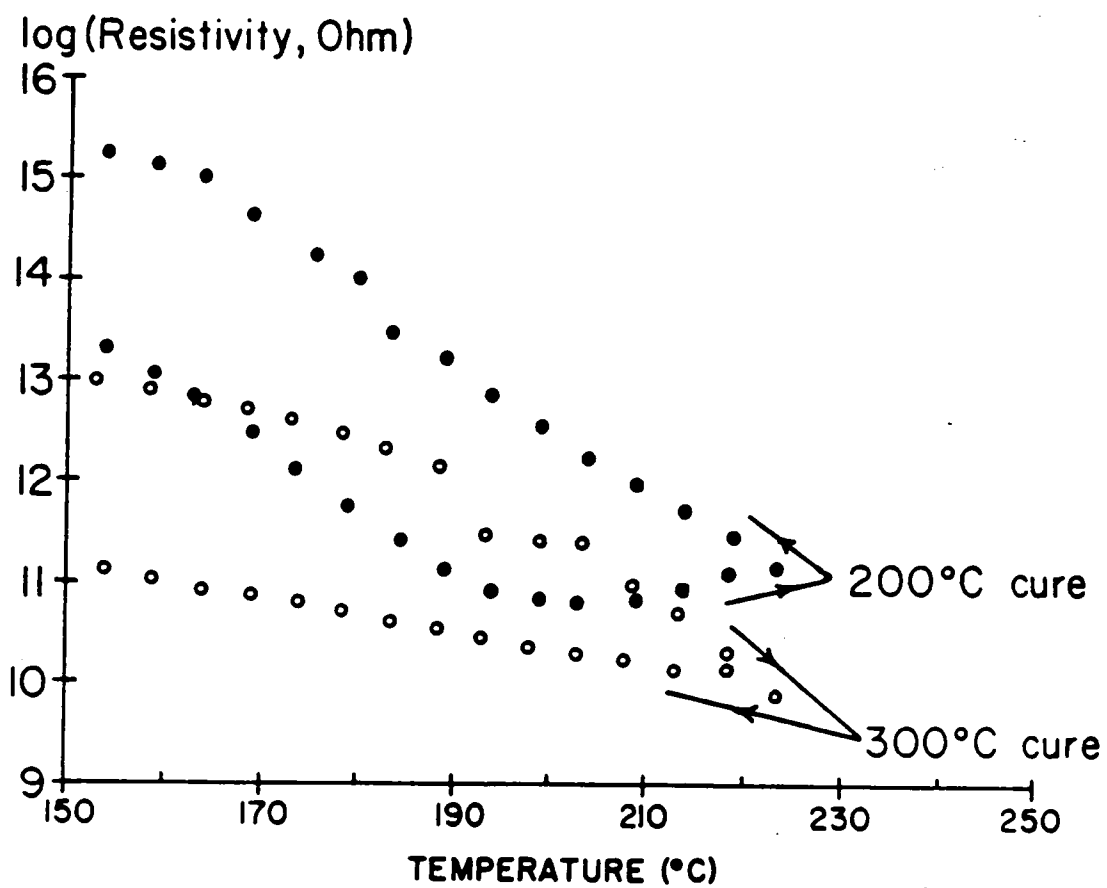


Figure 39. Resistivity versus temperature for  $\text{Cu}(\text{TFA})_2$  modified BTDA-APB films cured to 200°C and 300°C.

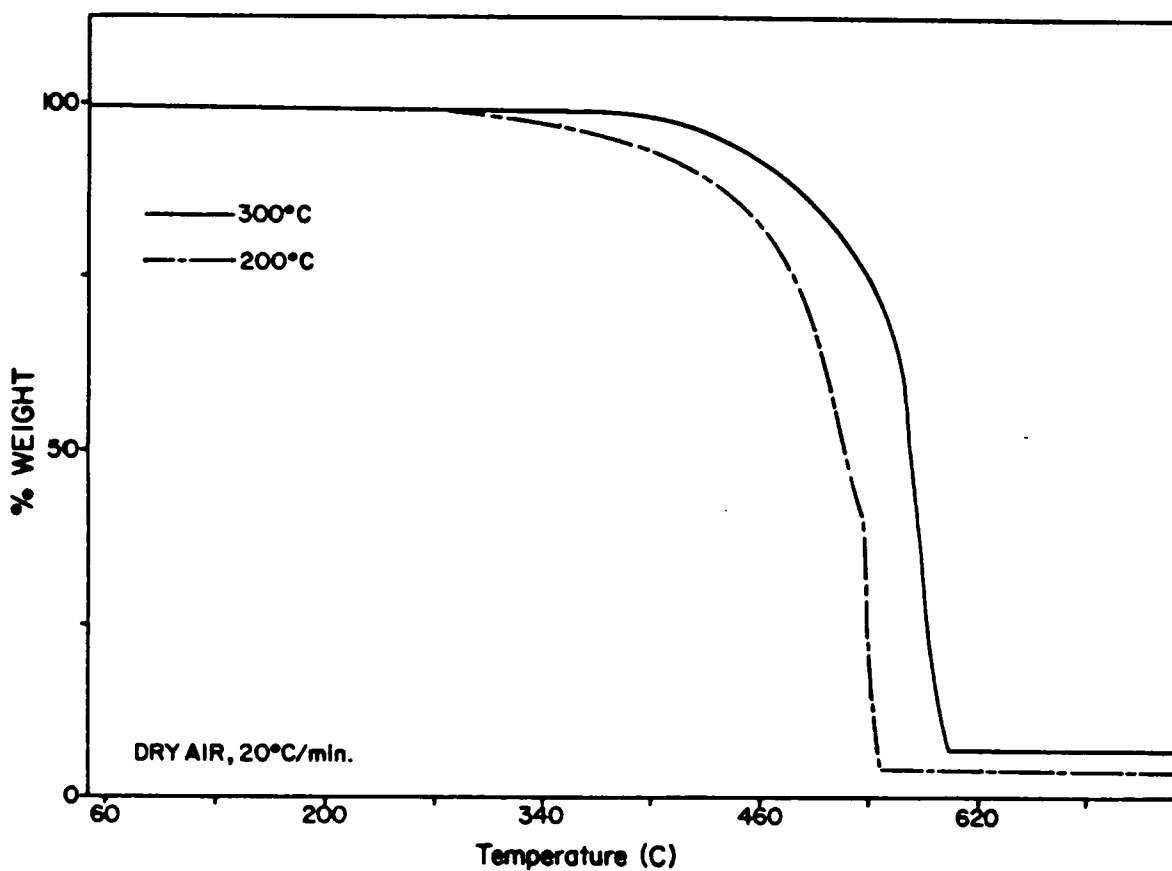


Figure 40. The thermogravimetric profile of  $\text{Cu}(\text{TFA})_2$  modified BTDA-APB films cured to  $200^\circ\text{C}$  and  $300^\circ\text{C}$ .

glass transition temperature shifts from an average value of 165°C during the first heating cycle to 199°C during the second heating cycle (Figure 41). The films cured to 300°C have glass transitions at 199°C and 200°C for the first and second heating cycles, respectively (Figure 42). Thus, the hysteresis is most likely due to the decrease in charge carrier concentration ( $H^+$ ,  $OH^-$ ) and a decrease in charge carrier mobility resulting from both the decrease in solvent content (plasticizer) and increase in polymer glass transition temperature (polymer viscosity) which occur upon heating these samples to temperatures above 200°C in the electrode system.

#### D. High Temperature Processing of Copper-Doped BTDA-APB

##### Polyimide Films

The factorial design provided four processing conditions that determine the observed structure and electrical properties of copper-doped BTDA-APB polyimide films. Metal-modified films were produced with significantly lower surface resistivities than those produced prior to the use of the factorial design, although poor mechanical properties were obtained by utilizing the optimum processing conditions. In some cases, a problem such as this may be overcome by applying the processing conditions beyond the boundaries set within the factorial design. In this way, one anticipates increased effectiveness from conditions already known to be important. In most cases increasing the conversion temperature was followed by an improvement in the specific property under inspection. Thermal processing to even higher temperatures than those defined in the factorial design was therefore undertaken. In this regard, several 2X copper-doped films were initially produced in wet-air and cured to a maximum of 300°C for 0.5 hr. At this point, the films were "post-processed" at 350°C, in

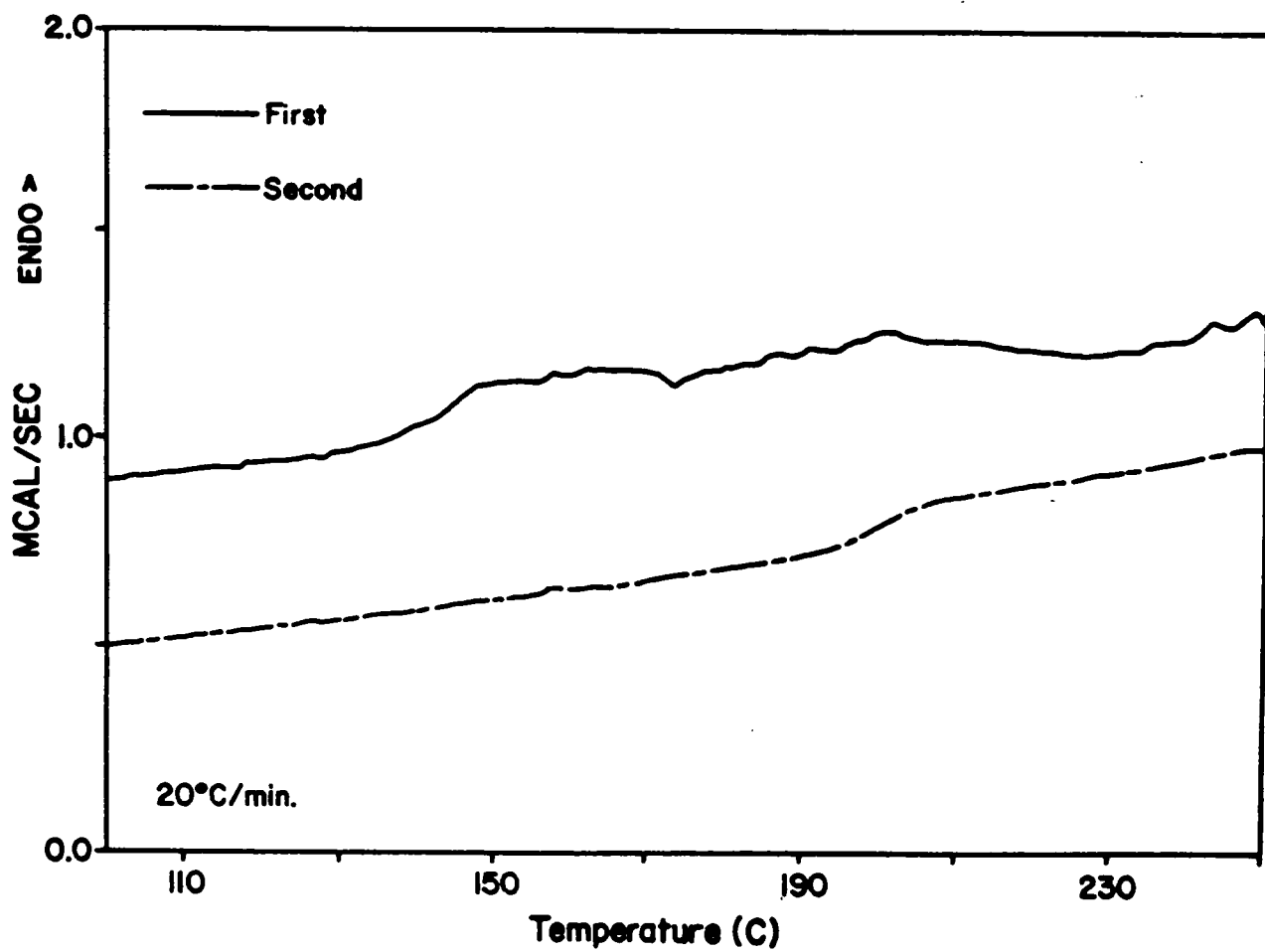


Figure 41. Differential scanning calorimetric analysis of a  $\text{Cu}(\text{TFA})_2$  modified BTDA-APB film cured to  $200^\circ\text{C}$ .

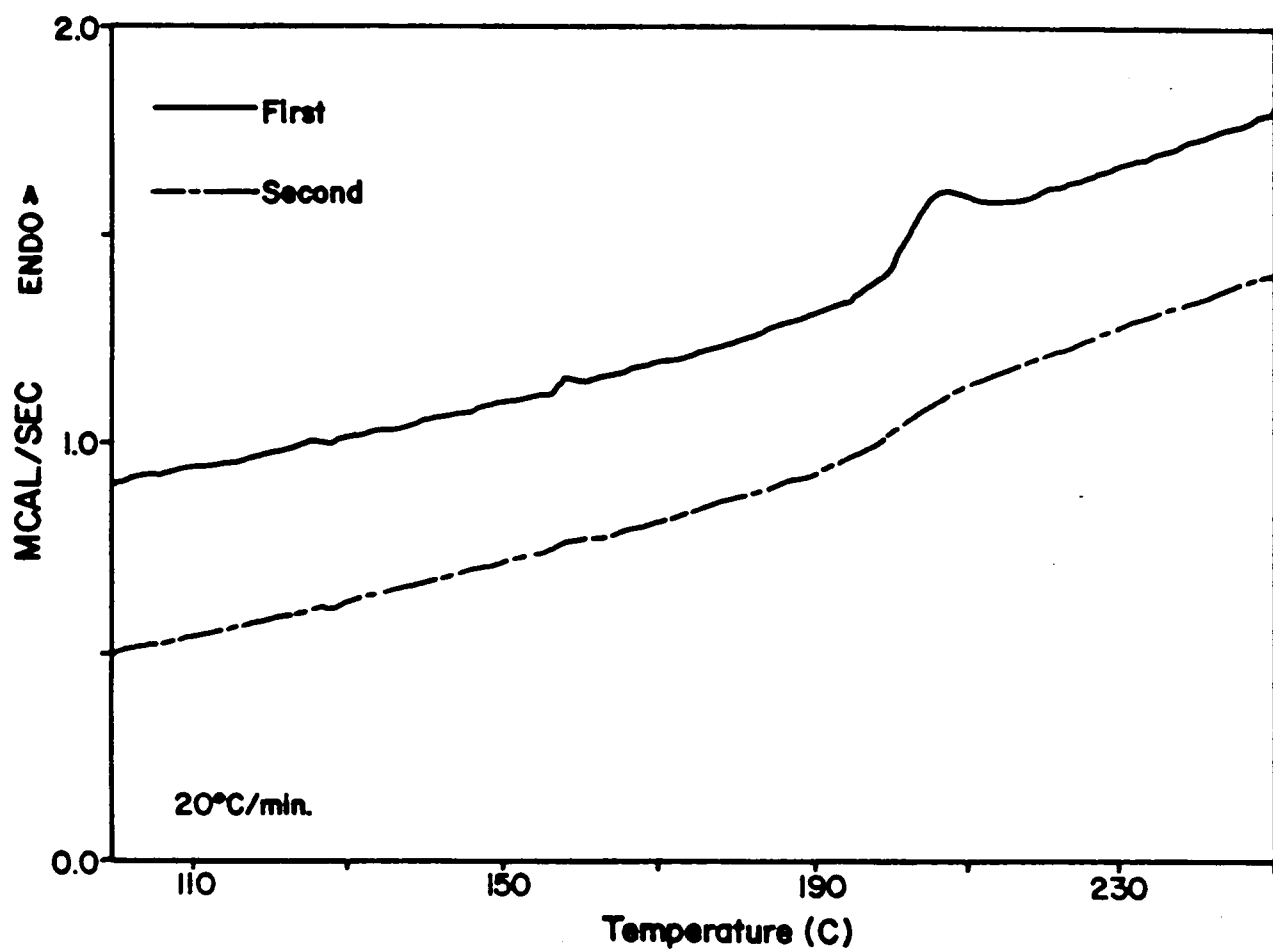


Figure 42. Differential scanning calorimetric analysis of a  $\text{Cu}(\text{TFA})_2$  modified BTDA-APB film cured to  $300^\circ\text{C}$ .

wet-air for an additional hour. Table XI compares the surface resistivities of a post-processed film with sample #3 of the factorial design. Upon inspection, post-processing produced a film with a resistivity as low as the best film produced in the factorial experiment. Comparing the experimental and calculated resistivities suggested that the continuity of the surface layer in the post-processed film approaches that of a wholly continuous medium. These properties are obtained with the added benefit of much improved mechanical properties. The films were more flexible and did not exhibit unusual surface phase separation. Figures 43 and 44 show the effect that post-processing had on the surface structure of these films. In each case, a comparison is made between a film prior to and after post-processing. Secondary electron microscopy (Figure 43) reveals an increase in the surface concentration of copper domains following additional cure. An increase in the thickness of the copper oxide layer from approximately 700 Å to 1300 Å is noted by transmission electron microscopy (Figure 44). The continuity of the CuO layer is also greater within the post-processed film, apparently formed from particles of much greater size. In this respect, post-processing could be considered analogous to sintering; wherein, small particles fuse to become a large solid mass.

If post-processing to 350°C produces superior films, it may be asked if higher cure temperatures might produce even better results. Post-processing to 400°C in air for up to one hour was attempted. But in each case the respective film exhibited significant decomposition and a drastic reduction in film thickness was observed (Table XIV). Films post-processed at 400°C for longer than one hour displayed total loss of integrity depositing a thin layer of copper oxide on the glass casting substrate. This behavior results from the fact that film thermo-oxidative stability is reduced upon doping by approximately 100°C as compared

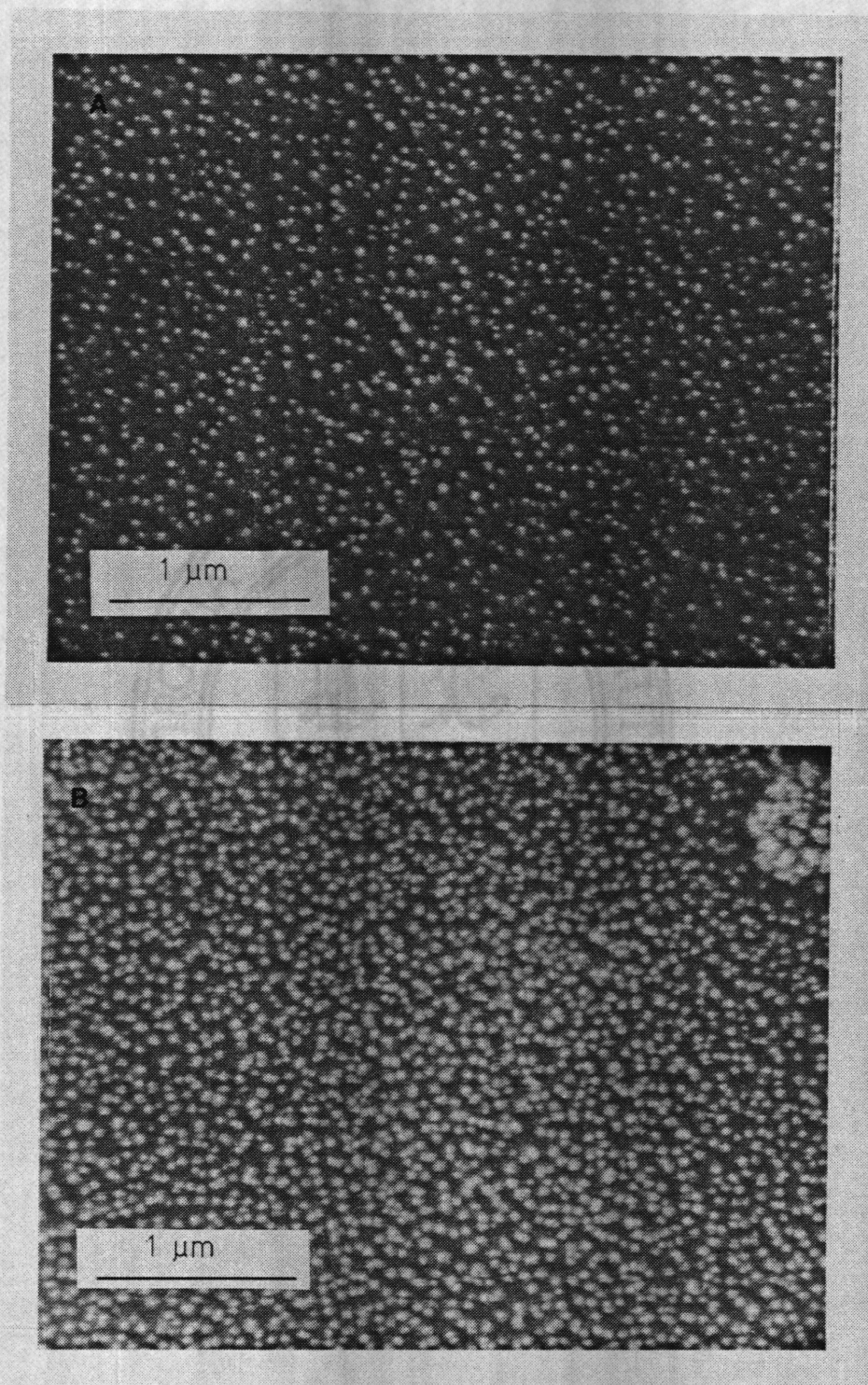


Figure 43. Scanning electron micrographs of a 2X-doped wet-air-cured BTDA-APB film (A) before and (B) after post-processing.

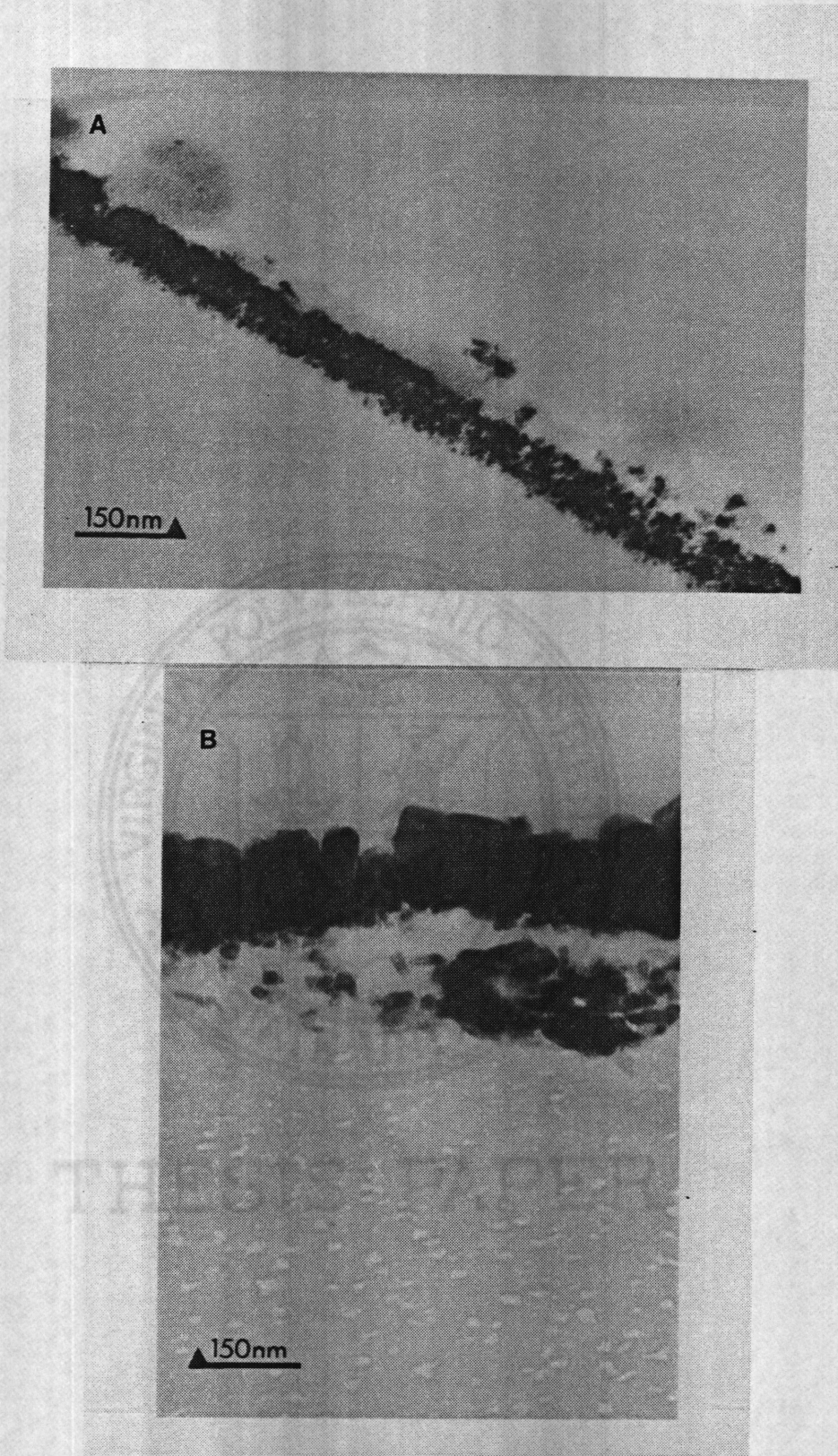


Figure 44. Transmission electron cross sections of the surface region of a 2X-doped wet-air-cured BTDA-APB film (A) before and (B) after post processing.

Table XIV

## General Characteristics of Post-Processed BTDA-APB Polyimide Films

<u>Sample</u>	<u>Post-Processing</u> <sup>a</sup>	<u>Color</u>	<u>Flexible</u>	<u>Film Thickness</u>
Dry Air/1X Doped	No	Gray	Yes	39.9 $\mu$
" "	Yes	Gold	Yes	23.0 $\mu$
Dry Air/2X Doped	No	Gray	Yes	36.4 $\mu$
" "	Yes	Gold	Yes	25.1 $\mu$
Dry Air/Nondoped	No	Yellow	Yes	41.7 $\mu$
" "	Yes	Amber	Yes	40.4 $\mu$

<sup>a</sup>T = 400°C for 1 hr in dry air.

to the non-doped films (Figure 45). As stated in Chapter V this is a result of a dopant-catalyzed decomposition mechanism. Post-processing then may be considered to have a ceiling temperature of about 350°C for copper-doped BTDA-APB films in an air atmosphere.

It has been shown in Chapter V that thermal stability in an inert atmosphere is ordinarily 50°C higher than the thermo-oxidative stability. Post-processing in a nitrogen curing atmosphere was therefore undertaken. It was found that films could be post-processed for longer periods of time at the elevated temperatures in nitrogen without any deleterious effects. Processing the films for longer time periods at 350°C or above allowed more dopant to migrate to the surface due to increased mobility at these temperatures. Consequently, the thickness of the surface CuO deposits were enhanced to even a greater extent than that observed for films post-processed in air (Table XV). However, films cured at 400°C still exhibited deterioration in nitrogen although at significantly slower rates. Reductions in film thickness of approximately 10% were observed for the samples post-processed in nitrogen for 1 hr compared to an approximate 30% reduction in films post-processed in air.

Analogous to the structural changes observed, the chemical composition of the surface copper containing layer is also altered relative to films post-processed in air. XPS has determined that the surface layer of films post-processed in nitrogen is formed from a mixture of CuO and Cu(0). Figure 46 exhibits the XPS Cu(2p) photopeak region of a Cu(TFA)<sub>2</sub>-doped BTDA-APB film post-processed in nitrogen for 2 hr at 350°C. The knees displayed on the right of the intense Cu(2p<sub>1/2,3/2</sub>) photopeaks indicate that copper metal is a minor component in a copper metal-copper oxide mixture. This was typical of all films post-processed in a nitrogen atmosphere. Curve resolution of the Cu(2p<sub>1/2</sub>)

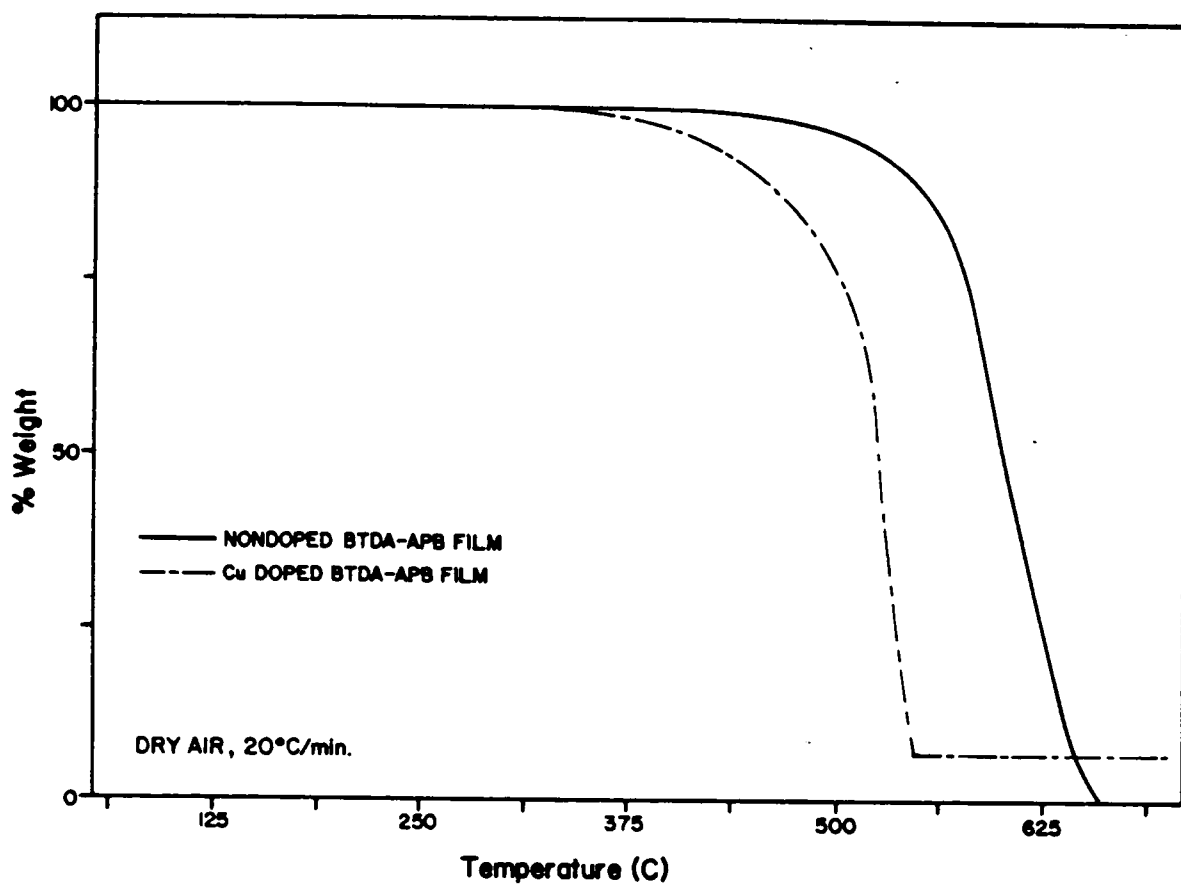


Figure 45. The thermogravimetric profile of  $\text{Cu}(\text{TFA})_2$ -doped and nondoped BTDA-APB films cured to  $300^\circ\text{C}$ .

Table XV

Morphological Features of Post-Processed<sup>a</sup> BTDA-APB Films as Deduced from TEM Data

<u>Sample</u>	<u>Post-Processing Atmosphere</u>	<u>CuO Layer Thickness (Å)</u>
Dry Air/1X Doped	Dry Air	2210
" "	Nitrogen	2750
Dry Air/2X Doped	Dry Air	2530
" "	Nitrogen	2830

<sup>a</sup>T=400°C for 1 hr.

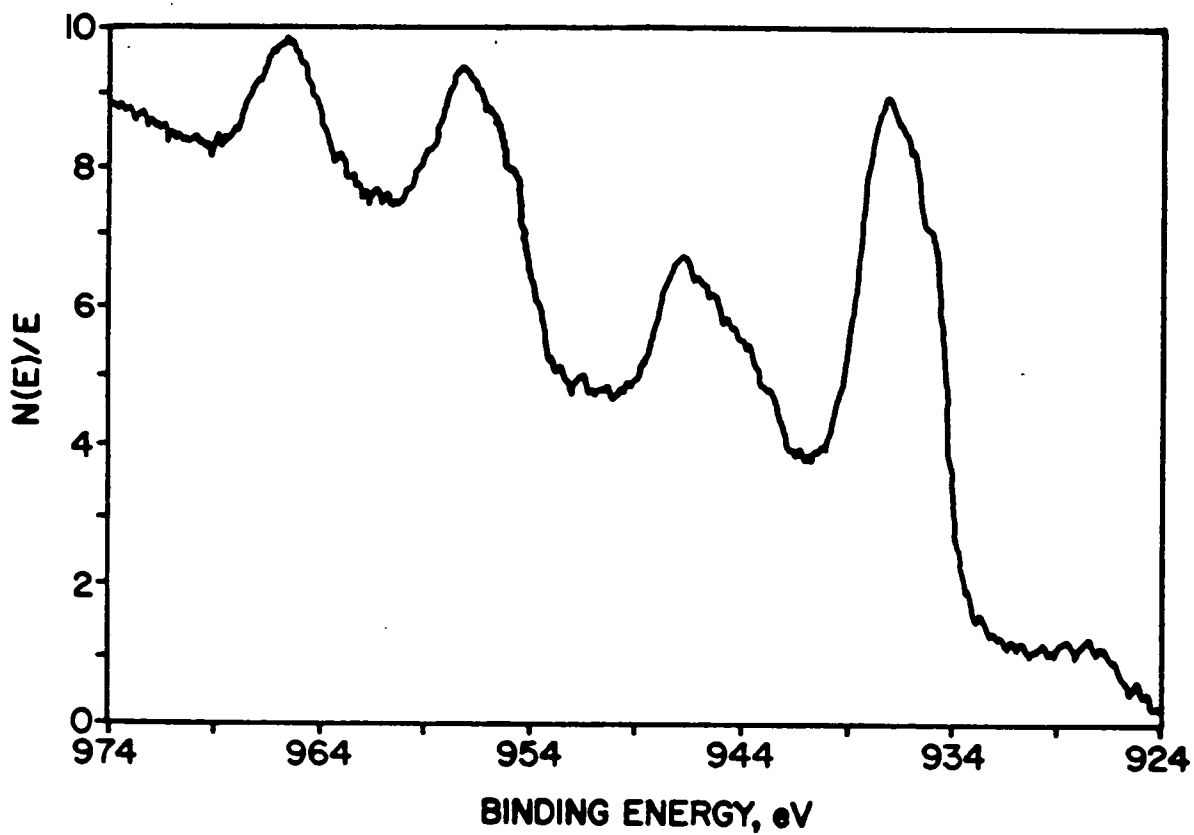


Figure 46. The XPS Cu(2p) spectrum of a 2X-doped dry-air-cured BTDA-APB film post-processed in nitrogen.

photopeak suggests that roughly 20% of the copper present on or near the surface is in the metallic state. As would be expected, the change in surface composition reduced the experimental surface resistivity by two orders of magnitude relative to films post-processed in air (Table XVI). A better than theoretical resistivity value is obtained assuming the surface layer was composed of homogeneous CuO. A number of films were post-processed at elevated temperatures in nitrogen for different periods of time, yet resistivities on the order of  $10^7$  ohm-cm were the lowest realized. The presence of both metallic copper and copper oxide in the surface region implies that the dopant first thermally decomposed to metal and subsequently partially formed the oxide in reaction with the water of imidization. However, some oxidation of the metallic copper component may have occurred when the sample was exposed to the laboratory atmosphere prior to analysis.

#### E. High Temperature Processing of Copper-Doped BTDA-ODA

##### Polyimide Films

Although the factorial design was limited to the study of one polymeric system (BTDA-APB), the important processing variables would likely be applicable to other doped polyimide matrices. The use of BTDA-ODA as the doped matrix, under appropriate conditions, produces either a bi-layered or tri-layered composite which contains copper oxide or copper metal surface strata respectively. BTDA-ODA is therefore more complex, in terms of processability than BTDA-APB polyimide. One variable that introduces this complexity is the surface structure dependence on the percent solids of the  $\text{Cu}(\text{TFA})_2/\text{poly}(\text{amide acid})$  solution. Figures 47, 48, and 49 display the effect of percent solids on the

Table XVI

Surface Electrical Resistivities of Cu(TFA)<sub>2</sub>-Doped BTDA-APB Polyimide Films<sup>a</sup>

<u>Sample</u>	<u>Experimental (ohm)</u>	<u>Calculated (ohm)</u>
Prior Doped Films	1.1 X 10 <sup>14</sup>	1.0 X 10 <sup>9</sup>
	5.2 X 10 <sup>15</sup>	1.3 X 10 <sup>9</sup>
Post-Processed Film <sup>b</sup>	9.5 X 10 <sup>9</sup>	5.6 X 10 <sup>8</sup>
Post-Processed Film <sup>c</sup>	5.0 X 10 <sup>7</sup>	1.0 X 10 <sup>8</sup>

<sup>a</sup>T = 25°C, Applied Voltage = 100 VDC.<sup>b</sup>T<sub>max</sub> = 350°C, Wet Air Cured, t<sub>max</sub> = 1 hr.<sup>c</sup>T<sub>max</sub> = 350°C, N<sub>2</sub> cured, t<sub>max</sub> = 1 hr.

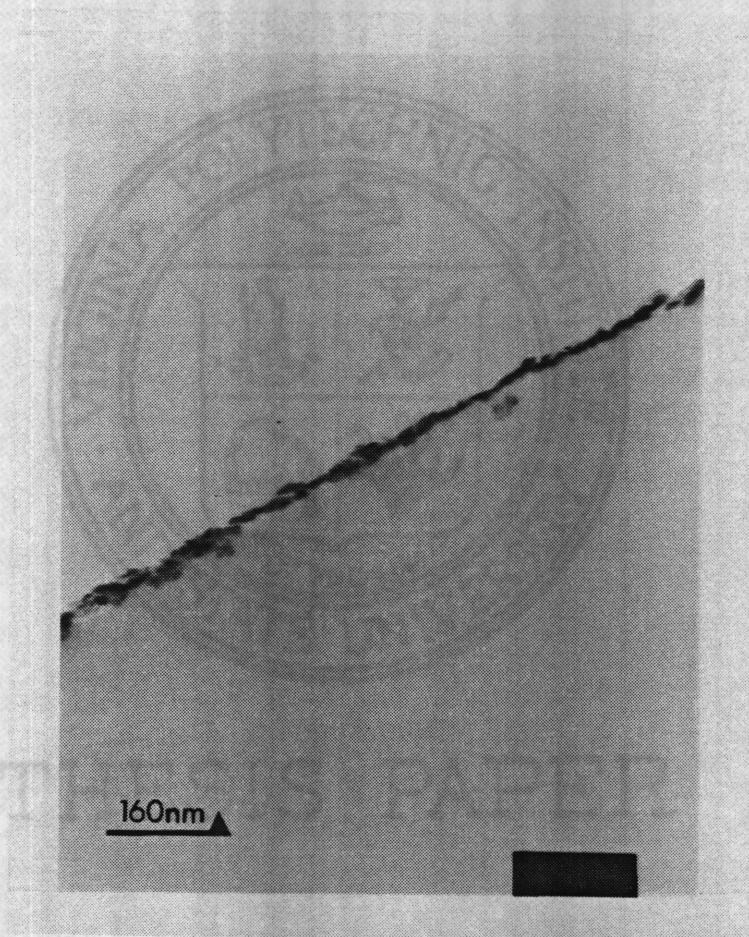


Figure 47. Transmission electron cross section of the surface region of a 20% solids 1X-doped wet-air-cured BTDA-ODA film.

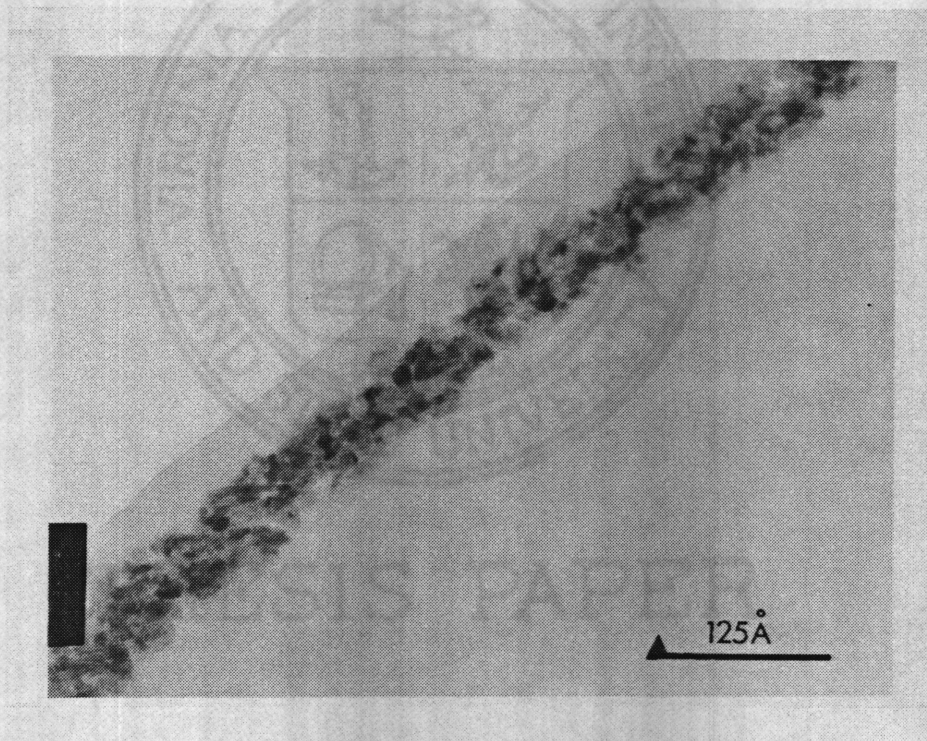


Figure 48. Transmission electron cross section of the surface region of a 23% solids 1X-doped wet-air-cured BTDA-ODA film.

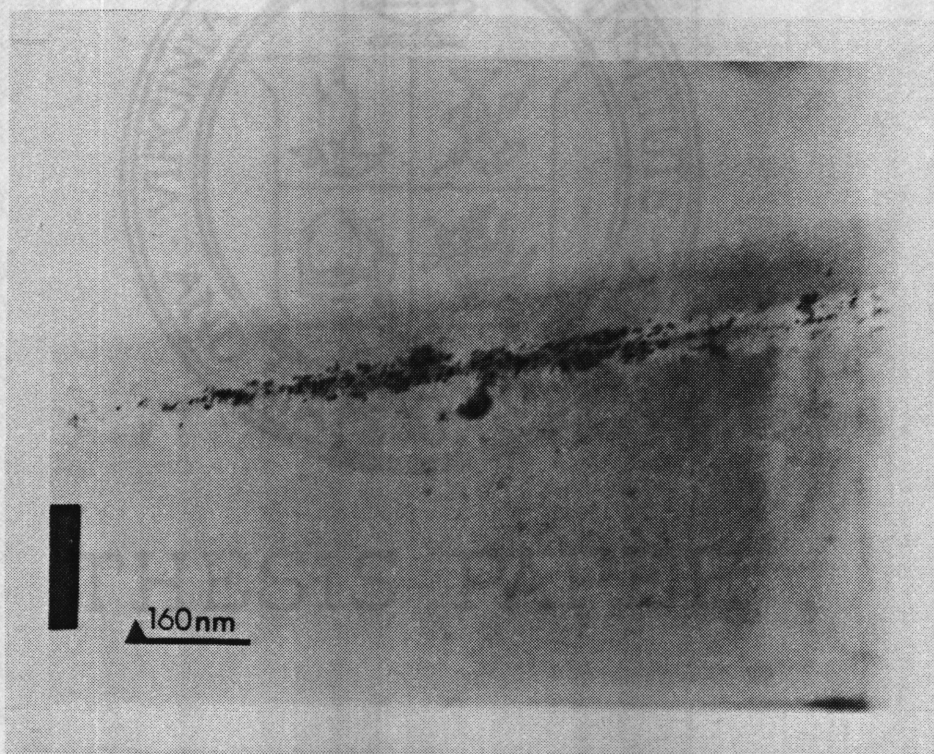


Figure 49. Transmission electron cross section of the surface region of a 25% solids 1X-doped wet-air-cured BTDA-ODA film.

surface structure of 1X-doped BTDA-ODA films. As one increases the solids content, the depth of the copper containing layer from the "air-side" surface increases while the continuity decreases. As the solids level increases, the mobility of the additive in the polymer is reduced due to the lower concentration of solvent present. The mobility reduction results in the formation of an overlayer because the additive is unable to reach the surface before the matrix is fully imidized hence locking it in place. The continuity of the copper layer may also decrease as a result of the reduced mobility producing a more dispersed phase of particles.

This phenomenon had a profound effect on the surface electrical properties of these films. The absence of an overlayer contributes to the formation of surface CuO as displayed by the copper-doped BTDA-APB films discussed above. Alternatively, formation of the overlayer prevents reaction of the resultant copper metal with the curing atmosphere. Table XVII provides the experimental and calculated resistivities for these films. The 23% solids film was the most conductive. This is expected since copper metal is orders of magnitude more conductive than copper oxide. The polyimide overlayer is also the thinnest ( $\sim 60$  Å) for this sample therefore electrical attenuation is minimized. It was shown previously (Chapter V) that the overlayer increased measured surface resistivity by 5 to 10 orders of magnitude dependent upon its thickness. The apparent continuity of the copper metal layer also appears equivalent to the copper oxide layer of the 20% solids film. The 25% solids film had the highest measured surface resistivity of the three copper-doped BTDA-ODA films due to a rather thick overlayer ( $1100$  Å) as well as extremely poor metal particle contact. The

Table XVII

Effect of Percent Solids On the Surface Electrical Resistivity Of Cu(TFA)<sub>2</sub>-Doped BTDA-ODA Polyimide Films<sup>a</sup>

<u>Sample</u> <sup>b</sup>	<u>Structure</u>	<u>Experimental</u> <u>(ohm)</u>	<u>Calculated</u> <u>(ohm)</u>
25% Solids	Tri-layer	6.7 X 10 <sup>16</sup>	1.2 X 10 <sup>-1</sup>
23% Solids	Tri-layer	2.3 X 10 <sup>11</sup>	5.6 X 10 <sup>-1</sup>
20% Solids	Bi-layer	3.2 X 10 <sup>15</sup>	2.0 X 10 <sup>9</sup>

<sup>a</sup>T = 25°C, Applied Voltage = 100 VDC.

<sup>b</sup>All films 1X, dry air cured.

20% solids film exhibited an intermediate resistivity resulting from the inherent conductivity and mediocre continuity of the copper oxide layer. Interestingly, the solids content of the poly(amide acid)/additive solution did not affect the structural characteristics of 2X-doped BTDA-ODA films. In all cases, bilayered films were formed. As stated earlier, the local dopant concentration must also play an important role.

Theoretically, the tri-layered BTDA-ODA composite films would be the most conductive (Table XVII); significantly more so than any bi-layered film that could be produced. Consequently, the 1X-Doped BTDA-ODA polyimide films would be excellent candidates for post-processing studies. Two results are likely, either improvement in the continuity of the copper metal layer will occur analogous to post-processed copper-doped BTDA-APB films; or, metal catalyzed thermal decomposition of the overlayer will arise producing a bi-layered CuO film. In the first case electrical resistivity will be reduced, potentially having near-theoretical values ( $10^{-1}$  ohm-cm). Or, the destruction of the overlayer will likely result in a decrease in surface resistivity on the same order as that exhibited by the post-processed BTDA-APB films. Several experiments were undertaken to answer this question.

1X-doped BTDA-ODA films prepared at the 23% solids level were post-processed at 350°C in nitrogen and dry air atmospheres. Following post-processing in either atmosphere, the films lost their brown metallic luster and became shiny gray. XPS analysis of the films found complete removal of the polyimide overlayer. In its place there now resided a CuO deposit exhibited by a dramatic increase in Cu(2p) photopeak intensity with concurrent satellite structure and the appearance of a new O(1s) photopeak indicative of oxide oxygen.

Auger electron spectroscopic depth profiling via argon ion etching also indicated complete loss of the polyimide overlayer after post-processing in nitrogen or dry air as displayed in Figure 50. A comparison of the spectra before and after the high temperature treatment revealed that the metal containing surface deposit increased in thickness similar to that observed upon post-processing BTDA-APB polyimide films. AES depth profiling did distinguish the effects of nitrogen versus dry air processing. For the films post-processed in nitrogen only the outer surface of the copper deposit is oxidized (Figure 51). In contrast, post-processing the doped BTDA-ODA films in dry air produced a homogeneous CuO layer (Figure 50).

In agreement with AES depth profiling, application of transmission electron microscopy revealed loss of the overlayer. The results of TEM analysis are given in Table XVIII.

The surface electrical properties are altered significantly following post-processing (Table XIX). As expected the removal of the overlayer results in a substantial decrease in surface resistivity. However, the protection it provided the underlying copper metal layer was also forfeit resulting in the layer's oxidation to CuO. Although near-theoretical or better resistivity values are realized for these films resulting from the complete or partial oxidation of the copper layer in dry air or nitrogen post-processing, respectively; the measured resistivity is substantially higher than what would be expected from the most continuous tri-layered film possibly produced.

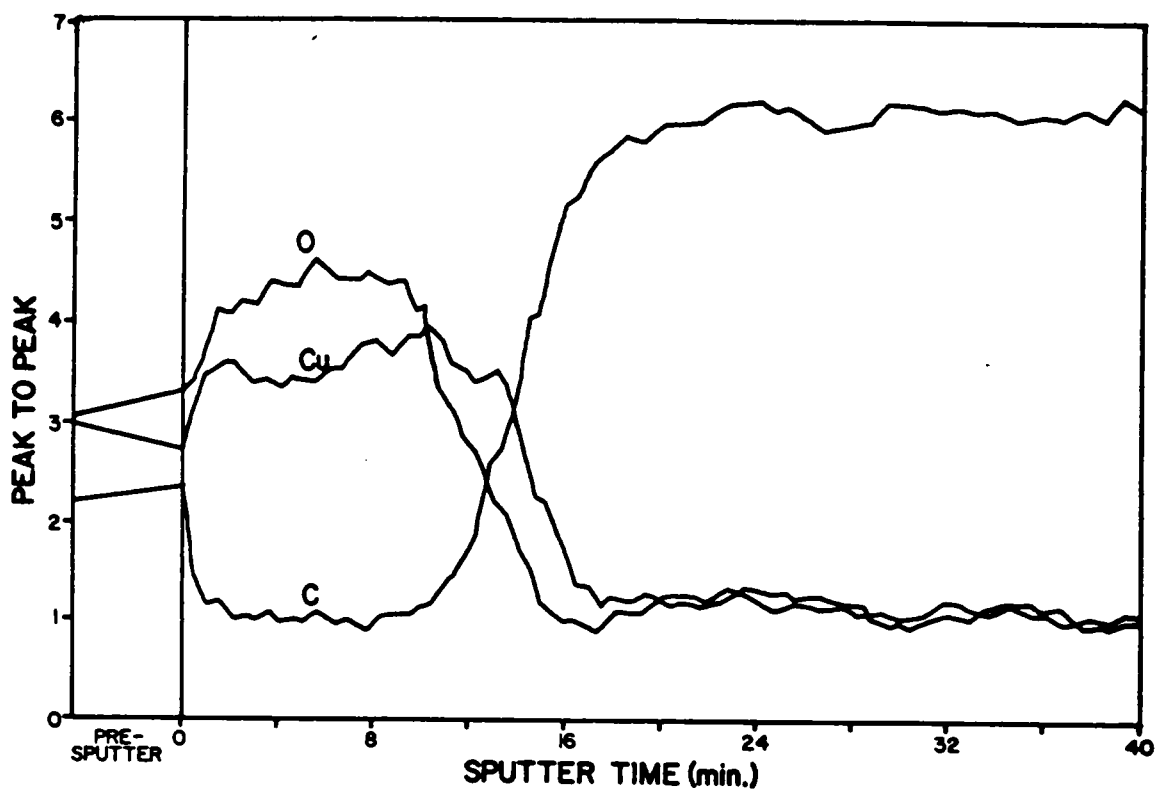


Figure 50. Auger electron spectroscopic depth profile of a 1X-doped BTDA-ODA film post-processed in dry air at 350°C for 1 hr.

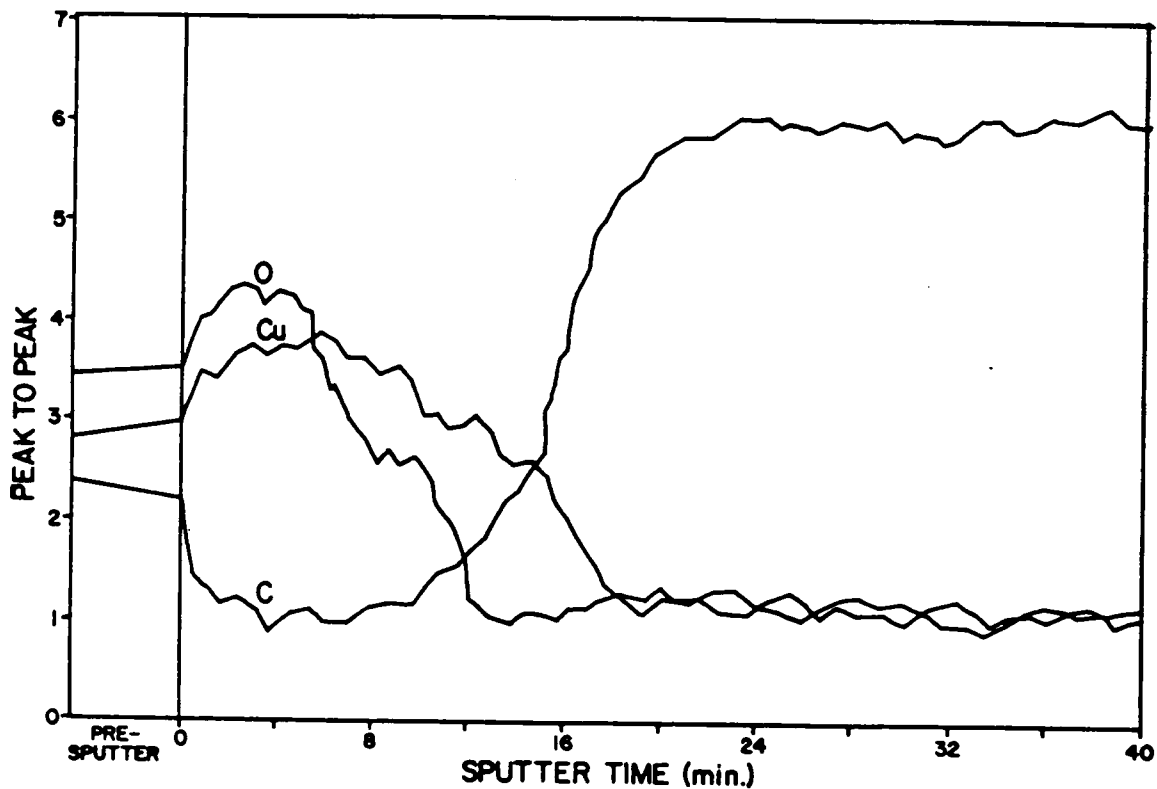


Figure 51. Auger electron spectroscopic depth profile of a 1X-doped BTDA-ODA film post-processed in nitrogen at 350°C for 1 hr.

Table XVIII

Morphological Features of Post-Processed<sup>a</sup> Cu(TFA)<sub>2</sub>-Doped BTDA-ODA Polyimide Films as Deduced from TEM Data

<u>Sample</u>	<u>Post-Processing Atmosphere</u>	<u>CuO Layer Thickness (Å)</u>
Wet Air/1X Doped	Dry Air	2200
Wet Air/1X Doped	Nitrogen	2700

<sup>a</sup>T=350°C for 1 hr.

Table XIX

Surface Electrical Resistivities of Post-Processed<sup>a</sup> Cu(TFA)<sub>2</sub>-Doped BTDA-ODA Polyimide Films

<u>Sample</u> <sup>b</sup>	<u>Post-Processing Atmosphere</u>	<u>Experimental (ohms)</u>	<u>Calculated (ohms)</u>
Wet Air/1X Doped	Dry Air	2.1 X 10 <sup>9</sup>	4.5 X 10 <sup>8</sup>
Wet Air/1X Doped	Nitrogen	1.1 X 10 <sup>8</sup>	3.6 X 10 <sup>8</sup>

<sup>a</sup>T=350°C for 1 hr.

<sup>b</sup>Samples produced at 23% solids.

## VII. CONCLUSIONS AND FUTURE WORK

The homogeneous incorporation of bis-(trifluoroacetylacetonato)copper(II) into a variety of poly(amide acid) precursors resulted in the formation of multi-layered copper metal- or copper oxide-polyimide composite films when thermally processed to 300°C. Several composite structures were produced which were dependent upon the precursor monomers, dopant level, and percent solids of the precursor/dopant solution. For Cu(TFA)<sub>2</sub> doped BTDA-ODA polyimide films either a tri-layered composite which consisted of a copper metal layer sandwiched between a thin polyimide overlayer and the bulk polyimide or a bi-layered composite film exemplified by a copper oxide layer residing on the surface of the polyimide film were produced. Doped BTDA-APB films, on the other hand, only exhibited the bi-layered structure. Cu(TFA)<sub>2</sub>-doped BDSDA-ODA polyimide films displayed either the bi-layered structure or no composite formation at all. However, polyimide sulfur/copper dopant complexation was observed for the doped BDSDA-ODA films resulting in improved dopant solubility. No interaction was observed between Cu(TFA)<sub>2</sub> and the other polyimide matrices.

A hypothesis was developed concerning the formation of the composite films and is described as follows: In all cases, phase separation of the additive occurs when the percent imidization reaches a certain level within the thermally curing film. A temperature gradient which exists in the film, due to continual solvent and water of imidization loss, propels a portion of the phase separated Cu(TFA)<sub>2</sub> to the air-side surface where it is most soluble. In the case of BDSDA-ODA, the solubility of the additive, regardless of temperature, gives rise to only small amounts of phase separated material accounting for the insubstantial layer, if

any, observed at the air-side surface. However,  $\text{Cu}(\text{TFA})_2$ -doped BTDA-ODA and BTDA-APB films where the solubility of the additive is much less, produce much larger surface or near-surface deposits of phase separated additive. The creation of the tri-layered or bi-layered structure is only dependent upon the mobility of the dopant in the matrix after phase separation. If mobility is high, the dopant reaches the air-side surface before substantial imidization has occurred, hence the bi-layered film is formed. If mobility is lessened, the additive only reaches the near-surface where it is locked in place resulting in the tri-layered composite.

Modification of soluble Polyimide XU-218 by this method supported the hypothesis. Since Polyimide XU-218 is pre-imidized, there exists no strong driving force to propel the additive to the surface once phase separation had occurred from solvent loss. As expected, there was no surface segregation of additive following cure. However, the poly(amide acid) analog to XU-218 (BTDA-DAPI) exhibited significant amounts of CuO on the air-side surface.

Surface electrical resistivity was altered by the formation of the conductive ( $\text{Cu}^0$ ) or semi-conductive (CuO) layers at the air-side of the BTDA-ODA and BTDA-APB polyimide films relative to the nondoped polyimide films. Substantial reductions in surface resistivity were realized, by up to seven orders of magnitude, but attenuation from the polyimide overlayer in the tri-layered composite films, the inherent resistivity of CuO, and discontinuity in both copper metal and copper oxide layers limited the attainment of the lowest possible values. Enhanced conductivity was, however, made with some sacrifice in thermal stability and glass transition temperature. The polymer decomposition temperature, indicated by 10% mass loss had decreased a minimum of  $70^\circ\text{C}$  for any of the doped polyimide films. An average reduction in glass transition

temperature by approximately 10<sup>0</sup>C was also found for the doped polyimide films.

Fractional factorial design methodology was used to determine process-property relationships for Cu(TFA)<sub>2</sub>-doped BTDA-APB films. Through the use of a screening analysis, a number of process variables have been determined that significantly affect the surface migration and/or chemical state of the dopant at the surface of a polyimide film. Films were produced with lower resistivities than those produced prior to the use of this method, although poor mechanical properties were obtained by utilizing the optimum processing conditions. This problem was overcome by applying the processing conditions beyond the boundaries set by the factorial design. By increasing the curing temperature to 350<sup>0</sup>C in dry air and nitrogen, films were produced that obtained or bettered near-theoretical surface resistivity, yet retained the flexibility inherent to nondoped polyimide films.

High temperature processing was also utilized to improve the conductivity of tri-layered 1X-doped BTDA-ODA films. However, decomposition of the polyimide overlayer above 300<sup>0</sup>C resulted in the oxidation of a copper metal layer to CuO. Surface resistivity was reduced substantially, but was still much higher than the copper metal deposit that may have resulted.

Several areas of this research project deserve additional study. Thermal curing is a relatively slow process wherein the gradients of temperature and imidization that exist in the film are long lived. To probe the stages of the phase separation process, microwave curing of the poly(amide acid)-dopant mixture would be useful. By microwave curing samples of a doped film after successive stages of thermal cure (i.e. thermally cured to 80<sup>0</sup>C, 150<sup>0</sup>C, 200<sup>0</sup>C) phase separation of the additive and the imidization process may be induced quickly at

higher temperatures allowing one to study the distribution of the additive in the matrix before dopant migration would occur.

Additionally, thermally curing doped films on a hot plate may instill a larger temperature gradient within them relative to an oven. This may allow more efficient dopant migration to the air-side of the film which would provide improved surface electrical properties.

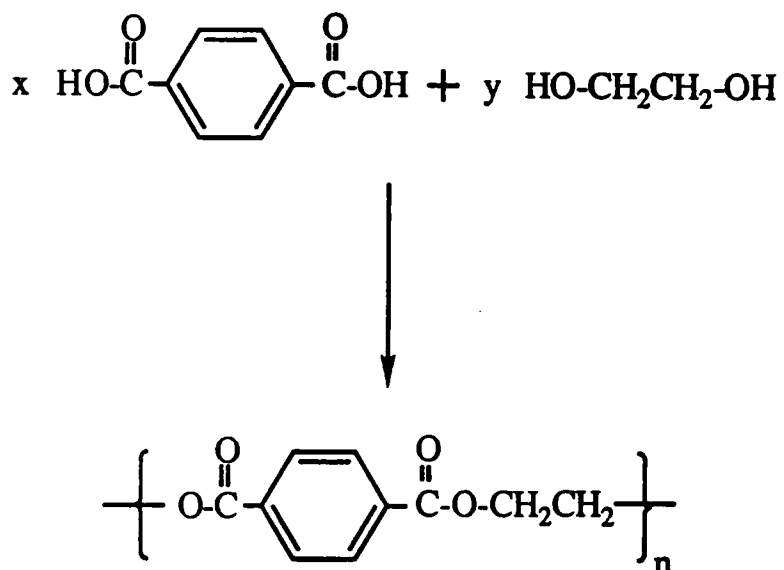
Alternative copper complexes and salts as well as alternative polyimide matrices may be employed. Copper oxalate, for example, decomposes to copper metal when exposed to an electron beam and may be useful in producing selective patterns on the surface of a film. One of the problems with using common monomers for condensation polyimide synthesis is the limited number of solvents useful for poly(amide acid) formation (e.g. N,N-dimethylacetamide, N-methylpyrrolidone, and Diglyme). Many copper additives, including copper oxalate, are insoluble in these solvents precluding homogeneous dispersal. However, by employing monomers such as 2,2-bis(3,4-dicarboxyphenyl)hexafluoro Dianhydride (6FDA), other solvents including methylene chloride and tetrahydrofuran may be used which increases the number of potential dopants.

## VIII. HISTORICAL

### A. Polyester Film

Polyesters belong to a large class of polymers called condensation polymers. Although, a large number of polyesters have been produced, few have made a commercial impact. Poly(ethylene terephthalate) (PET), however, is a polyester that dominates a number of commercial markets. Its commercial significance is attested by the 20 or more world producers of this polymer.[69] One of the largest areas of use for this polymer is as a film. Poly(ethylene terephthalate) film has found many applications in packaging, graphics, magnetic tape, and industrial capacities.[70] Consumption of polyester film has grown enormously in the past two decades, from approximately 55 million lb/yr (circa. 1966) to over 300 million lb/yr today.[71]

PET was first produced in experiments by Whinfield from the reaction between ethylene glycol and terephthalic acid (Scheme 4).[72] Subsequent experiments found that the polymerization was more controllable when the methyl ester of terephthalic acid was used instead of the free acid.[73] Once the polymer is formed it is processed into film. After the polymer is extruded from a die, it is quenched immediately to prevent it from crystallizing. It is then biaxially oriented by stretching it at a temperature just above the  $T_g$  ( $80^{\circ}\text{C}$ ). This has the usual effect of improving the mechanical properties and reducing brittleness. If the film is heated above  $80^{\circ}\text{C}$  at this point, it will shrink considerably, hence it finds uses as shrink wrap packaging material. In order to improve heat stability, a third processing stage may be added, wherein the oriented film is firmly held to prevent contraction and heated to  $200^{\circ}\text{C}$ . During this step the material



Scheme 4. Initial synthesis of poly(ethylene terephthalate).

undergoes considerable crystallization without affecting the orientation which provides dimensional stability to 200°C when finished.

The advantages of biaxially oriented and heat-set PET film are numerous.[70] The films are highly resistant to most organic solvents and mineral acids. No plasticizers are needed while moisture retention is very low. The films exhibit high strength and toughness, as well as, excellent flex life. They also have excellent electrical properties (i.e. low dielectric constant and loss).

Metallized polyester film is utilized as an aluminum foil replacement in the packaging industry.[70] Although a number of other polymeric films are now used as substrates for metallization, the superior properties of polyester still make it the film of choice for a number of applications. In particular, its thermal stability, and barrier properties, as well as, low moisture retention make it highly desirable for vacuum metallization techniques. Metallized plastic films are used because of their attractive appearance, use as gas, moisture and light barriers (alone or in laminates), and for optical reflectors and filters.

## B. Sputtering

As stated in the Introduction, vacuum sputtering is a method that is widely used to produce thin metal or oxide films on a large number of substrates.[74] Vacuum sputter deposition is a coating method wherein atoms of a specific material (metal, alloy, inorganic) are dislodged through momentum exchange arising from energetic particle bombardment of the material surface (target).[75,76,77] Substrates placed in front of the source intercept the influx of sputtered atoms which coalesce to form a continuous coating as the deposition proceeds. A low pressure glow discharge, allows use of a heavy inert gas, such as argon, to initiate the sputtering process. Argon ions generated in the plasma

are accelerated to high velocity before striking the source material. The sputtered species are primarily neutral atoms with relatively high energies (10-40 eV) dependent upon the target atomic mass.[75] Figure 53 displays a glow discharge sputtering apparatus of the simple planar diode type.[78,79]

Sputtering permits the use of many different type of materials, such as metals, alloys, and compounds which cannot be used readily with other vacuum-deposition techniques (i.e. evaporation methods). Due to the relatively low deposition rates and inability to deposit nonconductive materials, dc diode sputtering (Figure 52) has not been widely used. However, by application of a radio frequency potential to the target to permit continuous current flow, nonconductors may be sputtered efficiently.[80] In either dc or rf operation, the substrate in planar diode sputtering is in direct contact with the plasma therefore heating and/or degradation is possible.

One of the leading uses for this technique is to metallize plastic film [81] where high production speeds (30-60 meters/min.) are regularly encountered. The application of sputtering to plastics, however, has led to the introduction of new deposition sources with magnetic plasma confinement called magnetrons.[82,83] The magnetic confinement system contains the plasma/ionic component of the process such that substrate heating and damage by direct contact with the plasma is negligible. Magnetrons provide fairly high deposition rates (10-20 nm/sec) and can be engineered to allow deposition over large areas (many square meters).

### C. Surface Treatments

The performance of metallized plastic film or articles occasionally suffers due to poor metal-to-polymer adhesion. Over the years researchers have studied

# Planar Diode System

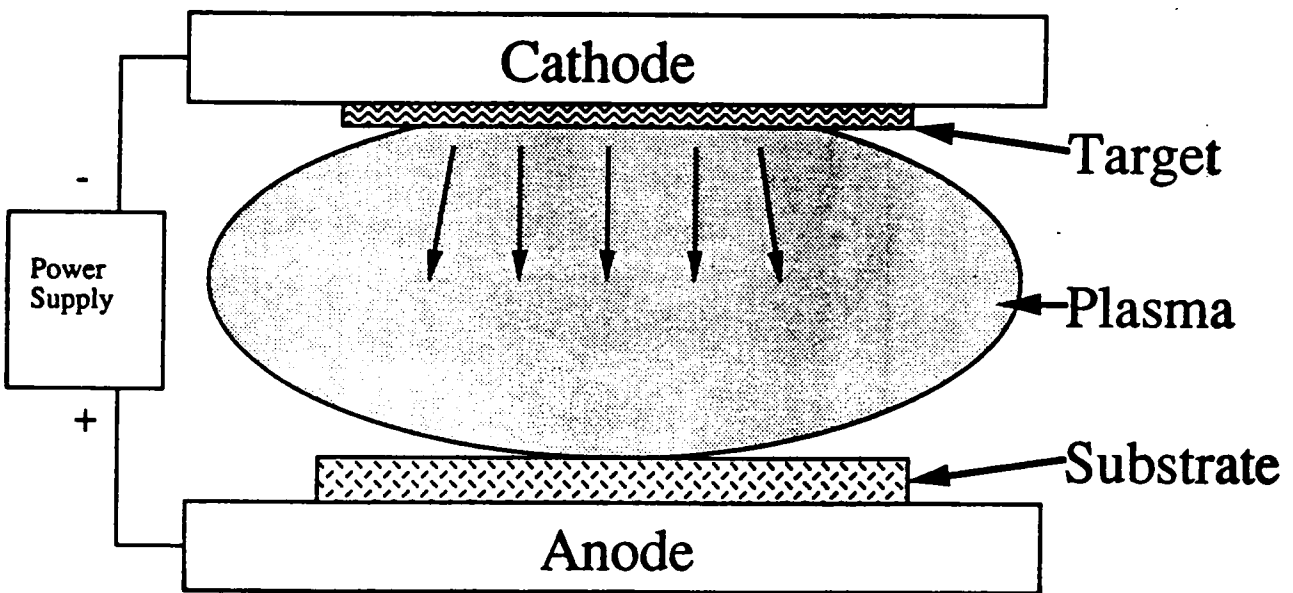


Figure 52. Schematic drawing of a glow discharge sputtering device of the planar diode type.

and developed numerous procedures to enhance existing levels of adhesion between polymer and deposited metal. Priming treatments that improve adhesion include: flame treatment [84], electrostatic discharge [85], electrostatic discharge in the presence of monomers [86], halogenation, chemical etching [87], and solvent etching. UV irradiation also introduces surface modifications that are effective in improving the bondability and wettability of plastics.[88]

Although a number of techniques have been discovered to improve adhesion to plastics, as shown above, two distinct methodologies have progressed and been commercially applied to improve metal/polymer adhesion. Both involve the modification of the plastic substrate in some way to benefit adhesion. The first method is to apply a thin metallic or polymeric coating which acts as a binding agent between the film and sputtered metal. The coating is usually applied under separate processing conditions prior to vacuum sputtering. Application of a thin layer (50 Å) of nickel between sputtered copper metal and polyvinyl alcohol has resulted in enhanced adhesion.[89] Likewise, thin polymeric coatings have been applied to commercial polymers during processing which contain amine [90], carboxylic acid [91], or sulfonyl [92] pendant groups which form chemical bonds through the nitrogen, oxygen, and sulfur atoms, respectively with deposited metals to improve adhesion. With each system of this kind, the binder or adhesive applied results in a planar composite structure having two interfacial regions. The chemistry that occurs at the metal-binder interface being different than that at the binder-polymer film interface.

The second method used to increase sputtered metal-to-polymer adhesion is to chemically modify or clean the surface of the substrate prior to metal deposition by the application of a gaseous plasma.[93] Jackson has used argon

plasma treatment to cleanse epoxy printed circuit boards prior to lamination resulting in improved adhesion between the laminates.[94]

A multitude of chemical modifications have been reported for plasma exposure of polymer surfaces. Glow discharges improve bonding to metals by cross-linking, which may strengthen weak boundary layers present on the surface of the plastic, and by generating reactive surface functionality.[95,96,97,98] Hansen and Schonhorn have reported that a polyethylene block exposed to a helium plasma for 15 minutes, when heated with a nontreated block kept its shape during heating even when the other deformed considerably.[99] The researchers concluded that a cross-linked shell formed on the outer surface of the plasma treated polyethylene sample preventing flow of the molten polymer above the melting temperature of the untreated sample. Similar effects have also been reported for polypropylene along with an increase in adhesive strength to metals.[91]

Surface chemical functionalization of polymers that do not contain oxygen or nitrogen heteroatoms can improve adhesion to metals by treatment with an oxidizing plasma prior to bonding.[100,101,102] Oxidation reactions produce oxygen-containing functional groups (i.e. carbonyl, hydroperoxide, hydroxyl) which are attached to the polymer surface.[103] The application of an oxygen plasma to polyethylene produced extensive oxygen surface functionality according to Nuzzo and Smolinsky.[95] These functional groups have surface densities on the order of the monomer density ( $\sim 10^{14}$  sites/cm<sup>2</sup>) as determined by chemical labeling techniques. Also, a 1-2 sec exposure to the plasma produces about the same degree of surface modification as longer treatments. In accord, K. Rossmann reported that plasma oxidation is a relatively fast process wherein observed changes are produced in seconds.[104]

A limited number of authors have described the effects of plasma processing on poly(ethylene terephthalate).[93,105] Yashuda et al. exposed PET to both argon and nitrogen plasmas.[106] Following treatment with either plasma, plasma-induced surface oxygen species are detected, however, no functional assignments are made. Other than the slight incorporation of nitrogen after N<sub>2</sub> plasma exposure, both plasmas induce similar types of surface change. In a study by Westerdahl, Hall, and Levi, a number of polymeric materials, including PET, were treated with oxygen and helium plasmas.[107] The adhesive bond strength of PET was found to increase at the same rate with either pretreatment. However, the rates of improved adhesion were less than those of the hydrocarbon based polymers (e.g. LD Polyethylene, HD Polyethylene, Poly(2-methylpentene)) under the same conditions. For the polar polymers (e.g. PET, Delrin, Nylon), chain degradation was probably more important than surface functionalization, hence the rate of improvement in bond strength is lower. Dunn, McClure and Grant have studied the effects of oxygen and argon plasma on the surface properties of poly(ethylene terephthalate) by both photoelectron [108] and infrared [109] spectroscopic techniques. Surface IR analysis determined that oxygen plasma treatment incorporated additional carbonyl functionality, however, argon plasma treatment resulted in the decrease of both C=O and C-O infrared bands indicative of surface carbonization. XPS analysis showed a decrease in the surface C-C signal for oxygen plasma treatment and an increase for argon plasma treatment, particularly at high power. These results suggest that the surface of the PET film is oxidized by O<sub>2</sub> plasma treatment and carbonized by the Ar plasma which is consistent with the surface IR results.

## IX. EXPERIMENTAL

### A. Plasma Pretreatment and Metallization of Poly(ethylene terephthalate) Film

#### 1. Polyester Film

The poly(ethylene terephthalate sheet used as a substrate was 75  $\mu\text{m}$  thick Melinex- type "s" obtained from ICI Ltd.

#### 2. Plasma Pretreatment Gases

The gases described below were used to sustain an r.f. plasma. All were purchased from Air Products, Inc.

Nitrous Oxide ( $\text{N}_2\text{O}$ )- technical grade (99.0%)

Argon (Ar)- ultrapure carrier grade (99.999%)

#### 3. Plasma Processing

An r.f. plasma was generated by a 0.30 KW automatically controlled and tuned supply. The apparatus was evacuated to  $2 \times 10^{-5}$  torr followed by introduction of the pretreatment gas through a variable leak valve to attain a system pressure of  $3\text{-}15 \times 10^{-3}$  torr. Following discharge initiation, the PET substrate was exposed to the plasma for times of up to one minute.

#### 4. Film Metallization

A titanium cathode (99.9% purity, grade 2) obtained from Astro Metallurgical Co. was used as the source for the sputter coating process. A planar magnetron sputtering system (Figure 53) operating at a pressure of 0.2 Pa in argon was used to metallize the polyester substrate. Sputtering power was varied between 3.9 - 8.0 kW.

The polyester metallization and plasma processing were performed by an industrial sponsor.

# Planar Magnetron System

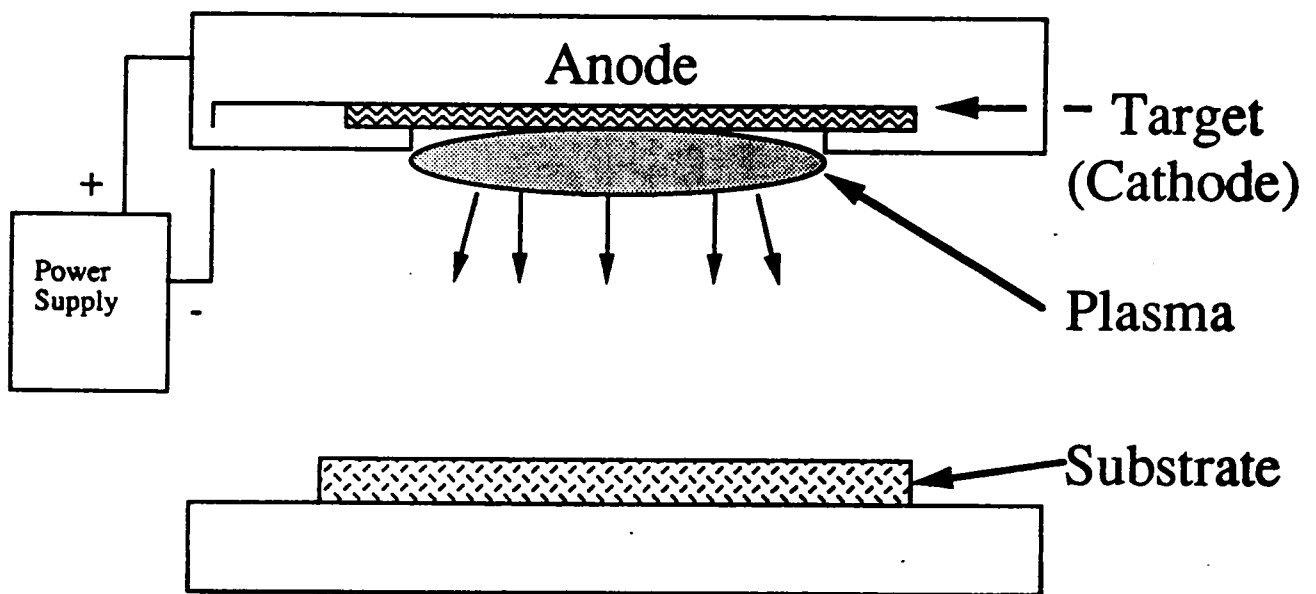


Figure 53. Schematic drawing of a planar magnetron sputtering system.

## B. Film Characterization

Listed below are the experimental techniques used to characterize metallized and nonmetallized PET film. Unless otherwise noted, the experimental conditions are the same as those listed in Chapter III. C.

1. X-ray Photoelectron Spectroscopy
2. Auger Electron Spectroscopy
3. Transmission Electron Microscopy
4. Fourier Transform Infrared Spectrometry

Surface Fourier transform infrared spectra were recorded on a Nicolet Model 6000 Infrared Spectrometer with an in-line Wilks Scientific Corp. Model 9000 Attenuated Total Reflectance Infrared Cell. Surface spectra of the films were measured using a KRS-5 internal reflection element at a nominal  $45^{\circ}$  angle of incidence. For each sample, a spectral average of 1024 scans was recorded with a resolution of  $4\text{ cm}^{-1}$  and an average intensity of approximately  $1.5\text{ V}/\text{scan}$  (gain = 8). Background was obtained by recording the spectrum of the empty ATR cell. The Nicolet "IR-Decon" routine was used to deconvolute certain infrared peaks of interest due to band overlap.

### 5. Contact Angle Analysis

Static contact angle measurements were obtained from a Ramé-Hart, Inc. Model 100-00 115 Goniometer. Distilled water was used as the wetting agent in all analyses. An average of five independent measurements was used in obtaining the final contact angle value.

### 6. Residual Gas Spectrometric Analysis

Residual gas mass spectra, before and after glow discharge initiation, were recorded on a Inficon Model IQ-200 Residual Gas Analyzer (RGA) by an

industrial sponsor. A faraday cup detector was utilized to resolve molecular and atomic species having mass-to-charge ratios between 1-200 amu.

## 7. Mechanical Analysis

180° Peel tests were carried out with a Instron Model 1130 testing instrument equipped with self-tightening jaws and a 500 gm load cell by an industrial sponsor. A jaw gap of 2" and a crosshead speed of 1"/min were used in all analyses. Before analysis, a polymeric coating obtained from Xerox Corp. consisting of Xerox Makrolan, Xerox Vitel, and methylene chloride was applied to the metallized surface of the film. After the appropriate drying period, 1 cm strips of each sample were prepared from uniform templates. A razor blade was used to cross-hatch a segment of the sample (coated surface) allowing one to begin the fracture necessary for the 180° peel test. In this experiment, analysis error was generally less than 15% for samples prepared from the same batch.

## **X. THE EFFECT OF PLASMA TREATMENT ON THE SURFACE PROPERTIES OF POLY(ETHYLENE TEREPHTHALATE) FILM**

### **A. Preliminary**

Unique surface modifications can be achieved by plasma processing polymeric materials. These effects are brought about by the presence of ultraviolet radiation and chemically active species produced by the plasma. However, details regarding the interaction of the reactive species generated in the discharge with the substrate immersed in the plasma, and the combined physical and chemical phenomena which occur during exposure have not been widely investigated. In this research, one of the primary effects of plasma treatment is that large increases in adhesion between treated polyester and a sputter deposited metal are gained. It is the object of this Chapter to determine the effects of N<sub>2</sub>O/Ar plasma treatment on the surface properties of commercial poly(ethylene terephthalate) film prior to metallization with titanium metal in order to account for the surface chemistry leading to improved adhesion.

### **B. X-ray Photoelectron Spectrometric Analysis of ICI-442 Polyester Film**

X-ray photoelectron spectroscopy (XPS) was applied to obtain reference spectra of raw (not plasma-treated) ICI-442 polyester film taken at normal incidence (90°) and grazing (15°) angles. In order to determine the surface uniformity of the film, several areas of a sheet measuring 11 X 8 inches were analyzed to ascertain the presence of any local inconsistencies. A comparison of survey and multiplex scans from each area showed insignificant change in C(1s) and O(1s) XPS spectral characteristics. This was considered important since fluorine was sporadically detected on the surface of plasma treated ICI-442 in

previous samples. This observation suggests that the intermittent fluorine content is a contaminant and is not a tag placed in the film by the manufacturer.

The carbon (1s) photoelectron spectrum of raw ICI-442 polyester film exhibits the pattern displayed in Figure 54. This signal may be computer curve resolved into three separate environments (Table XX) which would be expected based on the structure of poly(ethylene terephthalate) and in accord with measurements made by a number of other authors.[110,111,112] The higher binding energy carbon photopeaks correspond generally to those carbon atoms with slightly less electron density (a simplification) than the carbon species at lower binding energies. The area under a particular peak is proportional to the relative concentration of the specific carbon. The calculated carbon ratios for PET are 2:2:6 corresponding to the carboxyl, ester, and aromatic carbons, respectively. Experimental ratios obtained from the area below each peak gave a ratio of 2:2:7 which is in good agreement with the calculated ratio. The slight increase in the lowest binding energy peak (284.6 eV) is probably due to surface carbon contamination (adventitious carbon) which would appear at this binding energy. The observation is supported by the fact that this particular carbon (1s) photopeak is nearly 10% greater when XPS is conducted at a 15° rather than a 90° take-off angle.

The oxygen (1s) photopeak, as expected, exhibits two types of oxygen species (carbonyl and ester) (Figure 55). Theoretically, one would expect a 1.0:1.0 ratio of these oxygen species. Experiment yields a 1.0:0.95 ratio which shows excellent agreement. More total oxygen was detected on the polymer film surface relative to the theoretical expectation when the film was analyzed at a 90° take-off angle (Table XXI). XPS analysis at a 15° take-off angle, on the other hand, exhibited a decrease in the oxygen signal which was even lower than the

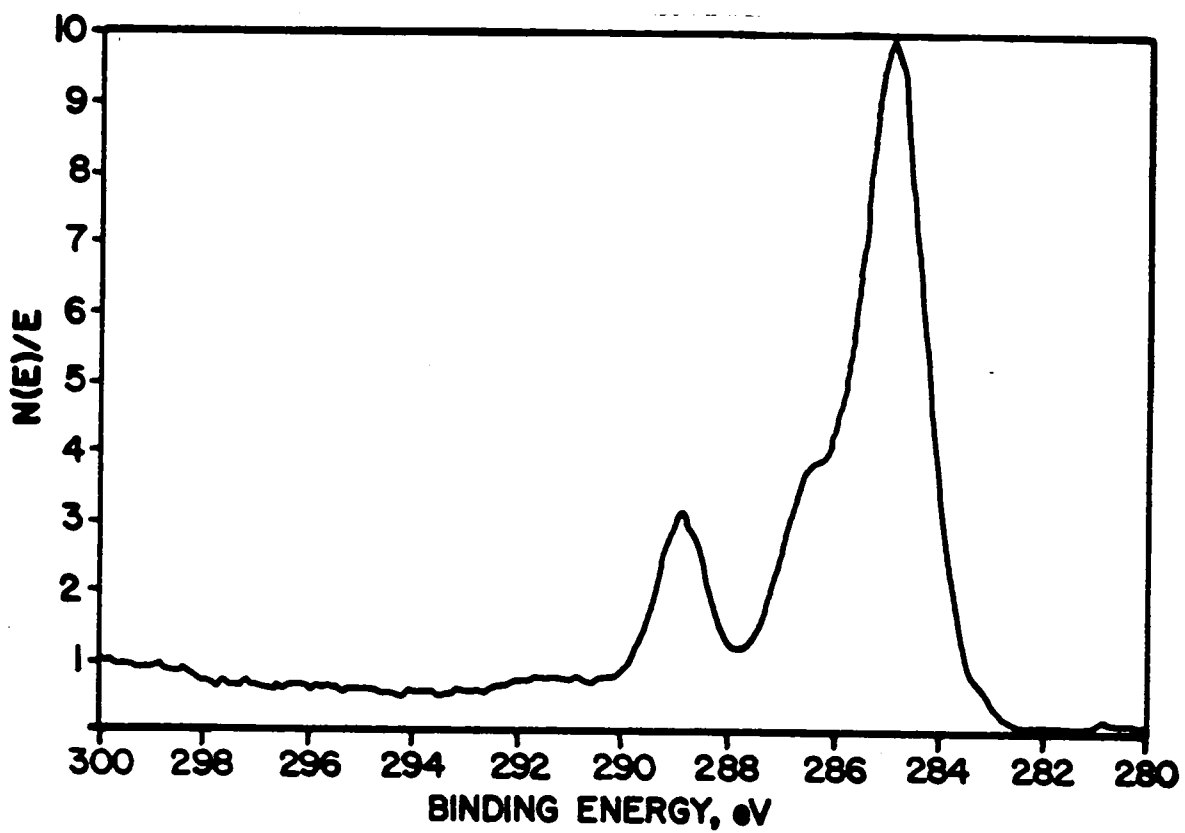


Figure 54. The XPS C(1s) spectrum of raw ICI-442 polyester film.

Table XX

Binding Energy Assignment for Nontreated ICI-442 Polyester Film

	<u>Substituent</u>	<u>E<sub>B</sub> (eV)</u>
Carbon (1s)	Carboxyl	288.8
	Ester	286.3
	Aromatic	284.6
Oxygen (1s)	Ester	533.3
	Carbonyl	531.6

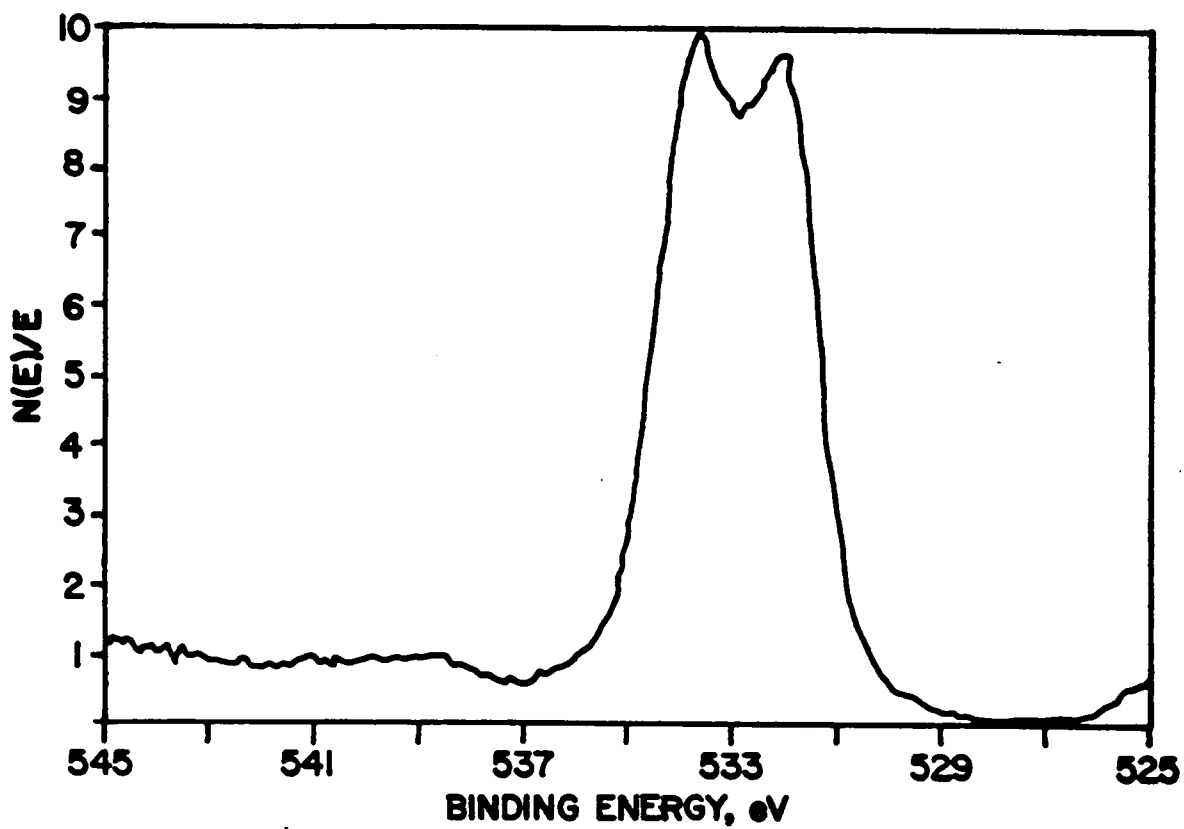


Figure 55. The XPS O(1s) spectrum of raw ICI-442 polyester film.

Table XXI

Surface Elemental Composition of Nontreated ICI-442 Polyester Film

<u>Condition</u>	<u>Atomic Concentration (%)</u>	
	<u>Carbon</u>	<u>Oxygen</u>
Theoretical	71.4	28.6
15 <sup>o</sup> Take-off Angle	75.6	24.4
90 <sup>o</sup> Take-off Angle	67.5	32.5

theoretical value suggesting, as stated earlier, the presence of surface hydrocarbon contamination.

### C. Surface Characterization of Plasma Treated ICI-442 Polyester Film by X-ray Photoelectron Spectroscopy

It has been shown previously that adhesion between a deposited metal and a polyester substrate increases significantly upon plasma pretreatment.[113,114] In order to characterize the surface of plasma treated polyester film, X-ray photoelectron spectroscopy was performed. Samples of plasma treated films were prepared on the sputter coater described in the Experimental. A gas mixture of argon/nitrous oxide was used as the pretreatment agent. Plasma exposures of 2.5, 5.0, 7.5, 15.0, 22.5, and 60.0 seconds were used in anticipation that a change in surface structure with time might be detected.

Surface characterization, via XPS, was obtained at both 15° and 90° take-off angles. Variation in take-off angle should determine whether surface modification affects the topmost monolayers of the substrate or whether changes occur deeper within the film. The calculated atomic percentages were determined by peak area analysis. Changes in surface composition relative to the nontreated film were noticeable for all plasma treated films regardless of plasma exposure and the XPS take-off angle. Figures 56 and 57 show the changes in elemental composition, in atomic percent, versus plasma exposure for both the 15° and the 90° take-off angles.

Nitrogen may be incorporated through the interaction of plasma activated nitrous oxide (metastable) or nitrous oxide decomposition products such as nitrogen radicals or ions with the polyester surface. Both Hellund [115] and Swartz [116] have proposed and observed  $N^+$  (cation), N (atomic),  $N^*$

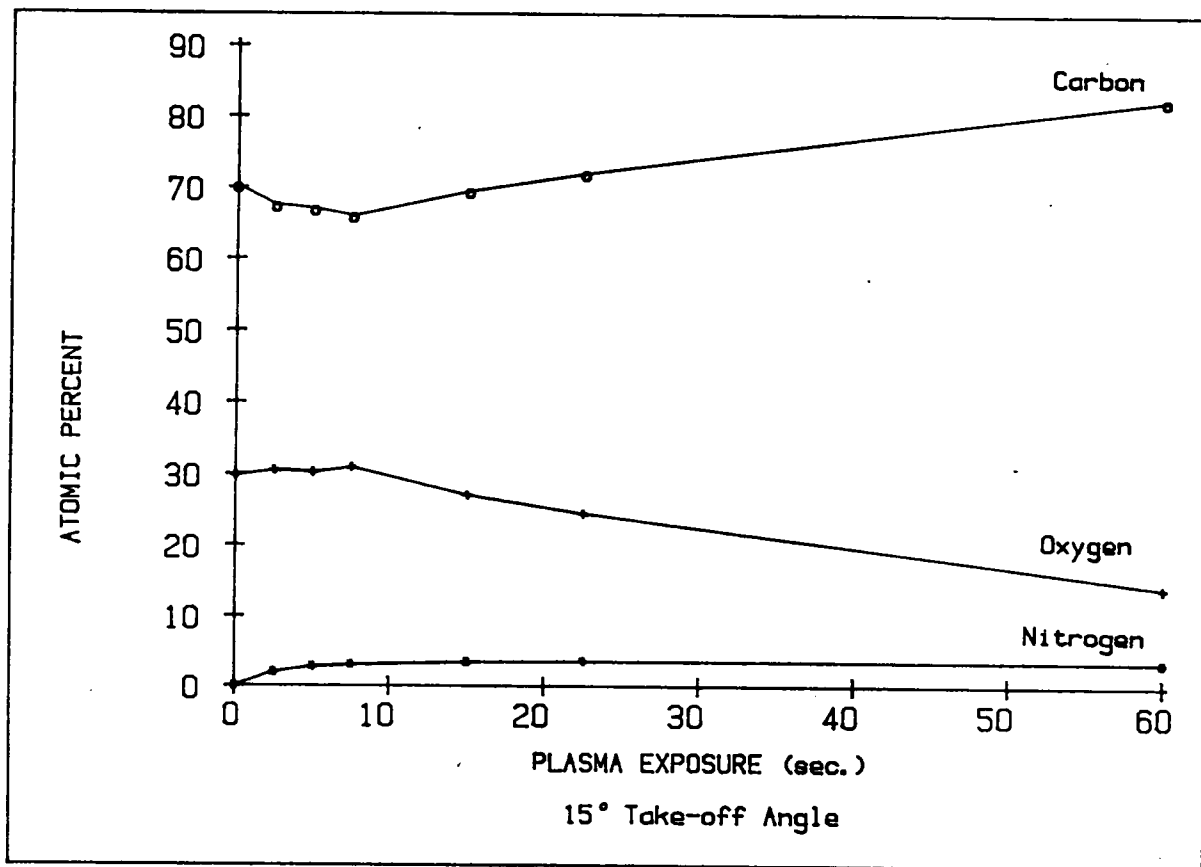


Figure 56. Plot of the change in elemental composition versus Ar/N<sub>2</sub>O plasma exposure for ICI-442 polyester film at a 15° take-off angle.

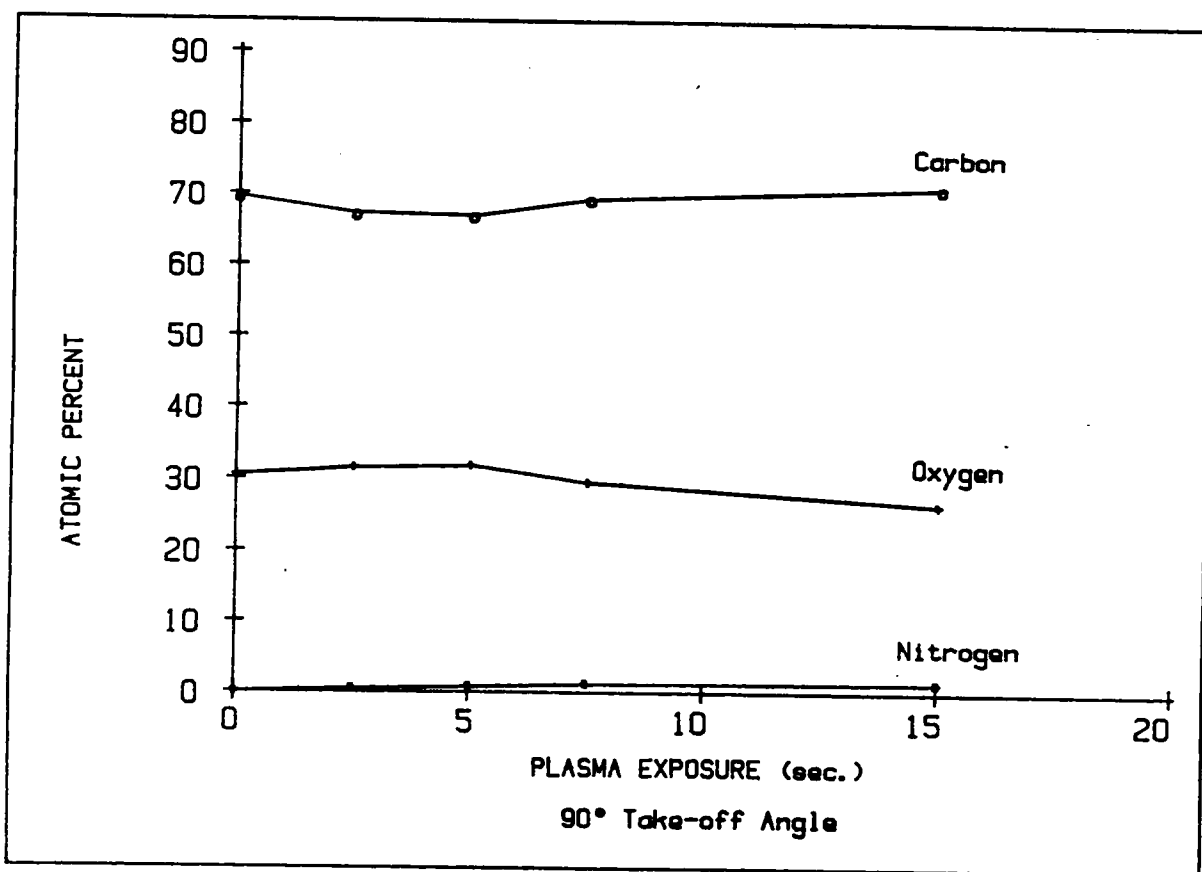


Figure 57. Plot of the change in elemental composition versus Ar/N<sub>2</sub>O plasma exposure for ICI-442 polyester film at a 90° take-off angle.

(metastable), and  $N_2^*$  (metastable) active nitrogen species among others in plasma environments. Schonhorn et al. [117] has shown similar incorporation of surface nitrogen when plasma treating polypropylene with  $N_2O$ . The concentration of nitrogen increases nearly 50% by changing the take-off angle from  $90^\circ$  to  $15^\circ$  indicating that this effect is limited to the outermost monolayers. Clark and Dilks [118] have proposed a model of plasma-surface interaction that suggests that ions and metastables only play an important role in modifying the outermost surface of polymer substrates in accord with the results discussed here. Aluminum was also discovered on the surface; however, it is probably a contaminant originating from the inner surface and/or the electrodes of the plasma pretreatment chamber. Aluminum is also more apparent at lower take-off angle. It was observed for this particular pretreatment power (300 W) that titanium-polyester adhesion, as determined by a  $180^\circ$  peel test, reached a maximum at approximately 5.0-7.5 sec. plasma exposure. At both longer ( $> 10$  sec.) and shorter ( $< 4$  sec.) exposures, measured adhesion decreased rapidly. Since surface coverage by aluminum occurs significantly at longer exposure ( $\sim 6$  atom % at 60 sec.), its presence may act as a barrier to adhesion between the deposited metal and the polyester film. XPS analysis suggested that the aluminum was in the form of  $Al_2O_3$ .

The length of plasma exposure has a profound effect on the carbon and oxygen surface composition. There are two noticeable trends in the data that are dependent upon the length of exposure. With less than 10 sec. exposure, comparison to the raw polyester indicated that while the total carbon concentration decreased slightly upon plasma treatment, the oxygen concentration was constant (Figure 56). This suggests that the pretreatment

may only clean the polyester surface of hydrocarbon contamination and otherwise not alter the surface composition other than through the addition of small amounts of nitrogen. Interestingly, the surface oxygen concentration was relatively unchanged, signifying that oxygen is not being incorporated into the surface during plasma treatment. An intriguing result since  $N_2O$  is considered to be an oxygenating gas. At pretreatment exposures exceeding 10 sec., there was substantial loss of surface oxygen that intensified with increasing exposure. This phenomenon implies that extensive deoxygenation has occurred in this time domain. Surface carbon increased at the same rate as oxygen loss.

The oxygen (1s) photopeak, however, revealed that there was a change in functionality due to the application of the plasma treatment (Figure 58). The presence of new oxygen functionality is independent of plasma exposure although exposure did affect the relative concentrations of surface oxygen species. Curve resolution of the oxygen (1s) photopeak for raw ICI-442 polyester film indicated the presence of two oxygen species both present in the ester functionality. Figure 59 displays a typical oxygen (1s) photopeak for a plasma treated polyester film following curve resolution. The photopeak binding energies and FWHM obtained from the functional groups of the nontreated film were used as a reference. Upon inspection, one notices that there are actually three types of oxygen present on the surface. Oxygens 1 and 2 correspond to the carbonyl oxygen and ester oxygen, respectively. Oxygen 3, which exhibited an intermediate binding energy ( $\sim 532.4$  eV), is a new functionality induced by the plasma pretreatment. Typically, aldehydes, ketones, and alcohols appear at these binding energies, however, XPS is not able to resolve these functional groups by analysis of the O (1s) signal. Curve resolution of the C (1s) photopeak of a plasma pretreated film was attempted, but the numerous

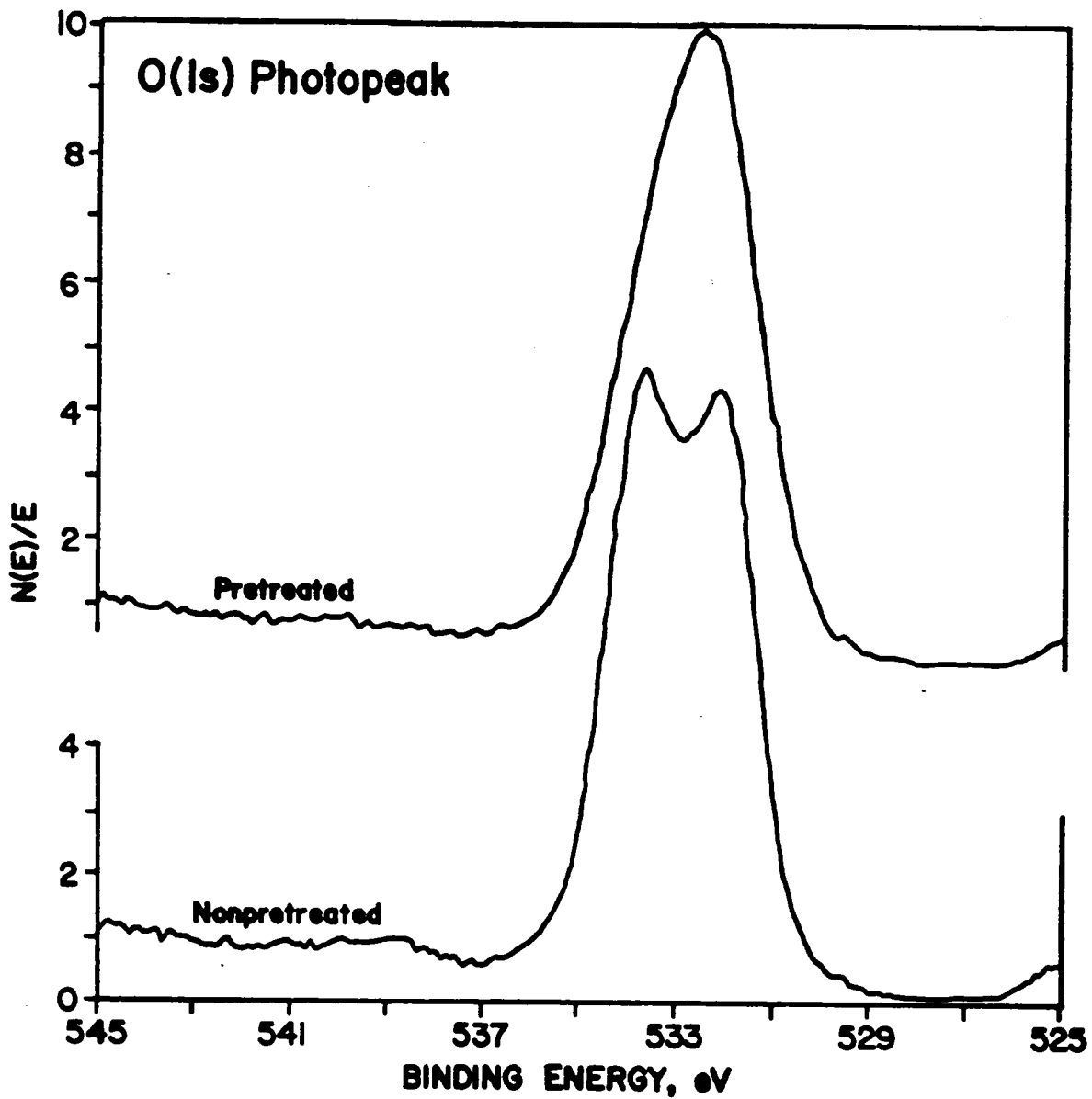


Figure 58. The XPS O(1s) spectrum of both plasma pretreated and nontreated ICI-442 polyester film.

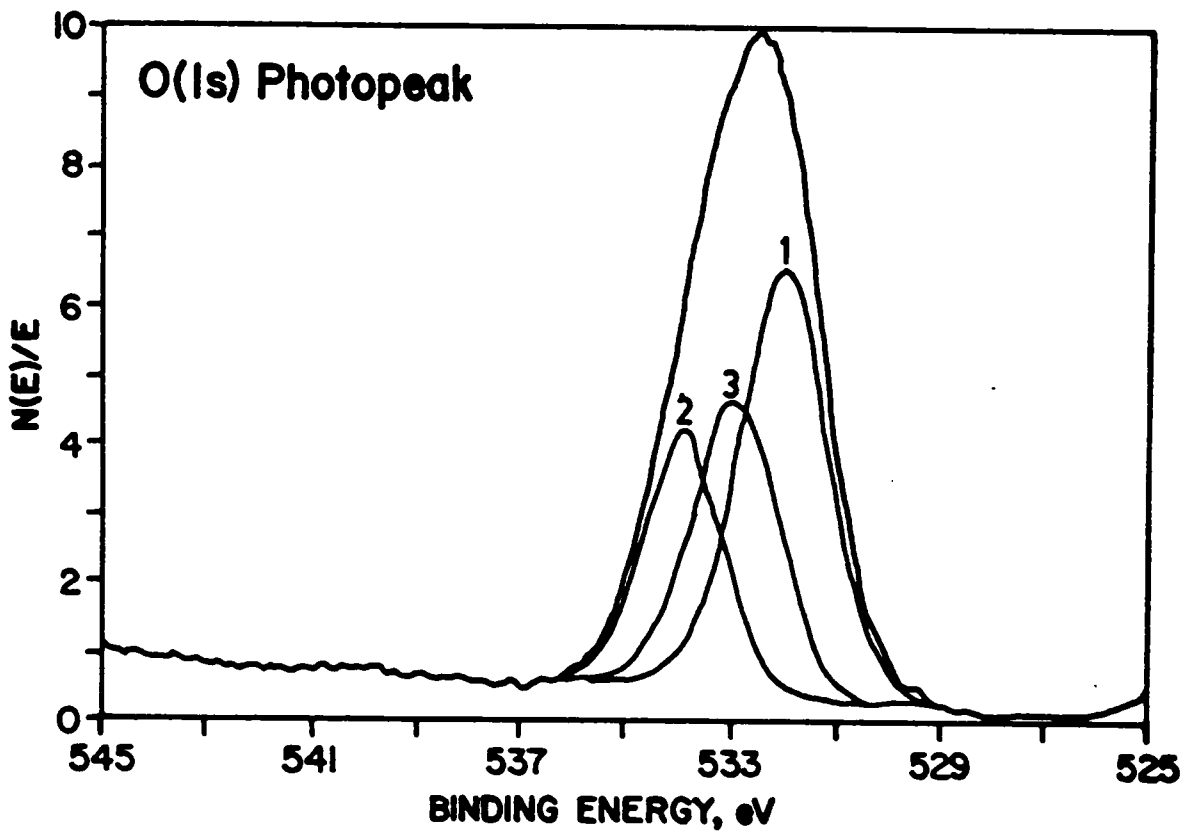


Figure 59. The curve resolved XPS O(1s) spectrum of plasma pretreated ICI-442 polyester film.

combinations of possible fits due to both oxygen-carbon and nitrogen-carbon functionalities precluded any definite results. However, one does notice a decrease in carboxyl carbon (288.8 eV) and an increase in the intermediate carbon binding energies (indicative of aldehydes and ketones following plasma treatment (Figure 60).

Since the total surface oxygen concentration is relatively constant, the new oxygen species produced must arise at the cost of another species rather than through incorporation of additional oxygen from the plasma or through atmospheric exposure. Figure 61 displays the changes in oxygen functionality with plasma exposure. The carbonyl oxygen concentration remained steady for the films produced at short and moderate exposures; yet, a significant decrease in the ester oxygen followed by an increase in the new species concentration is noted with increasing plasma exposure. Growth of the new species occurs at the same apparent rate as the decrease in ester oxygen. At high exposure, surface carbonyl oxygen is lost along with additional amounts of ether oxygen. It is therefore, probable that some energetic species (hv, electrons, ions, metastables) produced in the plasma pretreatment process impacts on or imparts sufficient energy to the ester functionality to cause its dissociation. The new oxygen functionality noted most likely results from the relaxation of radical species to a stable form. This is considered very probable since the samples were analyzed more than 24 hours after production and excited species in general have lifetimes a great deal shorter.

Insight into probable functional changes in the PET backbone may be gained by studying thermal and photochemical decomposition routes that have been shown to center around dissociation of the ester functionality. Many investigations [119,120,121,122] have been carried out on the thermooxidative

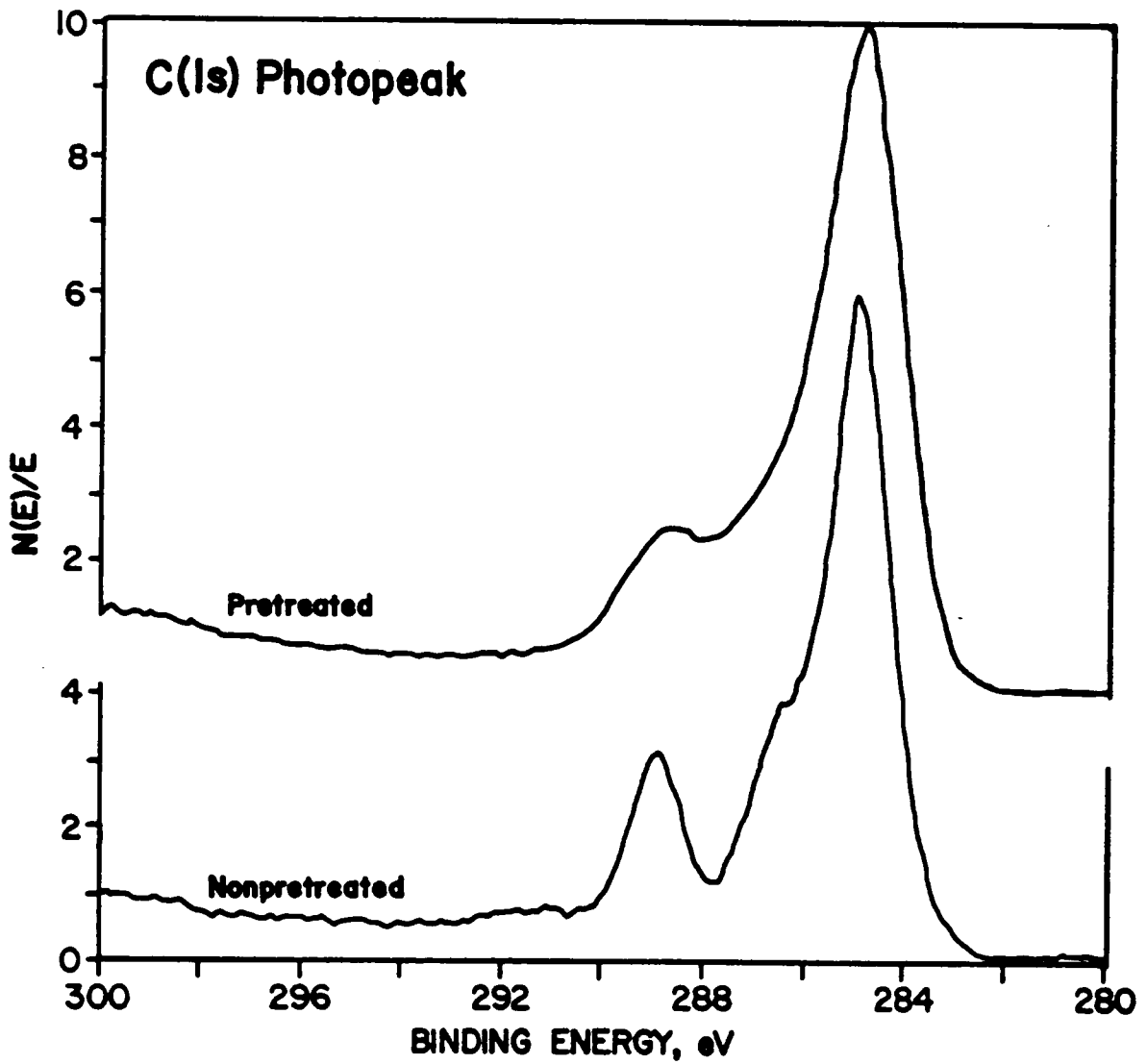


Figure 60. The XPS C(1s) spectrum of both plasma pretreated and nontreated ICI-442 polyester film.

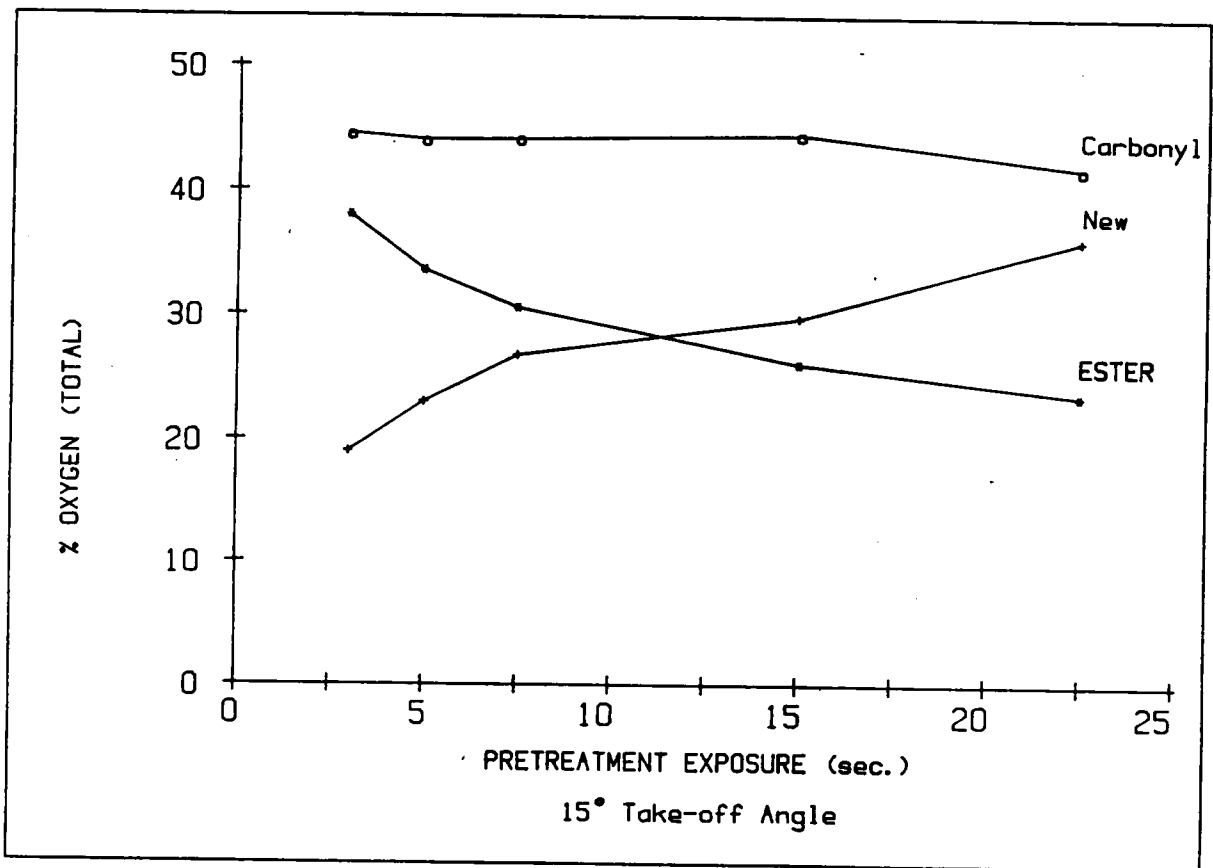
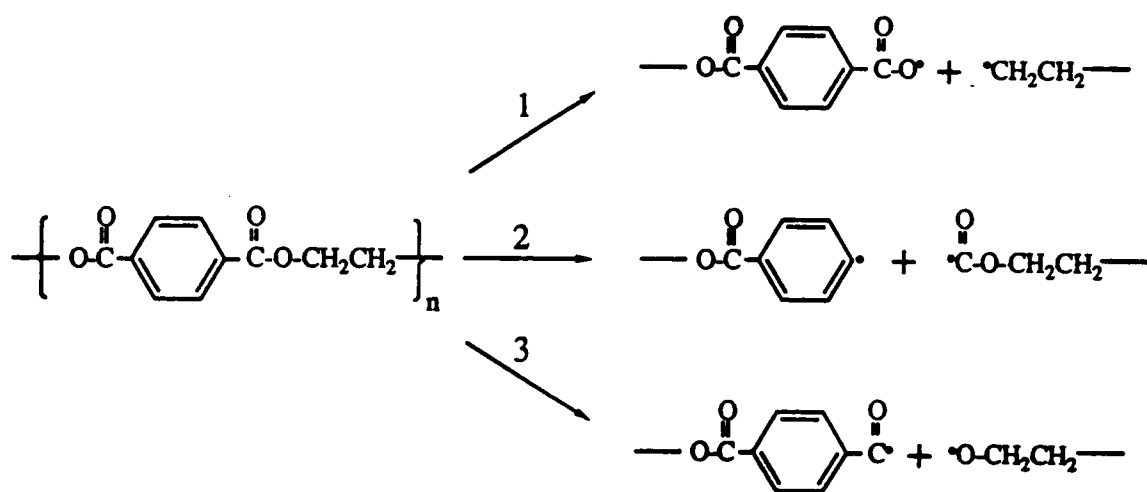


Figure 61. Plot of the change in concentration of oxygen species versus plasma exposure for ICI-442 polyester film at a 15° take-off angle.

degradation of poly(ethylene terephthalate). In summary, it is generally agreed that thermal dissociation of the ester functionality occurs between the ester oxygen and the primary methylene group in the backbone. The major functional products of thermoxidative degradation are carboxylic acids and vinyl groups. The photochemical degradation of poly(ethylene terephthalate) has also been studied extensively.[123,124,125,126] Photolysis of PET is more complex than thermal degradation and the possible mechanisms are more contested. But, typically two photolytic decomposition routes are reported. Scheme 5 provides a compendium of the more probable mechanisms. On energetic grounds, reactions (1) and (3), 84 and 88 kcal/mole, tend to seem more probable than reaction (2) with an estimated bond dissociation energy of 102 kcal/mole. Indeed in all reports, reactions (1) and (3) predominate. Reactions (1) and (3) are normally termed Norrish type II and type I decomposition, respectively. The major polymer functional products of photolytic decomposition were carboxylic acid and vinyl groups for reaction (1) and aldehydes for reaction (3).

In relation to the effects of the plasma pretreatment observed by XPS, it is most likely that either a carboxylic acid or aldehyde functional group is responsible for the appearance of the new oxygen functionality. Among these two choices, the aldehyde functionality agrees more closely with the observed changes in binding energy than the presence of a carboxylic acid; since the carboxylic acid C(1s) photopeak would most likely appear at a slightly higher binding energy than the ester carboxyl carbon and would not result in loss of signal intensity in this region. The evidence still does not preclude the existence of surface alcohol or ketone functionality, they are considered more unlikely in view of the evidence from previous decomposition studies.



Scheme 5. Commonly reported thermal and photolytic decomposition mechanisms of poly(ethylene terephthalate).

#### D. Attenuated Total Reflectance Fourier Transform Infrared Spectrometric (ATR-FT-IR) Study of Plasma Pretreated ICI-442 Polyester Film

Upon plasma treatment, evidence for the dissociation of the backbone ester functionality has been provided by X-ray photoelectron spectroscopy. From data obtained from this technique, an alcohol, ketone, aldehyde, or carboxylic acid surface species was predicted to result upon plasma pretreatment of ICI-442 polyester film. XPS, however, is not definitive in this case. In order to further define the nature of the new surface species as well as support one of the dissociative mechanisms described in the previous section, attenuated total reflectance Fourier transform infrared spectrometry has been used to study the effects of plasma pretreatment on ICI-442 polyester film. Day and Wiles [123] and Blais et al. [127] have used ATR-IR to study the effects of ultraviolet degradation on PET with success.

An ATR-IR spectrum of nonpretreated PET is exhibited in Figure 62. The IR spectrum of PET is characterized by the presence of intense bands due to the ester functionality and aromatic rings.[128,129] In the nonpretreated ATR-IR spectra there exists a relatively sharp band at approximately  $3430\text{ cm}^{-1}$ . Heating the sample in a vacuum oven at  $100^{\circ}\text{C}$  prior to IR analysis did not result in a decrease in its intensity suggesting that adsorbed water is not the explanation for its presence. However, the position and intensity are consistent with the band assignment as the first overtone of the fundamental carbonyl absorption located at  $1710\text{ cm}^{-1}$ . [122]

Study of the carbonyl region ( $1650\text{-}1800\text{ cm}^{-1}$ ) indicated significant changes in carbonyl peak shape following plasma pretreatment at low to moderate exposure (Figure 63). Growth of IR bands in this vicinity suggest the formation of new carbonyl species. However, at high plasma exposure reduction in carbonyl

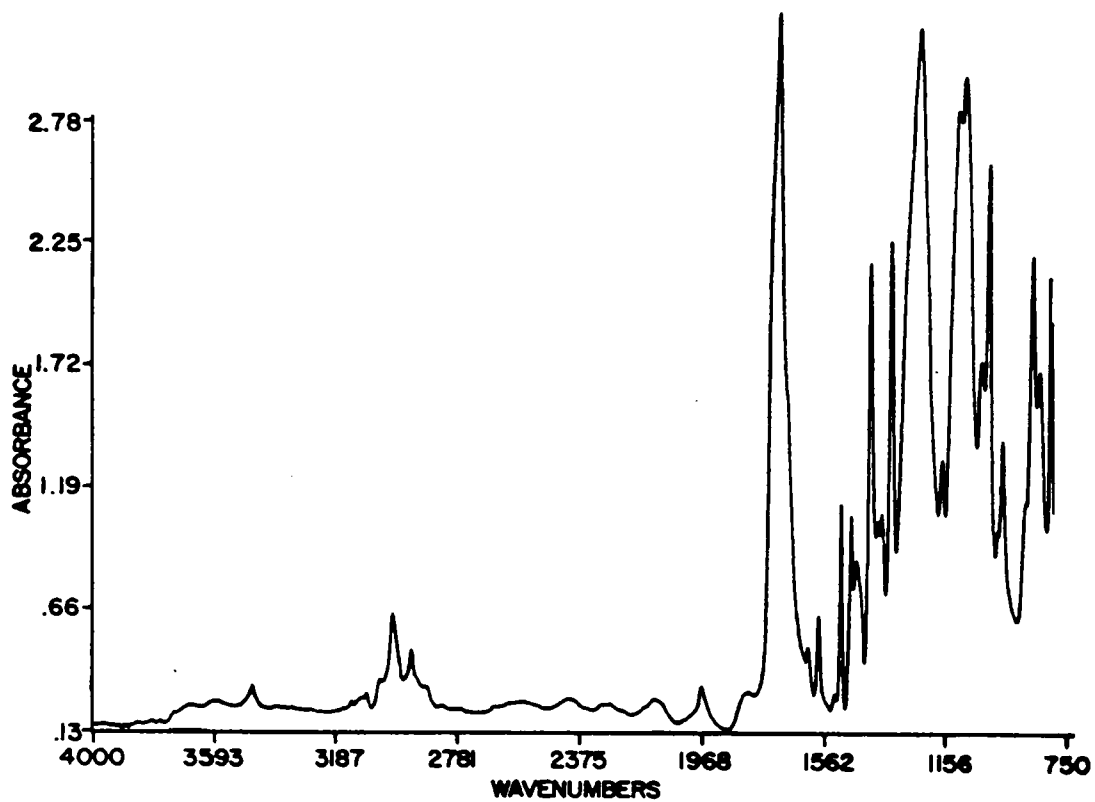


Figure 62. The ATR-IR spectrum of nontreated ICI-442 polyester film.

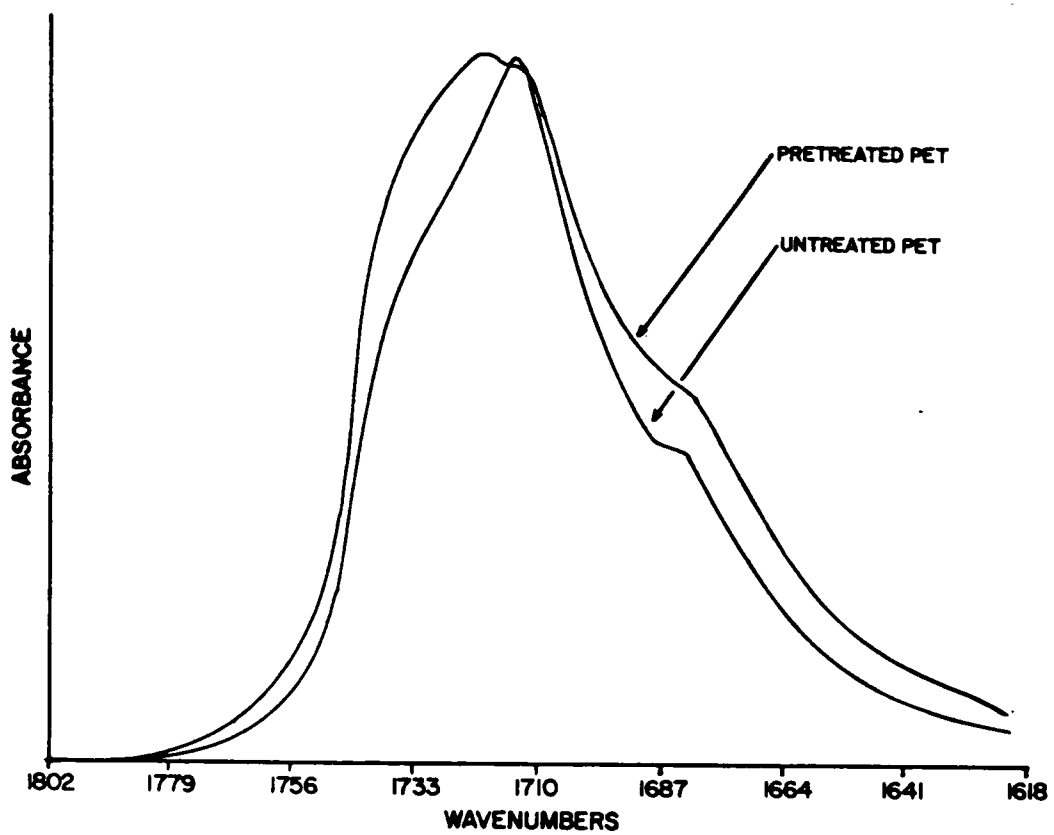


Figure 63. The carbonyl region of both plasma pretreated and nontreated ICI-442 polyester film obtained by ATR-IR.

band intensity is observed indicating loss of this functionality. It has been shown by XPS that plasma exposure has a profound effect on surface elemental composition. With short exposure, surface functionalization was evident, although long exposure reveals that extensive surface deoxygenation has occurred. Changes in carbonyl functionality follow this observed behavior. Figure 64 displays ATR-IR difference spectra of the carbonyl region of PET films which vary in plasma exposure. Initially, there was an increase in band intensity around  $1720\text{-}1745\text{ cm}^{-1}$  and  $1705\text{-}1670\text{ cm}^{-1}$ . The observed increase reaches a maximum in approximately 7.5 seconds. Pearce et al. have made tentative IR assignments to bands in this regime following thermal degradation of PET.[122] Carbonyl IR bands centering around  $1730$  and  $1740\text{-}1750\text{ cm}^{-1}$  have been assigned to generic "carbonyl" stretching frequencies, while bands observed below  $1710\text{ cm}^{-1}$  have been assigned to aldehyde and carboxylic acid (benzoic acid) species. Dunn and McClure[128] have reported the presence of carboxylic acids, aldehydes and esters on  $\text{O}_2$  plasma etched poly(ethylene terephthalate) films. Similar changes have also been found following photolytic decomposition of PET.[123,127] The presence of carboxylic acid functionality was substantiated by an -OH IR vibration of the -COOH group at  $3290\text{ cm}^{-1}$ . Figure 65 displays difference spectra for the IR region between  $3200$  and  $3550\text{ cm}^{-1}$  for PET samples with varying plasma exposure. Besides the first overtone of the carbonyl region ( $3440\text{ cm}^{-1}$ ), which changes in the expected manner with exposure, no other IR absorption is present suggesting that carboxylic acid formation is minor if occurring at all during plasma pretreatment. Additionally, the absence of -OH structure does not support the formation of surface alcohol functionality. It appears then, that surface aldehydes account for the primary growth of carbonyl species in the pretreated films. Of the decomposition

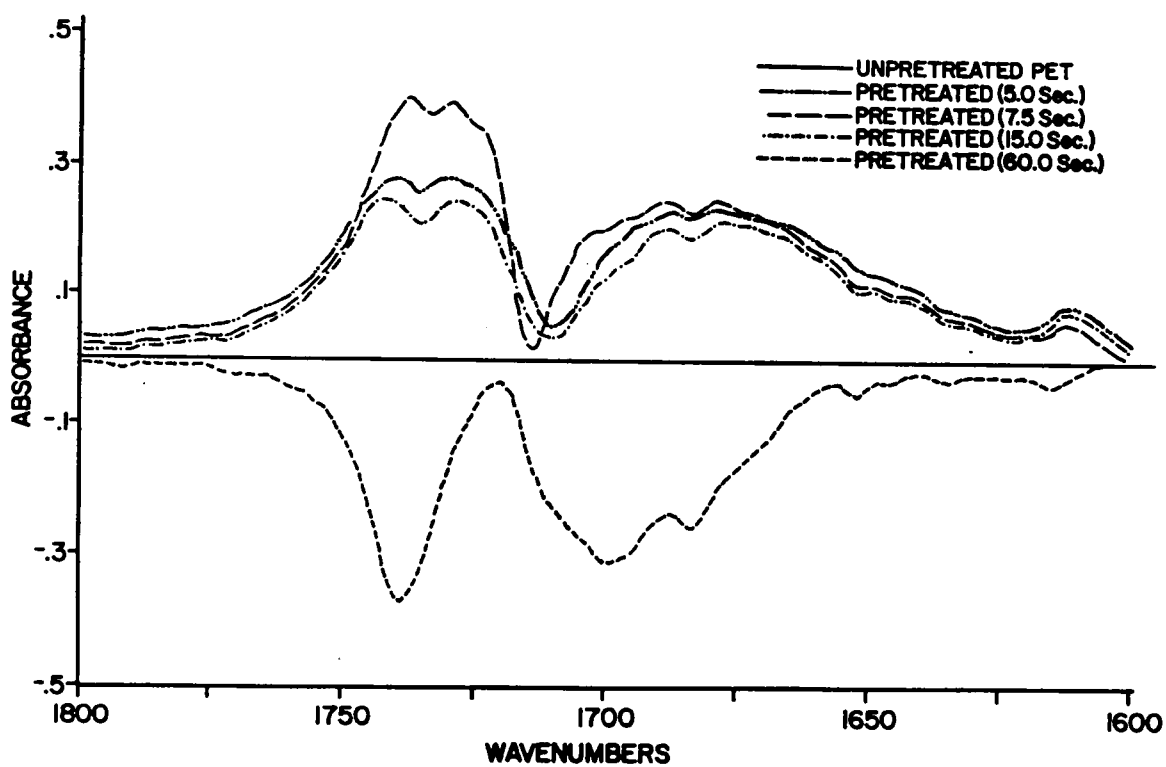


Figure 64. The effect of plasma exposure on the carbonyl region of ICI-442 polyester film obtained by ATR-IR. The difference spectra are shown (plasma treated spectrum - nontreated spectrum).

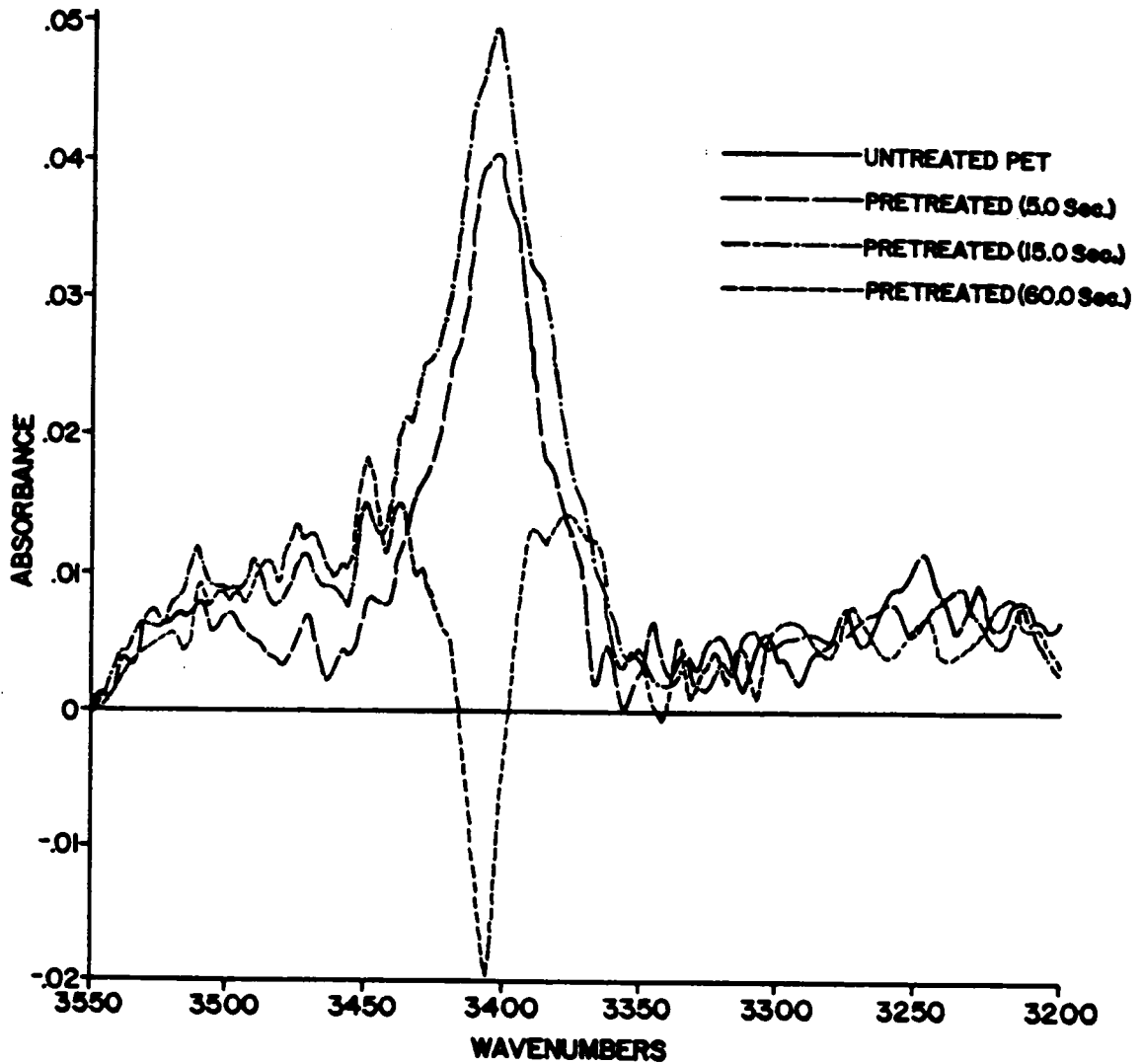


Figure 65. The effect of plasma exposure on the -OH stretching region of ICI-442 polyester film obtained by ATR-IR. The difference spectra are shown (plasma treated spectrum - nontreated spectrum).

mechanisms then, the Norrish type I scheme would most likely result in this phenomenon.

In accord with the changes observed by XPS, plasma exposure beyond 10 sec results in loss of carbonyl structure (Figure 64). After 15 seconds small amounts of carbonyl component are lost while 60 seconds exposure reveals a large loss of carbonyl functionality. If a Norrish type I decomposition route was in effect, the noted surface deoxygenation would probably result from either carbon-oxygen double bond breakage (energetically unlikely) or loss of carbon monoxide from the pretreated polymer backbone. As greater amounts of plasma energy are absorbed by the surface of PET (longer exposure), chances are that reactions such as carbon monoxide scission will predominate rather than relaxation of the intermediates to stable rearrangement products (aldehydes, etc.) which would account for the observed trend in surface composition with plasma exposure.

Dissociation of the ester functionality in PET through any of the possible mechanisms would result in reduced C-O (singly bonded) band intensity. Figure 66 displays the C-O IR stretching region ( $1200\text{-}1300\text{ cm}^{-1}$ ) for both plasma pretreated and nontreated ICI-442 polyester film. Indeed, in all cases, pretreatment leads to a reduction in the C-O stretching mode intensities at approximately  $1275$  and  $1250\text{ cm}^{-1}$ . Liang and Krimm [130] as well as D'Esposito and Koenig [131] have assigned these bands to C-O stretching of the -COO functionality in PET. Systematic changes in C-O band intensity are also produced by varying the pretreatment time (Figure 67). For either ketone/aldehyde formation or CO scission one would expect loss of C-O band intensity. Experimentally this is the case, as one increases plasma exposure

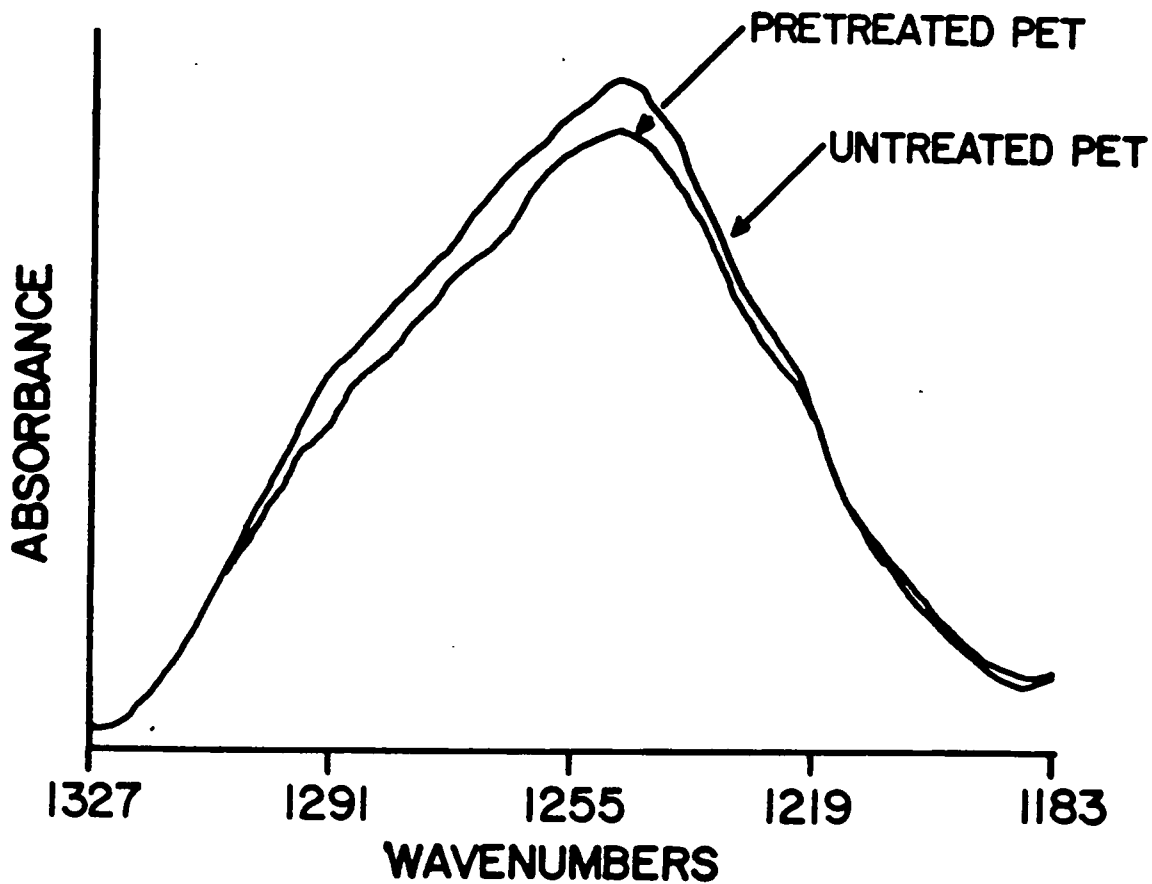


Figure 66. The C-O region of both plasma pretreated and nontreated ICI-442 polyester film obtained by ATR-IR.

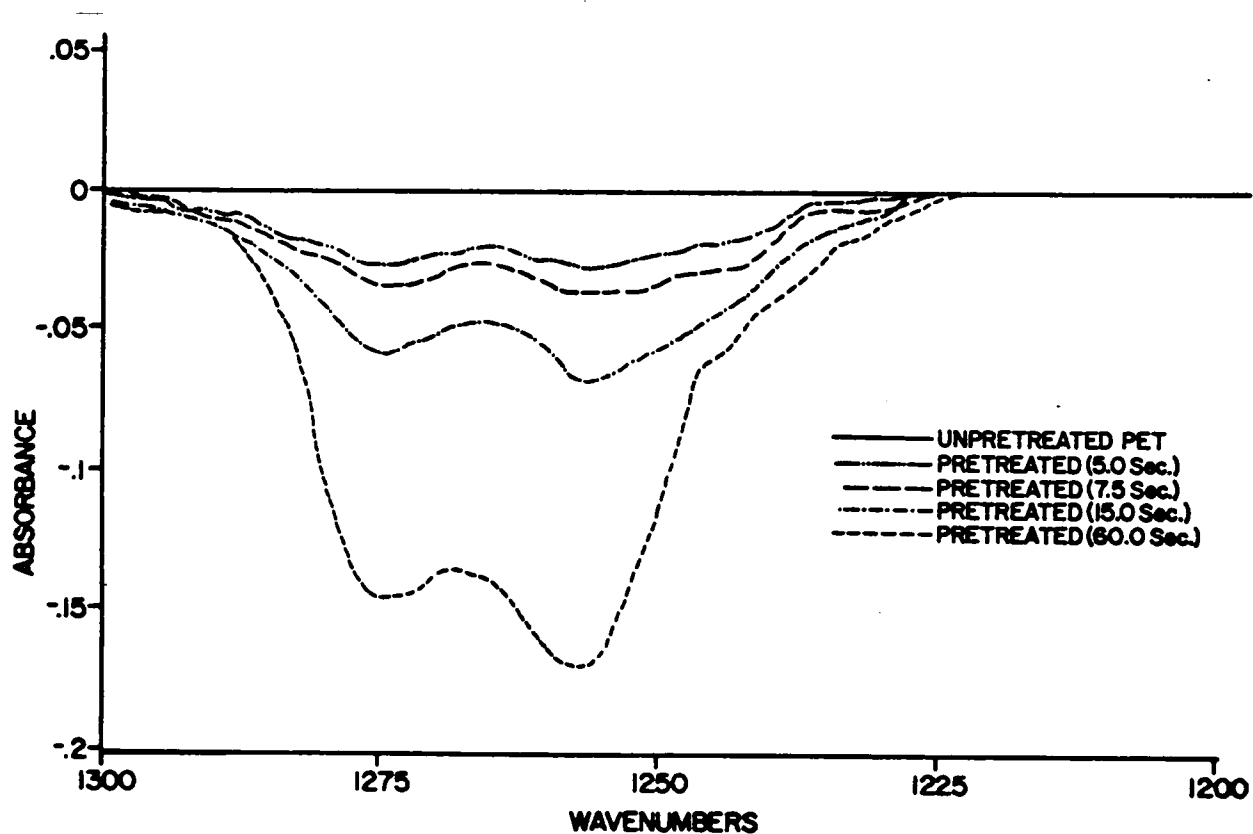


Figure 67. The effect of plasma exposure on the C-O region of ICI-442 polyester film obtained by ATR-IR. The difference spectra are shown (plasma treated spectrum - nontreated spectrum).

more C-O band intensity is lost. The bands at both 1274 and 1250  $\text{cm}^{-1}$  vanish at the same rates as more energy is input into the PET surface.

#### E. Residual Gas Analysis of the Treatment Gas Mixture Before and After Plasma Initiation

Residual gas analysis (RGA) provides one with a mass spectrum characteristic of a large volume of gas by regular sampling of small amounts over some set length of time. This technique is particularly well-suited for the study of gaseous plasma due to the numerous molecular and atomic species that arise under these conditions. As noted previously, with long plasma exposure, a prevalent effect of the pretreatment process may be chain scission followed by loss of carbon monoxide. The release of CO, if it occurs, should be easily observed by RGA. By monitoring the abundance before and after plasma initiation, relative to argon, a comparison of the values should indicate whether loss of CO is a viable decomposition route.

Table XXII compares RGA data obtained upon analyzing components in the pretreatment chamber before and after glow discharge initiation employing 100% argon and 60 seconds exposure. The possible number of gaseous components is relatively small due to the chemical inertness of argon. Accordingly, the mass spectrum is simple, allowing one to normalize all peaks to the singly ionized argon state at  $m/z$  40. The use of  $\text{N}_2\text{O}$  or a 50:50 mixture of argon and nitrous oxide resulted in more complex mass spectra arising from the decomposition of  $\text{N}_2\text{O}$  following plasma initiation. Production of new species, such as  $\text{N}_2$ , with the same  $m/z$  ratio as CO made interpretation impossible for these gases in this case.

Table XXII  
RGA Mass Spectral Data of the Glow Discharge<sup>a</sup>

<u>m/z</u>	Relative Abundance	
	<u>before initiation</u>	<u>after initiation</u>
18	6.4	5.8
20	20.9	19.8
28	0.9	6.6
40	100.0	100.0
44	0.0	0.2

<sup>a</sup>Pet film exposed to plasma for 60 sec. (avg.).  
100% argon used as pretreatment gas.

The mass spectra (Table XXII) obtained by using 100% Ar yield straightforward interpretation. Before plasma initiation, the presence of both singly (40 m/z) and doubly (20 m/z) ionized argon is expected. They are present in the anticipated 5:1 ratio.[132] There is also a rather large amount of water (18 m/z) and a small amount of carbon monoxide or possibly N<sub>2</sub> (28 m/z) detected. The water flux is most likely a result of the film off-gassing. Even though the film is under vacuum, it retains significant amounts of water because diffusion out of the tightly wound roll is slow. Since there is no change in the relative abundance of H<sub>2</sub>O before versus after plasma initiation, water must be diffusing out of the film at a fairly constant rate. To assess the moisture content of the ICI-442 polyester substrate, a sample was heated from 30°C to 600°C at 20°C per minute in a thermogravimetric analyzer. The moisture content (mass loss occurring up to 200°C) is approximately 0.15 wt %. A plasma pretreated ICI-442 film (60 sec exposure) had the same weight percent loss in this region indicating no permanent difference in the equilibrium moisture content of these two films (Figure 68).

Increases in both CO and CO<sub>2</sub> concentrations are observed in the RGA mass spectrum following plasma induction. CO generation alone accounts for the growth of the peak at 28 m/z, since there is no possible source of N<sub>2</sub> in the chamber except for the polymer substrate which contains none. The small amount of CO<sub>2</sub> (44 m/z) detected also precludes that CO resulted from substantial fragmentation of CO<sub>2</sub> in the plasma. The increase in carbon monoxide abundance can only occur through chain decomposition following a Norrish type I mechanism. Indeed, significant amounts of CO have resulted from the photolytic degradation of PET.[133,134,135] In general, the results of photolytic decomposition by both mass-spectrometric and gas chromatographic

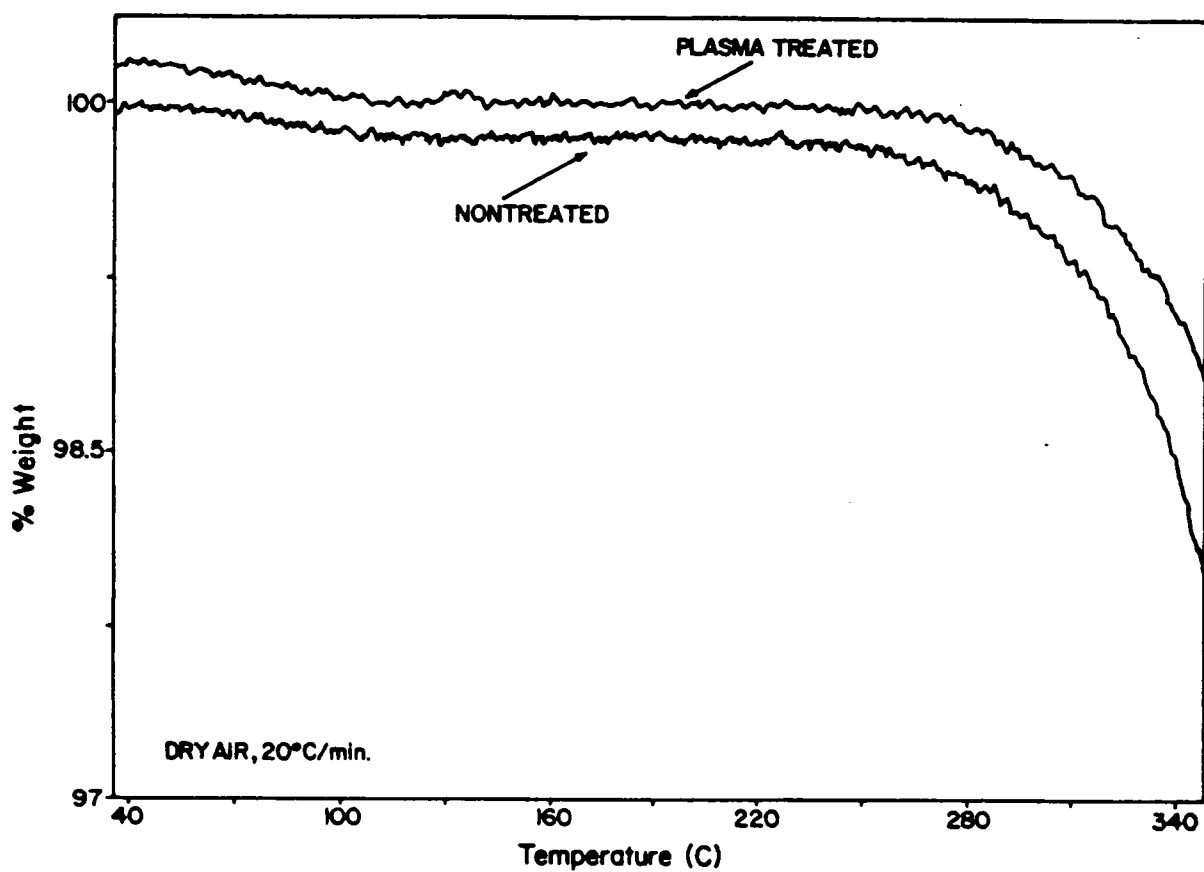
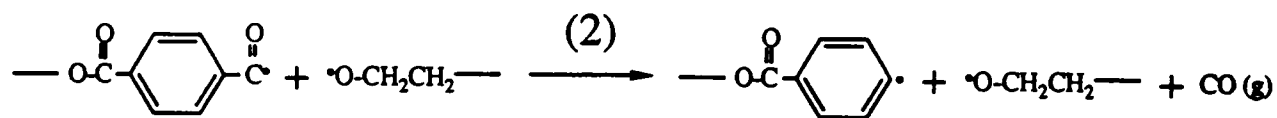
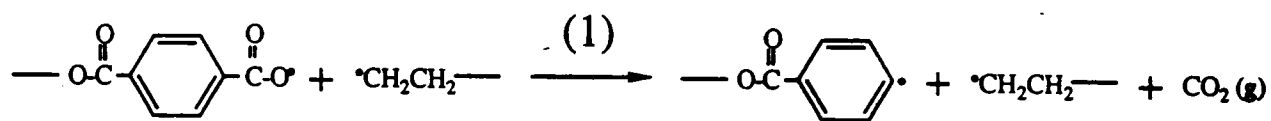


Figure 68. The thermogravimetric profile of nontreated and plasma pretreated ICI-442 polyester film.

analyses indicated CO and CO<sub>2</sub> to be the main volatile products, accounting for over 95% of the total volatiles. CO production, in most cases, was reported to be 2-4 times as great as CO<sub>2</sub> production dependent upon the length of UV exposure. Scheme 6 exhibits the primary mechanisms that have been suggested [126] to account for the presence of CO and CO<sub>2</sub>. Thermal decomposition results in CO<sub>2</sub> produced as the major volatile product. Therefore, the minor amount of carbon dioxide detected following plasma initiation as opposed to thermal decomposition indicates that ester dissociation following this route (same as Norrish type II) is of secondary importance.

A mechanism with two degrees of severity is therefore most probable. Initially, at low energy input a relaxation process which forms new carbonyl structure following a Norrish type I ester cleavage is favored. But, if the energy is higher, either through single or multiple plasma/polymer interactions, loss of carbon monoxide is favored. The adhesive strength of metallized PET follows this trend in behavior. That is at low plasma exposure the production of active surface species during plasma pretreatment may provide junctions between the polymer and the metal after metallization which allows increased adhesion. Alternatively, high plasma exposure leads to substantial chain scission from loss of CO before metallization. A weak boundary layer, consisting of low molecular weight polymer, is formed by this degradation thereby decreasing adhesion. The typical Lorentzian behavior of adhesive strength vs. plasma exposure is shown in Figure 69. The dashed line represents the point where the effects of either process are equal. The small amount of CO<sub>2</sub> detected suggests that chain scission may also be occurring between the ether oxygen and the primary methylene group (Norrish type II). If present, these results as well as the absence of -OH IR bands state that it is a minor mechanistic component.



Scheme 6. Poly(ethylene terephthalate) decomposition routes leading to the formation of CO and CO<sub>2</sub>.

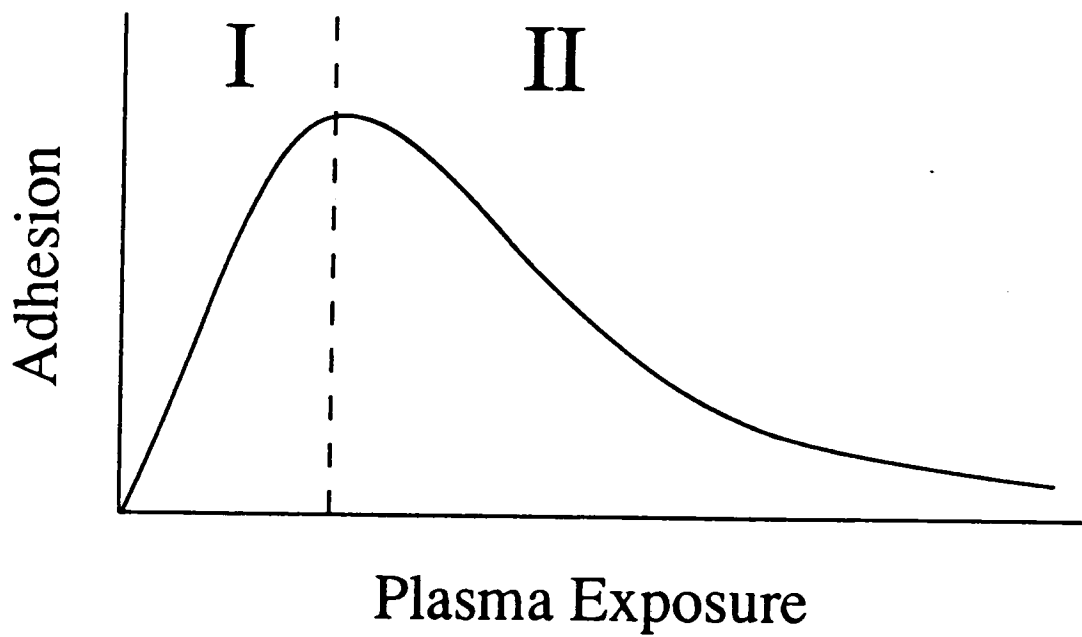


Figure 69. The behavior of titanium/polyester adhesion versus plasma exposure.

However, since plasma chemistry is complex, a variety of surface modifications would seem plausible.

#### F. Static Contact Angle Analysis of Nontreated and Plasma Treated ICI-442 Polyester Film

Good wettability is one of the ranking criteria for maximum bond strength between materials. Surface wetting characteristics are very sensitive, even small traces of contamination can adversely affect the contact angle. Surface hydrocarbon contamination as well as surface chemical modification has been observed for raw and plasma pretreated polyester film by XPS, respectively. Therefore, static contact angle analysis was performed on the raw and plasma pretreated polyester films described above to assess any changes in surface wettability. Distilled water was used as the wetting agent for all measurements.

The measured contact angle decreased significantly for the pretreated film as compared to the raw film suggesting an increase in surface energy of the polyester upon pretreatment. Water is a high surface energy liquid and will wet (e.g. exhibit a lower contact angle) a higher surface energy substrate. The measured contact angle for the nontreated polyester film was  $69.5^{\circ}$ . The contact angles measured for the pretreated films ranged from  $55.0$ - $58.5^{\circ}$  with no apparent trend for films exposed to the plasma for short to moderate intervals. At longer exposure (60 sec) however, an increase in contact angle to  $64.0^{\circ}$  is observed. Initially, it was thought that this measurement technique was detecting the difference between a clean and carbon contaminated surface. Although the presence of small amounts of nitrogen functionality may reduce the contact angle slightly. However, long exposure to the plasma shows that extensive surface compositional changes also affect wettability. The surface functional

changes that occur at low to moderate exposure would not be expected to change the surface energy significantly (i.e. ester vs. aldehyde). Nevertheless, the effects of surface deoxygenation are observed with longer exposure wherein the surface structure begins to resemble hydrocarbon-like material. Rose and Liston [136] profiled the effects of oxygen plasma treatment for a number of polymeric systems including PET. Following O<sub>2</sub> plasma exposure, poly(ethylene terephthalate) exhibited a water contact angle of 17.5°, much lower than observed here. An oxygen plasma, however, would not be expected to reduce the number of oxygen species with increasing exposure; it would increase surface oxygen functionality. The plasma pretreatment then, is not believed to alter the surface energy of a clean polyester surface until significant surface deoxygenation has occurred.

## **XI. THE INTERFACIAL CHEMISTRY OF TITANIUM COATED POLYESTER FILMS**

### **A. Preliminary**

One of the most important after-effects of plasma treatment is a substantial increase in adhesion between deposited titanium and the PET film relative to the untreated film. In the previous Chapter, the surface chemical effects of plasma treatment were determined by a variety of analytical methods. Surface functionalization, from the dissociation of the ester moiety, most likely results in new carbonyl species. The purpose of this Chapter is to probe the interfacial structure, chemically and physically, in order to determine how the plasma treatment induces additional adhesion. Further, the role that surface functionalization plays in this phenomenon will be addressed.

### **B. Auger Electron Depth Profiling and X-ray Photoelectron Spectroscopy**

The surface structure and composition of titanium sputter deposited on commercial ICI-442 polyester films were determined through the use of Auger electron spectroscopy (AES) with depth profiling via argon ion etching and X-ray photoelectron spectroscopy. To understand the adhesion of the titanium to the polyester, it is extremely important to know the composition of the material as close to the interface as possible to thereby determine the primary bonding agent. Three titanium coated films which differ in their plasma exposure (0, 2.5 and 60 sec) were examined in order to determine if the extent of plasma pretreatment affects (1) the bulk properties of the titanium deposit and (2) the structure of the titanium/polyester interface.

An Auger depth profile of a typical titanium coated polyester film (Figure 70) exhibits three distinct regions within the deposited layer (i.e. a layer, rather metallic in character sandwiched between two titanium oxide layers). In each of the films studied, the internal features of the deposited titanium were equivalent indicating that the extent of pretreatment does not affect bulk titanium structure. Information about the metal/polymer interface from the profile data, other than the fact that there is oxide present at or near this point, is not provided due to insufficient spatial resolution. It is expected that the outermost surface of the titanium metal would oxidize at room temperature. Typically, titanium has a native oxide layer of approximately 30 Å in air at room temperature. The appearance of oxide near the polyester/titanium interface, however, is unexpected. This observation may be explained in several ways. First, it has been shown [137] that atmospheric water and oxygen may travel along grain boundaries and interfaces which then react with components present in these regions. However, precautions taken to prevent this occurrence (dry conditions) as well as the length of atmospheric exposure do not seem to affect the size of the interfacial oxide. Another possibility is that the oxidation may occur through some chemical interaction between the titanium and polyester present at the interface. Again this does not seem likely, at least on a large scale, because the amount of titanium in direct contact with the polyester could not produce enough oxygen (if all were abstracted by the metal) to account for the expansiveness of this region even taking into account smearing by ion beam "knock-in" artifact effects. The most probable cause of the oxide formation in this area is the interaction of off-gassed water with the incoming or surface bound sputtered titanium atoms. RGA analysis has shown previously that a significant amount of water exists in the plasma pretreatment chamber. It is quite possible that water is

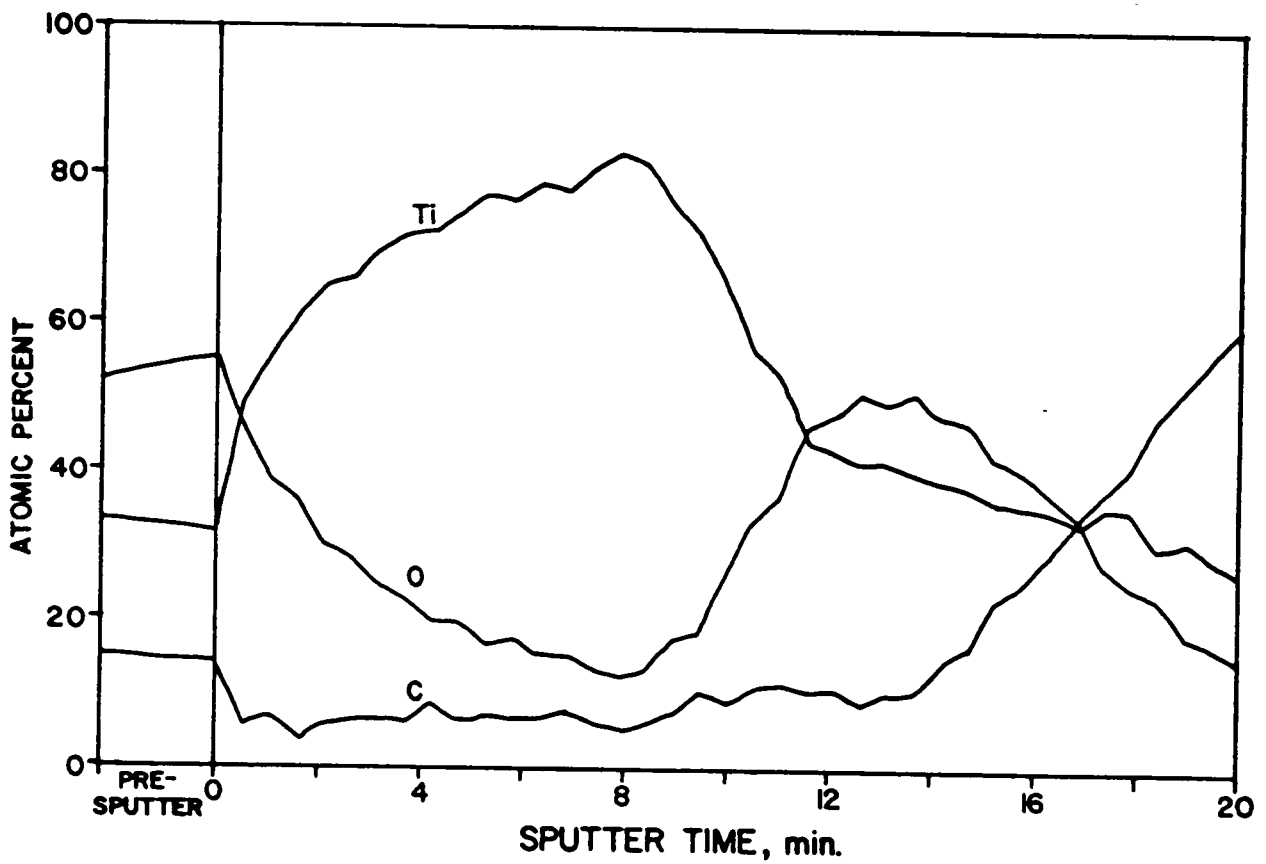


Figure 70. The AES depth profile of a typical titanium coated ICI-442 polyester film.

still being off-gassed into the metallization chamber which is encountered immediately after plasma processing. The highly reactive metal atoms would react with the water present to form an oxide state while continually getting the moisture so that its effects appear only near the interfacial region. Titanium is used commercially to getter oxygen and moisture in a large number of instruments where a high vacuum is required.

In order to inspect the interfacial composition of the metallized PET films, several studies which revolve around the use of X-ray photoelectron spectroscopy have been undertaken. In the first series of experiments, titanium coated PET films, both plasma pretreated and nontreated, with a titanium thickness of approximately 800 Å, were first rapidly argon ion sputtered in the Auger spectrometer, immediately removed from the instrument and placed into an X-ray photoelectron spectrometer for analysis. The location of the interface was determined in a separate experiment through the use of a reference Auger depth profile of the same sample, under similar etching conditions in the Auger spectrometer. Maximum raster size (10 mm X 10 mm) was used to produce a spot large enough for X-ray photoelectron analysis. The film was sputtered to within 50 Å of the titanium/polyester interface to minimize disturbance of the structure present. XPS was conducted at a 90° take-off angle to minimize edge effects from the crater produced in the etching process.

Analysis of the titanium 2p<sub>3/2,1/2</sub> photopeak region of an etched plasma treated titanium coated polyester film indicated that at least two distinct species were present at or near the interface (Figure 71). A peak assignable to carbidic titanium appeared at 454.7 eV in agreement with reported results.[138] A second peak attributable to TiO<sub>2</sub> also appears at 458.7 eV. However, the full-width-at-half-maximum (FWHM) for this peak is significantly greater (2.1 eV) than

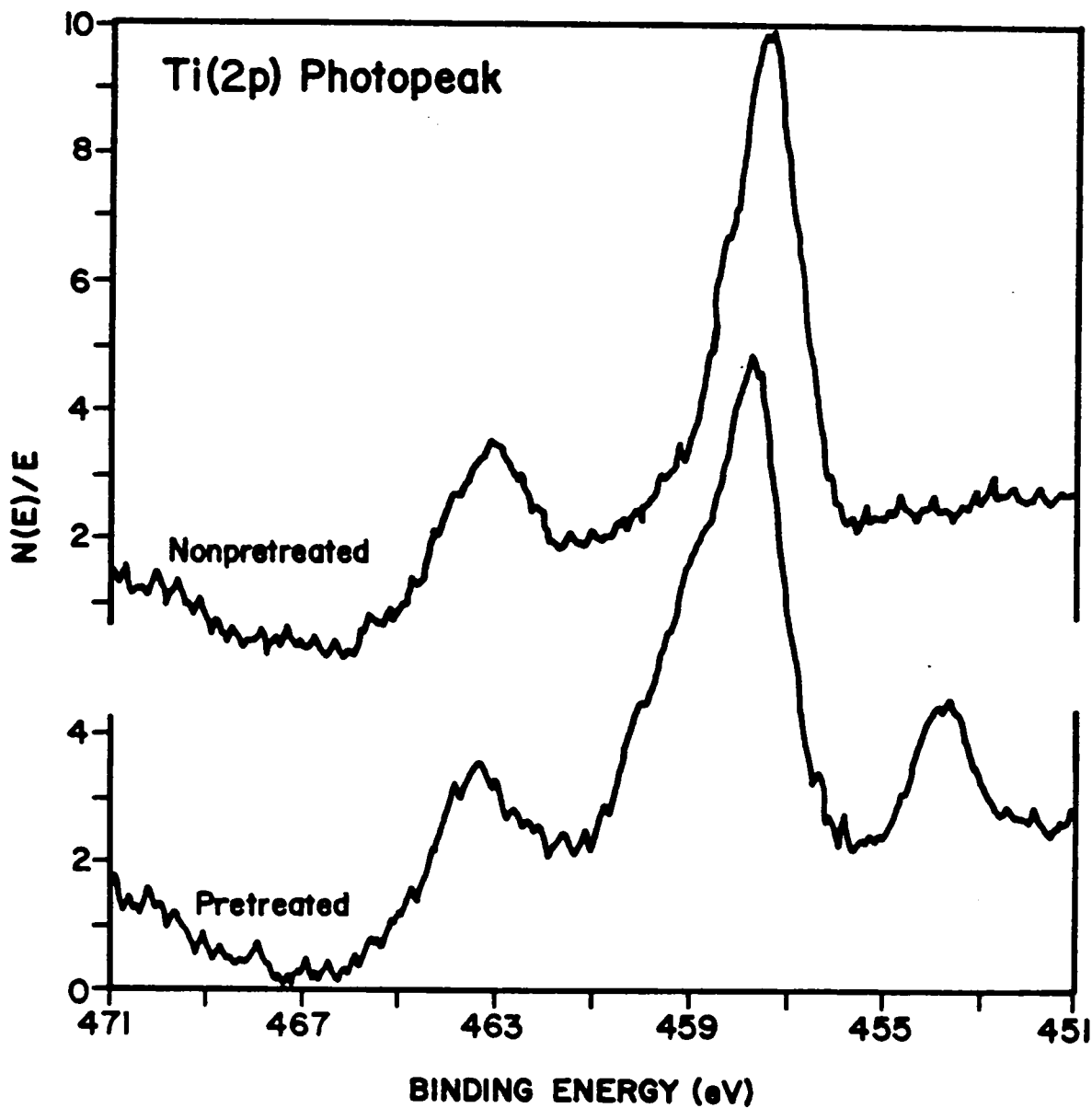
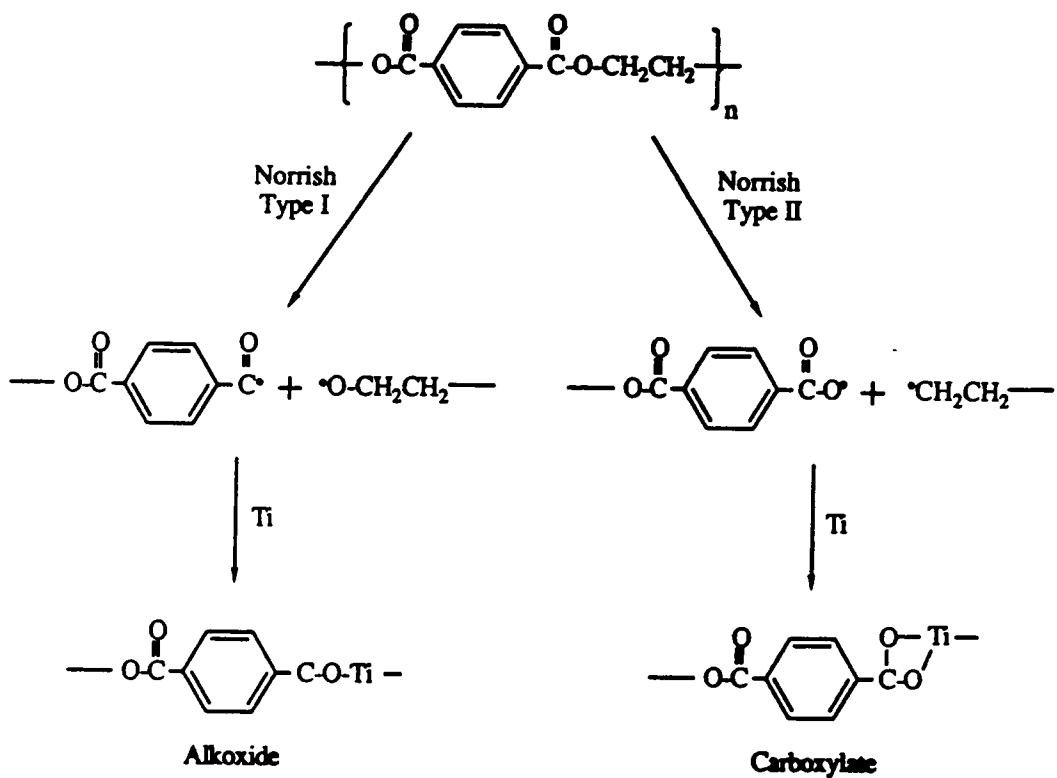


Figure 71. The XPS Ti(2p) spectrum of both plasma pretreated and nontreated titanium coated ICI-442 polyester film following argon ion etching.

that for a  $\text{TiO}_2$  standard (1.4 eV). The  $\text{Ti}(2p_{1/2})$  photopeak from the carbidic titanium species could not wholly account for this broadening since its intensity would be much lower than that of the  $\text{Ti}(2p_{3/2})$  photopeak at 454.7 eV. A variety of oxy-titanium species may therefore be present. It is possible that stoichiometric and non-stoichiometric oxides exist after argon ion etching. Baba and Sasaki [139] have reported chemical reduction of a  $\text{TiO}_2$  surface to  $\text{Ti}^{2+}$  and  $\text{Ti}^{3+}$  upon  $\text{He}^+$  ion bombardment resulting in non-stoichiometric oxides with slightly lower binding energies than that of  $\text{TiO}_2$ . It has also been found that  $\text{Ar}^+$  bombardment preferentially removes oxygen from a  $\text{TiO}_2$  surface which resulted in different oxide forms.[140] Alternatively, titanium alkoxide or carboxylate linkages to the polymer backbone may exist. For example  $\text{TiO}$  acetylacetonate has a reported binding energy of 458.4 eV [138], about the same as  $\text{TiO}_2$ . Species of this type are probable through reactions of titanium with the excited species produced in the polymer by plasma pretreatment. A Norrish type I mechanism could result in an alkoxide structure while a Norrish type II mechanism could result in a carboxylate bonded species, as shown in Scheme 7. Neither the carbidic titanium photopeak nor the increase in FWHM as great (1.7 eV) as that observed for the  $\text{TiO}_2$  region was exhibited in the  $\text{Ti}(2p)$  photoelectron spectrum of an etched metallized nontreated PET film. Therefore, the appearance of carbidic titanium and/or additional oxy-titanium species must result from an effect of the plasma treatment process.

Further elucidation of the titanium species occurred when the  $\text{O}(1s)$  and  $\text{C}(1s)$  photopeaks were evaluated after argon ion etching (Figures 72 and 73). The largest peak present in the oxygen (1s) spectrum had a corrected (aromatic  $\text{C}(1s) = 284.6$  eV) binding energy of 530.2 eV indicating the presence of oxide



Scheme 7. Possible polyester oxygen-titanium metal interactions and products.

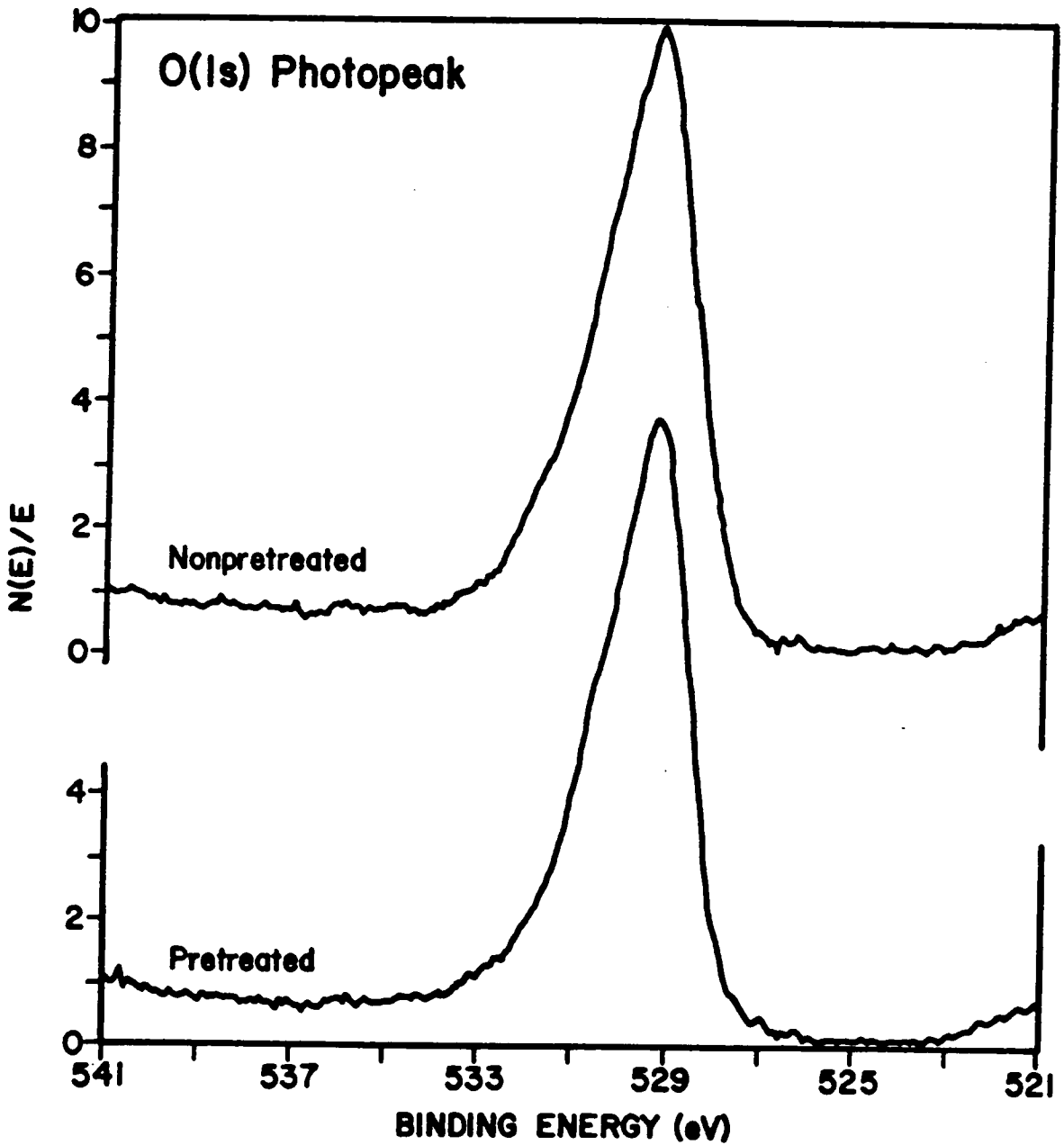


Figure 72. The XPS O(1s) spectrum of both plasma pretreated and nontreated titanium coated ICI-442 polyester film following argon ion etching.

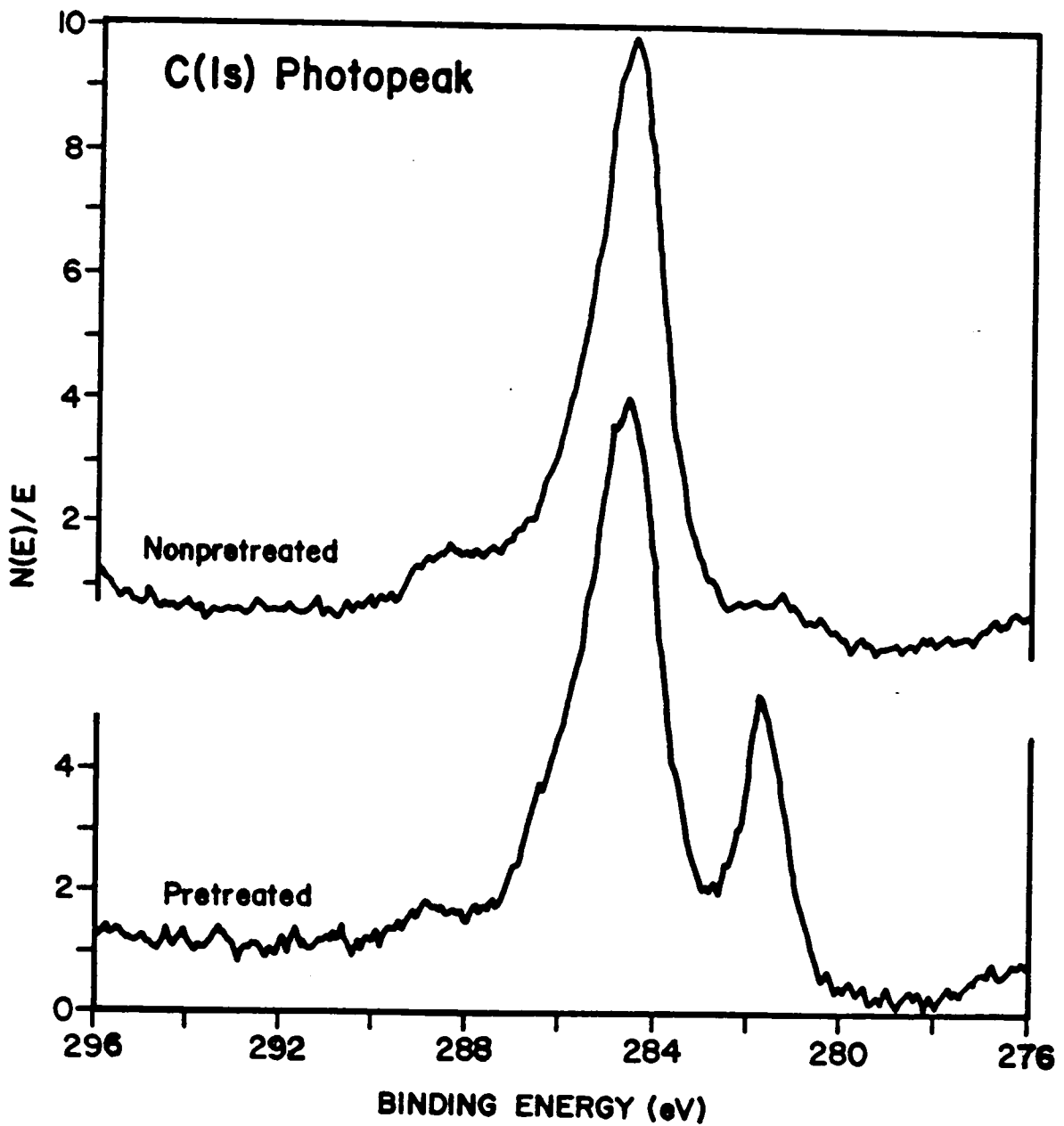


Figure 73. The XPS C(1s) spectrum of both plasma pretreated and nontreated titanium coated ICI-442 polyester film following argon ion etching.

oxygen, in agreement with Auger depth profiling. Weaker photopeak structure appeared at higher binding energies, and could be considered due to either polyester oxygens or various nonstoichiometric oxides and/or polymer-bound species. In the carbon (1s) photoelectron spectrum a peak assignable to carbidic carbon appeared at very low binding energy (281.6 eV corrected). This peak did not appear in the C(1s) photoelectron spectrum of the etched nontreated metallized PET film. Higher binding energy carbons were also detected indicative of the polyester substrate. Suzuki et al. have studied the effect of reactively ion plating PET films with TiO<sub>2</sub>. [141] TiC and carbide-like species were found in the interfacial region following metallization by this method.

Another route used to obtain information about the interfacial region of metallized PET films was to study the fracture specimens obtained from peel tests with XPS. A manual peel procedure was used in order to produce freshly fractured samples that could be placed directly into the photoelectron spectrometer. Samples were first prepared by application of a proprietary polymeric coating to the metallized surface of the polyester film so that the titanium layer could be peeled away. A cross-hatch across the metal layer was made with a razor blade. To this prepared fracture, scotch tape was applied and pulled by hand to manually delaminate the film. Four samples were studied, two were subjected to titanium deposition following plasma pretreatment; while, the other pair were metallized in the absence of pretreatment.

Cohesive failure occurred within the polyester substrate for the plasma treated/metallized films. XPS analysis of either fracture surface provides C(1s) and O(1s) photopeaks identical to that of raw ICI-442 polyester film. No titanium signal is observed on either surface. The nontreated/metallized polyester films exhibited mixed mode failure. Significant concentrations of both oxide oxygen

and polyester oxygen are present on the surface of both fracture surfaces (Figure 74). The titanium (2p) photopeak suggests that only  $\text{TiO}_2$  is present, in accord with that observed following argon ion etching.

Information regarding the interfacial characteristics of metallized polyester films via XPS with argon ion etching and fracture analysis was limited due to the inherent destructive nature, where artifacts are likely, in the first case and the cohesive failure encountered when plasma processing was applied in the second. A third method then was used to probe the interface. Polyester films were produced having a gradient of titanium thickness. It was thought that the thinnest sections produced would be below the effective depth resolution of XPS allowing a strong signal to be obtained from the interfacial region. Samples having a graded titanium thickness on both nontreated and plasma pretreated polyester film were produced by simply turning off the sputtering source power while the film was moving at a constant rate. It was estimated by optical measurements that the thickest titanium deposits at one end of the 8" X 11" sample were nearly 150 Å.

Selected sections from the length of the sheet were analyzed at both  $15^\circ$  and  $90^\circ$  take-off angles by XPS. Examination of the thickest deposit revealed a continuous coating of titanium dioxide. Significant concentrations of polyester were not detected until the upper third of the metallized sheet was reached. The detection of polyester oxygen and carbon photoelectron signals indicated that either the titanium coating was thin enough for the polyester photoelectrons to penetrate or that discontinuities were present in the titanium coating. The initial nucleation and growth of a sputtered film is acknowledged to occur through the formation of islands of the deposited material.[142] Once the islands become large enough, they coalesce to form a continuous film. It is most likely then that

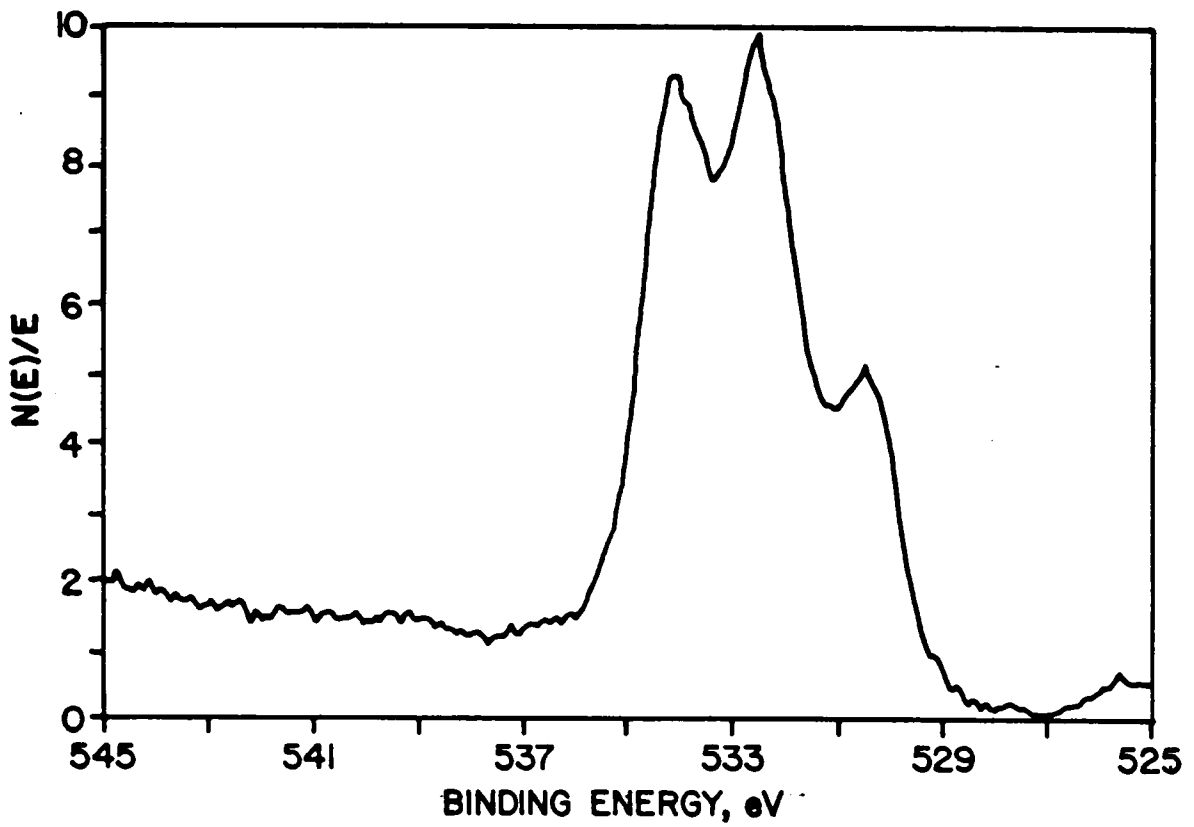


Figure 74. The XPS O(1s) spectrum of the metal containing fracture surface of a nontreated titanium coated ICI-442 polyester film.

discontinuities exist in the coating, with the thinnest portions formed of titanium/titanium dioxide islands.

Even with the presence of a discontinuous titanium layer, observation of the interface was difficult. The relative thickness of the deposited metal was thick enough that it interfered with XPS acquisition at a  $15^{\circ}$  take-off angle. Under these conditions, the C(1s) photopeak spectrum was typical of solely plasma pretreated or nontreated PET dependent upon which substrate was metallized. No carbidic carbon was observed. The O(1s) photopeak spectrum exhibited a mixture of polyester oxygen and oxide oxygen from the coated and noncoated regions (Figure 75). However, with the improved depth resolution of the  $90^{\circ}$  take-off angle, the interface was detected albeit not strongly. For example, a slight amount of carbidic carbon was detected at  $90^{\circ}$  in the C(1s) photoelectron spectrum for the plasma pretreated substrate (Figure 76). But, the Ti(2p) XPS spectrum did not correspondingly exhibit a photopeak at 454.7 eV. The sensitivity of XPS towards carbon is greater than towards titanium. The small amount of carbide detected in the carbon (1s) spectrum then would not be noticeable in the Ti(2p) spectrum. The observation of carbidic titanium in this study also indicates that its presence following argon ion etching is not an artifact of that process and that it is indeed located in the interfacial region. In accordance with the XPS data obtained following argon ion etching, the C(1s) photopeak region of the nontreated graded PET film did not display a carbide carbon signal. The oxygen (1s) photoelectron spectra at  $90^{\circ}$ , for both treated and nontreated PET, were consistent with those observed at a  $15^{\circ}$  take-off angle.

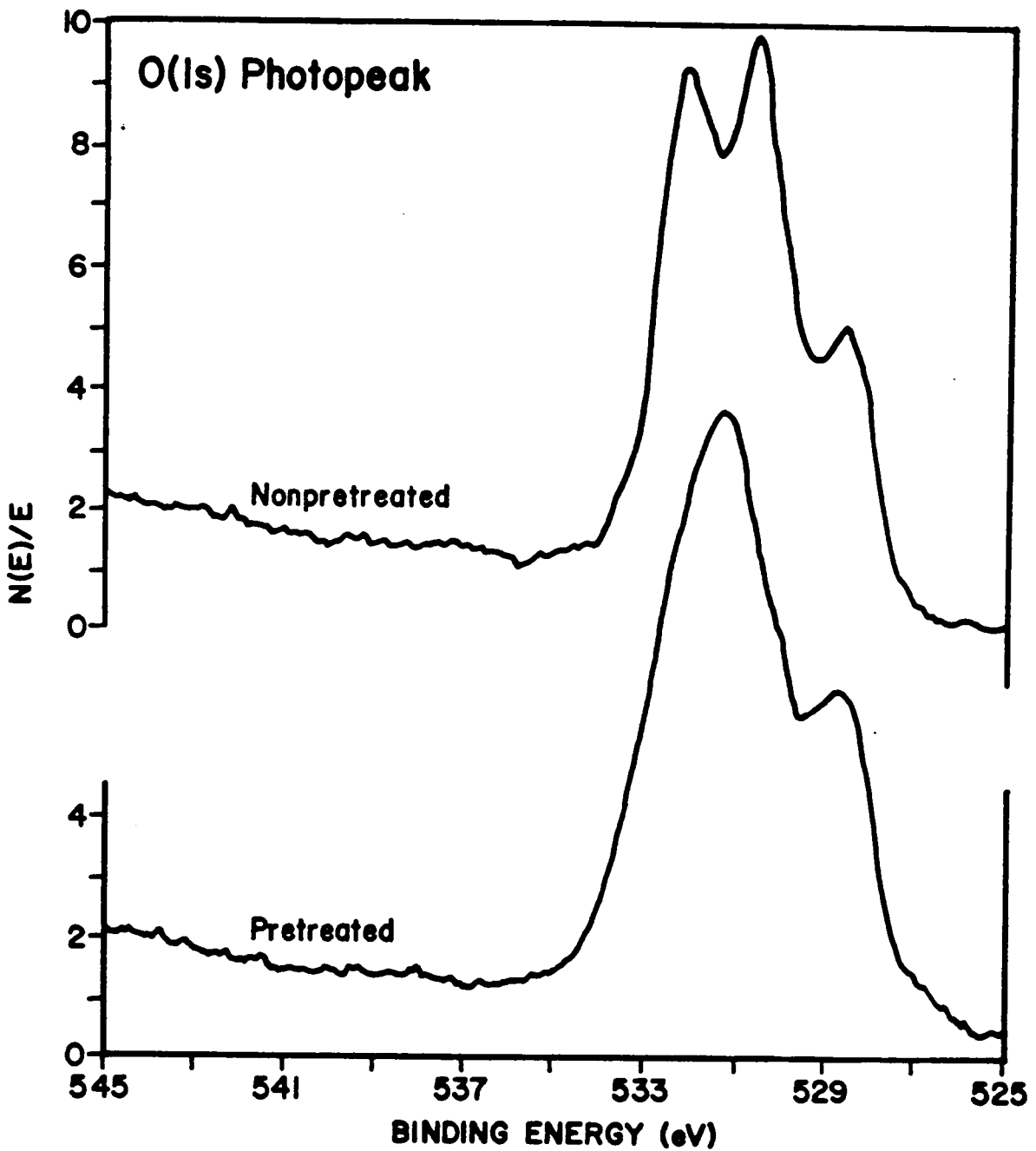


Figure 75. The XPS O(1s) spectrum of both plasma pretreated and nontreated ICI-442 polyester film coated with a thin layer of titanium.

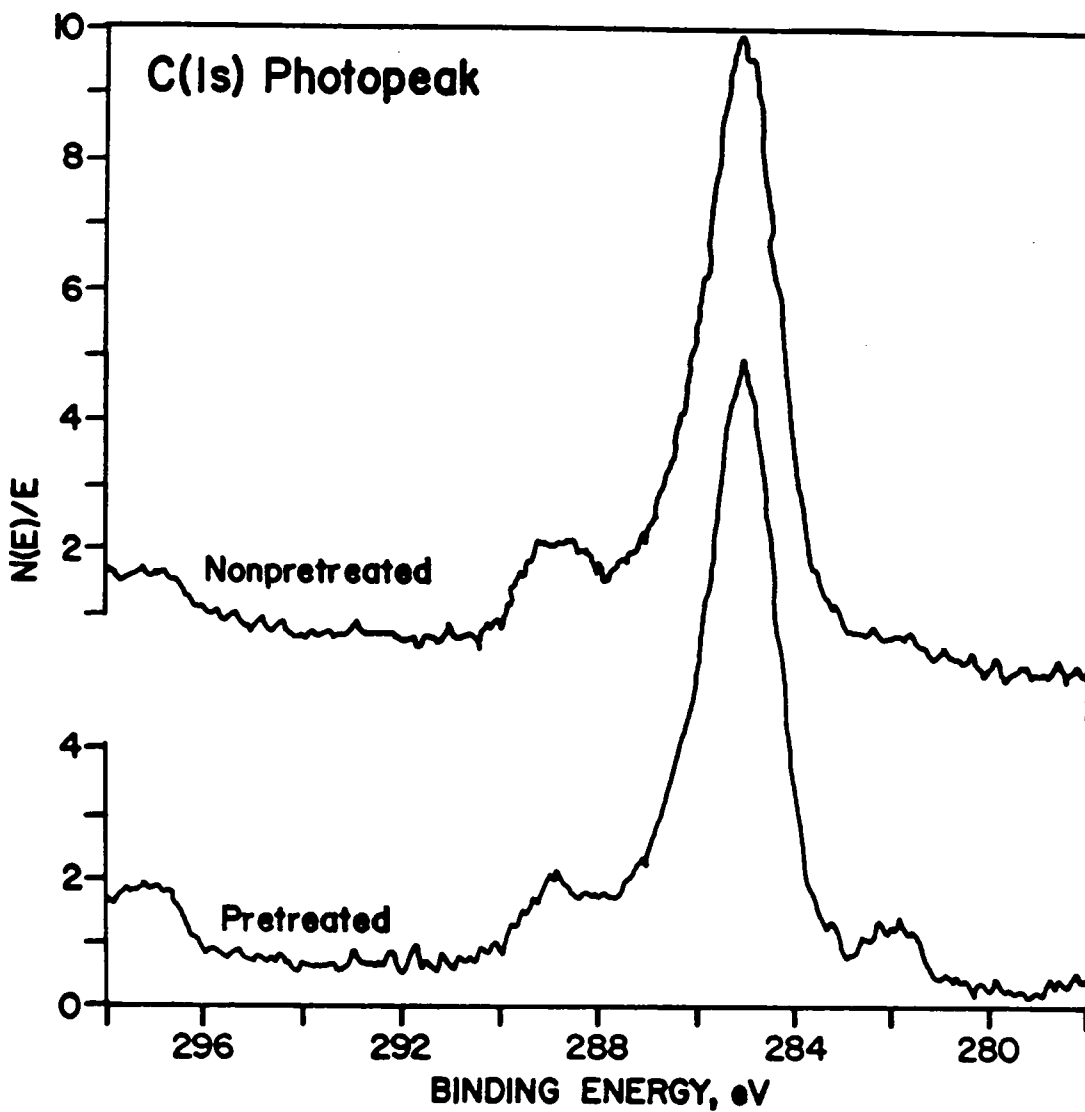


Figure 76. The XPS C(1s) spectrum of both plasma pretreated and nontreated ICI-442 polyester film coated with a thin layer of titanium.

### C. Transmission Electron Microscopic Analysis of Titanium Coated Polyester Films

Transmission electron microscopy (TEM) was used to analyze the metallized polyester film structure of the samples reviewed in the previous section. This particular technique, when the sample is prepared by ultramicrotomy, yields a micrograph of the cross-section of the sample in which both surfaces and the bulk material can be examined. The thickness and morphological character of a particular layer or region can then be inspected and measured from the micrograph. Micrographs of all samples, independent of plasma exposure, exhibited well-defined and consistent titanium deposits. In each case the titanium/polyester interface was extremely sharp (Figure 77) discounting a diffuse interface as suggested by Auger depth profiling. The cause of interfacial broadening in the depth profiles is most likely due to preferential sputtering and "knock-in" effects. Surface roughness would only have a slight influence, if at all, since it was minimal.

The thickness of the titanium layer in each of the films obtained from TEM is given in Table XXIII. It can be seen that TEM provides thicknesses significantly greater than those obtained by either profilometry or Auger depth profiling. TEM micrographs showed the titanium to be slightly embedded into the polyester substrate. Yet, profilometry would ignore any titanium located below the original plane of the uncoated polyester film. The resulting difference may then account for the low thickness values obtained using profilometry. The deviation between TEM and Auger depth profiling data may have resulted from an error in the assumed sputter rate. It was originally assumed that titanium sputters at a rate similar to that of tantalum oxide which is used as an instrumental standard. Normalization to the titanium thickness obtained from TEM yields an average

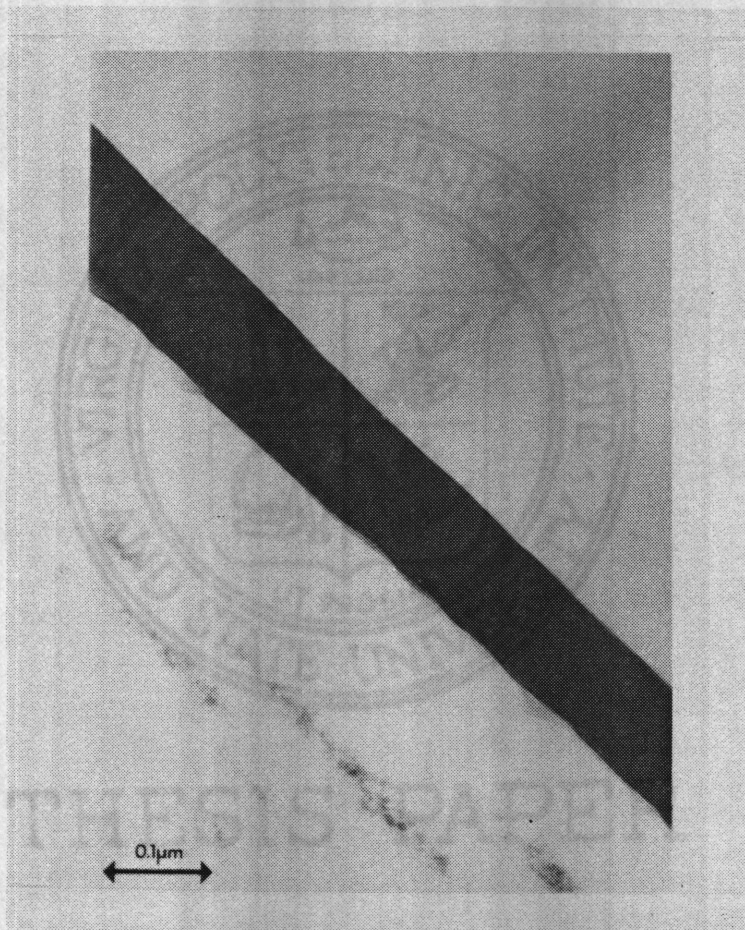


Figure 77. Transmission electron cross section of the metallized surface of a typical titanium coated ICI-442 polyester film.

Table XXIII

Deposition Characteristics of Titanium Coated Polyester Films

<u>Sample</u>	<u>Plasma Exposure (sec)</u>	<u>Metal Thickness (Å)</u>		
		<u>AES<sup>a</sup></u>	<u>TEM</u>	<u>Profilometry</u>
ICI-442	28.0	610	1480	850
ICI-442	22.0	580	1160	750

<sup>a</sup>Obtained through Auger Electron Spectroscopy with ion milling.

sputter rate of approximately 103 Å/min (i.e. more than double the rate assumed) for the titanium/titanium dioxide composition produced in these experiments.

## **XII. THE APPLICATION OF STATISTICAL EXPERIMENTAL DESIGNS TO DETERMINE PROCESS-PROPERTY RELATIONSHIPS OF TITANIUM COATED POLYESTER FILMS**

### **A. Preliminary**

The previous two Chapters have determined the chemical and physical effects that plasma treatment has on the surface and interfacial properties of ICI-442 polyester film before and after metallization with titanium. It is useful in many instances, to determine the effects that variation of processing conditions has on metal/polyester properties. A number of conditions may be varied in the plasma treatment, including; sample exposure, gas pressure, gas flow rate, plasma power, and type of treatment gas. In determining the important processing conditions, information may be obtained on the nature of the active species and/or surface effects of plasma treatment. In this Chapter, a variety of statistical methods have been used to relate the significance of the processing variables to titanium/polyester film adhesion.

### **B. Factorial I**

Statistically designed experiments have been shown to provide effective methods for determining process-property relationships.[143,144] Two types of experiments have been used here to derive the relationships between plasma processing parameters and measured adhesion between sputtered titanium metal and PET substrate. They are factorial and fractional factorial statistical designs. Both methods have the following advantages: (1) more efficient than typical one-factor-at-a-time experimentation where all variables are fixed except one which is varied, (2) hidden replication and randomization that exists in these

designs minimizes both random and bias errors, and (3) factorial experiments can determine whether process variable interactions exist which otherwise would go undetected by many other strategies. Fractional factorial methods, also known as screening designs, assume that variable interactions are negligible.

A  $2^2$  factorial design was used in the first statistical study of the pretreatment process. Pretreatment gas pressure and Ar:N<sub>2</sub>O gas ratio were the process variables assessed. A design matrix was created which consisted of six samples (Table XXIV). High (12.5 Pa) and low (2.5 Pa) gas pressures as well as 100% Ar and 100% N<sub>2</sub>O were used in combination to produce the four "end-point" samples. Two samples manufactured under 7.5 Pa pressure and with a 50:50 mixture of Ar and N<sub>2</sub>O were used as "mid-point" calibration. The results of the 180° peel tests, performed on each sample, are also given in Table XXIV.

Calculations specific to this type of design [145] provide one with a numerical value (factor effect) for each processing variable. Additional calculation yields a minimum significant factor effect (MIN) relative to a defined confidence interval (CI). Comparison of the factor effects for each variable with the MIN value determines whether the process variable in question is significant. If a factor effect is greater than or equal to the MIN value then that process variable is important; otherwise, it is insignificant. "Significant" in this context, means that changing the process variable will result in changing the dependent variable in question, which in this case is titanium/polyester adhesion. Table XXV displays the factor effects for gas ratio ( $X_1$ ), gas pressure ( $X_2$ ), and their interaction ( $X_1X_2$ ) along with the MIN value relative to a 90% confidence interval, obtained in this study. The factor effect for gas pressure (absolute value) is larger than the MIN, deeming this variable meaningful. Its negative value states that decreasing the gas pressure will result in higher levels of adhesion. Theoretically, an

Table XXIV  
Experimental Design of Factorial I

<u>Sample</u>	<u>Gas Ratio</u>	<u>Gas Pressure (Pa)</u>	<u>Xerox Adhesion (gm/cm)</u>
1	100% Ar	12.5	9.5
2	100% N <sub>2</sub> O	2.5	118.1
3	50 Ar/50 N <sub>2</sub> O	7.5	38.9
4	100% N <sub>2</sub> O	12.5	7.1
5	50 Ar/50 N <sub>2</sub> O	7.5	43.9
6	100% Ar	2.5	124.0

Table XXV  
Statistical Results of Factorial I

<u>Process Variable</u>	<u>Factor Effect<sup>a</sup></u>
Gas Ratio ( $X_1$ )	1.8
Gas Pressure ( $X_2$ )	-112.8
Interaction ( $X_1X_2$ )	-4.2

<sup>a</sup>Relative to a 90% confidence interval.  
Min Value = 30.9

increase in the mean free path of gaseous particles would result at lowered pressure.[146] By increasing the particle mean free path, more collisions of average higher energy with the PET substrate are made possible. This would be increasingly important if molecular bombardment plays a major role in producing the surface changes as evidenced by plasma exposure. Alternatively, collisions between particles will also occur at higher average energy with lower pressures increasing the probability that higher energy states will result. An increase in these states would produce larger amounts of active metastables, ions, and electrons per unit volume and increase the visible and ultraviolet photon flux within the plasma chamber. Again, the results would influence molecular bombardment characteristics, by increasing the chance that an active or charged species will come in contact with the substrate, but the radiative (photonic) nature of the plasma would be altered as well.

In contrast to the gas pressure, the factor effects for gas ratio and the interaction between gas ratio and gas pressure are below the MIN value (Table XXV). Whether or not 100% Ar, 100% N<sub>2</sub>O, or a 50:50 mixture is used in the plasma pretreatment process does not affect adhesion. In fact, XPS analysis has determined that each gaseous treatment produces the same surface functionality (i.e. as exhibited in Chapter X) all other factors being constant. An important result considering that N<sub>2</sub>O is a reactive gas while Ar is inert. A possible explanation for this phenomenon is that excited gaseous species (metastables, ions, free radicals) play far less of a significant role in the observed surface chemistry. It has been reported [147] that the use of N<sub>2</sub>O in plasma processing produces a highly functionalized surface incorporating substantial amounts of both nitrogen and oxygen. But in this study, although small amounts of nitrogen are added, surface oxygen is relatively constant. This may be in part due to the

orientation of the sample during plasma processing. In many studies [148,149,150], the sample is treated in the primary glow region, where the number of excited gas molecules are in highest concentration. Samples produced in this study, however, are in contact with the secondary glow discharge. In this region, the number of excited gaseous species as well as the average energy per molecule is less, since the molecules or atoms undergo numerous collisions before arriving. Therefore, plasma species such as free electrons and photons, which are capable of interacting with surface atoms, may play a more important role.

Processes such as photoexcitation, photoionization, and photoradicalization are all known to occur by vacuum UV radiation and have also been confirmed to exist in glow discharges.[151,152,153] UV radiation is strongly absorbed by polymers producing polymer free radicals. The polymer free radicals are active sites which can then react with gas components, other polymer chains, or relax to some stable form. In Chapter X, the effects of UV exposure and degradation have been thoroughly discussed. The ester functionality in PET is a known chromophore, and has been shown to dissociate by Norrish type I and II mechanisms under UV photolysis. The effects of UV exposure would also be deemed more selective than surface interaction with excited particles since the ester functionality alone would absorb radiation of these wavelengths while direct energy transfer (particle interaction) would be nonselective in effect. It could account for the predominance of one surface change (e.g. aldehyde functionality through Norrish type I cleavage) during plasma treatment.

E. Liston [154] has tabulated the vacuum UV spectral characteristics as well as photon energies for R.F plasmas excited in a number of gases, including argon and nitrous oxide. Table XXVI provides a partial listing of these results, providing

Table XXVI  
UV Spectral Characteristics of Gaseous Plasmas

<u>Gas</u>	<u>Wavelength (Å)<sup>a</sup></u>	<u>Photon Energy (kcal/mole)</u>
Argon	1048	273
Nitrous Oxide	1093	261

<sup>a</sup>Most intense resonance line.

the most intense resonance line and the corresponding photon energy. The predominant Ar and N<sub>2</sub>O resonance lines appear at similar wavelengths and have comparable photon energies. In both cases, the energies are more than sufficient to disrupt organic bonds. The resembling ultraviolet character of argon and nitrous oxide plasmas may account for their similarity in surface modification. If UV photolysis is responsible for the surface changes wrought by the plasma, indeed the chemical nature of the gas would not be of importance, in accord with the results of this experimental design.

The "mid-point" values are used to determine whether considerable curvature exists in the region between the "end-point" values. Curvature indicates that there exists a definite minimum or maximum between low and high values of a processing variable. In the absence of curvature, one assumes that a linear relationship governs variable behavior between "endpoints". A minimum significant curvature value (MINC) exists which is analogous to the MIN estimate described above. If the calculated curvature is equal to or greater than MINC, curvature is significant. The calculated curvature value for this study was 22.8, while MINC was determined to be 26.8 (90% CI); therefore a linear relationship (inverse) between gas pressure and Xerox adhesion is presumed.

### C. Factorial II

A second statistical design was devised to assess a larger number of processing variables. The use of a 2<sup>P</sup> factorial, equivalent to that used above, that encompasses all of the processing conditions (six) would require an excessive number of experiments (i.e. 64 experiments). Accordingly, a fractional factorial design was implemented which required the production of only 16 samples. Table XXVII provides a list of the processing variables under query and

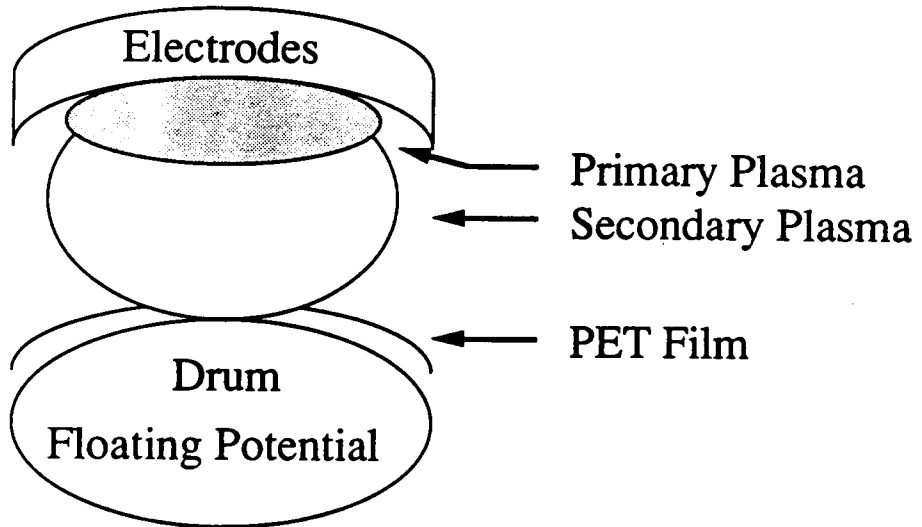
**Table XXVII**  
**Experimental Design of Factorial II**

<u>Sample</u>	<u>Pressure</u> <u>(Pa)</u>	<u>Exposure</u> <u>(sec)</u>	<u>Gas</u>	<u>Gas</u> <u>Flow Rate</u>	<u>Pretreat</u> <u>Power</u> <u>(W)</u>	<u>Film</u> <u>Bias(V)</u>
1	10.0	7.5	Ar	High	200	0
2	10.0	22.5	Ar	High	500	0
3	3.0	22.5	Ar	High	500	+25
4	3.0	7.5	Ar	High	200	+25
5	10.0	22.5	Ar	Low	200	+25
6	3.0	22.5	N <sub>2</sub> O	Low	500	+25
7	10.0	7.5	Ar	Low	500	+25
8	3.0	7.5	N <sub>2</sub> O	Low	200	+25
9	10.0	7.5	N <sub>2</sub> O	Low	200	0
10	3.0	7.5	Ar	Low	500	0
11	3.0	7.5	N <sub>2</sub> O	High	500	0
12	10.0	22.5	N <sub>2</sub> O	High	200	+25
13	10.0	7.5	N <sub>2</sub> O	High	500	+25
14	3.0	22.5	N <sub>2</sub> O	High	200	0
15	3.0	22.5	Ar	Low	200	0
16	10.0	22.5	N <sub>2</sub> O	Low	500	0

their value limits. Of the six processing variables, gas pressure and pretreatment gas were studied again to determine the reliability of this methodology. Film biasing was also studied in order to assist in the identification of the species inducing the chemical surface effects obtained during plasma treatment. By electrically biasing the drum roller of the plasma chamber (Figure 78), which is usually at a floating potential relative to the plasma, the PET film and/or drum act to disturb the electric field of the plasma. In this way charged gaseous species produced in the plasma, if near enough to the substrate, will be accelerated toward it enhancing any effect that the active particles might play.

Comparison of the factor effects of each processing variable with the MIN value (Table XXVIII) resulted in three out of six variables deemed significant. The reduction of gas pressure promoted higher levels of adhesion between titanium metal and PET substrate in full agreement with the results of the previous statistical design. Similarly, the type of pretreatment gas, argon or nitrous oxide, had no effect on adhesion proving the consistency of this type of experimental strategy. Plasma exposure was the second significant processing variable. An increase in exposure resulted in improving adhesion. It has been shown previously (Chapter X, Figure 69) that titanium/polyester adhesion goes through a maximum at an intermediate processing time frame. Under the conditions defined in this study, it is quite possible that each experimental sample was produced such that they show the character of the righthand side of the adhesion peak (e.g. adhesion decreases with a reduction in exposure). The maximum is also dependent upon the plasma pretreatment power which is the third significant processing condition. Typical behavior displays an increase of the peak maximum to lower plasma exposure time following an increase in plasma power. This may exaggerate the effects of the exposure period noted

### Normal Configuration



### Biased Configuration

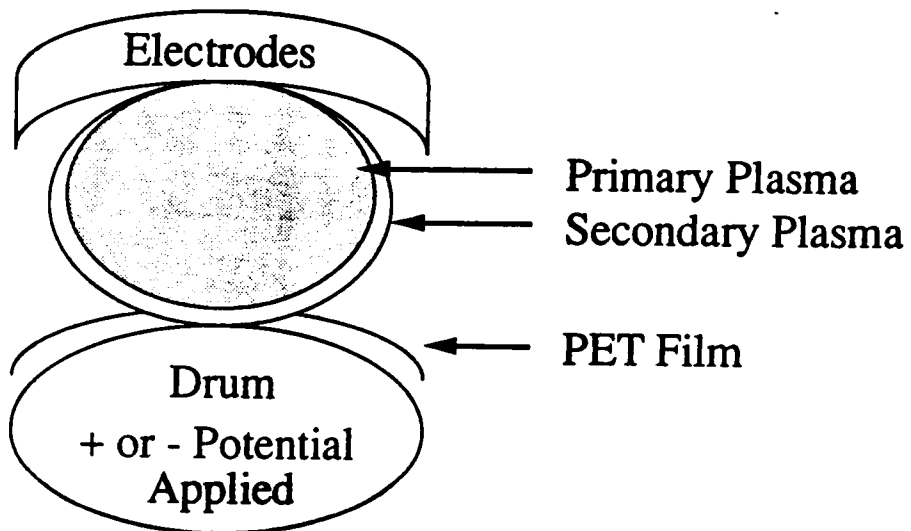


Figure 78. Schematic drawing of both normal and biased electrode configurations.

**Table XXVIII**  
**Statistical Results of Factorial II**

<u>Process Variable</u>	<u>Factor Effect<sup>a</sup></u>
Gas Pressure	-149.7
Plasma Exposure	55.9
Pretreatment Gas	13.5
Gas Flow Rate	-7.4
Pretreatment Power	-44.8
Film Biasing	-41.4

<sup>a</sup>Relative to a 90% confidence interval.  
MIN Value = 44.7.

above since higher power will improve the chance that the righthand side of the adhesion peak will be met.

Film biasing, gas flow rate, and pretreatment gas had no effect on measured adhesion. Nevertheless, questions were raised about the current experimental processing limitations. For example film biasing was deemed insignificant along with gas flow rate; but, in both cases, the variation of each within the design was minimal. The difference between low and high gas flow rate was only approximately 5% due to the limited adjustability of the exhaust valve used. Furthermore, for film biasing, the maximum voltage was relatively small (+25 VDC), the maximum allowed for the source used. In Part I, where the same type of design was used, it was stated that for this methodology to be effective, one must apply a wide range within each particular variable under study. In this case, the range for two variables was minimal. The windows of variation may be too small then for a significant effect to be observed. A question was also raised regarding whether a bias is actually generated on the surface of the PET film. Even though a positive bias was applied to the drum which the film revolves upon, is it the same bias produced on the opposite surface of the film facing the plasma? It was also not determined whether the magnitude of the bias, if generated, was strong enough to attract plasma generated species from the primary glow region. In order to provide answers to these questions, a third statistical design was implemented and is described below.

#### D. Factorial III

Three processing variables were studied in this design: film speed, gas throughput (flow rate) and film biasing. In order to avoid the pitfalls described in the previous section, a  $2^3$  factorial design was used encompassing 20

experiments (Table XXIX) which incorporated larger variations in the processing variables. Gas throughput was doubled with respect to the extremes and both negative and positive film biasing ( $\pm 100$  VDC) were included.

Gas throughput and plasma exposure were determined to be significant by comparing the MIN value with the calculated factor effects (Table XXX). In this third study, in contrast with the second statistical design, an increase in plasma exposure resulted in better adhesion. Correspondingly, it is quite possible that all third generation measurements now reside on the lefthand side of the adhesion maximum. A low pretreatment power level is used and not varied within this study so this notion is reasonable. As stated previously, higher power levels usually result in shifting the adhesion maximum to lower plasma exposure periods. In addition, reducing the gas throughput leads to an increase in titanium/polyester adhesion. Due to appreciable film off-gassing, as shown by residual gas analysis (Chapter X), the chemistry which occurs within a few millimeters of the film surface most likely differs from that which transpires within the bulk of the plasma. Increasing gas throughput may reduce the residence time or the concentration of active species in this above-surface region thereby reducing the overall effectiveness of the plasma treatment. The residence time of active species in the primary plasma region may also be affected by an increase in gas throughput.

In agreement with the second statistical design, film biasing, whether positive or negative in this case, had no effect on titanium/polyester adhesion. However, it has still not been determined if the film is actually being effectively biased by application of a voltage to the drum. But, if correct, significant evidence that particle bombardment does not play a role in the observed surface changes has been provided. A number of researchers [155,156,157] have reported that

Table XXIX

Experimental Design of Factorial III<sup>a</sup>

<u>Sample</u>	<u>Throughput</u> (X10 <sup>-4</sup> Pa l/s)	<u>Film</u> <u>Biasing (V)</u>	<u>Exposure</u> (sec)
1	11.0	0	15.0
2	4.4	+100	7.5
3	15.8	-100	22.5
4	15.8	+100	22.5
5	15.8	-100	22.5
6	4.4	-100	22.5
7	11.0	0	15.0
8	15.8	+100	7.5
9	4.4	-100	22.5
10	15.8	-100	7.5
11	4.4	+100	22.5
12	15.8	-100	7.5
13	4.4	-100	7.5
14	11.0	0	15.0
15	4.4	-100	7.5
16	4.4	+100	7.5
17	15.8	+100	22.5
18	15.8	+100	7.5
19	4.4	+100	22.5
20	11.0	0	15.0

<sup>a</sup>All samples produced at a constant gas pressure of 3.5 Pa, pretreatment power of 200 W, in argon.

Table XXX

Statistical Results of Factorial III

<u>Process Variable</u>	<u>Factor Effect<sup>a</sup></u>
Gas Throughput (1)	-36.6
Film Biasing (2)	-3.7
Plasma Exposure (3)	-115.9
Interaction (1,2)	12.8
Interaction (1,3)	19.0
Interaction (2,3)	5.1
Interaction (1,2,3)	-16.2

<sup>a</sup>Relative to a 90% confidence interval.  
MIN Value = 23.4.

biasing the substrate resulted in enhanced direct energy transfer through substantial increases in plasma particle/surface interactions. In these experiments, by biasing the substrate positively, the rate of negative ion and/or electron bombardment would be expected to increase. Alternatively, application of a negative bias would accentuate positive particle interactions. Since no prominent surface changes are observed upon application of either bias, further evidence for photon interaction is indicated. Photons are not charged species and would not be affected by successful application of film biasing.

Curvature in this third study had been determined negligible, hence linear behavior is assumed for each variable studied within the confines of the experimental design. As an overview of the results obtained by all three statistical designs, both significant and insignificant processing conditions related to adhesion are displayed in Table XXXI along with the highest relative confidence interval. The magnitude of the confidence interval may be used as a rough indication of variable importance.

Table XXXI

Statistical Significance of All Process Variables Studied

<u>Process Variable</u>	<u>Significance<sup>a</sup></u>	<u>Confidence Interval</u>
Gas Pressure	Yes	99%
Gas Mixture	No	---
Gas Throughput	Yes	95%
Film Speed	Yes	95%
Film Biasing	No	---
Pretreatment Power	Yes	90%

<sup>a</sup>Importance relative to measured adhesion.

### XIII. CONCLUSIONS AND FUTURE WORK

Poly(ethylene terephthalate) film which has undergone plasma pretreatment with a mixture of argon and nitrous oxide exhibits the effects of surface cleansing and surface functionalization at low to moderate plasma exposure. X-ray photoelectron spectroscopy has detected a new oxygen species resulting from the plasma/polymer interaction. Decreasing amounts of ester oxygen and carboxyl carbon have also been detected which suggest that dissociation of the polymer ester functionality has occurred. With longer plasma exposure, significant amounts of oxygen are lost from the surface with a concomitant increase in surface carbon concentration. A competing mechanism to surface functionalization wherein extensive chain degradation occurs is therefore suggested.

Attenuated total reflectance Fourier transform infrared spectrometry verifies the proposed mechanistic effects of plasma pretreatment. With this technique, the new oxygen species has been identified as primarily aldehydic although small amounts of surface carboxylic acid may also be present. Initial growth followed by loss of carbonyl band intensity and a constant decrease in C-O band intensity observed by ATR-IR suggest that a Norrish type I decomposition route accounts for aldehyde formation as well as most of the other surface functional changes observed with plasma exposure. Negligible amounts of carboxylic acid -OH functionality following plasma exposure indicate that a Norrish type II decomposition route wherein cleavage occurs between the primary methylene backbone linkage and the ester oxygen is of minor importance.

If a Norrish type I mechanism predominates; several specifics concerning the effects of plasma exposure are provided. First, a low energy process likely

dominates at low to moderate plasma exposure creating new carbonyl species through the dissociation of the carboxyl carbon and the ester oxygen while cleansing the surface of hydrocarbon contamination. With greater exposure, a higher energy process is more probable which results in chain scission followed by loss of carbon monoxide, rather than relaxation into an aldehyde species, creating a weak surface boundary layer. Residual gas analysis supports this hypothesis through observation of CO in the treatment chamber after plasma initiation at high exposure levels. Titanium/polyester adhesion also follows a trend in agreement with the proposed surface changes.

Examination of the titanium/polyester interfacial region with Auger electron spectroscopy revealed that a titanium oxide exists between the sputtered titanium metal and the polyester film.  $TiO_x$  formation most likely resulted from the interaction of the sputtered atoms with film off-gassing products such as water and oxygen. Further analysis by X-ray photoelectron spectroscopy indicates that titanium carbide or a carbide-like moiety resides at the interface. However, it was not determined whether this species exists as discrete units or is acting to covalently couple the titanium to the polyester substrate. Titanium-polyester oxygen interaction is also suggested by an increase in the full-width-at-half-maximum of the Ti(2p) photopeak following plasma treatment and metallization which may result in alkoxide or carboxylate linkages. In view of these results and the well defined interface as determined by transmission electron microscopy, a chemical bond not a mechanical effect must be responsible for the observed increase in adhesion relative to nontreated metallized poly(ethylene terephthalate) films.

The processing variables that determine the level of adhesion between sputter-coated metal and the PET substrate, under the conditions studied, were

identified. Six processing variables were considered using a variety of statistical experimental methods. Pretreatment gas pressure, gas throughput, pretreatment power, as well as film speed were the variables determined to significantly alter titanium/polyester adhesion. An increase in the mean free path of gaseous species, the residence time of the activated gaseous species, and the interaction between pretreatment power and film speed were deemed to cause these effects. Film biasing and the pretreatment gas mixture were determined not to affect adhesion. Since the nature of the pretreatment gas did not change the results of plasma exposure, evidence for a photon initiated mechanism is suggested. Argon, an inert gas, and nitrous oxide, an oxidizing gas, would not be expected to induce the same results if direct particle/polymer bombardment were an influence. However, both argon and nitrous oxide plasma contain a high energy vacuum-ultraviolet component capable of dissociating the only chromophore that exists in the polymer chain, the ester functionality. This specificity, relative to that observed in thermal decomposition or activated ion bombardment, may account for the predominance of the Norrish type I decomposition route and its after-effects.

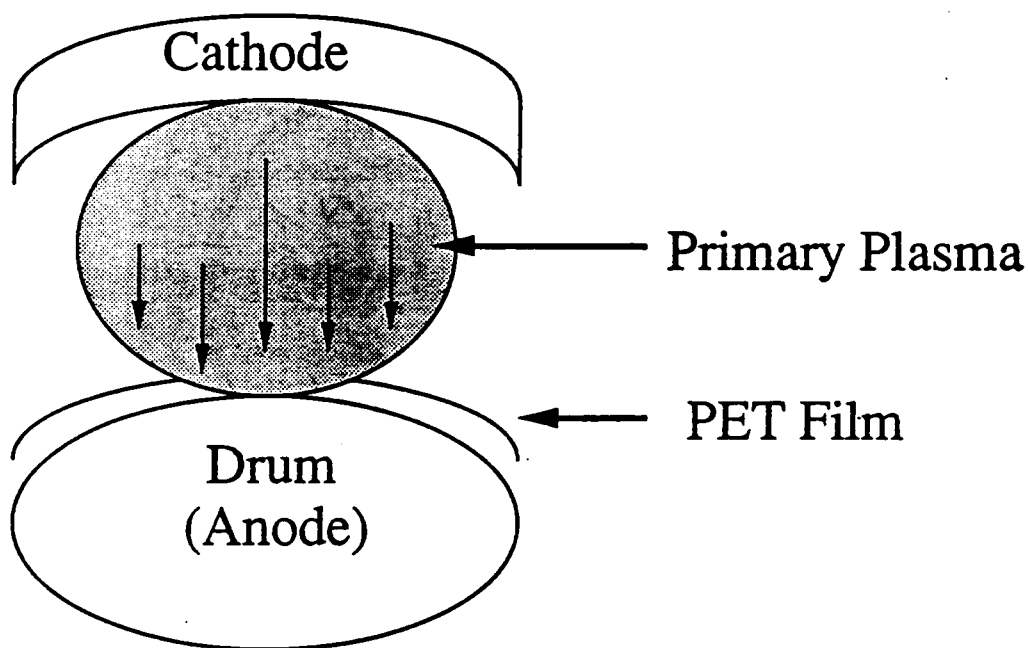
Although the determination of important processing variables was successful, the results indicated that near-optimum conditions were currently used. Any further "fine-tuning" would only allow minor improvements in titanium/polyester adhesion. With this thought, future work wherein chemical modifications to the process are considered. The most direct way to achieve this result is to study the effects of reactive gases and/or a series of inert gases as the pretreatment medium. Helium, for example has the most intense vacuum-ultraviolet output and its use in the pretreatment process may increase the effective rate of ester degradation allowing more adhesion at lower levels of exposure. Also, gases

such as SO<sub>2</sub>, CO, and CF<sub>4</sub> may induce surface functionality that would improve adhesion.

Radical plasma system reconfiguration may also prove fruitful providing additional information about the pretreatment process as well as an effective means of providing higher levels of adhesion at much lower exposure.

Modifications are currently underway on the drum assembly so that it functions as an electrode (Figure 79). In this way, study of the effects of direct particle bombardment will be assured as compared to the previous attempts at film biasing described here. Preliminary work suggests that extensive surface carbonization occurs even at plasma exposures of less than 3 seconds.

Further study of the plasma process by means of an optical probe would be useful. Even though studies have been cited concerning the vacuum-ultraviolet and ultraviolet emission of several gaseous plasmas, they were performed under the most stringent conditions (i.e high vacuum, low level of contaminants). With such problems as film offgassing, it would be important to monitor the emission spectrum during the plasma process to determine if high energy light could be a viable cause of the observed surface modifications.



**Note: Arrows in plasma indicate travel of positive particles.**

**Figure 79. Schematic drawing of the revised plasma chamber configuration where the drum cylinder is the anode.**

#### XIV. APPENDIX

The experimental volume fraction ( $V_f$ ) of particulate matter may be estimated from transmission electron microscopy through the following steps:

Calculate the total volume of a portion of a doped polyimide film from a TEM micrograph by using the measured film height, cross-section thickness (obtained from microtoming), and a representative film width.

Calculate the volume encompassed by the surface or near-surface layer (if present) by using the measured layer height, cross-section thickness, and the same film width determined above assuming the deposit is homogeneous.

Calculate the volume of particulate matter within the bulk of the polyimide, confined by the representative film width and height, assuming each particle is homogeneous and spherical.

From the information above

$$V_{\text{total}} = V_{\text{polyimide}} + V_{\text{spheres}} + V_{\text{layer}}$$
$$(V_{\text{spheres}} + V_{\text{layer}}) / V_{\text{total}} = V_f \text{ of particulate matter within the doped polyimide film}$$

For example, for a BTDA-ODA/Cu(TFA)<sub>2</sub> 1X-doped, wet-air-cured film

$$V_{\text{total}} = 9.85 \times 10^{-10} \text{ cm}^3 \quad V_{\text{spheres}} = 4.15 \times 10^{-11} \text{ cm}^3$$
$$V_{\text{layer}} = 8.0 \times 10^{-15} \text{ cm}^3$$

$$V_f = (V_{\text{spheres}} + V_{\text{layer}}) / V_{\text{total}} =$$
$$(4.15 \times 10^{-11} \text{ cm}^3 + 8.0 \times 10^{-15} \text{ cm}^3) / 9.85 \times 10^{-10} \text{ cm}^3$$
$$= 0.042$$

## REFERENCES

### Introduction.

1. A. R. Blythe, Electrical Properties of Polymers, Cambridge University Press, Oxford, UK., 1979.
2. R. B. Seymour, Conductive Polymers, R. B. Seymour, Ed., Plenum Press, New York, 1981, p. 1.
3. S. A. Halperin, Quality, February, 38 (1986).
4. The Silver Institute Letter, 15(6), February (1986).
5. G. E. Wnek, Handbook of Conducting Polymers, T. A. Skotheim, Ed., Marcel Dekker, Inc., New York, 1986, p. 205.
6. J. W. Bartha, P. O. Hahn, P. S. LeGoues, and J. Ho, J. Vac. Sci. Technol., A3, 1390 (1985).
7. G. A. Krulik, Electroless Plating, in Kirk-Othmer Encyclopedia of Chemical Technology, J. Wiley & Sons, New York, Vol. 8, 1980, p. 738.
8. P. R. Forant, Plastics Finishing and Decoration, D. Satas, Ed., Van Nostrand Reinhold Co. Ltd., New York, 1986, p. 320.
9. R. V. Stuart, Vacuum Technology, Thin Films, and Sputtering, Academic Press, New York, (1983).
10. R. P. Kusy, Metal-Filled Polymers: Properties and Applications, S. K. Bhattacharya, Ed., Marcel Dekker, Inc., New York, 1986, p. 1.

### Historical (Part I)

11. C. E. Scroog, A. L. Endrey, S. V. Abramo, C. E. Beer, W. M. Edwards, and K. L. Olivier, J. Polym. Sci., Part A., 3, 1373 (1965).
12. R. A. Dine-Hart, W. W. Wright, Makromol., 153, 237 (1972).
13. V. L. Bell, U.S. Patent 4,094,862 (June 13, 1978).
14. T. L. St. Clair, and A. Yamaki, in Polyimides: Synthesis, Characterization and Applications, Vol. 1, K. L. Mittal, Ed., Plenum Publishing Co., New York, 1984, p. 99.
15. J. H. Bateman, W. Geresy, and D. S. Neiditch, ACS Coatings and Plastics Preprints, 35, 77 (1975).

16. F. W. Harris, S. O. Norris, C. H. Lanier, B. A. Reinhardt, R. D. Case, S. Varaprath, S. M. Padaki, M. Torres, and W. A. Feld, in Polyimides: Synthesis Characterization and Applications, Vol. 1, K. L. Mittal, Ed., Plenum Publishing Co., New York, 1984, p. 3.
17. Torlon Engineering Resins, Technical Data Sheet, Amoco Corp., Naperville, Ill.
18. D. F. Loncrini, *J. Polym. Sci.: A-1*, 4, 1531 (1966).
19. J. D. Summers, C. A. Arnold, R. H. Bott, L. T. Taylor, T. C. Ward, and J. E. McGrath, *Polym. Prep.*, 27, 403, (1986).
20. S. Maudgal, and T. L. St. Clair, in Recent Advances In Polyimide Science And Technology, W. D. Weber, and M. R. Gupta, Eds., Society of Plastics Engineers, Poughkeepsie, New York, 1987, p. 37.
21. L. P. Fenocketti, EMI/RFI Shielding Plastics, Society of Plastics Engineers, Brookfield, CT, 1982, p. 57.
22. D. M. Bigg, Metal-Filled Polymers, S. K. Bhattacharya, Ed., Marcel Dekker, Inc., New York, 1986, p. 165.
23. J. E. Scheer, and D. J. Turner, *Adv. Chem.*, 99, 572 (1971).
24. R. J. Angelo, E. I. Dupont de Nemours and Co., U.S. Patent 3,073,785 (1959).
25. S. A. Ezzell, T. A. Furtch, E. Khor, and L. T. Taylor, *J. Polym. Sci.: Polym. Chem. Ed.*, 21, 865 (1983).
26. V. V. Korshak, E. E. Danilenko, M. T. Bryk, G. M. Tseitlin, M. S. Ustinov, and E. V. Dzhus, *Vysokomol. Soedin., Ser. B.*, 19, 230 (1977).
27. V. C. Carver, L. T. Taylor, T. A. Furtch, and A. K. St. Clair, *J. Am. Chem. Soc.*, 102, 876 (1980).
28. T. L. Wohlford, J. Schaff, L. T. Taylor, T. A. Furtch, E. Khor, and A. K. St. Clair, Conductive Polymers, R. B. Seymour, Ed., Plenum Publishing Co., New York, 1981, p. 7.
29. A. Auerbach, *J. Electrochem. Soc.*, 131(4), 937 (1984).
30. R. K. Boggess, and L. T. Taylor, in Recent Advances In Polyimide Science And Technology, W. D. Weber, and M. R. Gupta, Eds., Society of Plastics Engineers, Inc., Poughkeepsie, New York, 1987, p. 463.
31. R. K. Boggess, and L. T. Taylor, *J. Polym. Sci.: Part A*, 25, 685 (1987).
32. J. D. Rancourt, G. M. Porta, and L. T. Taylor, *Thin Solid Films*, 158, 189 (1988).

33. R. K. Boggess, and L. T. Taylor, *J. Polym. Sci.: Part A*, 25, 685 (1987).
34. A. Auerbach, *J. Electrochem. Soc.*, 132, 1437 (1985).
35. A. Auerbach, *Appl. Phys. Lett.*, 47, 669 (1985).
36. J. Krishnaswamy, L. Li, G. J. Collins, H. Hiraoka, and Mary Ann Caolo, Presented at the 1987 Fall Meeting of the Materials Research Society, Symposium B, Boston, Mass., December 1-3, 1987.
37. J. Krishnaswamy, M. Eyolfson, L. Li., G. J. Collins, H. Hiraoka, and Mary Ann Caolo, Presented at the SPIE 1987 Conference on "Microlithography", San Jose, California, 1988.
38. R. C. Haushalter, and L. J. Kraus, *Thin Solid Films*, 102, 161 (1983).
39. S. Mazur, and S. Reich, *J. Chem. Phys.*, 90, 1365 (1986).

#### Experimental (Part I)

40. C. D. Wagner, W. M. Riggs, L. E. Davis, and J. F. Moulder, *Handbook of X-ray Photoelectron Spectroscopy*, G. E. Muilenberg, Ed., Perkin-Elmer Corporation, Eden Prairie, Minnesota, 1979, p. 38.
41. J. D. Rancourt, J. L. Swartzentruber, and L. T. Taylor, *Amer. Lab.*, March, (1986).

#### Chapter IV

42. D. Dwight, *CHEMTECH*, July, 167 (1982).
43. C. Pantano, *Ceram. Bull.*, 60, 1154 (1981).
44. D. C. Frost, A. Ishtani, C. A. McDowell, *Mol. Phys.*, 24, 861 (1972).
45. J. D. Rancourt, R. K. Boggess, L. S. Horning, L. T. Taylor, *J. Electrochem. Soc.*, 134, 85 (1987).
46. D. G. Madeleine, S. A. Spillane, L. T. Taylor, *J. Vac. Sci. Technol.*, A5, 347 (1987).
47. K. S. Kim, W. E. Baitinger, J. W. Amy, N. Winograd, *J. Electron Spectrosc. Relatd. Phenom.*, 5, 351 (1974).
48. D. Briggs, J. J. Hearn, *Vacuum*, 11-12, 1005 (1986).

49. C. G. Pantano, *Ceram. Bull.*, 11, 1154 (1981).
50. J. D. Rancourt, L. T. Taylor, Cross-Linked Polymers; ACS Symposium Series, R. A. Dicket, S. S. Labana, R. S. Bauer, Eds., American Chemical Society, Washington, DC, 1988, p 395.
51. P. L. Buchwalter, A. I. Baise, Polyimides: Synthesis, Characterization and Applications, K. L. Mittal, Ed., Plenum Press, New York, 1984; p 537.
52. J. L. Slominski, A. Landau, *Plat. Surf. Finish.*, June, 96 (1982).
53. C. D. Wagner, D. Briggs, Ed., Handbook of X-ray and Ultraviolet Photoelectron Spectroscopy, Heyden & Sons, London, 1977, Chapter 7.
54. A. Okhi, M. Takagi, K. Ueno, *Analytica Chimica Acta*, 159, 245 (1984).
55. V. M. Koleshko, V. V. Sviridov, V. P. Boldyrev, B. S. Reznikov, I. V. Nekaryukin, K. D. Yashin, N. N. Goroshko, A. A. Kovalevskii, *Izvestiya Akademii Nauk SSSR, Neorganicheskie Materialy*, 12(10), 1730 (1975).
56. R. L. Hough, *Proceedings of the Third International Conference On Chemical Vapor Deposition*, F. A. Glaski, Ed., The American Nuclear Soc., 1972, p. 232.
57. J. E. Brady, and G. E. Humiston, General Chemistry: Principles and Structure, 4th Ed., J. Wiley & Sons, New York, 1986, p. 654.
58. R. A. Pike, J. P. Pinto, C. M. Brunette, Recent Advances in Polyimide Science and Technology; *Proceedings of the Second International Conference on Polyimides*, W. D. Weber, M. R. Gupta, Eds., Society of Plastics Engineers, Inc., Poughkeepsie, NY, 1987, p 92.
59. J. D. Rancourt, and L. T. Taylor, *J. Appl. Polym. Sci.*, 30, 4149 (1985).

## Chapter V

60. J. D. Rancourt, G. M. Porta, and L. T. Taylor, *Proceedings of the 19th International SAMPE Technical Conference*, October 13-15, 1987, p. 564.
61. G. D. Khune, *J. Macromol. Sci. Chem.*, A15, 241 (1981).
62. N. D. Ghatge, and U. P. Mulik, *J. Polym Sci. Polym. Chem. Ed.*, 18(6), 1905 (1980).
63. D. Hofer, Presented at the 1988 Fall Meeting of the Materials Research Society, Boston, Mass., December 1-3, 1988.

## Chapter VI

64. D. J. Golob, *Mod. Plas.*, 64, 158 (1987).
65. B. A. Jones, *Res. & Devel.*, 29, 54 (1987).
66. E. I. Dupont de Nemours & Co., Strategy of Experimentation, Professional Training Seminar Notes, Oct. 1975, p. 29.
67. R. L. Plackett, and J. P. Burman, *Biometrika*, 33, 311 (1946).
68. S. W. Gaarenstroom, and N. Winograd, *J. Chem. Phys.*, 67, 3500 (1977).

## Historical (Part II)

69. J. M. Hawthorne, and C. J. Heffelfinger, Encyclopedia of Polymer Science and Technology, H. M. Marks, N. M. Bikales, and N. Gaylord, Eds., J. Wiley & Sons, New York, Vol. 11, 1969, p. 42.
70. P. F. Stecher, Innovations In Plastic Films Technology, J. P. Harrington, Ed., Technomic Pub. Co., New York, 1985, p. 1.
71. *Mod. Plastics*, 44(4), 110 (1966).
72. J. R. Whinfield, and J. T. Dickson, E. I. Dupont de Nemours & Co., US. Pat. 2,465,319 (March 22, 1949).
73. C. R. Oswin, Plastics Films And Packaging, J. Wiley & Sons, New York, 1975, p. 108.
74. J. A. Thornton, *Thin Solid Films*, 80, 1 (1981).
75. G. K. Werner, and G. S. Anderson, Handbook of Thin Film Technology, L. I. Maissel, and R. Glang, Eds., McGraw-Hill, New York, 1970, p 3-1.
76. J. A. Thornton, Deposition Processes in Thin Films and Coatings, R. F. Bunshah et. al., Eds, Noyes Publications, Park Ridge, NJ, 1982, p. 170.
77. J. L. Vossen, and J. J. Cuomo, Thin Film Processes, J. L. Vossen, and W. Kern, Eds., Academic Press, New York, 1978, p. 11.
78. B. Chapman, Glow Discharge Processes, J. Wiley & Sons, New York, 1980.
79. I. Petrov, V. Orlinov, and A. Misiuk, *Thin Solid Films*, 120, 55 (1984).
80. G. N. Jackson, *Thin Solid Films*, 5, 209 (1970).
81. J. A. Thornton, and D. W. Hoffman, Plastics Finishing And Decoration, D. Satas, Ed., Van Nostrand Reinhold Co. Ltd., New York, 1986, p. 345.

82. J. A. Thorton, *Met. Finish.*, 74, 46 (1976).
83. R. K. Waits, *Thin Film Processes*, J. L. Vossen, and W. Kern, Eds., Academic Press, New York, 1982, p. 31.
84. S. Wu, *Polymer Interface and Adhesion*, Marcel Dekker, New York, 1982.
85. Minnesota Mining & Manufacturing Co., Brit. Pat. 891,469 (March 14, 1962).
86. L. E. Wolinski, E. I. Dupont de Nemours & Co., U.S. Pat., 3,274,089 (Sept. 26, 1966).
87. I. A. Abu-Isa, *Polym. Plast. Technol. Eng.*, 2, 29 (1973).
88. R. A. Bragole, *Adhesives Age*, 17, 24 (1974).
89. J. M. Burkstrand, *J. Vac. Sci. Technol.*, 21, 70 (1979).
90. W. R. Comboltz, and A. S. Hoffman, *Polym. Mater. Sci. Eng.*, 56, 720 (1987).
91. D. Satas, *Plastics Finishing And Decoration*, D. Satas, Ed., Van Nostrand Reinhold Co. Ltd., New York, 1986, p. 70.
92. F. G. Funderburk, E. C. Culbertson, and R. G. Posey, American Hoechst Corp., U.S. Pat. 4,493,872 (Jan. 15, 1985).
93. C. A. L. Westerdahl, J. R. Hall, E. C. Schramm, and D. W. Levi, *J. Colloid Interface Sci.*, 47, 610 (1974).
94. L. C. Jackson, *Adhesives Age*, Sept., 34 (1978).
95. R. G. Nuzzo, and G. Smolinsky, *Macromolecules*, 17(5), 1013 (1984).
96. J. R. Hollahan, and G. L. Carlson, *J. Appl. Polym. Sci.*, 14, 2499 (1970).
97. N. J. Delottis, *Rubber Chem. Technol.*, 46, 549 (1973).
98. J. R. Hall, C. A. Westerdahl, A. T. Devine, and M. J. Bodnar, *J. Appl. Polym. Sci.*, 16, 1465 (1969).
99. R. H. Hansen, and H. Schonhorn, *J. Polym. Sci.*, B4, 203 (1966).
100. R. M. Mantell, and W. L. Ormand, *I&EC Prod. Res. Devel.*, 3, 300 (1964).
101. K. L. Mittal, *J. Vac. Sci. Technol.*, 13, 19 (1976).
102. J. M. Burkstrand, *J. Appl. Phys.*, 52, 4795 (1981).
103. M. Hudis, *Techniques and Applications of Plasma Chemistry*, J. R. Hollahan, and A. T. Bell, Eds., J. Wiley & Sons, New York, 1974, p.113.

104. K. Rossmann, *J. Polym. Sci.*, 19, 141 (1956).
105. H. Schonhorn, F. W. Ryan, and R. H. Hansen, *J. Adhesion*, 2, 93 (1970).
106. H. Yasuda, H. C. Marsh, E. S. Brandt, and C. N. Reilley, *J. Polym. Sci., Polym. Chem. Ed.*, 15, 991 (1977).
107. C. A. L. Westerdahl, J. R. Hall, and D. W. Levi, ARRADCOM, Tech. Report., (1975).
108. J. L. Grant, D. S. Dunn, and D. J. McClure, *J. Vac. Sci. Technol. A*, 6, 2213 (1988).
109. D. S. Dunn, and D. J. McClure, *J. Vac. Sci. Technol. A.*, 5, 1327 (1987).

#### Chapter X

110. D. Briggs, *Polymer*, 21, 895 (1980).
111. G. Gillberg, *J. Adhesion*, 21, 129 (1987).
112. D. Briggs, *Polymer*, 25, 1379 (1984).
113. M. C. Ross, ARRADCOM, LCWSL, Tech. Report., ARLCD-TR-77088 (1978).
114. J. R. Hall, C. A. L. Westerdahl, M. J. Bodnar, and D. W. Levi, *J. Appl. Polym. Sci.*, 16, 1465 (1972).
115. E. J. Hellund, *The Plasma State*, Reinhold, New York, 1961, pp.65-101.
116. W. E. Swartz, *Anal. Chem.*, 45, 788A (1973).
117. H. Schonhorn, F. W. Ryan, and R. H. Hansen, *J. Adhesion*, 2, 93 (1970).
118. D. T. Clark and A. Dilks, *J. Polym. Sci. Polym. Chem. Ed.*, 15, 2321 (1977).
119. L. H. Buxbaum, *Angew. Chem., Int. Ed*, 7, 182 (1968).
120. H. Sobue, and J. Kajiura, *J. Chem. Soc. Japan, Ind. Chem. Sect.*, 62, 1766 (1959).
121. K. Yoda, A. Tsuboi, M. Wada, and R. Yamadera, *J. Appl. Polym. Sci.*, 14, 2357 (1970).
122. E. I. Pearce, B. J. Bulkin, and M. Y. Ng, *Polymer Characterization*, Adv. Chem. Series 203, C. D. Craver, Ed., American Chem. Soc., Wash., D.C., 1983, p.571.
123. M. Day, and D. M. Wiles, *J. Appl. Polym. Sci.*, 16, 175 (1972).

124. C. V. Stephenson, B. C. Moses, and W. S. Wilcox, *J. Polym. Sci.*, 55, 451 (1961).
125. F. B. Marcotte, D. Campbell, J. A. Cleaveland, and D. T. Turner, *J. Polym. Sci.*, A-1, 5, 481 (1967).
126. D. M. Wiles, *Polym. Eng. Sci.*, 13, 74 (1973).
127. P. Blais, M. Day, and D. M. Wiles, *J. Appl. Polym. Sci.*, 17, 1895 (1973).
128. D. S. Dunn and D. J. McClure, *J. Vac. Sci. Technol.*, A5, 1327 (1987).
129. S. K. Bahl, D. D. Cornell, and F. J. Boerio, *J. Polym. Sci., Polym. Lett. Ed.*, 12, 13 (1974).
130. C. Y. Liang, and S. Krimm, *J. Mol. Spectrosc.*, 3, 554 (1959).
131. L. D'Esposito, and J. L. Koenig, *J. Polym. Sci., Polym. Phys. Ed.*, 14, 1731 (1976).
132. ICI Ltd., Dyestuffs Division, Eight Peak Index of Mass Spectra, Mass Spectrometry Data Centre, Awre, UK, 1970, p. 2.
133. B. Ranby, and R. F. Rabek, Photodegradation, Photo-oxidation and Photostabilization of Polymers, J. Wiley & Sons, New York, NY, 1975, p. 231.
134. C. V. Stephenson, J. C. Lacey Jr., and W. S. Wilcox, *J. Polym. Sci.*, 55, 477 (1961).
135. D. M. Wiles, Degradation and Stabilization of Polymers, J. Wiley & Sons, New York, NY, 1975, p.137.
136. P. W. Rose, and E. M. Liston, *Plast. Eng., Oct.*, 40 (1985).

## Chapter XI

137. D. R. Lefebvre, The Durability Of Adhesive Joints, An Engineering Study, PhD Dissertation, VPI&SU, Blacksburg, Va (1988).
138. C. D. Wagner, L. H. Gale, and R. H. Raymond, *Anal. Chem.*, 51, 466 (1979).
139. Y. Baba, and T. A. Sasaki, *J. Nucl. Mater.*, 152, 295 (1988).
140. W. J. Lo, Y. W. Chung, and G. A. Somorjai, *Surface Sci.*, 71, 199 (1978).
141. K. Suzuki, A. B. Christie, and R. P. Howson, *Vacuum*, 36, 323 (1986).
142. J. A. Thorton, Semiconductor Materials and Process Technologies, G. E. McGuire, Ed., Noyes Publications, Park Ridge, N.J., 1982, p. 19.

## Chapter XII

143. R. A. Olivero, *Diss. Abstr. Int. B*, 48, 1028 (1987).
144. J. Usero, I. Gracia, *Ing. Quim. (Madrid)*, 19, 135 (1987).
145. G. E. P. Box, W. G. Hunter, and J. S. Hunter, *Statistics for Experimentors*, J. Wiley & Sons, New York, 1978.
146. P. W. Atkins, *Physical Chemistry*, 2nd Ed., Oxford University Press, UK, 1982.
147. H. Schonhorn, F. W. Ryan, and R. H. Hansen, *J. Adhesion*, 2, 93 (1970).
148. J. R. Hall, C. A. L. Westerdahl, A. T. Devine, and M. J. Bodnar, *J. Appl. Polym. Sci.*, 13, 2085 (1969).
149. R. G. Nuzzo, and G. Smolinsky, *Macromolecules*, 17, 1013 (1984).
150. H. Schonhorn, and R. H. Hansen, *J. Appl. Polym. Sci.*, 11, 1461 (1967).
151. H. V. Boenig, *Plasma Science and Technology*, Cornell Univ. Press, 1982.
152. R. E. Cohen, R. F. Baddour, and G. A. Corbin, *Proc. 6th Int'l Symp. on Plasma Chemistry, Montreal, Quebec, 1983*, p. 537.
153. H. V. Boenig, *Proc. 1st Ann. Int'l Conf. Plasma Chem. Technol., San Diego, CA.*, H. V. Boenig, Ed., Technomic Publ. Co., Lancaster, Pa 1983.
154. E. Liston, Presentation at VPI&SU, (April 19, 1989).
155. J. E. Curran, *J. Phys. E*, 14, 393 (1981).
156. S. Broydo, *Solid State Technology*, 1, 159 (1983).
157. S. J. Moss, A. M. Jolly, and B. J. Tighe, *Proc. 6th Int'l Symp. Plasma Chem., Montreal, Que., 1983*, p. 621.

**The vita has been removed from  
the scanned document**